# THE DYNAMIC BEHAVIOUR AND FEEDBACK CONTROL OF A TURBOCHARGED AUTOMOTIVE DIESEL ENGINE WITH VARIABLE GEOMETRY TURBINE

by

RICHARD JOHN BACKHOUSE

A thesis submitted to the University of Manchester for the degree of Doctor of Philosophy in the Faculty of Technology

April 1986

**Declaration**

No portion of the work referred to in the thesis has been submitted in support of an application for another degree or qualification at this or any other university or other institution of learning.

CONTENTS

## ACKNOWLEDGEMENTS

I am grateful to Professor Wallace of Bath University for permission to use their facilities and to the staff of the Wolfson Engine Test Unit for their cooperation: to Tony and Keith, the fitters, Ian, for help with soldering, Alex, for the use of his prototype Hall-effect position transducer, and in particular to Dave Howard, who was responsible for the engine, and gave a considerable amount of his own time to help.

I am thankful to the SERC for supporting me for two years as a research student and for funding the contract which enabled me to build the controller, carry out the experimental work, and to complete my third year.

I am grateful to the Holset Engineering Company for the opportunity to analyse the control stability of their boost pressure controlled variable geometry turbocharger, when fitted to an engine.

At UMIST, I am grateful to Hugh Frost who designed and built the controller to my specification. I am grateful also to Professor Munro, Dr. Wellstead and, in particular, Dr. Edmunds - all of the Control Systems Centre - for advice on the control aspects on the work. I am very grateful to my supervisor, Professor Winterbone, for his encouragement and practical help and for deflecting me away from some red herrings.

In writing up, I have been greatly helped and refreshed by the hard work of Val, typing text, and Pat Shepherd, typing equations and

appendices, and Clare, who traced most of the diagrams. Heather and Forrest looked after me and several people encouraged me and prayed on my behalf.

I am grateful to the one true God, the father of Jesus the Messiah, for enabling me to persevere and for helping me continually with the work.

**SUMMARY**

This thesis is concerned with the feedback control of a turbocharged automotive diesel engine with variable geometry turbine. To this end frequency response testing has been carried out on such an engine over much of its operating range. Both fuel rack position and turbine inlet area were perturbed and the responses of engine speed, output shaft torque, turbine inlet temperature and exhaust opacity measured. The interpretation of these responses is discussed and the time constants compared with predicted values. A dynamic mean effective pressure (d.m.e.p.) is derived from the speed and output shaft torque responses allowing the dynamic response of the effective engine torque to be examined in greater detail than previously achieved. From the d.m.e.p. response, values of the torque delay have been determined experimentally and were found to compare well with expected values when sampling of the rack position by the fuel injection pump occurs at the end of injection. Dynamic exhaust opacity is related to the dynamic trapped air-fuel ratio.

The choice of engine outputs to be used as control variables is discussed, and the stability of the engine is analysed when feedback loops are applied to control engine speed and either boost pressure or trapped air-fuel ratio. Interaction is small when boost is controlled, and improves the stability margin; when air-fuel ratio is the second controlled variable the effect of interaction is greater and is detrimental to the stability margins.

A digital controller to control such an engine has been designed and implemented onto the engine. This provides feedback control of speed

and air-fuel ratio (within the range allowed by the turndown ratio of the turbine inlet area); scaling is used to avoid singularity in the system steady state gain matrix and a precompensator, whose terms vary with the operating point of the engine, is used to reduce the effect of interaction.

| | | |
|---|---|---|
| G | transfer function matrix (MIMO systems) | - |
| G(0) | steady state gain matrix (MIMO systems) | - |
| i.m.e.p. | indicated mean effective pressure | bar |
| $I_E$ | moment of inertia of crankshaft and flywheel | $kg.m^2$ |
| $I_{t/c}$ | moment of inertia of turbocharger rotor | $kg.m^2$ |
| $I_{tot}$ | moment of inertia of crankshaft, flywheel, drive shaft and dynamometer | $kg.m^2$ |
| I.C. | internal combustion | - |
| IDI | indirect injection | - |
| IVC | inlet valve closing | - |
| j | imaginary operator (square root of -1) | - |
| k | constant; feedback gain term | - |
| Lp | pumping losstorque | Nm |
| m | number of sine wave periods (integer) | - |
| $m_{exm}$ | mass of gas in exhaust manifold | kg |
| $m_f$ | fuel injected per cylinder (or change of same) | mg/shot |
| $m_{im}$ | mass of air in the inlet manifold | kg |
| $\dot{m}_a$ | air mass flow rate | kg/sec |
| $\dot{m}_{ex}$ | exhaust mass flow rate | kg/sec |
| M | torque pulse | Nm |
| MIMO | multi-input, multi-output | - |
| n | indicial power; constant; signal noise | - |
| $n_E$ | change in engine speed | rev/min |
| N | number of cylinders | - |
| $N_E$ | engine speed | rev/min |
| $N_{t/c}$ | turbocharger speed | rev/min |
| $P_b$ | inlet manifold boost pressure (or change of same) | bar |
| $P_{exm}$ | exhaust manifold presssure (or change of same) | bar |
| $P_t$ | turbine power | kW |

| | | |
|---|---|---|
| PI | proportional plus integral | - |
| PID | proportional,integral and derivative | - |
| PRBS | pseudo random binary sequence | - |
| r | feedback reference value(s) | - |
| $r_t$ | reduction in turbine area (actuator movement) | mm |
| $r_{xy}(0)$ | measured cross-correlation (zero time offset) | - |
| $R_a$ | gas constant for air | kJ/kg.K |
| $R_e$ | Reynolds number | - |
| $R_{ex}$ | gas constant of exhaust gases | kJ/kg.K |
| $R_{xy}(0)$ | true cross-correlation (zero time offset) | - |
| RAM | random access memory | - |
| s | Laplace operator (complex exponent of e) | $sec^{-1}$ |
| S | exhaust opacity | % |
| SISO | single input, single output | - |
| t | time constant; time delay | sec |
| $t_{th}$ | thermocouple time constant | sec |
| $t_{we}$ | time constant of wall temperature $T_{we}$ | sec |
| T | sample period | sec |
| $T_{amb}$ | ambient air temperature | K |
| $T_c$ | compressor torque | Nm |
| $T_E$ | engine torque | Nm |
| $T_{im}$ | temperature of air in the inlet manifold | K |
| $T_L$ | load torque | Nm |
| $T_t$ | turbine torque | Nm |
| $T_{ti}$ | turbine inlet temperature | K |
| $T_{we}$ | temperature of walls affecting $T_{ti}$ | K |
| TDC | top dead centre | - |
| TFA | transfer function analyser | - |
| u | engine input | - |
| V | signal voltage (subscript indicates variable) | volts |

| | | |
|---|---|---|
| $V_{ex}$ | volume of exhaust manifold | $m^3$ |
| $V_{im}$ | volume of inlet manifold | $m^3$ |
| $V_{sw}$ | swept volume of each cylinder | $m^3$ |
| VG | variable geometry | - |
| $x_f$ | fuel rack position or change of same | mm |
| y | engine output | - |
| z | operator in sampled-data systems ($z=e^{sT}$) | - |
| $\alpha_{-1}$ | attenuation of first sideband | - |
| $\eta_c$ | compressor efficiency | - |
| $\eta_t$ | turbine efficiency | - |
| $\eta_{th}$ | thermal efficiency | - |
| $\eta_{vol}$ | volumetric efficiency | - |
| $\theta_{-1}$ | phase lag introduced into first sideband | degrees |
| $\rho$ | phase of first sample point relative to test sine wave | degrees |
| $\tau_E$ | change in engine torque | Nm |
| $\tau_L$ | change in load torque | Nm |
| $\tau_s$ | change in measured shaft torque | Nm |
| $\omega$ | sine wave test frequency | rad/sec |
| $\omega_b$ | break frequency | rad/sec |
| $\omega_E$ | change in engine speed | rad/sec |
| $\omega_s$ | sampling frequency | rad/sec |
| $\Delta T_e$ | temperature rise across engine | K |

# 1. INTRODUCTION

Both feedback control and turbocharging have been with us, at least in concept, for some time. The widespread use of feedback control probably began nearly 200 years ago when James Watt adapted the centrifugal flyweight device to operate a valve so as to adjust the torque of his beam engines and hence automatically control their speed (1).

The turbocharger was first proposed, early this century, by Dr. Buchi (2) who, later, went on to demonstrate its working on an engine. The diesel engine required the development of the liquid fuel injection pump before it became viable in the 1930's as an economical and reliable power unit for road transport. Turbocharging, although ideally suited to the diesel engine, had to await developments in materials before the turbocharger became sufficiently small, cheap and reliable to be a serious proposition for road transport power units; this occurred in the 1960's.

Nowadays turbocharging is standard on diesel engines of medium speed and larger, and is widespread on automotive direct injection diesels (i.e. of greater than about 100 b.h.p.) Apart from increasing the power per unit weight and per unit cost, a well-matched turbocharger gives improved brake specific fuel consumption (b.s.f.c.) over a large part of the engine operating range. This is a result of a reduction in the percentage of i.m.e.p. lost to friction, a reduction in pumping losses, and an increase in combustion efficiency at higher b.m.e.p.'s due to the higher trapped air-fuel ratios. In addition, combustion

noise and steady state smoke are reduced, and torque back-up can be increased to allow the use of gearboxes with fewer gear ratios. There are two main problems associated with turbocharging the automotive diesel; first is the inherent mismatch between the delivery characteristics of the rotodynamic turbocharger and the boost requirements of the metered flow through the engine cylinders. To a first approximation the compressor delivery pressure and mass flow are both proportional to turbocharger speed which is roughly proportional to engine power. The engine, however, requires a boost pressure that is proportional to torque but not to engine speed. The result is that at high engine speeds the turbocharger tends to provide unnecessarily high boost pressure and back pressure, while at low engine speeds insufficient boost is available to give the desired engine torque. As a result the full-load speed range of the engine may have to be limited, and the torque available for starting the vehicle from rest is generally poor.

The second main problem is related to the large changes in angular momentum required of the turbocharger rotor in comparison with the accelerating torque available. Since the turbocharger does not accelerate quickly enough to provide the boost pressure required by the engine during acceleration, the fuelling has to be cut back to avoid heavy smoke emissions and this results in poor vehicle acceleration. In engines of very high b.m.e.p., fuel limiting may be necessary to avoid stalling. Fuel delivery is limited during transients either by 'boost control' (where boost pressure is used to move the fuel rack stop) or by 'puff-limiting' (where a dashpot limits the rate of change of rack position). A substantial improvement in both problem areas can be

provided if it is possible to vary the inlet area to the turbocharger turbine (3,4). Reducing the area at low engine speeds and during acceleration raises the mean pressures in the exhaust manifold(s), substantially increasing the turbine torque available. This increases the boost available at low engine speeds and improves the acceleration of the turbocharger during transients. However, the greater back pressure seen by the cylinder adversely affects the pumping losses and depending on the extent of valve overlap, the proportion of residual gases left in the cylinder at exhaust valve closing. At low speeds and under load, these losses are more than offset by the increased inlet manifold pressures resulting from the raised turbocharger speed since pumping losses are moderated and combustion is substantially improved by the increase in trapped air-fuel ratio. The observed result is a significant increase in the torque that can be used without exceeding smoke limits.

At part load, and at full speed and maximum load, the extra air-fuel ratio is of no benefit since the ratio is already close to or greater than the optimum value for fuel consumption - normally about 30:1 (5). Under these conditions the turbine inlet area needs to be increased.

Typically the maximum inlet area will be chosen to be greater than that of a fixed geometry turbine matched to the engine for the same duty; this means that peak turbocharger speed is reduced and the fuel economy at rated output may be improved. If, alternatively, the maximum $A_t$ is kept similar to that of the fixed geometry turbine then the whole of the variable geometry turndown ratio ($A_t max/A_t min$) can be used to improve low speed torque and acceleration. This may be useful since

the turndown ratio achievable at present is 4:1 or 5:1. A typical desired scheduling of $A_t$ under steady state conditions is shown in figure 1.1.

One means of controlling an engine with a variable area turbocharger is to use simple feedback of the boost pressure to control $A_t$ so as to attempt to maintain a fixed inlet manifold pressure. In its simplest form this means that, at low loads, minimum turbine area is used giving unnecessarily high air-fuel ratios and poor fuel economy. However in applications where part load operation constitutes only a small part of the engine's duty, such a control scheme would seem to provide a simple, cost-effective solution. This is particularly the case where transient response is important, since this approach ensures that high turbocharger speed and boost pressure are available at part load, ready for any sudden increase in fuelling.

Where part load efficiency is significant, e.g. in rail traction and some automotive duties, maximum $A_t$ must be used during steady state running at part load. This may be achieved by:

a) scheduling $A_t$ according to speed and fuelling

b) using feedback control of boost, but varying the desired boost according to fuelling level.

c) using feedback control of air-fuel ratio.

None of these is easy to achieve under mechanical/pneumatic control and probably requires analogue electronic, or microprocessor-based digital control. As the complexity of control required increases so digital control becomes more attractive; and as the manufacturing costs of digital hardware continue to fall, so too does the degree of complexity

at which it becomes economically viable to use full microprocessor control. Once digital control is justified in financial terms, considerable improvements in engine diagnostics and complexity of control scheduling become available at little extra cost. In fact self-tuning control can then be used to tune the control parameters for optimum performance, compensating automatically for variations in ambient conditions, altitude, and engine behaviour (including the effects of friction and wear).

Microprocessor based control is already widely applied to spark-ignition engines and, as a result, considerable progress has already been achieved in the development of low cost, accurate and reliable sensors, actuators, integrated circuits and the associated leads and connectors.

With increasing demands for lower fuel consumption, better starting and increasingly strict emissions and noise regulations, it is almost certain that the more complex engines, or rather power systems, of the future will have full digital control.

Although feedback control of speed in automotive diesels normally occurs only at low and high speed idles, the increasing use of cruise control, including maximum speed limiters, will increase the demand for feedback control of speed. In addition, compound engines, and engines coupled with continuously variable transmissions (CVT) will require more complex control systems.

Meanwhile, there is a need for increased complexity, e.g. in the use of

variable geometry (VG) turbochargers, without the need to completely change the engine control system. The ability to add a VG turbocharger having a self-contained control system, and not requiring connection into the speed governor greatly increases the acceptability of the development to engine manufacturers and operators alike and allows for simple fitting to engines already in service.

In control terms all these systems are multi-input multi-output (MIMO). In order to predict steady state accuracy and feedback control stability, it is necessary to consider all the transfer functions between different input and output combinations. This also enables the correct choice to be made of output variable, or combination of outputs, by which to control each system input. The use of feedforward control avoids feedback instability that may result from the cross-coupling (or interactive) terms; knowledge of the interactions is still necessary in order to keep steady state errors in the system outputs within desired limits. This is the field of multivariable control theory and in the past fifteen years relatively simple methods have been developed for analysing and designing controls for such systems.

The work presented here considers the choice of control parameters to use, then examines the stability of the control system when an automotive diesel engine with VG turbocharger has feedback control of boost pressure or air-fuel ratio. First the dynamic behaviour of such an engine is measured and analysed; then its stability under different forms of feedback control is examined. Finally, a digital controller employing multivariable precompensation, is designed and applied to such an engine.

It is the thesis of the author that feedback control of boost pressure in a turbocharged, automotive, diesel engine with VG turbine is possible without multivariable precompensation, but that the same may not be assumed to be true when air-fuel ratio is to be controlled or in larger engines employing longer valve overlap periods, or spark ignited engines where the power is controlled by throttling.

# 2. LITERATURE SURVEY

## 2.1 Historical Overview

The basic principles of engine speed governing were laid out by Maxwell in 1868 (6) and extended by Routh (7) in 1877. Further development of feedback (or automatic) control theory did not come until the 1930's and 1940's when Nyquist (8) and Bode (9) published their papers. Further application of this theory to the diesel engine came in the 1950's, in Germany first with the publication of papers by Benz (10) and Welbourn and Allen-Williams (11), although Bujak (12) had produced a paper in England as early as 1945, but he died before he was able to explain his ideas more clearly (13). Otherwise the first publications in English were by Oldenburger (14) in the United States in 1958 and Welbourn et al (15) in the United Kingdom in 1959.

Oldenburger had been working in the field for some years previously without being permitted to publish his findings (13). Further papers followed from Taylor (16) and Benz (17, 18). Welbourn et al explained and solved many of the instability problems being experienced with diesel engines at the time. They recognised the sampled nature of the diesel fuel injection process but the application of sampled data theory to the diesel engine came with Bowns (19) and the team including Windett and Flower at Sussex (20, 21) in the early 1970's.

In the early and middle seventies, with the widespread use of digital computation, simulations of the diesel engine process began to appear that could be used for identifying transient behaviour. Initially these

were quasi steady state models (22, 23), which assumed that steady state characteristics were valid during engine transients. Later, filling and emptying models began to appear (24, 25), which treated the dynamics more accurately by allowing for the accumulation of gases in volumes. With care these could account for most non-steady effects and they began to be used to obtain transfer functions (26, 27), or simply to test different control strategies (28). In this manner, Aldren (27) obtained transfer functions for a turbocharged diesel engine with variable geometry turbine.

Also in the mid-1970's as a result of the advances in integrated circuit manufacture and due to the pressure of strict emissions and fuel economy legislation, mainly in the U.S.A., digital electronic control began to be applied to spark ignition engines. Initially this was simply to schedule spark timing as a function of engine operating point, but later it also included feedback control of air-fuel ratio, and now includes feedback control of timing to avoid knock. Feedback optimisation of timing to give optimum fuel economy and power (by means of timing dither) has been shown to work (29) and is beginning to be used in engine management systems.

In addition to the frequency response work carried out by Welbourn et al (15), Bowns (19) and Flower et al (21, 30), experimental frequency response measurements made on Diesel engines have been published by Thiruarooran (26) and Sawa and Hori (31). Flower et al (32) have analysed the effects of engine sampling and analyser sampling on measured frequency responses on engines.

Pseudo random binary sequences (PRBS) have been used to estimate the frequency responses of diesels (33, 26) and of an automotive gas turbine (34). Flower et al (35) have investigated the experimental techniques required to obtain repeatable results from PRBS testing of diesel engines.

With the past few years advances in electronics and digital control have begun to be applied to diesel engines mainly to improve the accuracy of the fuel injection process (36 - 41).

Pipho and Kittleson have demonstrated closed loop digital control of diesel injection timing (42) and Zanker and Wellstead demonstrated a self-tuning diesel controller, albeit with retuning times that were too long for automotive use (43).

## 2.2 Classical Control Theory Applied To Diesel Engines

Welbourn et al (15) applied to the diesel engine the 'modern' (now classical) control theory, developed by Nyquist (8) and Bode (9) from the foundation laid in the last century by Clerk Maxwell (6) and Routh (7). They analysed the engine/governor feedback loop, and by means of frequency response measurements were able to diagnose and cure speed instabilities (hunting) that were due, in part, to governor characteristics and, in part, to fuel injection system limitations at part load, low speed operation. Welbourn's approach was to identify the various contributions to phase lag in the forward path of the speed feedback loop and then reduce the phase lag where possible.

It was found that the performance of the flyweight-type governor depended on the damping ratio, which varied considerably with the number of hours run, and with slight variations in manufacturing and assembly technique. The damping ratio was found to vary between 40 and 10 and much of the damping was due to stiction.

The function of the flyweights is not only to sense speed but also to provide the force to move the fuel pump rack; if the governor gearing is changed to increase the speed of the flyweights (to increase the force available), the effects of coulomb friction and stiction are greatly increased and may cause instability. In hydraulic governors the two functions are separate and considerable force is available, by means of hydraulic actuation, to overcome any stiction effects. As a consequence the damping and the phase lags that result are considerably reduced.

Welbourn et al mention that a load in which the torque increases with engine speed (e.g. resistance to motion in vehicles or ships) can stabilise an otherwise unstable engine. E.g. where

$$T_L \propto N_E^n \quad [n > 0, \text{ and esp. } n > 1]$$

With such load characteristics the stiffness of the system increases with speed, and this contributes to the difficulty of obtaining satisfactory governing at low speed. They showed that a moderate increase of the speed 'droop' (by reducing the governor gain) does improve stability, but increasing inertia does not necessarily improve it.

From their frequency responses they estimated the time response to step load changes and found reasonable agreement with measured results.

They suggest derivative control to minimise the transient speed droop resulting from step load changes (as Clerk Maxwell had analysed earlier), and imply that this is best achieved by sensing the load. Webb and Janota (44) showed experimentally the improvement in speed droop that can be obtained by including a term proportional to load in the governor action. This is a feed-forward term and not derivative feedback action, but although Webb and Janota do not mention it, these two features have a similar effect since, where the transmission is stiff, the load change is inversely proportional to the initial angular acceleration. Load sensing avoids the problems of noise amplification associated with differentiating the speed signal, as well as avoiding any phase lag resulting from torsional flexibility in the transmission. Webb and Janota reduced the speed excursion by a factor of four (to 4% maximum) in experiments on a small petrol and a small diesel engine.

Blair (45), also by means of load feedforward, controlled the speed of a small petrol-driven generating set to $\pm$1%.

## 2.3 The Torque Delay of a Diesel Engine and the Sampled Nature of Diesel Combustion

Welbourn et al found that the phase lag in the engine speed response to rack movement increased to beyond the 90 degrees expected of a first order system. They concluded that the extra phase lag was due to the diesel torque delay. This is the time delay between the sampling of the

fuel pump rack position and the resulting torque appearing at the crankshaft. The delay appeared to be one firing period (120 degrees CA for their six cylinder, four-stroke engine) and they suggested that it comprised two parts:

1. a finite time delay equal to half the firing period.
2. a delay due to imperfect combustion and/or fuel delivery.

They do not elaborate on these two statements, and in their transfer functions they approximate the delay by a first order lag term.

The suggestion that the firing delay approximates one firing period has been used subsequently by others (46) and gives a correct order of magnitude for the delay in engines of six to eight cylinders (assuming four-stroke cycle and even firing).

Gant (47) suggests that the torque delay is 90 degrees CA plus one firing period, giving a total of 210 degrees CA for a six cylinder engine, and he admits this is conservative (48). It does give an upper bound that is useful in determing safe controller parameter values. Garvey (41) suggests that the delay is somewhere between 90 degrees CA and the value suggested by Gant.

Bowns (19) separated the delay into a switching delay (corresponding to the delay between rack position sampling and TDC), and then a zero order hold over the following firing period. This approximates the torque pulse to a torque of constant magnitude acting from TDC (top dead centre) until the next cylinder reaches TDC (see figure 2.1.(a)).

He discussed the exact timing of the sampling of the fuel rack position during the injection process. By reference to work by Eckert and Gauger (49) who had shown that resistance to the rotation of the injection pump plungers increased substantially as a result of the increase in cam loading during the injection process, he reasoned that the sampling point would vary with the actuating force available to move the fuel pump rack. With mechanical governors, lock-up would be likely to occur and sampling would therefore take place soon after the closing of the spill port (at the start of injection), whereas with hydraulic governors sufficient force would be available to prevent lock-up, in which case sampling would occur at the point of spill port reopening (i.e. at the end of injection). In this case the sampling point, and hence the torque delay, vary with engine load and speed.

Bowns pointed out that the control is not continuous, since the engine has no knowledge of the rack position except at the sampling instants. To take account of this ideally requires the application of sampled data theory and the concept of zero order hold.

Hazell and Flower (20) continued the analysis in terms of sampled data theory. They assumed that the hold started at the point of sampling and allowed for overlap of the torque into the following sample period. In this way they were better able to take account of the effect of the number of cylinders on the engine torque response. They suggested that only the 4 cylinder engine could be correctly modelled by a zero order hold, while the 6-cylinder required partial overlap and the 8-cylinder full overlap of torque into the second sample period. See figure 2.1 (c), (d) and (e). For these last two cases they proposed the names

'partial first order hold' and 'first order hold', terms which, strictly speaking, are not correct since there is no memory of the rate of change of the torque.

Their model suggests that the 6-cylinder torque diagram is not as smooth as that of the 4-cylinder or 8-cylinder engines; in practice the output torque becomes smoother as the number of (evenly firing) cylinders increases. However, because of the relatively large rotating inertia involved, these errors in modeling the variations in torque are negligible in their effect.

Bowns' transfer function for his model with switching delay and zero order hold is as follows:-

$$G(s) = \frac{n_E}{x_f} = e^{-aTs}\left[\frac{1 - e^{-Ts}}{s}\right]\left[\frac{k}{1 + t_1 s}\right]$$

where T is the sample period (firing period)

aT is the switching delay

$t_1$ is the time constant in the transfer function between torque and speed

k is the gain in the transfer function between torque and speed.

Transforming to the z-domain, and ignoring the switching delay gives:

$$G(z) = k(1-z^{-1})\left[\frac{z}{z-1}\right]\left[\frac{1 - e^{-T/t_1}}{z - e^{-T/t_1}}\right]$$

$$= k\left[\frac{1 - e^{-T/t_1}}{z - e^{-T/t_1}}\right]$$

$[z = e^{sT}]$.

Bowns recognised that this ignores the random delay (of up to one firing period) which occurs when a step change in input is not synchronised with the sampling point. He also pointed out that conventional sampled data theory applies to situations where the sampling rate is constant, whereas, in engine applications the sampling rate may vary widely, since it is directly related to the engine speed. Flower et al (32) found that a 10% variation in sampling rate did not have a significant effect on the results. Balestrino et al (50) developed a global model allowing for the variation in sampling rate, by relating the control variable to degrees CA. Local discrete models could be obtained from the global model. The model contained a complicated relationship between injection period and torque pulse period.

The Hazell and Flower (20) torque pulse has the form

$$M(s) = k\left[\frac{1 - e^{-Ts}}{s} + b\left[\frac{1 - e^{-cTs}}{s}\right] e^{-Ts}\right] x_f \qquad (2.1)$$

where k is the gain

T is the sample period

and for 4-cylinder engines, b = c = 0

for 6-cylinder engines, b = c = 0.5

for 8-cylinder engines, b = c = 1.0

These cases are illustrated in figure 2.1 (c), (d), and (e). Hazell and Flower determine the stability criterion for a speed feedback loop having a sampler and torque pulse transfer function of the above form. A solution requires that all the periodic terms (the

sidebands in the frequency response that result from the sampling action) be ignored. This assumption is reasonable, given the inertia of the engine and load; if the system time constants are large compared with the sampling time then the solution (for instability) simplifies to:-

$$M(jw)\ G(jw) = -T$$

or $$G^*(jw) = \frac{1}{T} M(jw)\ G(jw) = -1$$

where G(jw) is the response of the shaft speed to the torque, and M(jw) is equivalent to M(s) of equation 2.1 during frequency response testing.

They showed that little error resulted if the diesel torque delay were represented by a pure time delay alone at frequencies up to one sixth the sampling (firing) frequency. For a 6-cylinder engine running at 500 rev/min they showed that above 2 Hz the measured output frequency response may include a contribution of more than 10% from the first lower sideband and, for this important frequency range, they maintain that correct frequency response measurements require the use of discrete control techniques (see section 2.4).

The sidebands result from the sampling process (see figure 2.2) and cause greatest problems near half sampling frequency. In real systems sidebands other than the first can normally be neglected because of the attenuation of these frequencies by the system under investigation.

## 2.4. Frequency Response Testing of Diesel Engines

Bowns' (19) experimental results showed considerable scatter at frequencies greater than a fifth of the sampling frequency; Hazell and Flower (21) suggested this was due to the random phasing of the transfer function analyser's correlation period relative to the injection sampling instants. Flower et al (32) analysed the errors involved in using the correlation method to obtain frequency responses of sampled data systems and showed that if the start of the correlation period is not simultaneous with a sampling instant of the injection pump fuel rack position, scatter results and is worst at a test frequency equal to half the firing frequency. Synchronising the two and increasing the integration period improved repeatability.

They implemented a device to achieve synchronisation (to within practical limits of accuracy) and Windett and Flower (30) published frequency responses obtained with a 6-cylinder, medium-speed engine running at 600-720 rev/min. The results indicated that synchronisation was not required at frequencies below a quarter the firing frequency, and that as the test frequency approached half sampling frequency integration periods of at least 100 test cycles were necessary to minimise noise and sideband effects.

Their results show a gain slope in the speed response of 20 db/decade at 600 rev/min, and 17.5 to 18.5 db/decade at 720 rev/min, depending on engine load.

Bowns (19) found that frequency entrainment can occur when sampling rate is equal to the test frequency; the engine speed can become locked into the test cycle frequency in such a way that any change in speed is counteracted by a corrective change in fuelling. Similar effects may occur at test frequencies that are sub-multiples of the firing frequency.

Thiruarooran (26) obtained frequency responses of engine speed to perturbation of the rack position using white noise, band-limited at 5 Hz. This was for a 6-cylinder, turbocharged, 11 litre diesel engine. Although there is less confidence in the accuracy of his results at low frequency they do represent the response of an almost pure integrator. This can be attributed to the almost flat load characteristic (51) of the Heenan and Froude F-type dynamometer he used. What variation of load there is with speed, coupled with the variations in engine efficiency and fuelling with speed, will determine whether the large time constant is positive (stable) or negative (unstable). Because of the dynamometer load characteristic, Thiruarooran had to carry out his tests in closed loop mode (i.e. with the engine speed stabilised by a governor); the open loop responses were then extracted using estimated governor responses. His measurements were made at light load and low engine speed (3 operating points). He also carried out PRBS and square wave testing at 5 operating points, including high load and high speed.

The closed loop responses show a resonance at 3.5-4 Hz reflecting the second order (spring-mass-damper) response of the governor. However, in extracting the engine open loop response, he assumed a first order response for the governor. While incorrect, this will not seriously

affect the derived open loop response at low frequencies. From these frequency responses, and ignoring non-linear effects, he predicted with reasonable success the response to small step changes in rack position. However, at low speed high load (where air-fuel ratio is low and engine torque is most dependent on turbocharger response) the prediction was less accurate, indicating substantial non-linearity in the engine behaviour under these conditions. Under all other conditions he found engine response was dominated by the total rotating inertia, so that it was difficult to measure turbocharger dynamics from the engine speed responses.

The time constants in the engine transfer function varied little with mean torque; the gain increased with increase in engine speed and with decrease in mean torque.

Sawa and Hori (31) obtained engine speed frequency responses on three, small IDI diesels and one petrol engine. They perturbed the fuel and load settings and examined the speed responses at various mean loads and speeds, with different coolant temperatures and amplitudes of perturbation. They observed two break points in these responses, the first of which they attributed to the rotational inertia. The second, with a time constant of 0.2 - 0.6 seconds, they called the torque transfer time constant and suggested that it was related to the thermal inertia of the cylinder walls (which, in turn, affects the mechanical friction). Although the combustion chamber wall temperatures will have a more significant effect in IDI than in DI engines, it seems unlikely that this would cause a full first order lag effect in the frequency response. Had they been able to continue their tests beyond the maximum

1.6 Hz frequency they report, the results would make this clearer. Their maximum frequency was probably limited by the mechanical linkage they used to generate sine wave input perturbations; the radius arm and connecting rod mechanism would also generate significant second harmonics which they fail to mention. They also ignored time delays and sampling delays, but probably this is reasonable at their low test frequencies and high engine speed.

Chang and Sell (52) carried out frequency response measurements of output shaft torque and exhaust CO concentration in a 5.7 litre, normally-aspirated, spark ignition engine. They perturbed throttle position while keeping fuelling constant, then perturbed fuelling while keeping throttle position fixed, at 600, 1200 and 1800 rev/min engine speed. They were able to predict the time constant in the torque response and the time delay in the CO concentration response. Although they did not recognise it, their results show that the time delay in the response of shaft torque to throttle position is composed of a fixed part (roughly equal to the delay between IVC and torque pulse median timing), and a small part that increases in proportion to engine speed and is related to the filling of the cylinder from the inlet manifold; see table 2.1 and figure 2.3. They found that the transmission of CO concentration through the exhaust pipe had a second order transfer function, probably the result of wave action in the exhaust system.

They found that the shaft torque time constant was longer when the fuelling was perturbed than when the throttle position was perturbed. The latter case may be more representative of the process occurring in

diesel engines since the dynamics of wall-wetting are involved less. However, both tests will be affected by combustion saturation whenever the cyclically varying air-fuel ratio drops below stoichiometric, and therefore cannot be compared directly with the results for diesel engines.

## 2.5 Transient Behaviour of Turbocharged Diesel Engines

Marzouk and Watson (53) measured the step load responses of an automotive and a medium-speed diesel engine and compared them with results predicted using a filling-and-emptying model. The model took account of the thermal inertias of the cylinder walls and exhaust manifold.

The response of the medium speed engine was improved by reducing the valve overlap period so as to avoid substantial reverse scavenge flow. Increasing the flywheel inertia reduced the speed droop but increased total recovery time. Pulse turbocharging gave better transient response than constant pressure turbocharging, due to shorter exhaust manifold time constants and improved mean turbine efficiency during the transients. They suggested that transient air-fuel ratios could fall to stoichiometric without detriment to the speed recovery; boost control was used to avoid over-rich air-fuel ratios in order to minimise the speed recovery time. The b.m.e.p. developed by the automotive engine during transients however was smoke-limited, and boost control was used to maintain an approximate minimum air-fuel ratio which, in this application, was some way to the lean side of stoichiometric, so that

transient response was compromised. (Watson (54) shows how this deterioration in transient response becomes worse as the rating, or maximum b.m.e.p., of the engine increases). Their results indicated that cylinder pressure diagrams responded rapidly to changes in fuelling; they concluded that with pulse turbocharging the turbine torque also responds quickly to a change in fuelling, the delay in boost pressure being dominated by the response of the relatively high inertia of the turbocharger rotor relative to the turbine torque. Their model predicts that halving the turbocharger inertia reduces the rise time by a factor of three, the maximum droop by 60% and the recovery time by 50%. The model indicated that inlet manifold design had little effect on transient performance, provided any charge air cooler was mounted close to the inlet ports. Exhaust manifold design had more effect, presumably due to heat loss through the manifold walls and to attenuation of the pressure pulses in the manifold (likely to be overpredicted in a filling-and-emptying model).

Watson (28) also uses a simplified filling-and-emptying model to investigate the control of diesel engines. His model allowed for the response of the cylinder wall temperatures, since neglecting this effect can lead to errors of 2-3% in the air mass trapped during transients. This effect means that a normal boost control device allows the air-fuel ratio to become richer during transients than at steady state.

### 2.5.1. Friction and Combustion during Transients

Marzouk and Watson (53) did not allow for variations in f.m.e.p. during transients. They assume that their formula for calculating f.m.e.p. based on engine speed and peak cylinder pressure will hold true provided the peak cylinder pressure is correctly predicted. They do not mention transient effects on pumping losses, or the effect of wall temperatures on thermal efficiency, but both effects should be automatically calculated by their program.

Winterbone and Tennant (55) addressed the problem by first measuring carefully the steady state f.m.e.p. by Willans lines, by motoring tests and by subtracting measured b.m.e.p. from calculated i.m.e.p.. Correlating the f.m.e.p. with speed and peak cylinder pressure indicated a smaller constant term and smaller speed term than had been found in previous equations for f.m.e.p.. Moving to the transient case, they first investigated the variation in combustion coefficients required to adapt their Whitehouse-Way (56) single zone combustion model to accurately follow the cylinder pressure diagrams measured during transients. They calculated transient f.m.e.p. by subtracting from the calculated i.m.e.p.'s the instantaneous acceleration and brake m.e.p.'s (values averaged over one cycle). The results led them to conclude that, during the initial response to a step change in fuelling, f.m.e.p. reached values up to 50% higher than the steady state equation would predict from the corresponding instantaneous speed and cylinder pressure values.

Watson (54) again assumes that f.m.e.p. during transients can be calculated using equations based on steady state data, but admits that the difference in cylinder temperatures between the two cases will affect the friction during transients. Using a filling-and-emptying model he investigated the effect of increasing the f.m.e.p. during transients and found that a 20% increase affected the response time and that a 50% increase stalled the engine - a highly rated engine undergoing a step change from 30% to 70% load. Later, Watson (28) used the steady state f.m.e.p. equation but incorporated a simple means of allowing for the effect of oil temperature on f.m.e.p..

### 2.5.2. Transient Smoke

O'Neill (57) plotted the exhaust opacity under steady state conditions against air-fuel ratio on a log-log scale and obtained a straight line for a normally aspirated truck-size engine. This indicated that:

$$S \propto (AFR)^{-3.25}$$

He then measured instantaneous smoke and air-fuel ratios for a turbocharged engine of similar size and type, undergoing large step changes in load at different mean speeds. Adding these results to the same log-log plot he found that they fell onto the same straight line except at smoke values below 20% opacity. Differences might be accounted for by the increased proportion of fuel burning as a diffusion flame in the turbocharged engine. Using these results he then predicted the smoke produced by the same engine during a step change in load and obtained good results, although the recovery of the exhaust opacity at the end of the transient was slower than predicted from the

instantaneous air-fuel ratios.

Watson (28) also assumed smoke was proportional to a power of the air-fuel ratio in his simplified engine model for use in developing control systems. He also included terms allowing for the effect of engine speed and the proportion of fuel burning as a diffusion flame. The transient predictions are very similar to those of O'Neill, with the period of heavy smoke predicted well, but with too fast a recovery at the end of the transient.

## 2.6 Evaluation of Turbocharged Diesel Engine Transfer Functions

Windett and Flower (30) reported some frequency response measurements on a medium speed (720 rev/min) engine with single-stage turbocharging and charge cooling. The speed responses have slopes generally between 17.5 and 20 db/decade. One turbocharger speed response is shown, having a scope of 17 db/decade. The maximum load employed (8.5 bar b.m.e.p.) was well below the rating of the engine (12.4 bar b.m.e.p.). Windett and Flower did not evaluate the transfer functions, and the engine they used is much larger than the automotive type, which is the main subject of the present work.

Thiruarooran (26) used his results to plot the variation in steady state gain and transfer function pole positions for a turbocharged engine over the operating range 1000 - 1800 rev/min, 2-10 bar b.m.e.p. He suggested using a self-tuning controller to adapt to these variations in transfer function with operating point.

The only other identification of turbocharged automotive diesel engine transfer functions that has been published appears to have been made using computer simulations. In 1977, Aldren (27) used a filling-and-emptying model and frequency response correlation methods to determine the transfer functions of an 11 litre turbocharged diesel engine with variable geometry turbine. To achieve stability he included a governor model of 2.2 Hz resonant frequency, and extracted open loop responses from the closed loop results that he obtained. He suggested there were three important time delays:

i. Between compressor delivery and inlet valve.

ii. Between exhaust value and turbine inlet.

iii. Between fuel sampling and the resulting torque pulse.

Item (iii) is the torque delay discussed earlier; (i) should really be considered as a first order lag rather than a time delay, and (ii), is partly a transport delay, (due to the finite velocity of pressure waves) and partly a first order lag (due to the filling-and-emptying of the exhaust manifold volume). He suggests that the boost pressure response to turbine area is a pure integrator; but his lowest test frequency was only 0.3 Hz, and even at this frequency his measured phase lag was 50 degrees, much less than the 90 degrees of a pure integrator.

He suggests the following transfer functions for the engine running at 1400 rev/min, 4 bar b.m.e.p.:

$$\frac{n_E}{x_f} = \frac{k_1 \, e^{-0.048\,6s}}{s\,(1+0.525s)}$$

$\frac{n_E}{r_t}$ not evaluated owing to poor signal-to-noise ratio

$$\frac{P_b}{x_f} = \frac{k_2\, e^{-0.056s}}{s\,(1+0.525s)}$$

$$\frac{P_b}{r_f} = \frac{100\, e^{-0.03s}}{s}$$

$$\frac{T_{fi}}{x_f} = \frac{k_3\, e^{-0.069s}}{(1+0.23s)}$$

$$\frac{T_{fi}}{r_f} = \frac{k_4\,(1+0.68s)}{(1+0.24s)(1+0.025s)}$$

Hoff-Clausen (58) obtained the following transfer function for the speed response to rack motion; again using a filling and emptying model.

$$\frac{\omega_E}{u} = \frac{45.5\,(1+0.1s)(1+0.07s)e^{-0.04s}}{s(1+0.13s)(1+0.05s)}$$

While this expression no doubt fits his data, its form does not aid the physical interpretation of the response. Its basic form is that of an integrator implying either, that the dynamometer load did not vary with speed, or, that his minimum test frequencies were not sufficiently low. He mentions that the constants in the transfer function vary with engine operating point.

## 2.7 Multivariable Control of I.C. Engine Systems.

Ledger et al (59) suggested using multivariable principles to design a controller for a turbocharged diesel engine fitted with a pelton wheel to boost acceleration of the turbocharger during transients. However,

they found that the flow of oil was difficult to control other than by simply switching it on and off and that little advantage would have been gained by controlling it in any other way. Consequently, multivariable control theory was unnecessary.

Wallace et al (60) suggested using a 'multivariable' controller to avoid feedback instability in their engine systems with continuously variable transmissions (and three control variables). They proposed either open loop scheduling or hill-climbing methods to optimise the performance, but it is not clear whether they envisaged the use of a precompensator matrix or not.

Aldren (27) identified the turbocharged diesel with VG turbine at one (part load) operating point. His results, obtained with a filling-and-emptying simulation and using engine speed and boost pressure as the two controlled variables, indicated that the interaction terms were negligible so he applied two control loops without any attempt to compensate for the interaction.

Although his plots of the inverse Nyquist arrays indicate negligible interaction, there appears to be a large error in the gain of the response of speed to turbine area, which should be significantly larger. He found it necessary to reduce the feedback gain in the speed loop in order to maintain stability at different engine operating points. When he looked at using turbine inlet temperature, instead of boost pressure, as the second engine output, he found significant interaction and designed a precompensating matrix with constant terms.

Open loop control of gas turbine propulsion plant in ships having variable pitch propellors was found to give poor response. Kidd et al (61,62) showed that by use of suitable multivariable precompensation feedback control could be applied and gave significant improvements in response and plant safety.

Early automotive gas turbines had severe control problems as a result of non-minimum phase behaviour. A delay of about one second between throttle depression and vehicle response made driving dangerous. Winterbone et al (63,64), by analysing and modeling the plant, were able to discern the cause of the delay and designed a controller with multivariable precompensation, giving much improved response. As a result of the analysis, the manufacturers chose to change their choice of control variables but not to use precompensation, since this would have increased the complexity of setting up the controllers in production.

## 2.8 Electronic Control of Diesel Engines

Recently, electronic control has begun to be used in diesel engined cars in order to meet increasingly strict emissions regulations without serious loss of fuel economy. Much of the published work concerns open-loop scheduling (of injection timing, exhaust gas recirculation etc) and protective and diagnostic features (38-40). Feedback may be used in minor loops to obtain accurate, fast positioning of actuators but the basic strategy remains open-loop which is outside the scope of this thesis.

Garvey (41) considers the sampling rates necessary with digital controllers to minimise the reduction in phase margin, assuming a design based on classical (continuous) control theory. In his experience the phase margin in the speed loop needs to be at least 30 degrees, since a 25 degree margin causes noticeable ringing.

His analysis indicated that the sampling frequency needs to be 36 times the gain crossover frequency if the loss in phase margin is to be held to 5 degrees. If the gain crossover margin can be reduced by 30%, the sampling frequency can be reduced by a factor of 6. He advocates factors between 15 and 36, giving sampling frequencies between 60 and 144 Hz for a 4 Hz gain crossover frequency.

Pipho and Kittelson (42) applied true feedback control to the injection timing of a diesel engine to optimise torque and hence economy. The simple algorithm involves dithering the timing either side of the nominal setting and then stepping the timing in the direction which gives increased engine torque. The system had been developed previously by Schweitzer and Collins who had applied it to a spark ignition engine (29). A dither frequency of 2 Hz demonstrated the feasibility of the system, but for satisfactory response in automotive applications dither frequencies of 8 Hz or more will be required, together with a stored array of optimum timings under different operating conditions. The loss in efficiency due to timing dither (of 5 degrees CA amplitude) averages 0.5% compared with that obtained by fixing the timing at the optimum value, and $NO_x$ emissions are generally affected by 5%. The paper makes no mention of interaction between the speed and timing feedback loops.

Zanker and Wellstead (43) developed a self-tuning controller for an automotive diesel engine and ran an engine under its control. Although the response time (the retuning time) was too slow for automotive use, it demonstrated that with greater microprocessing power such a system could become feasible. In fact, since the basic transfer function of the engine should be known, self-tuning can be used just to fine-tune the model parameters to compensate for changes in ambient conditions, altitude, mechanical wear and fuel characteristics.

Considerable benefits in fuel injection pump performance and manufacture are also possible through the use of microprocessor control. Better cylinder-to-cylinder consistency of fuelling and timing can be achieved using cheaper actuators and wider manufacturing tolerances (36, 37, 39, 40). Dynamic low speed idle and the cold-start and warm-up procedure can be improved (38).

Further benefits will come in reduced development time for each new application of a pump, and greatly reduced inventory of pump types; the same hardware can be used in many applications, with the data appropriate to the application being programmed into the pump control unit before installation onto the engine (40).

Garvey (41) looks at the word length requirements and compares digital PI and PID controllers with their analogue equivalents. He concludes that, correctly set up, the digital unit will perform as smoothly as the analogue units. Removal of derivative action from the algorithm greatly reduces the dither of the fuel rack (of 1-4 Hz frequency), whose amplitude needs to be kept below .005" (0.5% of fuel rack

movement) if unacceptable FIE wear is to avoided.

Day and Frank (37) used boost pressure and engine speed signals to determine instantaneous, smoke-limited maximum fuel. Mischke and Frankle (65) monitored, in addition, the inlet manifold temperature to more accurately determine the trapped air mass. They demonstrated significantly improved torque curve shape and acceleration by limiting maximum fuel according to trapped air-fuel ratio rather than boost pressure.

Shiozaki et al (40) used a digital servo algorithm employing a switching surface for the feedback control of actuator positions and demonstrated fast, stable response.

Trenne and Nowak (66) and Walz et al (39) both report feedback control of exhaust gas recirculation, in the latter case to follow a desired air-fuel ratio schedule. Neither mentions the question of interaction with the speed feedback control.

## 2.9 Summary

The number of frequency response measurements made on turbocharged diesel engines and appearing in the literature is not great, and some of this has been obtained using filling-and-emptying simulations. No experimental results appear to have been published on the frequency response of engines to perturbations of turbine inlet area.

The non-linearity of the turbocharged diesel response has been

mentioned and in one case the variation in steady state gain and pole position, in the speed response, has been plotted against operating point. However, the effect of non-linearity on the shape of the frequency response plots has not been measured or discussed. The use of a diesel controller with gain or precompensator terms varying according to operating point has not been suggested or implemented.

From results obtained at one operating speed and load using a filling-and-emptying simulation, Aldren deduced that the turbocharged diesel with VG turbine was diagonally dominant provided boost pressure was used as one of the engine output variables. However, his analysis was made at one (part load) operating condition only, and involved a large error in the value of one of the gains. He did not determine whether the interaction between loops improved or impaired the feedback stability of the engine.

There is very little in the literature on the use of frequency responses to improve the understanding of engine transient behaviour. In particular there is no mention of the use of frequency response measurements to investigate the relationship between smoke and air-fuel ratio, or the development of torque/b.m.e.p. under dynamic conditions.

The diesel torque delay has been mentioned in the literature frequently and several estimates have been made of its length in terms of engine crankangle degrees. Whilst some of these are based on engine speed frequency response measurements, the implicit assumption is that all phase lag beyond 90 degrees is due to the diesel torque delay. No attempt has been made to relate the phase lag to any other cause.

# 3. THEORY

## 3.1 The Multivariable Control Problem

In multi-input multi-output (MIMO) systems such as that depicted in figure 3.1 each system output will, in general, have some response to each of the system inputs (or control variables). In applying feedback control to the system, it is necessary to assign one particular control variable to control each system output; the transfer functions between these assigned pairs will be called the 'direct path' transfer function and form the diagonal elements, $g_{ii}$, of the transfer function matrix. For a system of n inputs and n outputs:

$$\begin{bmatrix} y_1 \\ y_2 \\ \vdots \\ y_i \\ \vdots \\ y_n \end{bmatrix} = \begin{bmatrix} g_{11} & g_{12} & \cdots & g_{1n} \\ g_{21} & g_{22} & & \vdots \\ \vdots & & \ddots & \\ & & g_{ii} & \\ g_{n1} & \cdots & & g_{nn} \end{bmatrix} \begin{bmatrix} u_1 \\ u_2 \\ \vdots \\ u_n \end{bmatrix}$$

or $$\bar{y} = G\,\bar{u}$$

where $\bar{y}$ is the vector of system outputs

$\bar{u}$ is the vector of system inputs

G is the system transfer function matrix.

If the effect of the 'cross-coupling' or 'interaction' terms (the off-diagonal terms $g_{ij}$, where $i \neq j$) is ignored it is quite possible to choose inappropriate input-output pairs for the direct paths and to end up with an unstable sytem, or one with inferior transient response

(67).Where the chosen input-output pairs are appropriate, the effects of the interaction terms may still cause the system to become unstable even though each of the individual feedback loops appears to be stable. Finally, it is possible that the system is stable, but that the steady-state errors in output values, resulting from interaction, are unacceptable.

## 3.2 Feedback Versus Feedforward Control

Many stability problems may be avoided by dispensing with feedback control; the control variable values can be scheduled according to a predetermined strategy specifying the values for each system operating point. This is termed feedforward control, and there is no manipulation of the system inputs to optimise a given output (or combination of outputs) or to achieve a particular value of that output. Whilst care must be taken not to introduce feedback loops inadvertently, such control generally causes no instability (which would appear as oscillations or 'hunting' of the system variables). However, if the open loop system is unstable then feedback must be applied in order to obtain stable control.

Feedforward control includes, for example, the scheduling of injection or spark timing according to engine speed, load and coolant te mperature, or the adjusting of engine fuelling to allow for sensed changes in load. In practice, feedforward and feedback control may be combined in the same controller; e.g. scheduling of injection timing may be combined with feedback control of engine speed. In these cases the contribution of the scheduling scheme to the feedback loop

response, resulting from the interaction terms, needs to be taken into account in designing the feedback loop response.

Since feedforward control avoids many stability problems, what are the advantages of feedback control? Apart from the ability to stabilise systems that are open loop unstable, feedback can give the following:-

Greater accuracy in desired output.

Better transient response.

Reduced sensitivity to disturbances (68), which may include:

i) Changes in plant behaviour due to change in ambient conditions (including altitude)

ii) Changes in plant behaviour due to wear and friction.

iii) Reduced sensitivity to noise (e.g. sensor noise or electrical interference).

As a result of (iii) and because feedback control allows greater accuracy to be achieved with a given actuator it is possible to use cheaper sensors and/or actuators.

To illustrate the reduction in sensitivity, consider the SISO system of figure 3.2 in which r is the reference input value, f the sensor response, and k the feedback gain.

The system is subject to small variations, $\Delta g$, in plant transfer function due, for example, to wear and tear or ambient conditions, and to output noise, n:

$$y = (g + \Delta g)k(r - fy) + n$$

$$\therefore \quad y = \frac{k(g+\Delta g)r}{1 + fkg\left[1 + \frac{\Delta g}{g}\right]} + \frac{n}{1 + fkg\left[1 + \frac{\Delta g}{g}\right]}$$

If $|fkg| \gg 1$, which is true at low frequencies, then

$$y \doteq \frac{r}{f} + \frac{n}{fkg} \doteq \frac{r}{f}$$

The low frequency output of the system is independent of variations in the plant transfer function and is determined solely by f, the response of the feedback path. The effect of output noise is negligible.

If $|fkg| \ll 1$, which is true at high frequencies:

$$y = kg \left[1 + \frac{\Delta g}{g}\right] r + n$$

then plant output varies proportionately with plant gain and directly with the noise.

If $-1 < fkg < 0$, i.e. at an intermediate frequency such as the phase crossover frequency:-

$$y = \frac{kg}{1+fkg} \left[1 + \frac{1}{1+fkg} \frac{\Delta g}{g}\right] r + \frac{n}{1+fkg}$$

Under these conditions, the effects of noise and changes in plant behaviour are now amplified by an amount that depends on the gain margin (*). An 8 db margin leads to amplification of fractional errors by 66%. Amplification is generally greatest at some frequency between the gain and phase crossover frequencies (*). {Expressions marked (*) are control terms and fuller explanations will be found in standard textbooks on control theory, such as Raven (69)}

## 3.3 Stability Margins In Multivariable Control Systems

Consider the MIMO system G, figure 3.3, with transfer functions $g_{ij}$ and feedback gains $k_i$ (diagonal matrix K) which is to be controlled by independent feedback loops.

### 3.3.1 Inverse Nyquist Array Method

Rosenbrock's method (70) uses the inverse Nyquist array and, for each point in the diagonal elements draws a circle of radius equal to the sum of the off-diagonal row or column gains at that frequency; these circles form the Gershgorin bands and indicate the greatest possible effects of interaction on the stability of the system (figure 3.4). When a precompensator matrix (which may be necessary to make the array diagonally dominant) has been chosen, the reduced effect of interaction in each loop, when known feedback gains are applied to the other loops, is indicated by the Ostrowski bands. Rosenbrock showed that, provided the inverse Nyquist array is diagonally dominant, it can be used to determine the stability of the system when the feedback loops are closed (and with inverse Nyquist plots the effect of feedback gain on stability is particularly easy to determine). Diagonal dominance occurs when the bands exclude the origin, and is defined as:-

for all i, and at all frequencies,

$$\text{either} \quad |g_{ii}| > \sum_{\substack{j=1 \\ i \neq j}}^{n} |g_{ij}| \qquad \text{(row dominance)}$$

$$\text{or} \quad |g_{ii}| > \sum_{\substack{j=1 \\ i \neq j}}^{n} |g_{ji}| \qquad \text{(column dominance)}$$

Stability margins are determined by considering the edge of the Ostrowski bands closest to the critical point. This gives conservative values, since it assumes that the interaction has the worst possible effect.

### 3.3.2 Characteristic Equation Method

The linear MIMO system of figure 3.3 has the following closed loop response:-

$$\bar{y} = (I + GKF)^{-1}GK\bar{r}$$

Obtaining the inverse of (I + GKF) includes dividing each of its elements by the determinant. The system is unstable when, for any value of the complex variable s having positive real part,

$$\det |I + GKF| = 0 \qquad (3.1)$$

Equation 3.1 is called the characteristic equation of the closed loop system, and while its solution does not distinguish which loop causes instability, it does detect accurately the feedback gains under which instability occurs. The lines of instability can be plotted in the gain space (where the feedback gain values form the axes) and suitable margins can be obtained by ensuring, for example, that each feedback gain value is at least 10 db (a factor of 3) to the safe side of the instability surface. This is straightforward for two-input, two-output systems where the gain space becomes a gain plane and is simple to represent graphically.

For a two-input, two-output system the matrices become:

$$F = \begin{bmatrix} f_1 & 0 \\ 0 & f_2 \end{bmatrix} \quad K = \begin{bmatrix} k_1 & 0 \\ 0 & k_2 \end{bmatrix} \quad G = \begin{bmatrix} g_{11} & g_{12} \\ g_{21} & g_{22} \end{bmatrix}$$

and the characteristic equation becomes:-

$$(1 + f_1k_1g_{11})(1 + f_2k_2g_{22}) - f_1f_2k_1k_2g_{12}g_{21} = 0$$

or

$$f_1k_1g_{11} + f_2k_2g_{22} + f_1f_2k_1k_2(g_{11}g_{22} - g_{12}g_{21}) = -1 \qquad (3.2)$$

$$\left[1 + \frac{1}{f_1k_1g_{11}}\right]\left[1 + \frac{1}{f_2k_2g_{22}}\right] = \frac{g_{12}g_{21}}{g_{11}g_{22}} \qquad (3.3)$$

Without interaction ($g_{12} = g_{21} = 0$) the equation is solved when either of the two single feedback loops is unstable, but the gain and phase of the LHS of equation 3.2 are a combination of the values for the two loops and so cannot be used as a direct measure of the multivariable system stability margins. As described, though, stability margins (in gain) can be obtained once the lines of actual instability have been plotted in the gain plane.

Stability margins may be obtained in a similar manner from the characteristic loci (71); however, obtaining these loci requires evaluation of the eigenvalues of the matrix (I+ GKF), and it is simpler to use the characteristic equation method outlined above.

In single-input single-output (SISO) systems it is often preferred to define a phase margin (e.g. 60 degrees) and ignore the value of the gain margin, although Oldenburger (72) suggested ensuring a phase margin of 30 degrees as well as a gain margin of 8 db. Where phase or gain margin alone is to be used to define stability, some assumption

about the system response has to be made i.e. concerning the shape of the response between the gain and the phase crossover frequencies. This is reasonable where the system has a standard first or second order response, without excessive transport delays. In the multivariable case it will be assumed that if the same response (first order or second order) is true of each of the closed loop transfer functions then the stability margin of the system may be specified by quoting the value of just one margin, in this case a gain margin, which should be at least 10 db.

### 3.3.3 The Effect Of Interaction On Stability And Steady State Errors

For the two input, two output system without precompensator matrix the closed loop system gains are:

$$\frac{n_E}{\Delta N_{E_{ref}}} = \frac{1}{C}\left[k_1 g_{11}\left[1+f_2 k_2 g_{22}\right] - f_2 k_1 k_2 g_{12} g_{21}\right]$$

$$\frac{n_E}{\Delta P_{b_{ref}}} = \frac{1}{C} k_2 g_{12}$$

$$\frac{P_b}{\Delta N_{E_{ref}}} = \frac{1}{C} k_1 g_{21}$$

$$\frac{P_b}{\Delta P_{b_{ref}}} = \frac{1}{C}\left[k_2 g_{22}\left[1+f_1 k_1 g_{11}\right] - f_1 k_1 k_2 g_{12} g_{21}\right]$$

where $C = \left[1+f_1 k_1 g_{11}\right]\left[1+f_2 k_2 g_{22}\right] - f_1 f_2 k_1 k_2 g_{12} g_{21}$

The degree of interaction in an output may be defined as the change in its value resulting from a typical change in the reference value of the other output divided by its change in response to a typical change in its own reference value.

Where $^{\Delta N_E}_{ref}$ and $^{\Delta p_b}_{ref}$ are typical changes in the reference values. To consider the effect of interaction on stability consider the inverse version of the characteristic equation.

$$\left[1 + \frac{1}{f_1 k_1 g_{11}}\right]\left[1 + \frac{1}{f_2 k_2 g_{22}}\right] - \frac{g_{12}g_{21}}{g_{11}g_{22}} = 0$$

Where, in fact, any value of the expression between zero and -1 causes instability.

The term $g_{12}g_{21}/g_{11}g_{22}$ is a measure of the effect of the interaction on the stability of the system under feedback control, and since the inequality is double-sided, it is safest to minimise the magnitude of this term, without regard to its sign:

$$\left|\frac{g_{12}g_{21}}{g_{11}g_{22}}\right| << 1$$

This is effectively what Rosenbrock's Inverse Nyquist Array method does; it is unable to distinguish cases where the interaction actually improves the stability.

### 3.4. Response of Engine-Dynamometer System

A diesel engine coupled to a dynamometer has a response which is basically that of a first order system (see figure 3.5), with the engine torque exciting the system inertia. In figure 3.6 $\tau_E$, $\tau_L$ and $n_E$ are small perturbations about the steady state values $T_E$, $T_L$ & $N_E$. Initially the load characteristic is assumed to be linear, with the load torque proportional to engine speed:-

i.e.

$$T_L = k N_E + c$$

and

$$T_L + \tau_L = k (N_E + n_E) + c$$

therefore

$$\tau_L = k n_E$$

$$= \frac{T_L}{N_E} n_E \quad (\text{if } c = 0).$$

Applying Newton's Second Law to the angular acceleration of the inertia:

$$\dot{n}_E = \frac{30}{\pi}\left[\frac{\tau_E - \tau_L}{I_{tot}}\right]$$

$$= \frac{30}{\pi}\left[\frac{\tau_E - kn_E}{I_{tot}}\right]$$

In terms of the D operator, and assuming $n_E$ now in rad/sec,

$$(I_{tot}D + k)\, n_E = \tau_E$$

Then the transfer function is given by:-

$$\frac{n_E}{\tau_E} = \frac{1}{I_{tot}D + k} = \frac{\frac{1}{k}}{1 + \frac{I_{tot}}{k} D}$$

or in terms of the Laplace operator, s,

$$\frac{n_E}{\tau_E} = \frac{\frac{1}{k}}{1 + \frac{I_{tot}}{k} s}$$

In the frequency response work carried out all the input signals are sinusoidal and the s and D operators may be replaced by $j\omega$:-

$$\frac{n_E}{\tau_E} = \frac{\frac{1}{k}}{1 + \frac{I_{tot}}{k} j\omega}$$

At steady state, $\omega$ is zero and the gain becomes, as expected:-

$$\left.\frac{n_E}{\tau_E}\right|_{ss} = \frac{1}{k}$$

As frequency increases, so the gain is attenuated:-

$$\left|\frac{n_E}{\tau_E}\right| = \frac{\frac{1}{k}}{\sqrt{1 + \frac{I^2\omega^2}{k^2}}}$$

At the break frequency, real and imaginary parts are equal so that

$$\omega_b = \frac{k}{I_{tot}} \text{ rad/sec.}$$

The time constant is equal to $1/\omega_b$ seconds and the transfer function may be expressed in the following way:-

$$\frac{n_E}{\tau_E} = \frac{k}{1 + tj\omega}$$

## 3.5 Factors Affecting Engine Speed Response

### 3.5.1 Effect of Dynamometer Characteristic

The above response is that of a simple first order system; if the brake load remains constant, then k is zero and the transfer function becomes:-

$$\frac{n_E}{\tau_E} = \frac{1}{I_{tot}\, D}$$

In this case the inertia acts as a pure integrator of the engine torque. If brake load is a non-linear function of speed, where for

example:

$$T_L = k\, N_E^{\,n}$$

then
$$\tau_L = k\, n n_E\, N_E^{\,n-1}$$

$$= n n_E \frac{T_L}{N_E}$$

therefore
$$\frac{\tau_L}{T_L} = n \cdot \frac{n_E}{N_E}$$

and
$$\frac{n_E}{T_E} = \frac{1}{I_{tot} s + n \frac{T_L}{N_E}}$$

The time constant of the system now becomes

$$t = \frac{I_{tot} N_E}{n T_L}$$

instead of $t = \frac{I_{tot}}{k} = \frac{I_{tot} N_E}{T_L}$ for the linear case

The time constant is inversely proportional to the index of speed in the dynamometer load-speed characteristic. Figure 3.7 shows the modified transfer function diagram.

### 3.5.2 Effect of Variation of Fuelling Rate With Engine Speed

In automotive diesel engines the fuel injected per stroke generally varies with engine speed and in fact the fuelling characteristic is tailored to provide the desired variation of torque with engine speed. Figure 3.8 shows the transfer function block diagram adjusted to incorporate this.

Assuming negative feedback for the fuelling characteristic, i.e. where an increase of fuelling with decreasing speed (for constant rack position) gives a positive value for $k_3$, then

$$I_{tot}\dot{n}_E = k_2(k_1x_f - k_3n_E) - nkn_E$$

$$\therefore \quad (I_{tot}s + k_2k_3 + nk)n_E = k_1k_2x_f$$

$$\therefore \quad \frac{n_E}{x_f} = \frac{k_1k_2}{I_{tot}s + k_2k_3 + nk}$$

$$= \frac{\frac{k_1k_2}{k_2k_3 + nk}}{1 + \frac{I_{tot}s}{k_2k_3 + nk}}$$

(where $k = \frac{T_L}{N_E}$ as before)

The time constant is now $I_{tot}/(k_2k_3 + nk)$ seconds and the steady state gain is $k_1k_2/(k_2k_3 + nk)$ ; both are reduced for positive $k_3$, which is generally true at engine speeds above peak torque speed.

### 3.5.3 Effect of The Dynamic Response of the Dynamometer

If the dynamic response of the dynamometer with its associated valves and electronics is represented by a time delay and first order lag, the transfer function of the dynamometer load becomes

$$\frac{T_L}{n_E} = \frac{nke^{-t_1s}}{1 + t_2s}$$

and the overall transfer function becomes

$$\frac{n_E}{x_f} = \frac{k_1k_2}{k_2k_3 + I_{tot}s + \frac{nke^{-t_1s}}{1 + t_2s}}$$

The response is no longer that of a first order lag, and the effects of the values of $t_1$ and $t_2$ on the measured speed response are shown in figures 3.9 and 3.10.

The values of $t_1$ and $t_2$ vary with the mean hydrostatic supply pressure and this is a function of engine speed and load. Photographic records of the response of the supply pressure to changes in dynamometer control voltage had been obtained (using an oscilloscope) with a smaller (300 Nm maximum) swash-plate pump fitted with identical control gear. Values of $t_1$ and $t_2$ estimated from these results are plotted against hydrostatic supply pressure in figures 3.11 and 3.12. At medium and high load the supply pressure is always greater than 100 bar and $t_1$ and $t_2$ may be conservatively estimated at 20 and 10 msec respectively.

Since the control gear is identical to that used on the dynamometer used in the present work, it is assumed that the values of $t_1$ and $t_2$ given above apply to the present case, at the same mean hydrostatic supply pressures. Typical values of $t_1$ and $t_2$ are therefore 10msec and 20 msec respectively. From figures 3.9 and 3.10 it is clear that such values will have a small effect on the observed response of the engine speed to rack perturbation. However, it is possible to avoid the need to evaluate the dynamometer response by the method given below.

### 3.5.4 Dynamic Torque or Dynamic M.E.P. Response

Changes in shaft torque, $\tau_S$ , and engine speed, $n_E$ , can be monitored and, from these, the instantaneous or dynamic engine torque, $\tau_E$ , can

be reconstructed.

$$\tau_E = \tau_s + \frac{\pi I_E}{30} \frac{dn_E}{dt} \qquad (3.4)$$

assuming $n_E$ in rev/min

The dynamic engine torque is not a quantity that can be monitored directly and is probably best thought of as a dynamic mean effective pressure (d.m.e.p.), m.e.p. being closely related to engine torque. The d.m.e.p. is the instantaneous i.m.e.p. corrected for engine friction losses:-

d.m.e.p. = instantaneous (i.m.e.p. - f.m.e.p.)

While such a reconstruction of dynamic engine torque has been used before (73), it does not appear to have been used to obtain dynamic torque from engine frequency response testing. With sinusoidal perturbations, assuming that harmonics generated in the outputs are of negligible amplitude, equation 3.4 becomes:-

$$\bar{\tau}_E = \bar{\tau}_s + j\omega \frac{\pi I_E}{30} \bar{n}_E$$

Where $\omega$ is the test frequency (rad/sec) and $\bar{\tau}_E$, $\bar{\tau}_s$ and $\bar{n}_E$ are vectors having the amplitude and phase of the appropriate frequency response.

## 3.6 Frequency Response Measurements of Sampled Data Systems

Flower, Windett and Forge (32) showed that when digital correlation methods are applied to the frequency response measurement of sampled

data systems, serious errors can result from lack of control of the phasing between the sampling times and the driving sine wave. They showed that the measured sine and cosine correlations were subject to errors:-

the measured sine correlation is

$$r_{xy}(0) = \frac{1}{T} R_{xy}(0) + E$$

and the measured cosine correlation is

$$r'_{xy}(0) = \frac{1}{T} R'_{xy}(0) + E'$$

where T is the correlation period and E and E' are the errors.

E is reduced by using a large value of $[2\omega_s/\omega]\, m\omega_s m/\omega$; E' is reduced with a large value of $[2\omega_s/\omega]\, m\omega_s m/(\omega[1-\omega_s/\omega])$.

The integration or correlation period T can be expressed in terms of the number of test frequency cycles:-

$$T = \frac{2\pi m}{\omega}$$

$$m = \frac{\omega T}{2\pi} \qquad (3.5)$$

Sampling occurs once per injection, so that for a four-stroke engine with N cylinders running at $N_E$ rev/min,

$$\omega_s = \frac{2\pi N_E N}{2\times 60} \qquad (3.6)$$

then, using (3.5) and (3.6)

$$\frac{m\omega_s}{\omega} = \frac{T}{2\pi} \cdot \frac{2\pi N_E N}{120}$$

$$= \frac{TN_E N}{120}$$

If as in the present work, the minimum integration period is 20 seconds and the engine has six-cylinders, then at 1200 rev/min:

$$\frac{m\omega_s}{\omega} = 1200$$

If, in addition, the maximum test frequency is 10 Hz, then $\omega_s/\omega \geq 5$ so that

$$\left|\left[2 - \frac{\omega_s}{\omega}\right] \frac{m\omega_s m}{\omega}\right| \geq 11,300$$

and

$$\left|\left[2 - \frac{\omega_s}{\omega}\right] \frac{m\omega_s m}{\omega} \Big/ \left[1 - \frac{\omega_s}{\omega}\right]\right| \geq 2,800$$

Both the in-phase and out-of-phase components of the response have errors of less than 0.1%. The corresponding errors in the gain are generally $\approx \omega/\omega_s m$; again of the order of 0.1% in this case.

Any sampling introduced by the transfer function analyser (TFA) itself (i.e. digital TFA's) can also be assumed to contribute negligible errors since the sampling frequency used will be several orders of magnitude higher than the maximum test frequency used in this work (~10 Hz), and because of the relatively long integration period of 20 seconds.

# 4. IDENTIFICATION: EXPERIMENTAL DETAILS

## 4.1 Hardware

Figure 4.1 shows diagrammatically the engine and dynamometer with the sitings of the transducers and actuators used in the work.

### 4.1.1 The Engine

The engine is a turbocharged automotive diesel with a rating of 210 kW at 2100 rev/min. Details of the engine are given in table 4.1 and a maximum torque curve is shown in figure 4.2. Engine cooling is achieved by recirculating water from a static pond of large surface area through a heat exchanger mounted close to the engine. Water from the pond is drawn first through a coarse grid at the pipe inlet, and then through a fine mesh trap.

### 4.1.2 The Dynamometer

The dynamometer is a Lucas swash-plate hydrostatic pump. Hydrostatic system pressure determines dynamometer load and is controlled by means of a servo valve. The main valve position is controlled hydraulically by means of a spool valve whose motion is accurately determined via feedback position control. System pressure is controlled from the console by a DC signal in the 0 to 10V range, and the dynamometer steady state load versus speed characteristic can be tailored to follow a windage curve of the form:

$$T_L = kN_E^n$$

The value of the index n was found to be close to 1.60 except at light load (see fig. 4.3). The dynamometer may also be used in a mode which maintains constant brake torque, but this mode was not used for tests since the 'windage' mode more closely represents the behaviour of a real automotive load. The dynamic response of the dynamometer and its associated controls is not ideal and its effect on the measured speed response is not negligible. Campbell (74) had made experimental measurements of transients in a dynamometer with almost identical controls and associated piping. From his results (similar to those shown in figure 4.4) it has been possible to estimate the relevant transfer function (see section 3.5.3).

### 4.1.3 Actuators

The engine is fitted with actuators controlling rack position and turbine inlet area. Both are of the hydraulic ram type with cylinder diameters of 7/16 inch (11.11mm). Oil at a pressure of 60 bar from a single Bosch supply pack is admitted to the actuators under the control of servo valves. Feedback is used to obtain accurate positioning of the actuators, with position transducers monitoring rack position (the actuator acting directly onto the end of the fuel injection pump rack) and turbine inlet area actuator position. Due to lack of space a mechanical linkage connects the second actuator to the rods determining actual turbine inlet area (see figure 4.5), and since the linkage is not rigid its response needs to be allowed for. The response of both actuators is approximately that of a first order lag (of 5 msec time constant) and a time delay of 10 msec.

### 4.1.4 Instrumentation

Details of the engine output transducers are given in table 4.2, which includes the steady state calibrations obtained for each. Outputs are adjusted to be in the range 0 to 10 V, or 0 to -10 V.

#### 4.1.4.1 Dynamic Responses

Frequency response measurements were used to obtain the dynamic characteristics of some of the transducers with their associated amplifiers and signal conditioning circuits.

For example the measured response of the electronics associated with the turbine inlet thermocouple signal is shown as Bode plots in figure 4.6 indicating a first order system with break frequency at 2.83 Hz. In addition, the thermocouple itself has a first order lag due to its thermal inertia; the associated time constant varies with the Reynolds number of the exhaust gas flow since this affects the heat transfer to and from the thermocouple. The relation is assumed to be of the form:

$$t_{th} = kR_e^{\,n}$$

Winterbone and Nuske (34) used a value for n of -0.668 when measuring turbine inlet temperature in an automotive gas turbine, and the same value has been used in the present work. The value of k was estimated from the manufacturers' quoted time constant under given gas flow conditions.

Response of the infra-red absorption meter used to measure exhaust opacity was determined from a measurement of the rise time of the infra-red sensor output. This had been measured as 95 msec, indicating a time constant of about 32 msec and a break frequency of 5.0 Hz. A considerable transport delay occurs due to the length and volume of the exhaust system upstream of the opacity meter (see figure 4.7).

Measurement of engine speed involves the magnetic detection of the passing of teeth on a disc attached to the engine flywheel, one revolution consisting of 120 teeth. The positive voltage reversals in the transducer output are used to trigger the production of square pulses of standard amplitude and duration. Thus each tooth generates one standard pulse and standard frequency-to-voltage conversion techniques are used to generate a DC signal proportional to speed. Smoothing of this signal introduces a first order lag with 9.4 Hz break frequency.

The voltage representing inlet manifold pressure is obtained by DC amplification of a strain gauge signal. No attenuation or phase shift was introduced by this amplifier at or below 10 Hz. Remote siting of the transducer, 22cm from the inlet manifold at the end of a pipe of 5mm i/d, will cause resonance with a peak at about 330 Hz but this will have negligible effect below 10 Hz.

Drive shaft torque is measured by a process which involves frequency modulation and DC amplification. Neither the filters used to remove the carrier frequency (of 8 kHz) nor the DC amplification should introduce any detectable error at or below 10 Hz. A slight resonance

in the linkage used to arrest the rotation of the floating part of the torquemeter introduced small errors at around 3 Hz.

As mentioned above, lack of torsional rigidity in the turbine area control linkage resulted in noticeable deflection dependent on the resisting force seen by the turbine area restrictor, whether due to unbalanced gas forces or to sooting up of the surrounding clearances. In consequence the actuator position transducer could not be relied on to accurately reflect the actual turbine inlet area, particularly under dynamic conditions. Lack of space surrounding the turbine area control rods ruled out the use of standard position transducers capable of linear monitoring of the 6 mm of control rod movement. A small inductive device was installed and this was later replaced with a Hall-effect device with temperature compensation and water cooling. Linear calibration was obtainable over about 3 mm movement, but 4.5 mm could be covered with less than 5% error and this larger amplitude of turbine area perturbations was used in the tests.

### 4.1.5 Frequency Response Analysers (F.R.A.)

The theory of the correlation type frequency response analyser may be found in reference (32). Some early frequency responses in the present work were obtained using a 'Feedback' Transfer Function Analyser with associated Signal Generator. Errors in frequency calibration were found up to a maximum of +18% at a nominal $1.0 \times 10^{n}$ Hz. A facility allowing automatic, marching, ten-cycle averaging enabled greater accuracy and consistency of measurement. The running average was displayed on the instrument's analogue meter allowing an appreciation

of the consistency of the readings to be obtained. For accuracy it was also necessary to use the 'AC' filter at frequencies above 0.5 Hz; this is a simple first order R-C filter. Results had to be corrected for the filter response and this was complicated by the variation of the response, not only with the use of ten-cycle averaging, but also with the amplitude and harmonic content of the signal.

Despite its inaccuracy and inconvenience the 'Feedback' equipment allowed the consistency of the engine behaviour to be observed and this was useful in interpreting the results obtained later with a Solartron 1250 Frequency Response Analyser.

Apart from giving much greater accuracy, particularly with small signal amplitudes, the Solartron FRA was able to monitor two signals simultaneously and calculate the response of one relative to the other. In this way actuator responses could be removed automatically (figure 4.8) leaving the response of the engine itself (as coupled to the dynamometer).

The normal frequency range employed was 0.1 to 10 Hz with either 4 or 5 intermediate frequencies per decade. Four seconds or one complete cycle period, whichever was the greater, was allowed for the system to stabilise after a change in test frequency. Automatic adjustment of the signal integration period used in determining gain and phase was possible in two modes; a non-automatic mode was also available.

Automatic integration:

Short period - continues integration until 90% confident of giving a result with ± 10% accuracy.

Long period - continues integration until 90% confident of giving a result with ± 1% accuracy.

Preset integration:

The integration period can be chosen to be either a fixed time period or a fixed number of test signal cycles.

Normally the more accurate automatic integration procedure was used and the readings were repeated to check for consistency. Where this resulted in extremely long test times, or where the engine behaviour was very inconsistent, it was found better to use the shorter automatic integration mode and to repeat the readings several times, alternating the direction of frequency scan.

All frequency response testing was carried out with sinusoidal input perturbations.

## 4.2 Experimental Method

Engine coolant temperature was generally maintained between 80 and 90 degrees C with extreme values used of 70 and 95 degrees C.

Inadequacies in the flow of water in the heat exchanger circuit to and from the pond occurred as a result, first, of the use of a heat exchanger of insufficient capacity, and later as a result of frequent blocking of the mesh traps with debris from the pond. Consequently some tests had to be interrupted to allow the filters to be cleared or to allow the cooling water temperature to fall. To this end the water pressure downstream of the filters was monitored as well as engine coolant temperature.

Ambient air temperature in the cell during testing was generally between 20 and 25 degrees C.

Excessive cylinder pressures or turbine inlet temperatures were avoided during testing. Minimum turbine inlet area had to be limited at high engine power to avoid overspeeding the turbocharger, and during tests where the rack position was being perturbed, the turbine inlet area was fixed at a value that was approximately optimum for the mean operating condition.

Injection timing was held at the standard timing of 22 degrees CA BTDC (static) except at low speed, high torque when the timing had to be retarded 6 degrees CA to avoid excessive cylinder pressures.

Dynamometer oil boost pressure (pump inlet pressure) was kept above 15 bar to avoid pump damage by cavitation and to improve linearity (75).

## 4.3 Frequency Response Measurements Carried Out

Responses of the engine output variables to perturbations of the fuel injection pump rack position were obtained at engine conditions covering the whole operating range, apart from low idle. Table 4.3 indicates the operating conditions at which the tests were carried out and the corresponding output responses obtained at each. Engine speed and inlet manifold pressure were obtained at each operating condition; in addition, at some operating conditions, the responses of the drive shaft torque, exhaust manifold temperature or exhaust opacity were also obtained. Table 4.4 is the corresponding table of operating points of responses obtained when perturbing the turbine inlet area. In this case, little work was done at light load, since the turbocharger contributes little to engine efficiency under these conditions. While the amplitude of rack perturbations was varied between $\pm$ 38% and $\pm$ 2.5%, turbine inlet area perturbations had to be of as large amplitude as transducer linearity would allow in order to maintain adequate engine output signal amplitudes.

Actuator responses were measured under different engine operating conditions and repeated periodically. Frequency response measurements at 1200 rev/min, high load were also repeated on several occasions to check for repeatability of results over a period of time and under different ambient conditions.

All frequency responses are presented in the form of Bodé diagrams, the gain being relative to the steady state gain value.

# 5. FREQUENCY RESPONSE RESULTS AND DISCUSSION OF DYNAMIC RESPONSE

## 5.1 Engine Speed

### 5.1.1 Speed Response to Rack Perturbation

Figure 5.1 shows the effect of engine load, at a given mean speed, on the measured engine speed frequency responses. The slopes of the gain plots above 2 Hz are of the order of -20 db/decade. As expected, a first order response dominates and the time constant is reduced as the mean torque is increased; this is seen most clearly in the phase response since small errors in measured steady state gain significantly affects the frequency at which the gain crosses the -3db line. Above 2 Hz the phase lag is greater than 90 degrees and increasing, reflecting the presence of the torque time delay. Since the engine speed is similar in each case, the torque delay also is similar and the resulting phase plots are almost identical above 2 Hz.

When the mean speed varies (figure 5.2) the torque delay also varies and the resulting high frequency phase lags show more variation.

Table 5.1 shows the steady state gains measured under different engine operating conditions and figure 5.3 suggests contours of steady state gain on the engine operating trap (for data obtained using similar fuelling amplitudes and static injection timings).

The expected time constant (see section 3.5.2) is given by

$$t = \frac{\pi N_E I_{tot}}{30 (n-k) T_E} \text{ (sec)}$$

where $N_E$ and $T_E$ are mean values of engine speed and torque

n is the speed index in the dynamometer characteristic

k is the normalised variation of engine torque with speed

$I_{tot}$ is the combined rotational inertia of engine, flywheel, drive shaft and dynamometer.

The corresponding break frequency is given by

$$f_b = \frac{15\ (n-k)T_E}{\pi^2\ N_E\ I_{tot}}\ (Hz) \qquad (5.1)$$

Figure 5.4 shows some of the measured break frequencies plotted against values determined using expression 5.1, assuming n equal to 1.6 and k equal to 0. (The measured break frequency is taken to be the frequency corresponding to 45 degrees phase lag after the phase response has been corrected for phase lag due to the torque delay). At low load the index n may fall below 1.6, and k is negligible only at medium speeds (1100 - 1400 rev/min at medium to high fuelling). At higher speed (and at lower speeds where the load is light) k is generally negative (e.g. approx. -0.25 at 1600 rev/min, 600 Nm) so that n-k is greater than 1.6. This accounts for some of the deviation away from the line corresponding to n-k = 1.6; another factor affecting the measured values is the dynamic response of the dynamometer control system, which tends to increase the apparent engine break frequency.

### 5.1.2 Speed Response To Turbine Inlet Area.

Figures 5.5 and 5.6 show engine speed response to turbine inlet area perturbation at three engine speeds (constant mean fuelling) and the effect of fuelling at constant mean speed. Above 1 Hz the slope of the gain plot is close to or slightly greater than -20 db/decade, but the phase lag is greater than 180 degrees. At these frequencies variations in turbocharger speed are negligible and the engine speed response is determined by the effect of the turbine inlet area on the engine back pressure. Since a reduction in area is taken as positive, the resulting speed change is out of phase with the turbine area. At lower frequencies the turbocharger speed responds to the variations in turbine torque and the resulting changes in boost pressure serve to moderate the effect of the back pressure on the engine's pumping losses. In addition, the change in air-fuel ratio affects the thermal efficiency at the high fuellings employed (see figure 5.7). When the effect (at low frequency) of the boost pressure and air-fuel ratio is greater than the effect of the back pressure on the engine torque, then the steady state gain is positive and the phase lag at low frequency is small; as the frequency increases the turbocharger responds less and the effect of the back pressure becomes greater than that of the boost pressure and air-fuel ratio and the phase lag increases rapidly to more than 180 degrees. At engine operating conditions where the effect of the boost and air fuel ratio is always less than the effect of the back pressure (i.e. where air-fuel ratio is greater than about 25:1), the steady state gain is negative and the phase lag at low frequency is close to 180 degrees. This is generally the case at part load or at high engine speed. As the frequency increases so the amplitude of

engine torque increases until it reaches a plateau; the engine speed amplitude increases at first, then falls as the rotational inertia affects the response more significantly. This is the cause of the extra pole and zero seen in the speed response to turbine inlet area perturbations.

The response may be expressed as two terms in parallel, one representing the effects of boost pressure, and the other the effects of back pressure on engine torque.

$$n_E = \frac{k_1 p_b e^{-t_1 s} + \frac{k_2 r_t}{1 + t_3 s}}{1 + t_2 s}$$

The two terms have opposite signs as is seen in the values of $k_1$ and $k_2$:-

$$k_1 = \left.\frac{\partial n_E}{\partial \tau_E}\right|_{ss} \left[\frac{\partial \tau_E}{\partial (AFR)} \frac{\partial (AFR)}{\partial p_b} + \frac{\partial \tau_E}{\partial L_p} \frac{\partial L_p}{\partial p_b}\right] > 0$$

$$k_2 = \left.\frac{\partial n_E}{\partial \tau_E}\right|_{ss} \left[\frac{\partial \tau_E}{\partial L_p} \frac{\partial L_p}{\partial p_{ex}} \frac{\partial p_{ex}}{\partial r_t}\right] < 0$$

and $t_1 \doteqdot 200 + N_E/25$ degrees CA and is the time delay between changes in boost pressure occurring and the resulting change in engine torque.

$t_2$ is the engine speed time constant

$t_3$ is the exhaust manifold time constant

therefore

$$\frac{n_E}{r_t} = k_1 \frac{p_b}{r_t} \frac{e^{-t_1 s}}{(1+t_2 s)} + \frac{k_2}{(1+t_3 s)(1+t_2 s)}$$

Above 1 Hz the first term is negligible since the boost fluctuations are very small, so that in the frequency range determining stability

the response is dominated by the back pressure term (whose time constant is much shorter - see Appendix I)

Table 5.2 shows values of steady state gains obtained in response to changes in turbine inlet area, and in figure 5.8 suggested contours of steady state gain are superimposed on the engine operating map.

## 5.2 Output Shaft Torque

Figure 5.9 shows output shaft torque response measured with the Vibrometer torquemeter and compared with the corresponding engine speed response. Also shown is the expected shaft torque response given an assumed dynamometer response and assuming a rigid shaft. Clearly, the speed and shaft torque responses are closely related; however, a second order resonance appears in the measured torque response, with a natural frequency of approximately 3 Hz. A resonance of the torquemeter outer cylinder against its locating spring was observed at 3 Hz, but replacing the spring that was being used with a taut string caused very little change in the measured response. Other possible causes are a) torsional resonance of the engine/flywheel/drive shaft/dynamometer system, and b) resonance in the hydrostatic system due to compressibility of the oil.

Torsional resonance appears unlikely since the dynamometer inertia is low and the drive shaft is stiff (estimated resonant frequency is greater than 50 Hz, assuming that the shaft has less than 5 degrees windup at full load torque of 1000 Nm); nevertheless a similar resonance appears in the speed response measured using a toothed wheel

at the front end of the crankshaft (see figure 5.10).

If a torsional vibration is occurring it is likely that at such a low frequency the flywheel, being the largest component of inertia, will be close to the vibration node so that the speed response measured at the flywheel would be unaffected.

Resonance in hydrostatic systems is common (75) and Bowns and Worton-Griffiths (76) found resonances having natural frequencies of 2 to 4 Hz when analysing a hydrostatic system being used as an engine dynamometer. In their case, pump swash-plate angle was perturbed, while, in the present case the dynamometer control system varies the boost pressure. Whilst this constitutes a different excitation of the resonance it will not prevent its occurrence, and as a result, the amplitude of torque fluctuations produced by the dynamometer and sensed in the drive shaft will be affected. Although significant changes in flywheel speed amplitude may not follow, the torque fluctuations will be transmitted to the crankshaft and may be amplified by the crankshaft/damper system. This could explain the second order response seen in the speed measured at the damper end of the crankshaft.

## 5.3 Dynamic Engine Torque (and Dynamic M.e.p.)

Using the method described in section 3.5.4, dynamic engine torque was obtained from the measured shaft torque and engine speed responses. The resulting dynamic m.e.p. responses (for a given engine, m.e.p. is proportional to torque) as shown in figures 5.11 to 5.15 for several different engine operating conditions; some of these results have

already been published (77). Under all operating conditions except at light load there is a 5 to 8 db (40-60%) fall in dynamic m.e.p. with increasing frequency, the fall occurring mainly above 0.2 Hz and levelling out above 2 Hz. The knee at 0.2 to 0.35 Hz corresponds to the break frequencies observed in the engine speed responses and indicates that speed related effects (e.g. fuelling and f.m.e.p. changes) may be responsible for much of the attenuation of d.m.e.p., although effects related to the temperature of the cylinder walls may contribute since the corresponding break frequency is estimated to be of a similar value (0.5 Hz - see appendix II). Some attenuation of the d.m.e.p. occurs below 0.2 Hz and can be attributed to boost related effects since the break frequency in the boost responses is at a lower frequency, 0.12 Hz or less, than that in the speed responses. See schematic in figure 5.16. Boost related effects include pumping losses and the effect of air-fuel ratio on thermal efficiency. The different behaviour seen at light load (figure 5.15) is due to the characteristics of the FIE and of the dynamometer.

The attenuation in dynamic torque has been postulated by Winterbone et al (51) who found that in order to correctly predict the transient behaviour of a turbocharged diesel engine, it was necessary to reduce the torque calculated assuming steady state conditions by 5% during the first four seconds of the transient. Sawa and Hori (31) found that in their frequency response measurements of engine speed some attenuation occurred which could not be accounted for by the response of the rotational inertia, in fact it had a different break frequency. (This was apparent in their tests since the 2-cylinder diesel engine they were using had a relatively high rotational inertia). Their engines

were of the IDI and prechamber combustion type, with normal aspiration, so that changes in boost pressure can be neglected. They assumed that the effect was due to the thermal inertia of the cylinder walls and its effect on the oil temperature and f.m.e.p.. They introduced another first order lag in series to fit the data and found that its break frequencies were of the order of 0.5 Hz. In fact the response is almost certainly not that of a lag in series, but in parallel; however their maximum test frequency (1.6 Hz) was insufficient to make this apparent. Apart from the effect on oil temperatures, combustion in IDI engines is sensitive to cylinder wall temperatures since the surface to volume ratio and the charge velocity are much greater than in most DI diesel engines. They present a speed frequency response for one engine and, because of its relatively high inertia giving a break frequency of 0.1 Hz, it is easy to distinguish between speed- and temperature-related effects.

The method used in this section assumes a torsionally stiff drive shaft; appendix III analyses the effect of twisting of the shaft. The stiffness assumed is probably an order of magnitude too low, but the high frequency attenuation is unchanged, and the main break frequency is not increased greatly.

By applying inverse transformation to the transfer function a time response of torque can be estimated. Figure 5.17 shows the time response obtained by inverse transformation of the d.m.e.p. frequency response, obtained at 1200 rev/min (figure 5.12). This does not represent exactly the response to a large step change in fuelling, since the mean speed is fixed in the frequency response data; however,

the results give a good indication of the type of dynamic torque response to be expected.

After an initial time delay (corresponding to the diesel torque delay) the initial change in torque is 40% of the steady state change and does not reach 95% of the steady state change until 0.75 seconds have elapsed. If the shortfall in torque is integrated over four seconds the average attenuation is about 4.5% comparing favourably with the value of 5% deduced by Winterbone et al (51).

5.3.1 Prediction of D.m.e.p. Response

Ignoring the effects of cylinder wall and exhaust manifold thermal inertias and ignoring changes in volumetric efficiency, the amplitude of d.m.e.p. variations may be expressed in terms of the variations in engine speed, boost pressure and fuel rack position:-

$$\frac{\Delta T_E}{T_E} = A \frac{\Delta N_E}{N_E} + B \frac{\Delta P_b}{P_b} + C \frac{\Delta x_f}{x_f}$$

The coefficient A of the speed term may be expressed in terms of the variations of fuelling, back pressure and thermal efficiency with speed:-

$$A = \frac{N_E}{T_E} \frac{\partial T_E}{\partial m_f} \frac{\partial m_f}{\partial N_E} + \frac{N_E}{T_E} \frac{\partial T_E}{\partial \eta_{th}} \frac{\partial \eta_{th}}{\partial N_E} - \frac{N_E}{T_E} \frac{\partial T_E}{\partial (AFR)} \frac{AFR}{m_f} \frac{\partial m_f}{\partial N_E}$$

$$+ \frac{P_{exm}}{T_E} \frac{\partial T_E}{\partial p_{exm}} \left[ 1.25 + 0.25 \frac{N_E}{m_f} \frac{\partial m_f}{\partial N_E} \right] \qquad (5.2)$$

(assuming $p_{exm} \propto \dot{m}_{ex} \sqrt{T_{ti}}$ and $T_{ti} \propto (AFR)^{-0.5} N_E^{0.5}$)

Generally A, as expressed in equation 5.2 is negative or has a small

positive magnitude. At 1600 rev/min, medium load, the estimated values of the terms are:-

$$\frac{N_E}{T_E}\frac{\partial T_E}{\partial \dot{m}_f}\frac{\partial \dot{m}_f}{\partial N_E} \doteq +0.12$$

$$\frac{N_E}{T_E}\frac{\partial T_E}{\partial \eta_{th}}\frac{\partial \eta_{th}}{\partial N_E} \doteq -0.25$$

$$-\frac{N_E}{T_E}\frac{\partial T_E}{\partial (AFR)}\frac{AFR}{\dot{m}_f}\frac{\partial \dot{m}_f}{\partial N_E} \doteq -0.01$$

$$\frac{P_{exm}}{T_E}\frac{\partial T_E}{\partial P_{exm}}\left[1.25 + 0.25\frac{N_E}{\dot{m}_f}\frac{\partial \dot{m}_f}{\partial N_E}\right] \doteq -0.19$$

If A is negative, d.m.e.p. amplitude should increase as speed amplitude decreases. In fact, the opposite occurs with the measured d.m.e.p. amplitude being significantly attenuated as frequency increases and speed amplitude decreases (figure 5.11). Clearly other effects dominate in the dynamic variation of d.m.e.p. with frequency; effects such as the variations in thermal efficiency, frictional losses and volumetric efficiency with cylinder wall temperature, and the variation in frictional losses with engine speed under dynamic conditions. Variations in volumetric efficiency may be assumed to have negligible effect on the torque amplitude, and variations in thermal efficiency with cylinder wall temperature, while significant, are not considered large enough to explain the measured response. We are left with the conclusion that variations in frictional losses are substantial and dominate the d.m.e.p. response. This lends some support to the assumption made by Sawa and Hori, that variations in dynamic torque are due mainly to the variations in frictional losses resulting from the thermal inertia of the cylinder walls. Watson (54) using a computer

simulation has shown that changes in f.m.e.p. have a significant effect on engine transient response. In order to predict the d.m.e.p. response, more data is needed on the variation of frictional losses under dynamic conditions.

### 5.3.2 Experimental Measurement Of Diesel Torque Delay

The phase of the calculated d.m.e.p. responses does not have the form of a pure time delay; it contains phase lag related to the attenuation in gain caused by speed, temperature and boost effects. By assuming minimum phase behaviour the phase response corresponding to the d.m.e.p. gain responses can be determined. This was achieved by fitting a transfer function containing poles and zeros of non-integer power to the gain curves to obtain least square error, and then calculating the phase lag corresponding to this transfer function. When these phase responses are subtracted from the d.m.e.p. phase response, the residual phase is close to that of a pure time delay (see figures 5.11 to 5.15), although, because the d.m.e.p. gain is flat above 2 Hz, there is little change in the phase at 10 Hz . Values of the time delay calculated in this manner and the corresponding periods in crankangle degrees are shown in table 5.3; apart from two results all the calculated values fall within the range 62 to 80 degrees CA. The two remaining results are subject to significant error at the higher frequencies due to the small amplitudes being measured. The expected diesel torque delay for 60% maximum fuelling and an engine speed between 1000 and 1500 rev/min is estimated as follows:-

| | |
|---|---|
| sampling point (end of injection) | 4 to 8 degrees BTDC |
| Estimated median point of resulting torque | 60 to 65 degrees ATDC |
| Total torque delay | 64 to 73 degrees CA |

This compares well with the mean of the measured delays (68.5 degrees CA if the two readings that are high are omitted, 74.7 degrees CA if one is omitted). Had sampling been occurring at the start of injection, due to rack lock-up, the expected delay would be 76 to 79 degrees CA, but there was no experimental evidence of rack lock-up occurring. Errors in estimating the delay are probably due mainly to errors in estimating the median point of the torque pulses and may be up to 10 degrees CA.

The estimated and measured torque delay values are considerably less than the 210 degrees CA assumed by Gant's formula (47) for a six cylinder four-stroke diesel, and shorter even than the 120 degrees CA assumed by Ledger et al (46). Allowing for sampling at the beginning of injection rather than at the end of injection increases the delay to close to 80 degrees CA. This is the more likely value when mechanical governors are fitted, and will not be much greater at maximum engine speed. If, further, the extra random delay is added which occurs after a sudden step change in rack position, then the total delay is between 80 degrees CA and 80 degrees CA plus one firing period. This is slightly less than the value given by Garvey (41).

The torque delay does not alone explain the phase lag observed in the

d.m.e.p. responses, the extra phase lag being due to the temperature- and speed-related effects on d.m.e.p. discussed earlier.

## 5.4 Boost Pressure Response

### 5.4.1. Boost Response to Fuel Rack Perturbation

Figure 5.18 shows boost responses at one mean speed and three different mean fuellings. The response is basically first order although the slope of the gain curve reaches -30 db/decade and the phase lag is correspondingly increased. The break frequency varies with the mean rack position; when the mean speed is varied, however, (figure 5.19) the observed variation in break frequency is much less. This is due partly to the reduction in fuelling with increasing speed (for a given rack position) but this is not of itself a great enough effect to explain the results.

If the boost pressure response is assumed to parallel that of the turbocharger speed (true at lower frequencies, where the response of the inlet manifold can be ignored) then the expected break frequency in boost response is given by:

$$f_b = \frac{15\ (n_2 - n_1)\ T_t}{\pi^2\ N_{t/c}\ I_{t/c}} \quad (Hz)$$

$$= \frac{450\ (n_2 - n_1)\ P_t}{\pi^3\ N_{t/c}^2\ I_{t/c}} \quad (Hz) \qquad (5.3)$$

where $n_2 = \frac{N_{t/c}}{T_c} \frac{\partial T_c}{\partial N_{t/c}}$ and $n_1 = \frac{N_{t/c}}{T_t} \frac{\partial T_t}{\partial N_{t/c}}$

d.m.e.p. responses, the extra phase lag being due to the temperature- and speed-related effects on d.m.e.p. discussed earlier.

## 5.4 Boost Pressure Response

### 5.4.1. Boost Response to Fuel Rack Perturbation

Figure 5.18 shows boost responses at one mean speed and three different mean fuellings. The response is basically first order although the slope of the gain curve reaches -30 db/decade and the phase lag is correspondingly increased. The break frequency varies with the mean rack position; when the mean speed is varied, however, (figure 5.19) the observed variation in break frequency is much less. This is due partly to the reduction in fuelling with increasing speed (for a given rack position) but this is not of itself a great enough effect to explain the results.

If the boost pressure response is assumed to parallel that of the turbocharger speed (true at lower frequencies, where the response of the inlet manifold can be ignored) then the expected break frequency in boost response is given by:

$$f_b = \frac{15\,(n_2 - n_1)\,T_t}{\pi^2\,N_{t/c}\,I_{t/c}} \quad \text{(Hz)}$$

$$= \frac{450\,(n_2 - n_1)\,P_t}{\pi^3\,N_{t/c}^2\,I_{t/c}} \quad \text{(Hz)} \qquad (5.3)$$

where $n_2 = \frac{N_{t/c}}{T_c}\frac{\partial T_c}{\partial N_{t/c}}$ and $n_1 = \frac{N_{t/c}}{T_t}\frac{\partial T_t}{\partial N_{t/c}}$

and $N_{t/c}$ and $T_t$ are mean values of turbocharger speed and turbine torque

The value of $n_2$ is hard to determine but if $(n_2-n_1)$ is assumed to be equal to unity then estimates of the break frequency can be made; see table 5.4 for a comparison of calculated and measured values for those results where turbocharger speed was recorded. (Estimated values of turbocharger speed do not give good predictions because $f_b$ depends on the speed squared.) While the estimates are close to the measured value of $f_b$, the experimental break frequency is affected by other factors (primarily engine speed) which affect the amplitude of turbine torque (and which cause the slope of boost response to become steeper than -20 db/decade). And since the break frequency in the speed response is reduced as mean speed increases, this helps to explain why the break frequency in boost response to rack position does not increase with increasing mean speed.

Table 5.1 shows measured values of boost steady state gain and figure 5.20 plots contours of this gain on the engine operating map. Clearly, gain increases with both engine torque and engine speed, suggesting that it may be related to either engine power or fuel mass flow rate. Figure 5.21 plots the steady state gain against the fuel mass flow rate as determined from fuelling characteristics previously obtained for the same engine. Figure 5.22 plots the same gains against a dimensionless turbine mass flow and excellent correlation (0.97) is obtained for all tests carried out with maximum turbine inlet area. The dimensionless mass flow is represented by the term

$$\frac{N_E^{1.2}\, m_f^{0.5}}{P_b^{0.7}}$$

since these variables are more readily available than $\dot{m}$, $T_{ti}$ and $P_{exm}$. For derivation see Appendix IV.

That the variations in engine speed are responsible for the extra -10 db/decade slope in the boost responses is suggested by the frequency range over which the extra attenuation occurs; it is further supported by demonstrating the dependence of turbine torque on engine speed.

Assuming back pressure equal to 1 bar:

$$T_t \doteq \frac{30\ \dot{m}\ Cp_{ex}\ T_{ti}\ \eta_t\ (1 - P_{ex}^{-0.25})}{\pi\ N_{t/c}}$$

$$\propto N_E\ P_b^{0.6}\ T_{ti}^{1.25}\ N_{t/c}^{-1}\ \eta_t\ (1 - P_{ex}^{-0.25})$$

(assuming $\dot{m} \propto N_E\ P_b^{0.6}$ and $Cp_{ex} \propto T_{ti}^{0.25}$)

If it is assumed, further, that

$$T_{ti} \propto (AFR)^{-0.5}\ N_E^{0.5} \propto m_f^{0.5}\ P_b^{-0.3}\ N_E^{0.5}$$

$$P_{ex} \propto \dot{m}\sqrt{T_{ti}} \propto N_E^{1.25}\ P_b^{0.45}\ m_f^{0.25}$$

then $$T_t \propto N_E P_b^{0.3}\ m_f^{0.5}\ N_{t/c}^{-1}\ \eta_t\ (1 - N_E^{-0.31}\ P_b^{-0.11}\ m_f^{-0.06})$$

At low frequencies

$$N_{t/c} \doteq N_E^{0.5}\ m_f^{0.5}$$

so that

$$T_t \doteq N_E\ P_b^{0.3}\ \eta_t\ (1 - N_E^{-0.3}\ P_b^{-0.1}\ m_f^{-0.06})$$

The strong dependence of turbine torque on engine speed is therefore demonstrated at low frequencies. At higher frequencies, the

turbocharger speed variations are attenuated more quickly (in this case because of the small load inertia) than the changes in engine speed, so that the dependence still holds true.

### 5.4.2 Boost Response to Turbine Inlet Area Perturbation

Variations in engine speed which significantly affected turbine torque amplitude in the rack perturbation tests, are much smaller when the turbine inlet area is perturbed. As a result, turbine torque will be determined primarily by the turbine inlet area and its amplitude can be expected to vary less with frequency. The measured boost responses support this (see figures 5.23 and 5.24) since the gain slope is much closer to -20 db/decade. Above 4 Hz, the inlet manifold response begins to become significant introducing extra attenuation and phase lag into the responses (estimated break frequency at 2000 rev/min is 8 Hz). Most of the extra phase lag beyond -90 degrees is due to the inlet manifold response; the exhaust manifold response may contribute some phase lag, but its break frequency is estimated to be much higher than that of the inlet manifold (see appendix I). There is no pure time delay in the response of boost to turbine inlet area.

Break frequency increases with increasing speed (figure 5.23) but is affected little by changes in mean fuelling (figure 5.24).

Table 5.2 gives values of the steady state gain obtained experimentally and figure 5.25 suggests contours for the gain values on the engine operating map. Just as with the boost response to rack perturbation, the gain increases with both engine speed and load. Figure 5.21 shows a

plot of steady state gains against mean fuel mass flow rate; the correlation coefficient is better than 0.9.

Another means of expressing the turbine inlet conditions is to use the dimensionless mass flow. Figure 5.26 plots the gain against this; the correlation is 0.81. Figure 5.27 shows dimensionless boost gain against the turbine dimensionless mass flow. In this case the correlation coefficient is 0.97 and the relationship is:-

$$\frac{A_t}{P_b}\frac{\partial P_b}{\partial A_t} = 0.011\ \frac{\dot{m}_{ex}\sqrt{T_{ti}}}{P_{exm}}$$

## 5.5 Exhaust Opacity Response

### 5.5.1 Opacity Response to Rack Perturbation

Experimental opacity gain responses are shown in figure 5.28 together with the corresponding fuel-air ratio amplitudes, calculated from the boost response using the known compressor characteristics and engine volumetric efficiency. Both opacity and fuel-air ratio have similar responses, at first increasing in amplitude as frequency increases, reaching a peak and then settling to a steady amplitude above 1-2 Hz. The difference in gain between the two curves is constant with a very small standard deviation indicating (since the gain scale is logarithmic) that a power relationship exists between the two:

$$\Delta S = k' \Delta(FAR)$$

$$\frac{\Delta S}{S} = k \frac{\Delta(FAR)}{FAR}$$

$$S \propto (FAR)^k \propto (AFR)^{-k}$$

By measuring the offsets in the gain responses and taking into consideration the differences in steady state gains of the exhaust opacity and fuel-air ratio, the value of k has been determined under different engine operating conditions. Its value varies between -1.5 and -12, having greatest magnitude under conditions of highest mean opacity - figure 5.29 shows k plotted against mean opacity. When k is plotted against a relative spray penetration (the fuelling per shot divided by the inlet manifold relative density) the relationship is more linear (figure 5.30). Typically k lies between -2.5 and -4.0, comparing favourably with the value of -3.25 obtained by O'Neill (57) for a turbocharged diesel similar in size to the Leyland TL11. Watson (28) used a term involving the dynamic equivalence ratio to calculate transient smoke levels and found that an index value of 3.73 provided the best fit to data from two single-cylinder engines. For a six-cylinder turbocharged truck diesel the best fit was obtained with an index of 6.62 (Watson's indices are positive because equivalence ratio is inversely proportional to air-fuel ratio).

Both O'Neill and Watson assume constant values for the index, and this may be reasonable where all the tests involve fuelling close to full-load values; the present results indicate, however, that the index varies and that it appears to vary with fuel spray penetration.

### 5.5.2 Opacity Response to Turbine Inlet Area.

Engine speed fluctuations are relatively small when the turbine inlet area is perturbed so that variations in fuelling per injection can be ignored. Air-fuel ratio is therefore determined by the inlet manifold

density; the density is proportional to the 0.6 power (approx) of boost pressure so that logarithmic gain plots of the two will be parallel. Figure 5.31 shows dynamic responses of opacity and boost pressure compared. Below 1 Hz the gains are parallel confirming the power relationship between opacity and air-fuel ratio. Above 1 Hz the opacity signal amplitude is too small to distinguish clearly from the noise present. The much greater phase lag in the opacity response is the result of the large transport delay between the exhaust manifold and the opacity meter (figure 4.7) to which must be added the time taken for changes in boost pressure to affect the exhaust manifold (330 to 400 degrees CA, depending on engine speed). Also shown in figure 5.31 is the effect of removing a time delay of 150 msec from the opacity phase response - the phase now matches that of the boost pressure. The estimated time delay based on the dimensions of the exhaust system etc. for the conditions (1600 rev/min and 100 mg/shot fuelling) is 120-125 msec. The reason for the discrepancy between the two is not understood.

## 5.6 Turbine Inlet Temperature Response.

Turbine inlet temperature is also expected to be a function of air-fuel ratio, and to a lesser extent of engine speed. Figure 5.28 shows corrected turbine inlet temperature gain responses compared with the calculated air-fuel ratio gain. There is considerable similarity apart from the extra attenuation appearing in the temperature above 0.5 Hz. All possible experimental sources of this attenuation have been exhausted and it must be concluded that the attenuation above 0.5 Hz is due to the thermal inertia of the cylinder or exhaust manifold walls. The break frequency in response of the cylinder wall temperatures has

already been estimated to be 0.5 Hz (appendix II) and a first order lag of this break frequency would explain the observed response.

Variations in turbine inlet temperature can be expressed as:

$$\Delta T_{ti} = \Delta T_{im} + \Delta(\Delta T_e)$$

$$\Delta(\Delta T_e) = k_1 \Delta(AFR) + \frac{k_2 \Delta T_{we}|_{ss}}{1+t_{we}s}$$

where the last term allows for the effect of variations in wall temperatures (of the cylinders, exhaust valves and exhaust ports and manifold(s)). The time constant $t_{we}$ corresponding to these wall temperatures will not be identical to that affecting the engine d.m.e.p. response since the friction is dependent almost entirely on the cylinder wall and piston temperatures alone.

Changes in temperature rise across the engine under steady state conditions may also be represented by

$$\Delta(\Delta T_e) = k_3 \Delta(AFR) + k_4 \Delta N_E$$

where at steady state the speed term accounts to a great extent for the variations in wall temperature. If it is assumed that

$$AFR \propto p_b^{0.6} \dot{m}_f^{-1}$$

$$k_3 = k_4 = 0.5$$

then excellent prediction of changes in engine temperature rise results (figure 5.32). Observed temperatures were recorded about 30 seconds after step changes in rack position, so that significant changes in engine mean water and oil temperature will not have occurred.

## 5.7 Non-Linearity

The standard technique in determining the dynamic behaviour of non-linear systems is to linearise them locally; this assumes that for small changes in operating point a non-linear system may be approximated by a linear one. This is valid and may be successfully applied to regulator problems; what is not valid is to then assume that the same response occurs when much larger input perturbations are applied.

In the turbocharged automotive diesel the steady state torque gain in response to rack movement varies with the amplitude of rack movement as well as with mean speed and torque. In an attempt to investigate this, differing rack motion amplitudes were used at the same mean speed and torque, the maximum amplitude being about 3/4 of the maximum fuelling range. The speed responses are shown in figure 5.33 and indicate that the shape of the dynamic response is different in the case of the greatest amplitude ($\pm$38% of maximum fuelling). The other two responses ($\pm$13% and $\pm$3.5%) are very similar to each other. At this operating point (nominally 1200 rev/min, 68 mg/shot) fuelling amplitudes up to 11.5% of maximum fuelling (15 mg/shot) can therefore be used without significantly affecting the dynamic response. The degree of non-linearity varies with operating point and can be expected to be greatest at full load, low speed where combustion is closest to saturation.

Although the dynamic response (i.e. relative to the steady state value) is unchanged by increasing the fuelling amplitude to 11.5% maximum

fuelling, the steady state gain is affected. Figure 5.34 indicates that the steady state gains in speed are reduced as the fuelling amplitude increases, and this is consistent with saturation effects. The steady state gain in speed is reduced by approx 0.25% of the zero frequency limit gain per 1% of maximum fuelling amplitude.

The steady state gain in boost pressure at 1600 rev/min also appears to decrease as the fuelling amplitude increases; however, at 1200 rev/min no change in gain with fuelling amplitude was observed. The dynamic responses at 1200 rev/min (figure 5.35) show a similar consistency. It is reasonable to expect boost gain to be less affected than engine speed gain by non-linearities in the fuelling and torque response. The non-linearities affecting the speed gain are mainly in the variation of thermal efficiency with fuelling, and do not directly affect the boost pressure which is dependent on exhaust energy flux.

Harmonic analysis of the engine speed response was carried out at 1200 rev/min, 104 mg/shot mean fuelling in an attempt to further quantify the non-linearity. The operating point was chosen because of its low air-fuel ratio so that the effects of combustion saturation might be included. Figure 5.36 shows the amplitudes of the speed responses at each of the first six harmonics of the test signal - both speed response relative to the rack position and speed response relative to the transducer signal. From these two responses the harmonic content of the rack motion can be deduced and is shown also; harmonic content of the rack motion is better than -55 db. The harmonic content of the speed response relative to the test signal at the fourth, fifth and sixth harmonics can largely be attributed to noise or harmonic content

in the rack motion. However, at the second and third harmonic frequencies there is a significant amplitude which can not be attributed to harmonic content of the rack motion, and which is therefore generated by the non-linearity of the engine behaviour. The second harmonic is -25 db (~6%) relative to the amplitude of the fundamental, and the third is at -44 db (~0.6%); only the second harmonic can be considered significant, and its amplitude is not great.

## 5.8 Accuracy of Measurements

Results given in table 5.1 and 5.2 show a considerable spread in measured gains under nominally similar operating conditions. While this is partly explained by small differences in the mean operating conditions, it is also a result of difficulty in obtaining consistent steady state readings. Long thermal time constants exist, e.g. of the exhaust manifold walls, turbine casing, engine lubricant and coolant as well as that of the test cell air temperature. Winterbone et al (34) also had difficulty in obtaining consistent steady state readings for an automotive gas turbine.

Some error is due to inaccuracy in determining the actual engine fuelling (mg/shot) from the rack position. The FIE fuelling characteristics had been measured previously but inaccuracy in these measurements and subsequent wear in the FIE may cause errors up to $\pm$5% in the fuelling amplitude.

Over the 21 month period of the present tests the change in dynamic behaviour of the engine has been small as is seen in figures 5.37 and

5.38 which show speed and boost response obtained under nominally similar conditions over a period of more than a year. Only the speed response measured in August 1985 shows significant deviation and this may be due to the warm ambient conditions.

Owing to the difficulty of measuring accurately the turbine inlet area, discussed in section 4.1.4, errors in the estimated turbine area amplitudes may be up to $\pm$10%. While this will significantly affect the steady state gains (as seen in figure 5.26) the dynamic relative responses are unlikely to be greatly affected. Figure 5.39 shows boost responses to turbine area perturbations, obtained, again under nominally similar conditions, but over a period of more than a year.

# 6. CONTROL IMPLICATIONS OF ENGINE DYNAMIC BEHAVIOUR

## 6.1 Choice of Control Variables

The two outputs from the controller are clearly the demand voltages for rack position and turbine inlet area actuator position. It is necessary to choose which control inputs (i.e. engine outputs) to use, and which input-output pairs are to be used if two feedback control loops are to employed.

### 6.1.1 Engine speed

Despite the fact that, in many automotive diesel applications, speed governing is not used over much of the engine operating range, feedback control of engine speed is necessary not only to achieve stable, economical idling but also to prevent overspeeding.

With petrol engines, overspeeding is unlikely unless the throttle is opened wide while the transmission is in neutral; at high speeds, the S.I. engine torque decreases with increasing engine speed (due to the reduction in volumetric efficiency) and the vehicle drag rises sharply with increasing vehicle speed.

The torque produced by the automotive truck diesel at high speed is much less sensitive to changes in volumetric efficiency and the vehicle drag rises less steeply with speed, since the ratio of rolling drag to aerodynamic drag is greater than is the case with petrol-engined passenger cars.

In addition to the need to prevent the high wear rates and valve damage that may result from overspeeding, legislation limiting commercial vehicle maximum speed is likely and cruise control is also becoming more common. Cruise control allows a given vehicle speed to be maintained without further action by the driver. In some applications, for example bulldozing and digging, speed governing is required over a wide range of engine speeds.

### 6.1.2 Engine Torque

For many automotive applications engine torque is attractive for use as a control variable, since torque (or more precisely variations in torque with a given torque-speed characteristic) is really the commodity demanded by the driver's right foot. This is, to a large extent, what is provided by S.I. engines and by diesel engines fitted with 2-speed governors; the carburettors and fuel injection pumps are developed to give the required torque-speed characteristic and movement of the driver's right foot moves the torque curve up and down. This is achieved without the use of feedback control of the torque (apart from the control applied by the driver himself).

Feedback control of torque requires sensing of the engine torque and this is difficult and expensive at present. If torque sensing were to become feasible, this would allow more sensitive optimising of engine efficiency (some current S.I. engines use engine speed variations to indicate increasing torque and this is used to set the ignition timing for best economy). In a diesel engine with variable-geometry turbocharger the torque signal would allow the turbine inlet area to be

controlled for optimum efficiency and acceleration.

### 6.1.3 Exhaust Opacity

In automotive applications exhaust opacity is an important parameter. Legislation governs the maximum opacity allowed and social considerations require that the exhaust be practically invisible most of the time. Sensitive opacity meters, such as the infra-red absorption type, suitable for transient control, are currently expensive and prone to sooting. While the costs can no doubt be reduced substantially there remains the problem of extracting the mean smoke level from a very noisy signal (see section 5.5.2). The sensor would have to be placed, almost certainly, downstream of the turbine outlet and this will mean that there will be a significant transport delay. Control techniques exist to cope with large time delays (78), but the optimum control achievable is prejudiced by the length of the delay. However, if opacity sensors become cheap and reliable enough for automotive use, this would allow the greatest possible torque to be achieved during vehicle acceleration without exceeding specified limits on exhaust opacity.

### 6.1.4 Air-Fuel Ratio

While torque sensing allows the air-fuel ratio to be controlled (by means of turbine inlet area) for optimum efficiency, it provides no control over exhaust opacity. Sensing of the air-fuel ratio allows both efficiency and exhaust opacity to be controlled, although the final result cannot be as good as when torque and exhaust opacity are sensed

directly and each regulated by means of feedback control. The air-fuel ratio must be scheduled to give the best efficiency over the engine operating map and a minimum air-fuel ratio used to limit the transient exhaust opacity. These air-fuel ratio values will have to be determined empirically.

Until exhaust oxygen sensors are developed sufficiently to give continuous control under the very lean conditions found in turbocharged diesel engine exhaust gases, the best means of sensing air-fuel ratio is probably to sense inlet manifold boost pressure and temperature.

A knowledge of volumetric efficiency and fuelling as functions of engine speed and rack position is then required to determine the air-fuel ratio. While this approach ignores the variation of volumetric efficiency with cylinder wall temperature under transient conditions, it has the great advantage of allowing the trapped air mass to be estimated before the fuel rack position is sampled for the next cylinder to fire. Where controller sampling takes place once per cylinder firing, this allows the fuelling to the next cylinder to be limited according to the specified minimum air-fuel ratio (provided that the rack actuator has a sufficiently fast response).

An alternative method is to measure total air mass flow rate - e.g. by orifice flow meter or hot-wire probe upstream of the turbocharger compressor inlet. This requires the monitoring of an extra parameter (either pressure drop or local air velocity) in addition to the ambient temperature and pressure. The cost of sensors and their associated wiring probably rules this option out since the cost of adding software

to calculate the volumetric efficiency will normally be negligible.

### 6.1.5 Turbine Inlet Temperature

In the gas turbine, turbine inlet temperature determines maximum cycle temperature and thermal efficiency; in order to maximise efficiency within the constraints of material creep resistance and to obtain the best transient response Winterbone et al (64) chose turbine inlet temperature as one of the two control inputs.

Aldren (27) considered controlling turbine inlet temperature in a turbocharged diesel, but in this case peak temperatures occur intermittently and within the confines of the closed cylinder. Burnt gases are not released to the exhaust manifold until they have cooled substantially. In addition, air-fuel ratios are generally high, and as a result turbine inlet temperature is usually satisfactory if the turbocharger is well-matched to the engine (79). This is also true with variable geometry turbines except that at peak torque, the turbine inlet temperature may rise if the maximum increase in b.m.e.p. made possible by the increased air flow is used.

The measurement of turbine inlet temperature currently involves a compromise between response time and robustness and at present the minimum usable time constant (due to the thermal inertia of the thermocouple probe and protective shielding around it) will be at least one second. This is insufficient to allow the temperature to be controlled satisfactorily without derivative action, and derivative action increases signal noise.

For these reasons, it was decided not to use turbine inlet temperature as a control input. It will be assumed that any limit on turbine inlet temperature (e.g. due to the specification of a less expensive turbine wheel or housing material) will be compensated during engine development either by matching the turbocharger to give higher air-fuel ratios, or by increasing the valve overlap period in order to dilute the exhaust with cooler air.

### 6.1.6. Inlet Manifold Boost Pressure

Apart from its possible use in determining trapped air fuel ratio, boost pressure may be used as a control input in its own right; it can be used (without knowledge of the inlet manifold temperature) as a crude measure of trapped air mass which, to a great extent, automatically compensates for changes in ambient pressure (whether due to atmospheric conditions or altitude). In its simplest form, a fixed reference value of boost pressure may be used so that the feedback loop attempts to maintain a constant boost pressure, and this has advantages where transient response is most important (see chapter 7).

In applications where part load fuel economy is important the reference boost pressure would have to be varied, in addition, as a function of engine fuelling and/or speed. This relationship is potentially complicated and in the limit becomes equivalent to controlling the air-fuel ratio. However, because of the limited turndown ratio achievable with current variable geometry turbines the turbine area will be either fully open or fully closed over much of the engine operating range; as a result, a simple scheduling of desired boost pressure can probably

achieve a good compromise between thermal efficiency and transient response. It will not be able to compensate for changes in ambient temperature.

## 6.2 Effect of Interaction when Engine Speed and Boost Pressure are used as the control inputs

### 6.2.1 Effect on Steady State Conditions.

Table 6.1 shows the effect of the interaction terms at steady state when the control inputs are engine speed and boost pressure. All-speed governing is assumed and typical feedback gains are used for the two feedback loops. The system assumed is that of figure 6.1 and the results give the magnitude of the effects of interaction without indicating whether the effect is beneficial or not. The effect of interaction on steady state speed is greatest at low speed high load and at high speed high load; in the mid-speed range the effect of interaction is much less.

The effect of interaction on steady state boost is greatest at low speed and high load, falling gradually with increasing speed and reducing load.

The term $g_{12}g_{21}/g_{11}g_{22}$ which gives an idea of the magnitude of the effect of interaction on stability (see section 3.3.3) has greatest magnitude when the engine is operating at low speed, high load and at high speed, high load; these are the same conditions under which the effect of interaction on steady state speed is greatest.

### 6.2.2 Effect on stability under feedback control

In order to determine properly the effect of the interactions on stability when controlled by two feedback loops, the dynamic responses must be taken into account. The value of the interaction stability term under steady state conditions indicates that the effect on stability is likely to be greatest at either low speed, high load or at high speed, high load. At high speed high load, turbine inlet area will be fully open and interaction has no effect on stability; however at medium load high speed (2200 rev/min 4.4 V fuelling) the term is still significant and its effect on feedback stability needs to be examined since, if a fixed value of reference pressure is used, the turbine inlet area will be partly open under these conditions. Stability with such a system is examined in chapter 7, using the characteristic equation method.

Where the reference pressure is varied with engine operating point the turbine inlet will be fully open at high speed, whatever the load. In this case the problem of possible feedback instability due to interaction is removed at high speed and the stability need be examined only at the peak torque condition.

The approximate transfer function under peak torque condition, with gains expressed in terms of actuator and sensor output signal voltages, is given below:-

$$\begin{bmatrix} V_{N_E} \\ V_{P_B} \end{bmatrix} = \begin{bmatrix} \dfrac{1.3e^{-0.017jw}}{(1+0.38jw)(1+0.039jw)^{0.33}} & \dfrac{0.019e^{-0.024jw}}{(1+0.6jw)} \\ \dfrac{2.68e^{-0.029jw}}{(1+0.87jw)^{1.5}} & \dfrac{0.145e^{-0.0275jw}}{(1+1.25jw)(1+0.029jw)^{0.3}} \end{bmatrix} \begin{bmatrix} V_{x_f} \\ V_{r_t} \end{bmatrix}$$

where $V_{x_f}$ , $V_{r_t}$ are voltages corresponding to rack position and turbine area actuator

The responses given above do not include the responses of the actuators. Since the two actuators have very similar responses their inclusion in the transfer functions will not significantly change the effect of interaction on the stability, although they may change the crossover frequencies. The only significant difference between the responses of the two actuators is the response of the turbine area actuator linkage; at peak torque this introduces an extra 1 db attenuation and 10 degrees phase lag at 6 Hz.

The quoted transfer function for speed response to turbine inlet area does not describe the increase in amplitude at low frequency but is valid above 0.5 Hz.

Figure 6.2 shows the array of Nyquist plots for these responses. Attempts to diagonalise the matrix by means of a pre-compensator proved fruitless, indicating that the array as it stands is singular. This was confirmed by looking at the eigenvalues of the matrix $G_t(0)G(0)$; the ratio of square roots of the largest and smallest eigenvalues is about

50 (a value greater than 10 indicates that the matrix G(0) is singular). This is not entirely surprising since the choice of calibrations for the actuator and engine output signal voltages had been made on the basis of convenience for signal handling alone. Scaling of the controller input and output voltages is necessary to restore satisfactory relative magnitudes of the different transfer functions (see figure 6.3). A precompensator can now be applied to optimise the diagonal dominance (the 'Align' algorithm available in the suite of programs at the UMIST Control Systems Centre will do this for any chosen frequency).

Figure 6.4 shows the Nyquist plots when the precompensator optimising the diagonalisation at 3.3 Hz is included. The Gershgorin bands are shown and, since these do not include the origin, may be used to examine the maximum effect of the off-diagonal (interaction) terms on stability under feedback control. Figure 6.5 shows the same responses expanded to show more detail in the region closest to the critical point $(-1+j0)$ . As is clear from the size of the Gershgorin discs, the chosen precompensator has reduced to a small amount the effect of interaction on stability.

Plotting the corresponding closed loop responses (figure 6.6) confirms that the amplitudes of the off-diagonal terms is less than those of the diagonal terms at all frequencies up to the maximum shown (7 Hz). The analysis of chapter 7, however, shows that this kind of precompensation is not necessary to ensure stability when boost pressure is used as the second variable.

## 6.3 The Effect of Interaction when engine speed and trapped air-fuel ratio are used as control inputs.

### 6.3.1 The Effect on Steady State Conditions

Table 6.2 gives steady state interactions and values of the interaction stability term for the same engine when the second input to the controller is air-fuel ratio. These values assume no precompensation and the typical interactions assume changes in reference speed and air-fuel ratio (AFR) of 500 rev/min and 3 ratios respectively.

Changes in AFR due to interaction are not great, even when speed governor action is applied, but these values ignore possible saturation of the actuators.

At steady state the interaction stability term $r_{12}r_{21}$ $r_{11}r_{22}$ has a magnitude similar to that when boost pressure is used as the second variable. In the case when the second variable is air-fuel ratio, however, the interaction appears to be greater at high speed than at peak torque.

### 6.3.2 The Effect of Interaction on stability under feedback control.

Using the characteristic equation to determine the limits of stability in the gain plane, confirms that at high speed the interaction has a significant and, in fact, detrimental effect on stability under feedback control (figure 6.7).

The analysis assumes no precompensation, a load inertia equal to that of the engine, flywheel and dynamometer and assumes actuator responses similar to those fitted to the TL11 engine. Under these assumptions the feedback gain in the air-fuel ratio loop must be reduced to less than 1 mm of actuator movement (approximately 9% reduction in turbine inlet area) per AFR if a satisfactory governor runout is to be maintained (0.83 mg/shot per rev/min is equivalent to a runout of about 150 rev/min). When the increased load inertia seen in a vehicle is taken into account, the air-fuel ratio feedback gain may be increased to about 2 mm per AFR. However, since the turbine inlet is likely to be fully open at all loads at high speed, possible stability problems will only occur at the highest speed at which turbine area reduction takes place. The stability margin will be further reduced if the moment of inertia of the turbocharger rotor is reduced.

At peak torque (figure 6.8) the effect of interaction is less significant, confirming the impression obtained from looking at the amplitude of the term $g_{12}g_{21}/g_{11}g_{22}$ at steady state. A satisfactory margin of stability is almost maintained with the desired feedback gains even under all-speed governing, and the situation is improved when the increased load inertias seen in service are taken into account.

In conclusion, where air-fuel ratio and engine speed are used as the two controlled variables there should be no problem with instability resulting from the interaction terms in engines with 2-speed governing. Where all-speed governing is employed, some feedback instability may occur at full load just below maximum speed, where turbine area

reduction is beginning to take place. In this case a reduction in the air-fuel ratio feedback gain will solve the problem, if multivariable precompensation is not to be used.

## 6.4 Turbine area scheduling as a function of engine speed.

Turbine inlet area may be scheduled to vary with engine speed, with minimum area required at peak torque speed and maximum area at high engine speeds. This means that part-load efficiency at higher engine speeds is not sacrificed substantially, while at low speed the best possible boost is available at all times to provide optimum transient performance.

From the viewpoint of feedback control stability this is a simple problem, since there is now only one engine output (engine speed) subject to feedback control. Figure 6.9 shows the corresponding transfer function diagram.

$$n_E = k_1 g_{11} (N_{E_{ref}} - f_1 n_E) + k_2 g_{12} f_1 n_E$$

$$\therefore \quad \frac{n_E}{N_{E_{ref}}} = \frac{k_1 g_{11}}{1 + f_1 k_1 g_{11} \left| 1 - \frac{k_2 g_{12}}{k_1 g_{11}} \right|}$$

For an automotive (truck) diesel engine, assuming a governor runout of 150 rev/min and a change from maximum to minimum turbine area in 600 rev/min, the steady state values are within the ranges:

$$5 \leqslant k_1 g_{11} \leqslant 25$$

$$0.1 \geqslant k_2 g_{12} \geqslant -0.3$$

$$\therefore \quad \left| \frac{k_2 g_{12}}{k_1 g_{11}} \right| \ll 1$$

Clearly, the stability of the speed feedback loop is not affected greatly.

# 7. CONTROL STABILITY UNDER SIMPLE BOOST FEEDBACK CONTROL OF TURBINE AREA

Ideally in a turbocharged engine with VG turbine a multivariable controller should be applied to control engine speed and boost simultaneously, making due compensation for interaction; this will probably require digital control methods.

Such an approach undoubtedly increases the first cost of the engine and requires integration of turbine area control with the engine speed governor, which has until now been the responsibility of the fuel injection equipment (FIE) manufacturer. In the short term at least, there is believed to be a market for variable goemetry turbochargers having simple control technology and which can be fitted to the engine independently of the FIE. This also allows easy fitting to engines already in service.

One simple control strategy is to adjust turbine inlet area so as to try to keep inlet manifold pressure constant. This produces variations in turbine inlet area under steady state engine conditions as shown in Figure 7.1. Such a system requires no integration of the turbine area control with the speed governing function; it gives good full load performance and good transient performance, and can be achieved using the boost pressure itself to actuate the changes in $A_t$. Engine part load efficiency is impaired by high back pressure, but in some applications this is not a major problem. The transfer function diagram of such a system is shown in figure 6.1.

This chapter examines the control stability of a 200-250 kW automotive diesel engine having such boost feedback control of VG turbine area. Stability is considered under different engine operating conditions, with both 2-speed and all-speed governing. The effects on stability of effective load inertia, turbocharger rotor inertia and actuator response are considered.

For automotive diesel systems the gain crossover frequency, at which phase margin is measured, and the phase crossover frequency, at which gain margin is measured, are generally within the range 1 to 5 Hz, although as electronic control (analogue or digital) is applied together with faster actuators, the upper end of the range may approach 10 Hz.

## 7.1 Method

The analysis uses the characteristic equation to determine limits of stability for the system, plotted in the gain plane (where the two axes represent the gains in the two feedback loops) as described in Section 3.3.2. The characteristic equation may be written as:-

$$\underbrace{f_1 k_1 g_{11}}_{A} + \underbrace{f_2 k_2 g_{22}}_{B} + \underbrace{f_1 f_2 k_1 k_2 (\overbrace{g_{11}g_{22}}^{C_1} - \overbrace{g_{12}g_{21}}^{C_2})}_{C} = -1 \qquad (7.1)$$

The analysis makes use of frequency response obtained on the TL11 engine and also some responses from a 10 litre engine. Each engine is fitted with a Holset VH2C turbocharger - essentially an H2C turbocharger with prototype variable geometry mechanism and pneumatic

(boost pressure) actuation. Some responses were measured on the turbocharger itself.

The assumed speed governor response is shown in Figure 7.2 where it is compared with measured responses typical of mechanical governors fitted to this type of engine. The assumed response is equal to the best of the measured responses which all refer to a mid-speed, 60% load condition. Steady state speed governor gain is varied in the range 8 to 160 per cent maximum fuel per change in speed (as per cent of rated speed). Values of 10 to 14 per cent are typical for automotive diesels of this type at maximum speed.

Boost feedback response including actuator response was measured on the turbocharger and steady state gain is varied between 2.5 and 60 per cent $A_t$(i.e. per cent of fully open area) per change in boost pressure (as per cent of absolute boost reference pressure); the preferred value for good transient and steady state performance, 5% $A_t$ per % $P_b$ (abs), implies a narrow pressure range within which the turbine area actuator may operate free of the stops (as indicated in figure 7.1).

## 7.2 Stability Analysis in the Absence of Speed Governor Action

In many automotive applications a 2-speed governor is used so that explicit speed feedback occurs only at maximum speed and low speed idle. There is implicit feedback, however, since fuelling varies with engine speed, the fuel injection characteristics being chosen to give a small increase in fuelling with decrease in speed in order to achieve the desired torque back-up.

At high load and with engine speed close to peak torque speed the estimated steady state gain values for the functions in equation 7.1 are given in table 7.1 for a typical 200-250 kW turbocharged diesel engine; the estimated ranges of uncertainty are given in brackets.

The terms in equation 7.1 then have the following steady state magnitudes, assuming boost feedback gain has the desired value of 5% $A_t$ per % change in absolute boost pressure:-

| | | | |
|---|---|---|---|
| A | - | 0.32 (0.0 - 0.4) | Dimensionless |
| B | - | 2.54 (1 - 6 | |
| C | - | 0.716 (0 - 3.1) | |
| $C_1$ | - | 0.4 (0.24 - 0.6) | |
| $C_2$ | - | 0.042 (0.026 - 0.08) | |
| $C_2/C_1$ | - | 11% rising to 15% above 1Hz. | |

At steady state, term $C_2$ , the product of the interaction terms is small compared to $C_1$ , the product of the direct gains $g_{22}$ and $g_{11}$ ; at higher frequencies of interest (2-10 Hz) the interaction becomes more significant and will affect the system stability. The low frequency interaction between loops can probably be ignored since small steady state errors in speed are unlikely to be important in automotive applications (although steady state errors in boost may affect the smoke-limited torque curve).

In the absence of speed governor action there is clearly sufficient margin in the speed feedback loop; figure 7.3 shows the stability margin in the boost feedback loop is also sufficient and that, if

anything, interaction improves the stability slightly.

## 7.3 Stability analysis with speed governor action

### 7.3.1 Idle Speed Control

Since boost pressure at engine idle speed is well below the range within which actuator motion occurs, no feedback occurs in the boost control loop. This is so even if, for the sake of improved transient response, the turbine area is reduced to its minimum value at engine idle in order to raise the minimum boost pressure. In this latter case the actuator is at the other limit of its range; and in both cases k is zero and the system is effectively single-input single-output with stability determined solely by the speed feedback loop.

### 7.3.2 Maximum Speed Control (Governor Runout)

Typical steady state gain values for the transfer functions under maximum speed governing (point 3 of figure 7.1) are given in Table 7.2 with ranges in brackets.

#### 7.3.2.1 Effect of Engine Load Inertia

Since speed response break frequency is generally well below the range determining control stability, any increase in load inertia reduces gain more significantly than it increases phase lag and thus improves the stability margin. Instabilities that appear on the test-bed, therefore, will not necessarily appear when the engine is operating in a

vehicle.

The engine is under load, other than momentarily, only when a gear is engaged; total effective inertia increases with vehicle load and inversely with gear ratio. Minimum effective inertia under load is estimated to be at least 2.5 times that of the engine and flywheel alone (see appendix V).

The assumption that the transmission is torsionally rigid is valid provided the natural frequency of torsional oscillations is not close to the frequency determining control system stability. At frequencies close to the transmission natural frequency, typically between five and ten Hz, the effective load inertia seen by the engine may be substantially reduced; this will reduce the stability margin and may cause hunting.

The stability with an effective inertia of 2.5 times that of engine and flywheel is shown in fig. 7.4. Stability margin in the speed loop is now ample and stability in the boost loop is also improved.

7.3.2.2 Effect of Improved Boost Actuator Response.

Figure 7.5 shows stability limits after improving boost feedback response to simulate that of a 10 Hz bandwidth actuator controlled digitally with total time delay of 20 msec. In the 1-5 Hz range determining stability, such a feedback path has negligible attenuation of gain but moderate phase lag. Whilst improving resonse time this can be expected to reduce stability margins in the boost feedback path as

can be seen when comparing with figure 7.4. Interaction now has negligible effect on boost loop stability but does affect speed loop stability.

#### 7.3.2.3 Effect of Reduced Turbocharger Inertia

Turbocharger response break frequency is usually well below one Hz, so that reducing the turbocharger inertia increases the gain in the 1-5 Hz range without significantly reducing the phase lag. As expected this reduces the stability margin (figure 7.5); however, the margin appears sufficient even with the turbocharger inertia reduced by 60%.

Where reference boost pressure is varied with engine load (i.e. to optimise part load b.s.f.c.), turbine inlet area will generally be fully open at or above engine rated speed and the boost loop will no longer affect stability.

### 7.3.3 Mid Speed Range

With an all-speed governor, the stability margins form a continuum covering the whole of the engine full load speed range and stability at higher engine speeds (point 2 of figure 7.1) is similar to that at maximum speed.

Figure 7.6 shows stability near peak torque speed (point 1 of figure 7.1), assuming a load inertia of 2.5 times engine inertia. When the turbocharger inertia is reduced the stability margin in the boost loop is again reduced and an improvement in the boost actuator response

further reduces the boost loop stability. Interaction actually improves the stability of the boost loop and in the case of reduced turbocharger inertia (lines labelled A-A) will help to maintain sufficient margin in the desired feedback gain operating range. When the boost feedback response of the form used in the section above is combined with reduced turbocharger inertia (lines B-B) the stability margin in the boost loop is insufficient.

## 7.4 Summary

The use of boost pressure instead of trapped air-fuel ratio as the second variable, while compromising the part load fuel economy, considerably simplifies the feedback control of the engine.

Interactions between the boost feedback loop and the speed feedback loop are small in an engine of this type and generally improve stability margin. Feedback control of boost pressure can therefore be applied without the need for multivariable precompensation.

Stability margin in the boost loop is least at the peak torque condition and instability is likely to result at this operating point if a reduced turbocharger inertia is combined with fast actuation and digital control of the turbine inlet area.

Provided that the frequency of transmission torsional resonance is not close to the frequency determining control stability, minimum load inertia seen by an installed engine under load will be several times that of the engine and flywheel alone. This implies that control

instabilities seen on the test bed may not appear under installed conditions.

# 8. DESIGN OF A SUITABLE MULTIVARIABLE DIGITAL CONTROLLER

## 8.1 The Hardware

An Apricot Xi10 microcomputer was used to implement digital control onto the TL11 engine. The computer has an Intel 8086 16-bit microprocessor, an 8087 floating point arithmetic co-processor and 256 kilobytes of random access memory (RAM). A hard disc stores programs, data files etc.

A high-speed, 12 bit analogue-to-digital converter (ADC) was connected to the microcomputer communication bus and linked via a multiplexer to ten input channels. Eight channels may be scanned repeatedly at 40 microseconds per scan - equivalent to a data transfer rate of 2.4 megabaud. Three 12-bit digital-to-analogue converters (DAC's) enable the controller outputs to be converted into voltages to operate the actuators on the engine.

A clock/timer programmable from one microsecond to one second was included to control the ADC, but timing pulses originating from the engine flywheel may also be used (flywheel markers are less prone to error due to torsional oscillations than markers located at the free end of the crankshaft).

The specification is higher than will be required for production automotive diesel engines since the same equipment is to be used for a wide variety of research identification and control work.

## 8.2 The Control Algorithm

The algorithm provides all-speed governing and control of the air-fuel ratio for best efficiency (within the limits of the turndown ratio of the turbine inlet area). Optimum air-fuel ratio, determined from steady-state tests, is specified as a function of engine speed and the difference between this and actual air-fuel ratio is used to generate a corresponding boost pressure error. This optimum air-fuel ratio involves a compromise between combustion efficiency and pumping losses and is generally less than the 30:1 ratio that is optimum for combustion.

The rack position voltage corresponding to the maximum torque curve is specified as a function of speed, but during transients (and at low speed, high load) the maximum fuelling may be overridden by the need to maintain a minimum specified air-fuel ratio. In addition the rate of change of rack position and turbine inlet area are limited.

Engine speed demand voltage is input via the ADC and the speed error can be integrated, if required, for more accurate steady state speed control.

In order to calculate trapped air-fuel ratio the controller requires knowledge of the volumetric efficiency (specified at a function of engine speed), swept volume and the inlet manifold boost pressure and temperature. In addition fuelling (in mg per shot) needs to be known as a function of speed and rack voltage, but this can be simplified since accurate knowledge of the air-fuel ratio is required only at medium and

high loads; at low loads exhaust opacity is not a problem and turbine area has little effect on air-fuel ratio. A flow diagram of the algorithm is given in figure 8.1.

The following relationships are assumed for the TL11 engine with Majormec fuel injection pump:

$$\eta_{vol} = 0.93 - 0.9 \times 10^{-7} (N_E - 1500)^2$$

$$(AFR)_{opt} = 29 \qquad [N_E > 2100 \text{ rev/min}]$$

$$= 29 - 0.2 \times 10^{-6} (N_E - 2100)^2 \qquad [1100 < N_E < 2100]$$

$$= 22.5 \qquad [N_E < 1100]$$

$$m_f = 10 - m_f' \left[\frac{V_{x_f} - 3.13}{5.67 - 3.13}\right] \text{ mg/shot}$$

where $m_f'$ is the fuelling when $V_{x_f} = 5.67$

$$m_f' = 103 - 0.005 (N_E - 1500) (1 - 0.21 \times 10^{-5} (N_E - 1500)^2)$$

To reduce signal noise all inputs were scanned eight times in quick succession; the first scan was discarded, since data in the first scan was occasionally corrupted, and the remaining scans were averaged to obtain the inputs to the algorithm. In addition, small values of speed error and boost error were divided by three; this effectively reduces the gain applied to signal noise and makes for smoother engine running, and reduced actuator wear. Larger values of the errors were reduced by the amount necessary to avoid discontinuity of the gain values.

high loads; at low loads exhaust opacity is not a problem and turbine area has little effect on air-fuel ratio. A flow diagram of the algorithm is given in figure 8.1.

The following relationships are assumed for the TL11 engine with Majormec fuel injection pump:

$$\eta_{vol} = 0.93 - 0.9 \times 10^{-7} (N_E - 1500)^2$$

$$(AFR)_{opt} = 29 \qquad [N_E > 2100 \text{ rev/min}]$$

$$= 29 - 0.2 \times 10^{-6} (N_E - 2100)^2 \qquad [1100 < N_E < 2100]$$

$$= 22.5 \qquad [N_E < 1100]$$

$$m_f = 10 - m_f' \left[ \frac{V_{x_f} - 3.13}{5.67 - 3.13} \right] \text{ mg/shot}$$

where $m_f'$ is the fuelling when $V_{x_f} = 5.67$

$$m_f' = 103 - 0.005 \ (N_E - 1500) \ (1 - 0.21 \times 10^{-5} (N_E - 1500)^2)$$

To reduce signal noise all inputs were scanned eight times in quick succession; the first scan was discarded, since data in the first scan was occasionally corrupted, and the remaining scans were averaged to obtain the inputs to the algorithm. In addition, small values of speed error and boost error were divided by three; this effectively reduces the gain applied to signal noise and makes for smoother engine running, and reduced actuator wear. Larger values of the errors were reduced by the amount necessary to avoid discontinuity of the gain values.

## 8.3 Scaling and Precompensation.

The controller can operate without multivariable precompensation and in this case control is effectively by two independent feedback loops (although the boost error depends on the output signal to the rack actuator). However, since the controller operates by controlling air-fuel ratio rather than boost pressure the stability of the feedback control system will correspond to the analysis with air-fuel ratio as the second variable. Since this analysis (Section 6.3.2) indicated insufficient gain margin at high load, high speed (particularly if the load inertia is small) it was decided to include a precompensator matrix with non-dynamic terms to reduce the effect of interaction on the control stability. Inverting the steady state gain matrix often results in a beneficial precompensator; in this case since the matrix of steady state voltage gains had been found to be singular (section 6.2.2), it was necessary to apply scaling before inverting the matrix.

Table 8.1 shows suitable input and output scaling matrices, $S_i$ and $S_o$ respectively, determined at different engine operating points. The elements of $S_o$ do not vary greatly and may be approximated by fixed values of 0.8 and 0.18 for the diagonal elements.

The steady state gain matrix G(0) has been determined from experimental results:

$$Y(0) = G(0)\ U(0)$$

where Y is the vector of engine outputs

U is the vector of engine inputs

Scaling is applied to G(0) to obtain the best diagonalising of G*(0):

$$G(0) = S_o G^*(0) S_i$$

In order to calculate the engine inputs (i.e. control outputs) necessary to achieve the desired outputs (i.e. the reference values of the control inputs) it is necessary to invert:

$$U(0) = (G^*(0)S_i)^{-1} S_o^{-1} Y(0)$$

Table 8.2 gives the values of the matrices $G^*(0)S_i$ and $(G^*(0)S_i)^{-1}$ when the value of $S_o$ is fixed as above. The controller input scaling, $S_o^{-1}$, has diagonal elements of 1.15 and 5.55, which can be simplified conveniently to the integer values 1 and 5. This means that input scaling need only be applied to the boost error value. Output scaling can be combined with the precompensator matrix.

Applying less weight to the values at 1600 rev/min, where interaction has less effect, the resulting terms of the precompensator matrix, $(G^*(0)S_i)^{-1}$ may be approximated by:

$$P_{11} = 2.0 - 0.7 \times 10^{-3} N_E$$
$$P_{12} = -0.5 + 0.28 \times 10^{-3} N_E$$
$$P_{21} = -1.1 + 0.45 \times 10^{-3} N_E$$
$$P_{22} = 0.7 - 0.3 \times 10^{-3} N_E$$

In order to vary the gain in the speed feedback loop with engine load,

an extra term was introduced into the relationship for $p_{11}$ :-

$$P_{11} = (2.0 - 0.7 \times 10^{-3} N_E)\ (0.25 + 0.75\ \frac{V_{x_f}}{6})$$

During program initialising the precompensator terms are multiplied by the appropriate constant feedback gains.

8.4 Program execution time.

The program consists of 400 lines of FORTRAN (See appendix VI) of which 200 are repeated each sample period. This repeating section executes in about 10 milliseconds, allowing cylinder-to-cylinder control at engine speeds up to 2000 rev/min on a 6-cylinder four-stroke engine. This has been achieved by using 16-bit integer numbers wherever possible and placing repeated calculations in the initialising part of the program. Real numbers are used when necessary for accuracy. Further reductions in computing time may be achieved by, for example, omitting actuator slew rate control and integral action and averaging three rather than seven scans of the input signals.

To reduce the time delay between the sampling of the engine outputs and the resulting output of new voltages to the actuators, the calculation of slowly-varying parameters such as volumetric efficiency, optimum air-fuel ratio and precompensator terms is carried out after the outputs have been put to the DAC'S.

The engine flywheel has just one timing marker and the extra two sampling instants per revolution are generated by means of the timer.

The timer periods are determined from the known instantaneous engine speed and corrected for the execution time that elapses before the timer is set.

## 8.5 Controller Performance

The controller gave smooth control at engine speeds up to nearly 2000 rev/min. When sampling was not synchronised to the flywheel pulses, a sample frequency of 25 Hz was insufficient to give smooth control; increasing the sample frequency to 75 Hz gave smoothness of engine running equal in smoothness to that obtained with the analogue controllers installed with the test cell instrumentation. Sampling once per cylinder firing, synchronised with the engine marker also gave smooth control.

Several tests were carried out with the digital controller where a step increase in demand speed was applied. The feedback gains were adjusted to values suitable for automotive use i.e., approximately 0.8 mg/shot per rev/min and 2 mm turbine area actuator movement (18% of maximum turbine inlet area) per air-fuel ratio. In order to obtain a consistent time base for the data, sampling frequency was fixed at 80 Hz and not synchronised with the engine cycle.

Figure 8.2 shows the engine response with multivariable, digital control compared with the response obtained with the test cell analogue speed controller (without control of turbine area). Engine speed is stepped from 1200 to about 1900 rev/min along a windage curve of the dynamometer. There is little to choose between the two responses, since

the feedback gains in the speed loops are similar. With the digital controller, however, it is possible to increase the gain at higher engine fuellings without causing instability at part load (since the gain can be varied with operating point) and the best performance with the digital controller is better than that achievable with analogue control. In applications where exhaust opacity must be limited, the resulting improvement in engine performance may not be great.

The boost signal appears very noisy; much of the fluctuation is removed when the controller sampling points are synchronised with the engine cycle. The inlet manifold pressure is subject to large fluctuations resulting from the unsteady outflow as the airflow is alternately restricted and released and switched from one inlet port to another. The fluctuations have the same periodicity as the engine firing, so that sampling once per firing significantly reduces the variation seen by the controller. Sampling the inlet manifold pressure shortly before IVC for each cylinder would enable a good estimate to be obtained of the air mass to be trapped in that cylinder.

Figure 8.3 shows the effect of changing the minimum air-fuel ratio specified to the controller from 19:1 to 18:1. Maximum fuelling is cut back slightly and exhaust opacity significantly reduced without a large change in speed response.

The instability predicted when feedback control of air-fuel ratio is used and the engine is operating at high speed, high load with a small inertia (section 6.3.2) was not noticed on the test bed, but this may be a result of the conservative slew rate limit applied to the turbine

inlet area actuator (full actuator movement in 0.5 seconds).

# 9. CONCLUSIONS AND FURTHER WORK

## 9.1 Overview

The stability of a turbocharged automotive (200-250kW) diesel engine with variable geometry turbine under feedback control has been examined. Towards this end, frequency response measurements have been made on such an engine.

Frequency response measurements were used because of their particular advantages in identifying non-linear systems and because they allow greater insight into the dynamic behaviour of the system to be gained (than when step responses alone are used). A significant contribution to the use and interpretation of frequency response measurements on internal combustion engines, particularly diesel engines, has been made. These include dynamic torque and smoke responses and, it is believed, the first experimental measurements to be published of engine response to turbine area perturbations. The results give further insight into the dynamic behaviour of turbocharged diesel engines.

## 9.2 Engine Frequency Response Results

All the engine transfer functions, except that of the engine speed response to turbine inlet area under certain conditions, were found to be dominated by a single first order response and the time constants have been related to the inertia of the engine (with its load) and of the turbocharger. The exact break frequency depends on the dynamometer load-speed characteristic and the variation of fuelling and thermal

efficiency with engine speed. The turbocharger time constant depends on the normalised variations of the turbine and compressor torque with turbocharger speed; the difference between these two is approximately unity.

The slope of the gain curve in the response of boost pressure to fuel rack perturbation is significantly steeper than the -20 db/decade of a first order system and it has been shown that this is a result of the variations in engine speed.

Frequency responses of dynamic engine torque (or dynamic mean effective pressure - d.m.e.p.) have been derived from measured shaft torque and engine speed responses. These show a substantial drop in engine torque amplitude with frequency at most engine operating points. The changes in slope of these responses correspond with the changes of slope in the boost and engine speed responses, the greater effect being associated with the speed changes. Attempting to predict the speed-related effects by taking account of the variations with speed of fuelling, thermal efficiency and pumping losses proved fruitless and indicated that wall temperature effects (on volumetric efficiency, f.m.e.p. and thermal efficiency) must dominate the dynamic torque response and cause the measured 6-8 db (50-60%) attenuation above 2 Hz. The time constant of the wall temperature variation is estimated in this case to be close to that of the speed responses, so that it is difficult to distinguish between the two effects in the frequency response plots. In order to successfully predict dynamic torque using computer simulations it will be necessary to take account of these effects of temperature on frictional losses.

The phase curve in the dmep response is not that of a pure time delay, but when the phase corresponding to the slope of the gain curve is subtracted, the resulting phase curve is very close to that of a pure time delay - the diesel torque delay. The average measured value was 69 degrees CA, and if the extra delay is added to allow for sampling at the beginning, instead of at the end, of injection then the total delay is close to 80 degrees CA. On top of this is a random delay of up to one firing period, when step changes in rack position take place that are not synchronised with the instants at which the fuel injection pump samples the fuel rack position. The results support the value suggested by Garvey of between 90 degrees CA and 90 degrees CA plus one firing period.

Inverse transformation of the dmep response indicated that 95% of steady state torque would not be achieved until 0.75 seconds after a step change in fuelling. Averaging the loss in torque over 4 seconds gave a mean loss of 4.5% of the final (steady state) value, and this compared well with the 5% loss that Winterbone et al had to introduce into their simulations to correctly predict the transient performance of a turbocharged diesel engine.

Frequency response of the exhaust opacity to fuel rack perturbation showed clearly the dependence of opacity on a negative power of the air-fuel ratio, as Watson had assumed and O'Neill had shown previously. In this case the index in the relationship while mainly being in the range -2 to -4 was found to increase substantially as the mean air-fuel ratio decreased (and mean opacity increased). The index varied approximately linearly with a simple parameter representing injection

spray penetration.

## 9.3 Feedback Control Stability

Feedback control of engine speed and boost pressure was shown to suffer only small effects from the interactions between the two feedback loops. The interaction was shown, in this case, to actually improve the stability margin of the feedback control system, so that precompensation is not necessary and it is possible to bolt a VG turbocharger with built-in boost pressure control unit onto the engine without the need to interface with the engine speed governor.

If air-fuel ratio is chosen as the second control variable, instead of boost pressure, the interaction between the feedback loops is greater and is detrimental to the stability of the control system. The worst engine operating point for stability was shown to be when the engine operates at high speed and high load and the analysis indicated instability under these conditions, when the load inertia is small. Future reductions in the moment of inertia of the turbocharger rotor will reduce the stability margin further, and multivariable precompensation may be necessary to avoid large reductions in the air-fuel ratio feedback again.

Scheduling the turbine inlet area according to engine speed was shown to have a negligible effect on the stability of the speed governing loop.

## 9.4 A Digital Multivariable Controller

A control program has been written for a digital controller, giving feedback control of engine speed and air-fuel ratio and the controller has been successfully implemented on the engine, giving smooth control at speeds up to 2000 rev/min. The engine transfer function voltage gain matrix was found to be singular when the boost pressure, engine speed and actuator signals are all normalised to the 0 to 10 V range. As a result the controller incorporates input scaling as well as precompensation to reduce the effect of interaction on steady state errors (and stability).

The controller is able to give better response than that achievable with standard electronic analogue control; this is a result, not so much of the precompensation, but of the ability to vary the feedback gain in the speed control path with engine fuelling.

## 9.5 Further Work

More work needs to be done to clarify the mechanisms by which the dynamic m.e.p. is attenuated during transients. Steady state tests where the effect of engine coolant temperature on b.m.e.p. is measured will enable a qualitative appreciation of the effect of cylinder wall temperature on f.m.e.p. to be gained. Quantitative results will require direct measurements of the cylinder wall and ring groove temperatures, and possibly also of the temperature of the oil in the sump. It would also be worth looking at the d.m.e.p. response of an engine having markedly different wall temperature behaviour, e.g. one with ceramic

liner coatings. The effect of oil pressure on f.m.e.p. should be investigated too.

Measurement of wall temperatures will also allow a more accurate determination of the time constant of cylinder wall temperature variations.

In order to predict more accurately the time constant of the turbocharger speed (and boost) responses, the variation of compressor and turbine torques with turbocharger speed needs to be investigated.

Once the above effects have been quantified, it will be possible to develope a simple program predicting frequency responses of engine speed, boost pressure, d.m.e.p. and exhaust opacity for turbocharged automotive DI diesel engines. The effect of load inertia and load-speed characteristics can be predicted.

The analysis of stability under multi-loop feedback control should be extended to petrol engines, where torque is related closely to boost pressure, and to medium speed diesel engines, where, as a result of the increased valve overlap period, back pressure has a significant effect on trapped air mass and torque. In both cases interaction between feedback loops is likely to be much greater than is the case with the automotive diesel.

The feedback control of exhaust opacity should be attempted, in order to obtain maximum acceleration within given constraints on exhaust opacity. The feedback control of engine torque should also be attempted

since this allows automatic tuning of parameters to give optimum torque and, therefore, efficiency. D.m.e.p. as defined in this work cannot be measured directly; the best obtainable measure of dynamic torque is probably to detect torque at a point in the crankshaft just behind the flywheel. Monitoring this torque will also make possible powerful diagnostic features - e.g. in detecting malfunctioning fuel injectors or cylinder bores that are picking up.

For the turbocharged automotive diesel engine the air-fuel ratio giving the best efficiency is a compromise between the effects of air-fuel ratio and pumping losses on thermal efficiency. The variation of optimum air-fuel ratio with ambient temperature and altitude for a given turbocharger needs to be investigated.

REFERENCES

1. FULLER, A.T., 'The early development of control theory', Trans. ASME, J. of Dyn. Sys., Meas. and Control, Vol. 98, June 1976, pp 109-118.

2. BUCHI, A., 'Uber Brennkraftmaschinen', Zeitung Gasturbinenwesen, 1969

3. WALLACE, F.J., WAY, R.J.B. and BAGHERY, A., 'Variable geometry turbocharging - the realistic way forward', SAE paper 810336, 1981.

4. FLAXINGTON, D. and SZCZUPAK, D.T., 'Variable area radial inflow turbines', Turbocharging and Turbochargers Conf., I. Mech. E., 1982.

5. WATSON, N., Course notes, Turbocharging course, Imperial College, London, Sept. 1984.

6. CLERK MAXWELL, J., 'On Governors', Proc. Roy. Soc., Vol. 16, p270, 1868.

7. ROUTH, E.J., 'On the stability of motion' (Adams Prize Essay), Macmillan, London, 1877.

8. NYQUIST, H., 'Regeneration Theory', Bell Syst. Tech. J., Vol 13, pl, 1932.

9. BODE, H.W., Network Analysis and Feedback Amplifier Design, Van Nostrand, Princeton, N.J., 1945.

10. BENZ, W., 'Der Einfluss der verzogerten Drehmomentabgabe auf die Stabilität der Regulierung', MTZ, Jahrg. 17, Heft 1 (January), 1956.

11. WELBOURN, D.B. and ALLEN-WILLIAMS, D.J., 'The application of simple control theory to the governing of diesel engines', Proc. of Conf. 'Regelungstechnik', Heidelberg, 1957.

12. BUJAK, J.Z., 'The variable speed hydraulic governor', Proc. I. Mech. E., Vol 153, p193, 1945.

13. WELBOURN, D.B., Discussion to Bowns et al (ref. 19).

14. MASSEY, A.G. and OLDENBURGER, R., 'Scientific design of a diesel governor', ASME paper 58-OGP-11, 1958.

15. WELBOURN, D.B., ROBERTS, D.K. and FULLER, R.A., 'The governing of compression ignition oil engines', Proc. I. Mech. E., Vol 173, p575, 1959.

16. TAYLOR, G.W., 'Development of a speed and load sensing governor', ASME paper 60-OGP-4, 1960.

17. BENZ, W., 'Stabilitätsuntersuchungen für die Drehzahlregulierung von Verbrennungskraftmaschinen', MTZ, Jahrg. 22, Heft 8 (August), 1961.

18. BENZ. W., 'Stabilitätsuntersuchung der Drehzahlregulierung, insbesondere bei parallelgeschaltenen Diesel-Elektroaggregaten', MTZ, Jahrg. 25, Heft 10 (October), 1964.

19. BOWNS, D.E., 'The dynamic transfer characteristics of reciprocating engines,' Proc. I. Mech. E., Vol. 185, paper 16/71, pp 185-201, 1970-71.

20. HAZELL, P.A. and FLOWER, J.O., 'Sampled data theory applied to the modelling and control analysis of compression ignition engines -Part I', Int. J. Control, Vol 13, No. 3, pp 549-562, 1971.

21. FLOWER, J.O. and HAZELL, P.A., 'Sampled data theory applied to the modelling and control analysis of compression ignition engines -Part II', Int. J. Control, Vol 13, No. 4, pp 609-623, 1971.

22. LEDGER, J.D. and WALMSLEY, N.D., 'Computer simulation of turbocharged diesel engines operating under transient load conditions', SAE paper 710177, 1971.

23. BOWNS, D.E., CAVE, P.R., HARGREAVES, M.R.O. and WALLACE, F.J., 'Transient characteristics of turbocharged diesel engines', I. Mech. E. conf. on Engine Performance Modelling, paper C143/73, p 13-23, London, 1973.

24. WATSON, N. and MARZOUK, M., 'A non-linear digital simulation of turbocharged diesel engines under transient conditions', SAE paper 770123, 1977.

25. WINTERBONE, D.E., THIRUAROORAN, C. and WELLSTEAD, P.E. 'A wholly dynamic model of a turbocharged diesel engine for transfer function evaluation ', SAE paper 770124, 1977.

26. THIRUAROORAN, C., 'Control studies of a turbocharged diesel engine', Ph.D. thesis, UMIST, 1978.

27. ALDREN, D.B., 'Control studies of a turbocharged diesel engine', M.Sc. Dissertation, UMIST, 1977.

28. WATSON, N., 'Dynamic turbocharged diesel engine simulator for electronic control system development', ASME J. of Dyn. Sys., Meas. and Control, Vol 106, pp 27-41, ASME paper no. 83 - WA/DSC-1, 1984.

29. WINDETT, G.P. and FLOWER, J.O., 'Sampled-data frequency response measurements of a large diesel engine', Int. J. Control, Vol 19, No. 6, pp 1069-1086, 1974.

31. SAWA, N. and HORI, S., 'Measurement of transfer time constant of effective torque in internal combustion engines', Bull. JSME, Vol 26, No 215, pp 805-811, May 1983.

32. FLOWER, J.O., WINDETT, G.P. and FORGE, S.C., 'Aspects of the frequency response testing of simple sampled systems', Int. J. Control, Vol 14, No. 5, pp881-896, 1971.

33. FLOWER, J.O., and WINDETT, G.P. 'Dynamic measurements of a large diesel engine using p.r.b.s. techniques. Part 2; Instrumentation, experimental techniques and results'. Int. J. Control, Vol 24, No 3, pp 393-404, 1976.

34. WINTERBONE, D.E., MUNRO, N. and NUSKE, D.J., 'A multivariable controller for an automotive gas turbine', ASME paper 79-GT-73, Gas Turbine Conf., San Diego, 1979.

35. FLOWER, J.O. and WINDETT, G.P., 'Dynamic measurements of a large diesel engine using p.r.b.s. techniques. Part 1; Development of theory for closed loop sampled systems', Int. J. Control, Vol 24, No 3, pp 379-392, 1976.

36. IVES, A.P. and TRENNE, M.V., 'Closed loop electronic control of diesel fuel injection', I. Mech. E. Conference paper C201/78, 1978.

37. DAY, E. and FRANK, H.L., 'Electronic diesel fuel controls', SAE paper 820905 (SAE special publication P-111),1982.

38. KIHARA, R., MIKAMI, Y. and NAKAO, H., 'The performance advantages of electronic control diesel engine for passenger cars', SAE paper 830528, 1983.

39. WALZ, L., WESSEL, W. and BERGER, J., 'Progress in electronic diesel control', SAE paper 840442, 1984.

40. SHIOZAKI, M., HOBO, N. and AKAHORI, I., 'Development of a fully capable electronic control system for diesel engines.' SAE paper 850172, 1985.

41. GARVEY, D.C. 'A digital control algorithm for diesel engine governing', SAE paper 850174, 1985.

42. PIPHO, M.J. and KITTELSON, D.B., 'Closed loop digital electronic control of diesel engine timing', SAE paper 830579, 1983.

43. ZANKER, and WELLSTEAD, P.E., 'A self-tuning governor for a diesel engine', Chap. 12, Self-Tuning and Adaptive Control (Harris and Billings, Eds.), 2nd Ed., Peter Peregrinus, Stevenage, 1985.

44. WEBB, C.R. and JANOTA, M.S., 'Governors with load sensing', Proc. I. Mech. E., Vol 184, Pt 1, No 9, pp 161-174, 1969-70

45. BLAIR, J.R.,'Governing: an examination of a torque feed-forward loop', Proc. I. Mech. E., Vol 186, No. 47/72, pp603-622, 1972.

9. BODE, H.W., Network Analysis and Feedback Amplifier Design, Van Nostrand, Princeton, N.J., 1945.

10. BENZ, W., 'Der Einfluss der verzogerten Drehmomentabgabe auf die Stabilität der Regulierung', MTZ, Jahrg. 17, Heft 1 (January), 1956.

11. WELBOURN, D.B. and ALLEN-WILLIAMS, D.J., 'The application of simple control theory to the governing of diesel engines', Proc. of Conf. 'Regelungstechnik', Heidelberg, 1957.

12. BUJAK, J.Z., 'The variable speed hydraulic governor', Proc. I. Mech. E., Vol 153, p193, 1945.

13. WELBOURN, D.B., Discussion to Bowns et al (ref. 19).

14. MASSEY, A.G. and OLDENBURGER, R., 'Scientific design of a diesel governor', ASME paper 58-OGP-11, 1958.

15. WELBOURN, D.B., ROBERTS, D.K. and FULLER, R.A., 'The governing of compression ignition oil engines', Proc. I. Mech. E., Vol 173, p575, 1959.

16. TAYLOR, G.W., 'Development of a speed and load sensing governor', ASME paper 60-OGP-4, 1960.

9. BODE, H.W., Network Analysis and Feedback Amplifier Design, Van Nostrand, Princeton, N.J., 1945.

10. BENZ, W., 'Der Einfluss der verzogerten Drehmomentabgabe auf die Stabilität der Regulierung', MTZ, Jahrg. 17, Heft 1 (January), 1956.

11. WELBOURN, D.B. and ALLEN-WILLIAMS, D.J., 'The application of simple control theory to the governing of diesel engines', Proc. of Conf. 'Regelungstechnik', Heidelberg, 1957.

12. BUJAK, J.Z., 'The variable speed hydraulic governor', Proc. I. Mech. E., Vol 153, p193, 1945.

13. WELBOURN, D.B., Discussion to Bowns et al (ref. 19).

14. MASSEY, A.G. and OLDENBURGER, R., 'Scientific design of a diesel governor', ASME paper 58-OGP-11, 1958.

15. WELBOURN, D.B., ROBERTS, D.K. and FULLER, R.A., 'The governing of compression ignition oil engines', Proc. I. Mech. E., Vol 173, p575, 1959.

16. TAYLOR, G.W., 'Development of a speed and load sensing governor', ASME paper 60-OGP-4, 1960.

17. BENZ, W., 'Stabilitätsuntersuchungen für die Drehzahlregulierung von Verbrennungskraftmaschinen', MTZ, Jahrg. 22, Heft 8 (August), 1961.

18. BENZ. W., 'Stabilitätsuntersuchung der Drehzahlregulierung, insbesondere bei parallelgeschaltenen Diesel-Elektroaggregaten', MTZ, Jahrg. 25, Heft 10 (October), 1964.

19. BOWNS, D.E., 'The dynamic transfer characteristics of reciprocating engines,' Proc. I. Mech. E., Vol. 185, paper 16/71, pp 185-201, 1970-71.

20. HAZELL, P.A. and FLOWER, J.O., 'Sampled data theory applied to the modelling and control analysis of compression ignition engines -Part I', Int. J. Control, Vol 13, No. 3, pp 549-562, 1971.

21. FLOWER, J.O. and HAZELL, P.A., 'Sampled data theory applied to the modelling and control analysis of compression ignition engines -Part II', Int. J. Control, Vol 13, No. 4, pp 609-623, 1971.

22. LEDGER, J.D. and WALMSLEY, N.D., 'Computer simulation of turbocharged diesel engines operating under transient load conditions', SAE paper 710177, 1971.

23. BOWNS, D.E., CAVE, P.R., HARGREAVES, M.R.O. and WALLACE, F.J., 'Transient characteristics of turbocharged diesel engines', I. Mech. E. conf. on Engine Performance Modelling, paper C143/73, p 13-23, London, 1973.

24. WATSON, N. and MARZOUK, M., 'A non-linear digital simulation of turbocharged diesel engines under transient conditions', SAE paper 770123, 1977.

25. WINTERBONE, D.E., THIRUAROORAN, C. and WELLSTEAD, P.E. 'A wholly dynamic model of a turbocharged diesel engine for transfer function evaluation ', SAE paper 770124, 1977.

26. THIRUAROORAN, C., 'Control studies of a turbocharged diesel engine', Ph.D. thesis, UMIST, 1978.

27. ALDREN, D.B., 'Control studies of a turbocharged diesel engine', M.Sc. Dissertation, UMIST, 1977.

28. WATSON, N., 'Dynamic turbocharged diesel engine simulator for electronic control system development', ASME J. of Dyn. Sys., Meas. and Control, Vol 106, pp 27-41, ASME paper no. 83 - WA/DSC-1, 1984.

29. WINDETT, G.P. and FLOWER, J.O., 'Sampled-data frequency response measurements of a large diesel engine', Int. J. Control, Vol 19, No. 6, pp 1069-1086, 1974.

31. SAWA, N. and HORI, S., 'Measurement of transfer time constant of effective torque in internal combustion engines', Bull. JSME, Vol 26, No 215, pp 805-811, May 1983.

32. FLOWER, J.O., WINDETT, G.P. and FORGE, S.C., 'Aspects of the frequency response testing of simple sampled systems', Int. J. Control, Vol 14, No. 5, pp881-896, 1971.

33. FLOWER, J.O., and WINDETT, G.P. 'Dynamic measurements of a large diesel engine using p.r.b.s. techniques. Part 2; Instrumentation, experimental techniques and results'. Int. J. Control, Vol 24, No 3, pp 393-404, 1976.

34. WINTERBONE, D.E., MUNRO, N. and NUSKE, D.J., 'A multivariable controller for an automotive gas turbine', ASME paper 79-GT-73, Gas Turbine Conf., San Diego, 1979.

35. FLOWER, J.O. and WINDETT, G.P., 'Dynamic measurements of a large diesel engine using p.r.b.s. techniques. Part 1; Development of theory for closed loop sampled systems', Int. J. Control, Vol 24, No 3, pp 379-392, 1976.

36. IVES, A.P. and TRENNE, M.V., 'Closed loop electronic control of diesel fuel injection', I. Mech. E. Conference paper C201/78, 1978.

37. DAY, E. and FRANK, H.L., 'Electronic diesel fuel controls', SAE paper 820905 (SAE special publication P-111),1982.

38. KIHARA, R., MIKAMI, Y. and NAKAO, H., 'The performance advantages of electronic control diesel engine for passenger cars', SAE paper 830528, 1983.

39. WALZ, L., WESSEL, W. and BERGER, J., 'Progress in electronic diesel control', SAE paper 840442, 1984.

40. SHIOZAKI, M., HOBO, N. and AKAHORI, I., 'Development of a fully capable electronic control system for diesel engines.' SAE paper 850172, 1985.

41. GARVEY, D.C. 'A digital control algorithm for diesel engine governing', SAE paper 850174, 1985.

42. PIPHO, M.J. and KITTELSON, D.B., 'Closed loop digital electronic control of diesel engine timing', SAE paper 830579, 1983.

43. ZANKER, and WELLSTEAD, P.E., 'A self-tuning governor for a diesel engine', Chap. 12, Self-Tuning and Adaptive Control (Harris and Billings, Eds.), 2nd Ed., Peter Peregrinus, Stevenage, 1985.

44. WEBB, C.R. and JANOTA, M.S., 'Governors with load sensing', Proc. I. Mech. E., Vol 184, Pt 1, No 9, pp 161-174, 1969-70

45. BLAIR, J.R.,'Governing: an examination of a torque feed-forward loop', Proc. I. Mech. E., Vol 186, No. 47/72, pp603-622, 1972.

46. LEDGER, J.D., BENSON, R.S. and WHITEHOUSE, N.D., 'Dynamic modelling of a turbocharged diesel engine', Paper C142/73, I. Mech. E. conf. on Engine Performance Modelling, London, 1973.

47. GANT, G.C., 'The governing of diesel engines', Chap. 4 of Principles and Performance in Diesel Engineering (Haddad, S.D. and Watson, N., Eds.), Ellis Horwood, Chichester, 1984.

48. GANT, G.C., private communication.

49. ECKERT, K. and GAUGER, R., 'Das Drehmomentverhalten ein nichtaufgeladenen Dieselmotors bei sinusformig schwankenden Einspritzmengen', MTZ, Jahrg. 26, Heft 7 (July), 1965.

50. BALESTRINO, A., EISINBERG, A. and SCIAVICCO, L., 'A new approach to modelling of internal combustion engines', Fourth Int. Symp. on Engine Test Automation. Vol 2; Performance, Emissions and Diagnostics, Naples, 1975.

51. WINTERBONE, D.E., BENSON, R.S., CLOSS, G.D. and MORTIMER, A.G., 'A comparison between experimental and analytical transient test results for a turbocharged diesel engine', Proc. I. Mech. E., Vol 190, No 22/76, 1976.

52. CHANG, M-F. and SELL, J.A., 'A linearised model of engine torque and carbon monoxide emissions', SAE paper 830427, 1983.

53. MARZOUK, M. and WATSON, N., 'Load acceptance of turbocharged diesel engines', I Mech. E. conf. on Turbochargers and Turbocharging, paper C54/78, 1978.

54. WATSON, N., 'Transient performance simulation and analysis of turbocharged diesel engines, ' SAE paper 810338, 1981.

55. WINTERBONE, D.E. and TENNANT, W.H., 'The variation of friction and combustion rates during diesel engine transients', SAE paper 810339, 1981.

56. WHITEHOUSE, N.D. and WAY, R.J.B. 'A simple method for the calculation of heat release rates in diesel engines based on fuel injection rate', SAE paper 710134, 1971.

57. O'NEILL, G., 'Measurement and prediction of exhaust smoke of a turbocharged diesel engine', M.Sc. dissertation, UMIST, 1974.

58. HOFF-CLAUSEN, N.E., 'On modeling and model identification of a turbocharged diesel engine system', M.Sc. dissertation, Control Systems Centre, UMIST, 1977.

59. LEDGER, J.D., BENSON, R.S. and FURUKAWA, H., 'Improvement in transient performance of a turbocharged diesel engine by air injection into the compressor', SAE paper 730665, 1973.

60. WALLACE, F.J., WINKLER, G. and BOWNS, D.E., 'Multivariable control for engine transmission systems with infinitely variable ratios', SAE paper 770752, 1977.

61. KIDD, P.T., MUNRO, N. and WINTERBONE, D.E. 'Multivariable control of a ship propulsion system', Proc. 6th Ship Control Systems Symp., Ottawa, Canada, 1981.

62. KIDD, P.T., MUNRO, N., THIRUAROORAN, C. and WINTERBONE, D.E., 'Linear modeling of ship propulsion plants', Proc. I. Mech. E., Vol 199, No A1, paper 21/85, 1985.

63. WINTERBONE, D.E., MUNRO, N. and LOURTIE, P.M.G., 'A preliminary study of the design of a controller for an automotive gas turbine', ASME paper 73-GT-14, 1973.

64. WINTERBONE, D.E., MUNRO, N. and NUSKE, D.J., 'A multivariable controller for an automotive gas turbine', ASME paper 79-GT-73, 1979.

65. MISCHKE, A. and FRANKLE, G., 'Elektronische Dieselregelung EDR fur Nutzfahrzeuge', ATZ, Vol 85, No 9, pp539-548, 1983.

66. TRENNE, M.U. and NOWAK, V.J., 'An overview of electronic controls for passenger car diesel engines', IEEE conf. on Vehicular Technology Society, 1980.

67. PATEL, R.V. and MUNRO, N., Multivariable System Theory and Design, Chap. 9, Pergamon Press, Oxford, 1982.

68. EDMUNDS, J.H.,'Frequency responses to minimise output disturbances caused by parameter variations and noise', Int. J. Control, Vol 38, No 1, pp 47-60, 1983.

69. RAVEN, F.H., Automatic Control Engineering, McGraw-Hill, New York, 1961.

70. ROSENBROCK, H.H., Computer Aided Control System Design, Academic Press, London, 1974.

71. MACFARLANE, A.D.J. (Ed), Complex Variable Methods for Linear Multivariable Feedback Systems, Taylor and Francis, London, 1980.

72. OLDENBURGER, R.C., 'Frequency response data, standards and design criteria', ASME paper 53-All, 1953.

73. WINTERBONE, D.E. and TENNANT, D.W.H. 'The variation of friction and combustion rates during engine transients'. SAE paper 810339, 1981.

74. CAMPBELL, N., Ph. D. thesis, Bath University, to be submitted.

75. SHEARER, J.L., Fluid Power Control, MIT Press, Cambridge, Mass., 1960.

76. BOWNS, D.E. and WORTON-GRIFFITHS, J., 'The dynamic characteristics of a hydrostatic transmission system', Proc.I. Mech.E., Vol 186, No 55/72, pp755-773, 1972.

77. BACKHOUSE, R.J. and WINTERBONE, D.E. 'Dynamic behaviour of a turbocharged diesel engine', SAE paper 860453, 1986.

78. PALMOR, Z.J. and SHINNAR, R., 'Design and tuning of dead-time compensators', Joint Automatic Control Conf. (JACC),Vol 2, pp59-70, 1978.

79. WATSON, N. and JANOTA, M.S., Turbocharging the Internal Combustion Engine, p389, MacMillan, London, 1982.

80. WELBOURN, D.B., Essentials of Control Theory for Mechanical Engineers, pp97-98, Arnold, London, 1963.

## APPENDIX I

## ESTIMATION OF MANIFOLD TIME CONSTANTS

Welbourn analyses the time constant of a volume filled with gas[80], showing that the time constant is equal to the change in mass in the volume per unit change in pressure, divided by the change in mass flow rate out of the volume per unit change in pressure. For the inlet manifold:-

$$t_{im} = \frac{\partial m_{im}}{\partial p_b} \Big/ \frac{\partial \dot{m}_a}{\partial p_b}$$

$$= \frac{V_{im}}{R_a T_{im}} \Big/ \frac{\eta_{vol} V_{sw} N_E N}{2 \times 60 \times R_a T_{im}}$$

$$= \frac{120\ V_{im}}{N V_{sw} N_E \eta_{vol}}$$

Assume the following values for the TL11 engine:

$$V_{im} \doteqdot 0.006 \ m^3$$
$$V_{sw} = 0.00185 \ m^3$$
$$N = 6$$
$$\eta_{vol} \doteqdot 0.9$$

then

$$t_{im} \doteqdot \frac{72}{N_E} \text{ sec.}$$

At 1600 rev/min this gives a time constant of 25 msec and a break frequency of 6.4 Hz.

For the exhaust manifold

$$t_{exm} = \frac{\partial m_{exm}}{\partial p_{exm}} \Big/ \frac{\partial \dot{m}_{ex}}{\partial p_{exm}}$$

Assuming turbine dimensionless mass flow remains fixed:

$$\frac{\dot{m}_{ex}\sqrt{T_{ti}}}{p_{exm}} = \text{constant}$$

then

$$\frac{\partial \dot{m}_{ex}}{\partial p_{exm}} = \frac{\dot{m}_{ex}}{p_{exm}}$$

and

$$t_{exm} = \frac{V_{exm}}{R_{ex}\, T_{ti}} \Big/ \frac{\dot{m}_{ex}}{p_{exm}}$$

Now

$$\dot{m}_{ex} = \dot{m}_a + \dot{m}_f \doteq 1.03\, \dot{m}_a$$

$$= \frac{1.03\, \eta_{vol}\, V_{sw}\, N_E\, N\, p_b}{120\, R_a\, T_{im}}$$

therefore

$$t_{exm} = 120\, \frac{R_a}{R_{ex}}\, \frac{V_{exm}}{V_{sw} N}\, \frac{p_{exm}}{p_b}\, \frac{T_{im}}{T_{ti}\, 1.03\, \eta_{vol} N_E}$$

$$\frac{t_{exm}}{t_{im}} = \frac{R_a}{R_{ex}} \frac{V_{exm}}{V_{im}} \frac{p_{exm}}{p_b} \frac{\dot{m}_a}{\dot{m}_{ex}} \frac{T_{im}}{T_{ti}}$$

Assume

$$\frac{R_a}{R_{ex}} \doteq 0.95$$

$$\frac{V_{exm}}{V_{im}} \doteq 0.5$$

$$\frac{p_{exm}}{p_b} \doteq 0.8 - 1.0 \text{ at full load}$$

$$\doteq 1.1 - 1.25 \text{ at light load}$$

$$\frac{\dot{m}_a}{\dot{m}_{ex}} \doteq 0.96 \text{ at full load}$$

$$\doteq 0.99 \text{ at light load}$$

$$\frac{T_{im}}{T_{ti}} \doteq 0.5 \text{ at full load}$$

$$\doteq 0.75 \text{ at light load}$$

then

$$\frac{t_{exm}}{t_{im}} \doteq 0.18 - 0.23 \quad \text{at full load}$$

$$\doteq 0.38 - 0.43 \text{ at high load}$$

and

$$t_{exm} \doteq \frac{15}{N_E} \text{ seconds at high load}$$

$$\doteq \frac{30}{N_E} \text{ seconds at light load.}$$

## APPENDIX II

## ESTIMATE OF TIME CONSTANT OF CYLINDER WALL THERMAL INERTIA

If the actual cylinder wall temperature variation is of the order of 20 K at 1600 rev/min, whilst the equilibrium wall temperature varies by about 500 K (one third the amplitude of the mean gas temperature), then, assuming a first order system

$$\text{gain} = \frac{1}{\sqrt{1 + \omega^2 t^2}} = \frac{20}{500}$$

where $\omega$ is the perturbation frequency and $t$ the time constant of the cylinder wall temperature.

$$1 + \omega^2 t^2 = 625$$

$$\omega t = \sqrt{624} \doteq 25$$

therefore

$$t = \frac{25}{\omega} = \frac{25 \times 60 \times 2}{1600 \times 2\pi} \doteq 0.3 \text{ sec.}$$

The corresponding break frequency is 0.5 Hz.

In fact the variation in equilibrium wall temperature is not sinusoidal and the amplitude of the fundamental component will be considerably less

than 500 K. Higher harmonics will contribute little to the actual wall temperature variation, due to the greater attenuation at the higher frequencies.

If the fundamental amplitude is 350 K then

$$t = 0.21 \text{ sec}$$

and the break frequency is 0.76 Hz.

## APPENDIX III

## CORRECTION TO D.M.E.P. RESPONSE TO ALLOW FOR DRIVE SHAFT TWISTING

Figure A3.1 is a diagram of the engine crankshaft, flywheel and dynamometer torsional system. Using the notation of this diagram the calculated dynamic torque may be corrected for lack of torsional stiffness in the drive shaft in the following way:-

Assume:

$$\theta_E - \theta_s = \theta_s - \theta_d = 0.5\ (\theta_E - \theta_d)$$

$$\tau_d = \frac{k_1\, e^{-t\,s}}{1 + t_2 s}\ n_d$$

$$= \frac{k_1\, e^{-t\,s}}{1 + t_2 s}\ \left[ n_s + (n_d - n_s) \right] \qquad \text{(A3.1)}$$

Now

$$\tau_d = \tau_s + k_2\ (\theta_d - \theta_s) \qquad \text{(A.3.2)}$$

where $k_2$ is the torsional stiffness in Nm/radian.

Assuming that the system is linear and that there is a sinusoidal perturbation of frequency $\omega$ rad/sec:-

$$\theta_d - \theta_s = \frac{n_d - n_s}{j\omega} \qquad \text{(A3.3)}$$

Substituting A3.3 into A3.2 and combining with A3.1

$$\tau_s + k_2\ \frac{(n_d - n_s)}{j\omega} = \frac{k_1\, e^{-t\,j\omega}}{1 + t_2 j\omega}\ \left[ n_s + (n_d - n_s) \right]$$

Now

$$n_s = n_E + (n_s - n_E)$$

$$= n_E + (n_d - n_s)$$

then

$$\tau_s - \frac{k_1 e^{-t_1 j\omega}}{1+t_2 j\omega} \; n_E = (n_d - n_s) \left[ \frac{2k_1 e^{-t_1 j\omega}}{1+t_2 j\omega} - \frac{k_2}{j\omega} \right]$$

therefore

$$n_d - n_s = \frac{\left[ \tau_s - \frac{k_1 e^{-t_1 j\omega}}{1+t_2 j\omega} n_E \right]}{\left[ \frac{2k_1 e^{-t_1 j\omega}}{1+t_2 j\omega} - \frac{k_2}{j\omega} \right]} \qquad (A3.4)$$

But

$$\tau_E = \tau_s + k_2 (\theta_E - \theta_s)$$

$$= \tau_s - \frac{k_2 (n_d - n_s)}{j\omega} \qquad (A3.5)$$

Substituting A3.4 into A3.5 gives the dynamic engine torque $\tau_E$ in terms of the measured shaft torque response $\tau_s$ and the measured engine speed response $n_E$ :-

$$\tau_E = \tau_s - \frac{k_2}{j\omega} \; \frac{\left[ \tau_s - k_1 e^{-t_1 j\omega} n_E \right]}{\left[ \frac{2k_1 e^{-t_1 j\omega}}{1+t_2 j\omega} - \frac{k_2}{j\omega} \right]}$$

$$= \tau_s \frac{\left[ \frac{2k_1 e^{-t_1 j\omega}}{1+t_2 j\omega} - \frac{2k_2}{j\omega} \right]}{\left[ \frac{2k_1 e^{-t_1 j}}{1+t_2 j\omega} - \frac{k_2}{j\omega} \right]} + n_E \left[ \frac{k_1 k_2 e^{-t_1 j\omega}}{2k_1 j\omega e^{-t_1 j\omega} - k_2 - k_2 t_2 j\omega} \right]$$

Assume

$$k_2 = 10^4 \text{ Nm/rad}$$

$$t_1 = 0.01 \text{ sec.}$$

$$t_2 = 0.02 \text{ sec.}$$

$$k_1 = \frac{\partial \tau_d}{\partial n_E} = 1.6 \frac{T_d}{N_E}$$

Figures A3.2 and A3.3 show the effect of this correction on the d.m.e.p. response at two operating conditions.

## APPENDIX IV

### DERIVATION OF ALTERNATIVE TERM REPRESENTING TURBINE DIMENSIONLESS MASS FLOW

Assume:

$$\dot{m}_{ex} \propto \dot{m}_a \propto p_b^{0.6} N_E$$

$$T_{ti} \propto AFR^{-0.5} N_E^{0.4}$$

$$P_{ex} \propto P_b$$

$$AFR \propto p_b^{0.6} m_f^{-1}$$

and assume fuel mass flow and variations in volumetric efficiency can be neglected, then

$$\frac{\dot{m}\sqrt{T_{ti}}}{P_{ex}} \propto \frac{N_E^{1.2} m_f^{0.5}}{p_b^{0.7}}$$

## APPENDIX V

## ESTIMATION OF MINIMUM TOTAL EFFECTIVE LOAD INERTIA

Assuming torsional rigidity of the transmission, total effective inertia seen by the engine is given by:

$$I_{tot.eff.} = I_e + \frac{I_w n_w}{r_1 r_2} + \frac{MR^2}{(r_1 r_2)^2} \qquad (A5.1)$$

where $I_e$ is polar inertia of engine, flywheel and clutch (ignoring gearbox input shaft and layshaft inertias).

$I_w$ is polar inertia of each road wheel ($kgm^2$)

$n_w$ is number of road wheels.

M is vehicle gross mass (kg)

R is rolling radius of driving wheels (m)

$r_1$ is gearbox ratio

$r_2$ is rear axle ratio.

This assumes that the inertias of gearbox output shaft, propeller shaft, differential, half shafts and driving hubs are negligible compared with the aggregate inertia of the road wheels.

From equation A5.1 it is clear that minimum effective inertia occurs when $r_1 r_2$ is maximum.

If it is assumed in addition that the gearing is chosen such that bottom gear is sufficient to enable the engine to take the vehicle, fully

laden, up the steepest gradient encountered, and that the gear ratio, $r_1 r_2$, required to climb this hill is proportional to the vehicle mass

i.e. $$r_1 r_2 \propto M$$

then

$$\frac{MR}{(r_1 r_2)^2} \propto \frac{1}{M}$$

The third term of equation A5.1 is now inversely proportional to vehicle mass, and the minimum total effective inertia occurs not only in bottom gear but also with the vehicle fully laden.

For a 32 tonne articulated vehicle, fully loaden, we assume:

$I_e = 3 \text{ kg m}^2$

$I_w = 20 \text{ kg m}^2$

$R = 0.55 \text{ m}$

$r_1 r_2 = 55$

$M = 32 \times 10^3 \text{ kg}$

$n_w = 14$

Then

$$I_{tot.eff.} = 3 + 5.1 + 3.2 \text{ kg m}^2$$
$$= 3.76 \, I_e.$$

Allowing for errors in the assumptions, a value of 2.5 times that of the engine and flywheel is assumed to be a safe estimate of the minimum total effective inertia seen by the engine under load in service.

APPENDIX VI Listing of Digital, Multivariable Diesel Engine Control Program.

```
      PROGRAM DGLINE
      DIMENSION XAA(8),XA(8),XLI(8,2),VI1(8),VI2(8),VIG(8),
     *          PCL(2,2),PCL2(2,2),PCL3(2,2),S0(2),
     *          SC1(2),SC2(2),SC3(2),SMS(8),SAM(8)
      REAL IG,AAS,AS1,AS2
      INTEGER*2 X(8),XL(8,2),ST(5MX,8),XFV1,XFV4,FS1,FS2,XEVS,AFS1,
     *   AF1,FM1,XSL,XPL,X01,X01L,X01M,X02,X02L,X02M,X1L,X1M,X2L,X2M,
     *   AS(8),ASMG,M,A,NI,NO,NN1,NN,L,XSP,XPB,ASS(8),NCYL,NSTR,LL,
     *   XFMA,XLFX,XPB1,AFM,DFS,XSMX,XSMN,DSP,T(64),POL(8),XSF,
     *   AFS2,PCL2,PCL3,PCL4,PCL5,I,J,FLAG,XFX,MDF,MUM,NPT,KM,XFLS,
     *   ASS1,XFP,XMP,DAF,DAS,XNUM,XFXM,ASL,X2,X3,X4,X5,XTB,XTO,TAMB,
     *   ASG4,NC,NCC,XPL,LE2P,XE2P,XM1M,XUEL,NCT
      LOGICAL TEST
      CHARACTER IFIL*8,OFIL*8
      CALL CLEAR
      WRITE(*,300)
300   FORMAT(1H*,///32X,'MULTI-DECK',//,32X,'**********',//
     *,17X,'MULTIVARIABLE DIESEL ENGINE CONTROLLER',////
     *,' TYPE IN NAME OF DATAFILE TO BE USED (MAX 8 CHRS)')
      READ(*,310) IFIL
310   FORMAT(1A8)
      OPEN(1,FILE=IFIL,STATUS='OLD')
      CALL SETINT
*** READ IN DATA ****
*** NO OF INPUT & OUTPUT CHANNELS TO CONTROLLER ***
      READ(1,*)NI,NO
      NNP1=NO
      NNN=NN+1
      NN1=NI+1
*** POLARITIES OF INPUT SIGNALS ***
      READ(1,*) POL2,POL3,POL4,POL5
      POL(2)=POL2
      POL(3)=POL3
      POL(4)=POL4
      POL(5)=POL5
*** ENGINE DATA ***
      READ(1,*)NCYL,NSTR,8,5
      VSM=3,1416*8*8*5/4,
      ATX=VSM*1,E5/(1024,*208,)
      NCC=NCYL*2/NSTR
*** MAX FUEL DATA (AS OUTPUT VOLTS) ***
      READ(1,*)FV1,FV2,FV4,FV5,FSP1,FSP2,FVM,FVL
*** CONVERT VOLTS TO ADC READINGS (5V=1024) ***
      FV1=FV1*204,7
      FV4=FV4*204,7
*** CONVERT SPEEDS TO ADC READINGS (5V=1240REV/MIN) ***
      FSP1=FSP1*0,82
      FSP2=FSP2*0,82
      FVM=FVM*204,7
      XFV1=IFIX(FV1)
      FV2=FV2*204,7*1,22
      XFV4=IFIX(FV4)
      FV5=FV5*204,7*1,22
      FS1=IFIX(FSP1)
      FS2=IFIX(FSP2)
      XFM=IFIX(FVM)
      FVL=FVL*204,7
      XFL=IFIX(FVL)
*** VOLUMETRIC EFFICIENCY DATA ***
      READ(1,*)EV1,EV2,EVSP
      EVSP=EVSP*M,82
      XEVS=IFIX(EVSP)
```

```
      EV2=EV2*0.02*0.02
*** OPTIMUM AIR FUEL RATIO DATA ****
      READ(1,*) AFL,AF1,AF2,AFSP1,AFSP2,AF4
      AFSP1=AFSP1*0.02
      AFSP2=AFSP2*0.02
      AFS1=IFIX(AFSP1)
      AFS2=IFIX(AFSP2)
      AF2=AF2*1.22*1.22
*** INITIALISE PRECOMPENSATOR TERMS FOR FIRST CYCLE ***
      PM11=1.
      PM12=0.
      PM21=0.
      PM22=1.
***PULLING IN TERMS OF AG/SHOT ***
      READ(1,*) PL1,PL2,PL3,PL4,PLSP
      PL1=PL1*204./
      XP1=IFIX(PL1)
      PL3=PL3*0.02
      PL4=PL4*0.02*0.02
      PLSP=PLSP*0.02
      XPLS=IFIX(PLSP)
      PL12=PVM*PL1
      PM1=XPM*XP1
*** INTEGRATION FEEDBACK CONSTANT ****
      READ(1,*) IG
*** DATA FOR DETERMINING CORRECT TIMING VOLTAGE ****
C     TP1=.0025
C     TM2=0.5
C     TM3=0.0
C     TMSP=150.
*** READ IN CALIBRATION DATA FOR BOOST TEMPERATURE ***
*** TD IS DEGREES K PER VOLT FROM INLET MAN TRANSDUCER ***
*** TAMB IS INTEGER DEGS K ***
      READ(1,*) TD,TAMB
      TD=204./*/,/TD
      XTD=IFIX(TD)
*** READ LIMIT VALUES, CALIBRATIONS, PRECOMPENSATOR MATRIX COEFFICIENTS***
      READ(1,*)((XL1(I,J),I=1,4),J=1,2)
      READ(1,*)(XAD(I),I=1,4),(AK(I),I=1,4)
      READ(1,*)((PC1(J,I),I=1,2),J=1,2)
      READ(1,*)((PC2(J,I),I=1,2),J=1,2)
      READ(1,*)((PC3(J,I),I=1,2),J=1,2)
*** READ OUTPUT SCALINGS, VOLTAGE LIMITS AND DATA TO CALCULATE SAMPLING PER.
      READ(1,*)(SO3(I),I=1,2),(SO2(I),I=1,2),(SO1(I),I=1,2)
      READ(1,*)(V11(I),V12(I),I=1,6)
      READ(1,*)(SMS(I),I=1,5)
      READ(1,*)(SMR(I),I=1,5)
*** READ ACTUATOR SLEW RATE LIMITS AND FEEDBACK GAINS ***
      READ(1,*)VSM1,VSM2
      READ(1,*)FG1,FG2,E2PM
      S1=SO3(1)
      S2=SO3(2)
*** MULTIPLY PRECOMPENSATOR COEFFICIENTS BY APPROPRIATE FEEDBACK GAIN ***
      DO 15 I=1,2
        PC1(1,I)=PC1(1,I)*FG1
        PC2(1,I)=PC2(1,I)*FG1
        PC3(1,I)=PC3(1,I)*FG1
        PC1(2,I)=PC1(2,I)*FG2
        PC2(2,I)=PC2(2,I)*FG2
15      PC3(2,I)=PC3(2,I)*FG2
*** USE CONSTANTS RATHER THAN MATRIX NOTATION (TO REDUCE EXEC. TIME) ***
      PC11A=PC1(1,1)
      PC11B=PC3(1,1)
```

```
      PC11C=PC2(1,1)
      PC11C=1.-PC11C
      PC12A=PC1(1,2)
      PC12B=PC3(1,2)
      PC21A=PC1(2,1)
      PC21B=PC3(2,1)
      PC22A=PC1(2,2)
      PC22B=PC3(2,2)
      DO 20 I=1,N1
        XL11=XLI(1,1)*204.7
        XL12=XLI(1,2)*204.7
        XL(I,1)=IFIX(XL11)*POL(I+1)
        XL(I,2)=IFIX(XL12)*POL(I+1)
20      V1G(I)=(V12(I)-V11(1))/(-2048.)
*** SPEED AND BOOST UPPER LIMITS ONLY - OTHER LIMITS NOT USED ***
      XSL=XL(1,2)
      XPL=XL(2,2)
*** OUTPUT VOLTAGE LIMITS ****
      READ(1,*) V01L,V01M,V02L,V02M,VSUM
      V01L=V01L*204.7
      V01M=V01M*204.7
      V02L=V02L*204.7
      V02M=V02M*204.7
      VSUM=VSUM*204.7*7.
      XSUM=IFIX(VSUM)
      X01L=IFIX(V01L)
      X01M=IFIX(V01M)
      X02L=IFIX(V02L)
      X02M=IFIX(V02M)
*** DATA FOR CALCULATING SAMPLING PERIOD ****
      READ(1,*) RKS,RK,SRL,NCT,XDEL
*** NCT IS NO OF SAMPLINGS TO BE MADE PER ENGINE REV.(0 INDICATES THAT
*** SAMPLING NOT TO BE SYNCHRONISED TO ENGINE MARKERS) ***
***
*** SRL IS MIN. SAMPLING RATE WHEN NCT=0 ***
***
*** RK IS TIME TO BE SUBTRACTED FROM TIMER PERIOD TO ALLOW FOR EXECUTION
*** TIME OF INITIAL PART OF ALGORITHM ***
***
*** XDEL IS DELAY PERIOD FOR USE WITH ENGINE MARKER ***
      AKIG=RKS/16
      SMS1=SMS(1)*0.02
      KSS1=IFIX(SMS1)
      KS1=RKS/SMR(1)*30.*60.*0.02*FLOAT(NSTR)
      IF(NCT.NE.0) KS2=RKS*60.*60.*0.02/FLOAT(NCT)
      DO 50 I=2,6
        IF(SMR(I).EQ.0.) GO TO 40
        SMSI=SMS(I)*0.02
        AKS=RKS/SMR(I)
        KSS(I)=IFIX(SMSI)
50      KS(I)=IFIX(AKS)-KD
40    AA=RKS/SRL
      KSM1=IFIX(AA)
      AA=KS1/AA
      XSMN=IFIX(AA)
*** CALCULATE CONSTANTS FOR SLEW RATE CONTROL ***
      VSM1=VSM1*204.7/RKS
      VSM2=VSM2*204.7/RKS
*** SET STARTING VALUES FOR CONTROL VARIABLES, ZERO COUNTERS ETC ****
      ATMM=VSM*1.25/(2MM,*3.14.)
      FM=ATMM/APL
      M=0
50    WRITE(*,*)'TYPE IN ACTUATOR VOLTS FOR FUEL AND TURBINE AREA'
```

```
      READ(*,*) V01,V02
      VM1=V01*204./
      VM2=V02*204./
      XM1=IFIX(VM1)
      XM2=IFIX(VM2)
      X01=XM1
      X02=XM2
      E2PL=ABS(E2PM/POL3(2,2))
      E2PX=E2PL*PM12
      LE2P=IFIX(E2PL)
      MTEST=.FALSE.
      E11=0.
      NC=0
      CALL CLEAR
99    WRITE(*,320)
320   FORMAT(1H+,8X,'CONTROLLER OPERATING'///8X,'TYPE  0 <CR>  TO STOP
     + ENGINE'//14X,'1 <CR>  TO DISABLE CONTROL'//
     +14X,'2 <CR>  TO RE-ENABLE CONTROL'//
     +14X,'4 <CR>  TO START ACCUMULATING DATA'//)
      CALL SETCLK(20,2)
***
*** START OF REPEATING CALCULATIONS ****
***
*** READ DATA FROM INPUT CHANNELS ***
***   DATIN1 SCANS 8 CHANNELS 8 TIMES (TOTAL 64 READINGS)
***   DATIN2 IS USED TO DETECT OUTPUT SIGNAL FROM TIMER
***   DATIN3 DETECTS ENGINE MARKER, THEN MAKES 8 SCANS AFTER DELAY XDEL***
60    NC=NC+1
      IF(NCT.EQ.0.OR.NC.LT.NCT) THEN
        CALL DATIN2(X,8,8,L)
        CALL SETCLK(20,2)
        CALL DATIN1(Y,8,64,L)
        IF(L.NE.M) CALL DATIN1(Y,8,64,L)
      ELSE
        NC=0
        CALL SETCLK(20,2)
        CALL DATIN3(Y,8,64,L,XDEL)
        IF(L.NE.0) CALL DATIN1(Y,8,64,L)
      END IF
*** AVERAGE INPUTS OVER SEVEN SCANS (DISCARD FIRST) ***
      X2=Y(10)+Y(18)+Y(26)+Y(34)+Y(42)+Y(50)+Y(58)
      X3=Y(14)+Y(22)+Y(30)+Y(38)+Y(46)+Y(54)+Y(62)
      XSP=X2/7*POL2
      XPB=X3/7*POL3
*** IF SPEED OR BOOST LIMITS EXCEEDED SHUT ENGINE DOWN ***
      IF(XSP.GT.XSL.OR.XPB.GT.XPL) THEN
        CALL DACOUT(0,X01L)
        CALL CLEAR
        WRITE(*,*) 'EMERGENCY SHUTDOWN  ',XSP,XPB
        CALL DACOUT(1,X02L)
        GO TO 200
      END IF
*** CALCULATE PRESENT SAMPLE PERIOD ****
      IF(NCT.NE.0) THEN
        AKP=KS2/FLOAT(XSP)
        KSL=IFIX(AKP)+KM
      ELSE IF(XSP.LE.KSS1) THEN
        IF(XSP.LE.XSMN) THEN
          KSL=KSMX
          NC=1
        ELSE
          AKP=KS1/FLOAT(XSP)
          KSL=IFIX(AKP)+KM
```

```
          END IF
        ELSE
          DO 130 I=2,6
            IF(XSP.LT.RSS(I)) THEN
              RSL=RS(I)
              GO TO 132
            END IF
130       CONTINUE
        END IF
*** SET TIMER FOR APPROPRIATE PERIOD ***
132     CALL SETCLK(2M,RSL)
*** SET OUTPUT LIMITS FOR CURRENT STEP ACCORDING TO ACTUATOR SLEW RATES **
        RRSL=FLOAT(RSL)
        ADP=RRSL*VSR1
        MDP=IFIX(ADP)
        ADM=RRSL*VSR2
        MDM=IFIX(ADM)
        X2L=XU2-FDM
        X2M=XU2+FDM
        X1L=XU1-FDP
        X1M=XU1+FDP
*** COMPARE MAX PUFFLING (TURN) WITH AIR TRAPPED: DETERMINE MAX F VOLTS **
        IF(X2L.LT.XU2L) X2L=XU2L
        IF(X2M.GT.XU2M) X2M=XU2M
        IF(XSP.LT.FS1) THEN
          USP=FS1-XSP
          AUSP=FLOAT(USP)
          AA=AUSP/FV2
          XFMX=XFV1+IFIX(AA)
          IF(XFMX.LT.XFM) XFMX=XFM
        ELSE IF(XSP.GT.FS2) THEN
          USP=XSP-FS2
          AUSP=FLOAT(USP)
          AA=AUSP*FV5
          XFMX=XFV4+IFIX(AA)
        ELSE
          XFMX=XFM
        END IF
*** DETERMINE PUFFLING EQUIVALENT TO 5.0/V (BACK V) AT CURRENT SPEED ***
*** REQUIRED FOR CALCULATING VOLTAGES EQUIVALENT TO PUFFLINGS ***
        XSP=XSP-XFLS
        USP=FLOAT(XSP)
        FDV=FL2-USP*(1.-USP*USP/FL4)/FLS
        XFX=XFMX-XF1
        DFX=FDV/FM1
        FMT=DFX*FLOAT(XFX)
        IF(FM.LT.FMT) THEN
          FMM=FM1*FM/FMT
          XFFX=IFIX(FMM)+XF1
        END IF
*** COMPARE LIMITS WITH ALLOWED MAX, AND MIN, VOLTAGES TO ACTUATORS ***
        IF(X1L.LT.XU1L) X1L=XU1L
        IF(XFMX.LT.X1L) THEN
          XFFX=X1L
        ELSE IF(XFMX.GT.X1M) THEN
          IF(X1M.GT.XFM) THEN
            XFMX=XFM
          ELSE
            XFMX=X1M
          END IF
        END IF
*** DETERMINE DESIRED A/F RATIO ****
        IF(XSP.LT.AFS2) THEN
```

```
          APP=APP4
        ELSE
          XSP=APS1=XSP
          ADS=FLOAT(XSP)
          APP=AP1+AP2*ADS*ADS
        END IF
*** CALCULATE SPEED CONTROL ERROR VALUE (E1P) AND INTEGRATE ****
*** THIS REQUIRES DETERMINATION OF SPEED DEMAND SIGNAL (X5) ***
        APDX=APP*DPX/ATMP
        X5=Y(13)+Y(21)+Y(29)+Y(37)+Y(45)+Y(53)+Y(61)
        IF(-X5.GT.XSUM) X5=-XSUM
        DX5=X2-X5
*** APPLY INPUT SCALING (S1) AND REDUCE GAIN FOR SMALL ERRORS IN SPEED ***
        IF(IABS(DX5).LT.45) THEN
          SPS1=FLOAT(DX5)*S1/21.
        ELSE IF(DX5.GT.0) THEN
          DX5=DX5-30
          SPS1=FLOAT(DX5)*S1/7.
        ELSE
          DX5=DX5+30
          SPS1=FLOAT(DX5)*S1/7.
        END IF
*** INTEGRATE SPEED ERROR ***
        E11=E11+SPS1*HRSL/ARIG
        E1P=SPS1+E11
*** CALCULATE BOOST ERROR (E2P) AND APPLY INPUT SCALING (S2)***
*** THIS INVOLVES ASSUMPTIONS ABOUT FUELLING TO BE APPLIED ***
        XPD1=XPD*1024
        FPD1=FLOAT(XPD1)*S2
        PRDS=PR12*FPD1
        APPR=PRDS*APDX
        APXP=APPR*XP1*PRDS
        E1PR=E1P*PR11
        XM1P=XP1*IFIX(E1PR)
        XNUM=XM1P-IFIX(APXP)
        IF(APPR.EQ.1.) THEN
          XPP=XPMX
        ELSE
          FP=FLOAT(XNUM)/(1-APPR)
          XPP=IFIX(FP)
        END IF
        DXP=XPP-XP1
        E2P=FPD1*(APDX*FLOAT(DXP)-1)
        XE2P=IFIX(E2P)
*** CHECK THAT BOOST ERROR VALUE IS NOT BEING ALLOWED TO BECOME
*** UNREALISTICALLY LARGE ***
        IF(XE2P.LT.-LE2P) THEN
          XPP=XM1P-IFIX(E2PX)
        ELSE IF(XE2P.GT.LE2P) THEN
          XPP=XM1P+IFIX(E2PX)
        END IF
*** CHECK THAT FUELLING OUTPUT VOLTAGE IS WITHIN LIMIT VALUES
*** IF OUTSIDE LIMITS ADJUST BOTH ACTUATOR OUTPUT VOLTAGES (SINCE
*** IN MULTIVARIABLE CASE THE OUTPUTS ARE NOT INDEPENDENT) ***
        IF(XPP.LT.X1L) THEN
          XPP=X1L
          XAP=X2L
        ELSE IF(XPP.GT.XPMX) THEN
          XPP=XPMX
          E2PR=(APP*PMT/ATMP-1.)*FPD1*PR22
          DXP=XPMX-XM1
          E1PR=E1P*PR21*FLOAT(DXP)/(E1PR+E2P*PR12)
          XAP=IFIX(E1PR)+XM2+IFIX(E2PR)
```

```
        ELSE
          DXP=XPP-XP1
          E2PR=(APDX*FLOAT(DXP)+1.)*PR01*PR22
          E1PR=E1P*PR21
          XRP=XM2+IFIX(E1PR)+IFIX(E2PR)
        END IF
*** CHECK THAT TURBINE AREA OUTPUT WITHIN CURRENT LIMITS ***
        IF(XRP.LT.X2L) THEN
          XRP=X2L
        ELSE IF(XRP.GT.X2H) THEN
          XRP=X2H
        END IF
*** PUT OUTPUTS TO DAC ****
        X01=XPP
        X02=XRP
C       X03=TM3+TM1*(XSP-XTMS)+TP2*(X01-XP1)
C       IF(X03.GT.X03H) THEN
C         X03=X03H
C       ELSE IF(X03.LT.X03L) THEN
C         X03=X03L
C       END IF
        CALL DACOUT(0,X01)
        CALL DACOUT(1,X02)
C       CALL DACOUT(2,X03)
*** STORE DATA VALUES INTO STORE ARRAY ***
*** A4 IS INLET MANIFOLD THERMOCOUPLE SIGNAL ***
        X4=Y(15)+Y(23)+Y(31)+Y(39)+Y(47)+Y(55)+Y(63)
        SP=FLOAT(X2)*.174
        SPD=FLOAT(X5)*.174
        XTB=X4/XTD+TAMB
*** IF TEST IS BEING RUN, STORE DATA IN ARRAY ***
        IF(ITEST) THEN
          M=M+1
          ST(M,1)=IFIX(SP)
          ST(M,2)=XPB1
          ST(M,3)=XTB
          ST(M,4)=IFIX(SPD)
          ST(M,5)=X01
          ST(M,6)=X02
          ST(M,7)=(Y(16)+Y(24))*5
          IF(M.EQ.MPT) THEN
            ITEST=.FALSE.
            WRITE(*,*)'DATA TAKE COMPLETE!  CONTROL CONTINUES'
          END IF
        END IF
*** CALCULATE CURRENT VALUES OF SLOWLY-VARYING PARAMETERS ***
        DXS=XSP-XEVS
        DNE=FLOAT(DXS)
        EV=EV1+EV2*DNE*DNE
        ATM=EV*ATX*FLOAT(XPB1)/FLOAT(XTB)
        FM=ATM/AFL
*** RE-CALCULATE PRECOMPENSATION TERMS ***
        PR11=(PC11A*SP+PC11B)*(PC11D*V01/D+PC11C)
        PR12=PC12A*SP+PC12B
        PR21=PC21A*SP+PC21B
        PR22=PC22A*SP+PC22B
*** RE-CALCULATE LIMIT FOR IMPLIED BOOST ERROR IN CALC. OF OUTPUT FUELLING
        E2PL=ABS(E2PM/PR22)
        LE2P=IFIX(E2PL)
        E2PX=E2PL*PR12
*** DETECT INPUT FROM KEYBOARD ***
        CALL BREAK(FLAG)
        IF(FLAG.NE.0) THEN
```

```
      READ(*,*) LL
      IF(LL.EQ.0) THEN
        CALL DACOUT(0,XO1L)
        CALL DACOUT(1,XO2L)
        CALL CLEAR
        WRITE(*,*) 'KEYBOARD ENGINE STOP'
        LL=99
        GO TO 200
      ELSE IF(LL.EQ.4) THEN
        MTEST=.TRUE.
        M=0
        LL=99
        WRITE(*,*)'READY!  TYPE IN NO. OF POINTS (500 MAX)'
        READ(*,*)NPT
        GO TO 60
      ELSE IF(LL.EQ.1.OR.LL.EQ.3.OR.LL.EQ.7) THEN
        LL=99
        CALL CLEAR
        GO TO 200
      ELSE
        GO TO 60
      END IF
    ELSE
      GO TO 60
    END IF
200 WRITE(*,340)
340 FORMAT(1H1,8X,'CONTROL DISABLED'///8X,'TYPE  2 <CR>  TO RE-
   +ENABLE CONTROL'//14X,'3 <CR>  TO QUIT TO APRICOT SYSTEM'//
   +14X,'7 <CR>  TO TRANSFER DATA TO DISC')
    READ(*,*)LL
    IF(LL.EQ.2) THEN
      LL=99
      GO TO 50
    ELSE IF(LL.EQ.3) THEN
      STOP
    ELSE IF(LL.EQ.7) THEN
      LL=99
      WRITE(*,*) 'TYPE IN DATAFILE NAME (MAX 6 CHRS)'
      READ(*,310) DFIL
      OPEN(3,FILE=DFIL,STATUS='NEW')
      WRITE(3,*) DFIL
      IF(M.NE.NPT) THEN
        IF(M.GT.NPT.AND.NPT.GT.50.AND.NPT.LE.500) THEN
          M=NPT
        END IF
      END IF
      IF(M.LT.1) THEN
        CALL CLEAR
        WRITE(*,*)'NO DATA'
        GO TO 200
      END IF
      DO 220 I=1,M
220     WRITE(3,250) I,(ST(I,J),J=1,NNN)
    ELSE
      GO TO 200
    END IF
250 FORMAT(Y10)
    STOP
    END
```

Data file for feedback control without precompensator.

```
4 2
1 -1 1 1
6 4 0.127 0.140
0.0 -0.2425 0.0 -0.000803 0.0 2350. 0.0 1.00
0.99 -9.E-6 1000.
17. 31. -3.E-6  2100. 1100. 20.
2.9  1.23E-4  1.E0  4.0E0  1500.
0.000001
20.0  200
0. 0. 0. 0. 9.2 -0.4 10. 10.
0. 1.0 270.0 0. 1.00 9.70E-4 0.0009/0 1.00
0. 0. 0. 0.
0. 0. 0. 0.
1. 0. 0. 1.
1. 1. 0. 0. 0. 0.
0. 10. 0. 10. 0. 10. 0. 10. 0. 10. 0. 10. 0. 10.
0000. 2500. 1600. 2100. 2500. 0. 0. 0.
2.0 00. 00. 00. 20. 0. 0. 0.
1000. 200.
4.0 5.0  2000.
1.00 0.0 0.10 9.0 0.0
50000  00 10. 0 1
```

Data file for feedback control with precompensator

```
4 2
1 -1 1 1
6 4 0.127 0.140
0.0 -0.0425 0.0 -0.000803 0.0 2350. 0.0 1.00
0.99 -9.E-6 1000.
17. 27. -3E-6  2100. 1100. 22.
2.9  1.23E-4  1.E0  4.0E0  1500.
0.000001
20.0  200
0. 0. 0. 0. 9.2 -0.4 10. 10.
0. 1.0 270.0 0. 1.00 9.70E-4 0.0009/0 1.00
-7.E-4  2.0E-4  4.0E-4  -3.E-5
0.20  -1.0  -0.0  0.0
2.0  -.5  -1.1  0./
1.10 5.55 0. 0. 0. 0.
0. 10. 0. 10. 0. 10. 0. 10. 0. 10. 0. 10. 0. 10.
0000. 2500. 1600. 2100. 2500. 0. 0. 0.
2.0 00. 00. 00. 20. 0. 0. 0.
1000. 200.
4.0 5.0  2000.
1.00 0.0 0.10 9.0 0.0
50000  00 10. 0 1
```

TABLE 2.1 Experimental Time Delays in Speed Response to Throttle Movement in a 5.7 litre S.I. Engine.

| Speed (rev/min) | Load | Delay (sec) | Delay ($^{o}$CA) |
|---|---|---|---|
| 600 | Light load | 0.066 | 238 |
| 1200 | Medium load | 0.036 | 259 |
| 1800 | Light load | 0.026 | 281 |

Based on data in paper by Chang and Sell (49).

TABLE 4.1 Engine Data

| | |
|---|---|
| Type | Leyland TL11, direct injection turbocharged. |
| Configuration | In-line six cylinder, 4-stroke |
| Bore and Stroke: | 127 mm x 146.05 mm |
| Swept Volume: | 11.1 litre |
| Fuel Injection Pump: | CAV Majormec, governor removed |
| Maximum Fuelling: | 125 mg/shot approx. |
| Injection Timing: | $22^{\circ}$ BTDC (static). |
| EVO | $135^{\circ}$ ATDC |
| IVC | $135^{\circ}$ BTDC |
| Overlap Period: | $46^{\circ}$ CA |
| Rated Power | 210 kW approx. at 2200 rev/min. |
| Moment of Inertia of Rotating Parts: | 2.95 kg $m^2$ (including flywheel) |
| Turbocharger: | Holset VH2C with variable geometry turbine. |
| Turndown ratio: | 2.2:1 (turbine inlet area). |
| Moment of inertia of turbocharger rotor: | 0.000244 kg $m^2$. |

TABLE 4.2 Transducer Details

| | | |
|---|---|---|
| Boost pressure: | Druck PDCR 10 | strain gauge types with water cooling |
| Exhaust manifold pressure: | Schaevitz P722 | |
| Turbine inlet temperature: | 1 mm chromel-alumel thermocouple (mineral insulated and with stainless steel sheath). | |
| Exhaust opacity: | Infra-red absorption type. | |
| Engine speed: | Orbit magnetic pick-up from 120-tooth wheel on engine flywheel. Ancom f-v converter. | |
| Shaft torque: | Vibrometer TG200 torque meter in drive shaft between flywheel and dynamometer. | |
| Turbine area control rod position: | Prototype Hall-effect device with temperature compensation and water cooling. | |
| Other position transducers: | Linear inductive types. | |

TABLE 4.3 Operating Conditions at which Responses to Fuel Rack Perturbation were made.

| Mean Fuelling / Mean Speed (rev/min) | 3.4 V 39 mg/shot | 4.4 V 67 mg/shot | 5.1 V 88 mg/shot | 5.4 V 104 mg/shot |
|---|---|---|---|---|
| 1000 | - | $n_E$ $p_b$ $T_{bi}$ opacity $\tau_s$ $p_{ex}$ | - | $n_E$ $p_b$ |
| 1200 | $n_E$ $p_b$ $T_{ti}$ opacity $p_{ex}$ | $n_E$ $p_b$ $T_{ti}$ opacity $\tau_s$ $p_{ex}$ | - | $n_E$ $p_b$ $T_{ti}$ opacity |
| 1600 | $n_E$ $p_b$ $T_{ti}$ opacity | $n_E$ $p_b$ $T_{ti}$ opacity $p_{ex}$ $\tau_s$ | $n_E$ $p_b$ $T_{ti}$ opacity | $n_E$ $p_b$ $T_{ti}$ opacity $\tau_s$ |
| 2000 | $n_E$ $p_b$ $T_{ti}$ $\tau_s$ | $n_E$ $p_b$ $T_{ti}$ | $n_E$ $p_b$ $T_{ti}$ opacity $\tau_s$ | - |
| 2200 | (4.0 V) $n_E$ $p_b$ | $n_E$ $p_b$ | (4.75 V) $n_E$ $p_b$ | - |

TABLE 4.4 Operating Conditions at which Responses to Turbine Inlet Area Perturbations were made.

| Fuelling (volts) / Mean Speed (rev/min) | 3.4 V | 4.4 V | 5.4 V |
|---|---|---|---|
| 1000 | - | $n_E$ $p_b$ | $n_E$ $p_b$ $T_{ti}$ opacity $\tau_s$ |
| 1200 | - | $n_E$ $p_b$ $T_{ti}$ opacity $\tau_s$ | $n_E$ $p_b$ $T_{ti}$ |
| 1600 | $n_E$ $p_b$ | $n_E$ $p_b$ | $n_E$ $p_b$ $T_{ti}$ opacity $\tau_s$ |
| 2000 | $n_E$ $p_b$ $\tau_s$ | $n_E$ $p_b$ | (5.0V) $n_E$ $p_b$ |
| 2200 | - | $n_E$ $p_b$ | - |

TABLE 5.1 Steady State Gains in Response to Changes in Fuelling.

| Nominal Speed | Mean Fuelling (mg/shot) | Steady State Gains (per mg/shot) Speed (rev/min) | Boost (bar) |
|---|---|---|---|
| 1000 | 66 | +8.8*, +10.3 | +0.0042*, +0.008 |
| | 104 | +6 | +0.01 |
| 1200 | 39 | +17.7 | +0.0032 |
| | 68 | +10.8*, 14.7†, 13.4 | +0.006*, 0.0058, 0.006† |
| | 104 | +6.0, +8.3, +5.9 | +0.0116, +0.0136, +0.0095 |
| 1600 | 40 | +22.6, +31 | +0.0063, +0.006 |
| | 68 | +12.5*, +17.7 | +0.008*, +0.011 |
| | 88 | +11.5 | +0.012 |
| | 102 | +10.2 | +0.013 |
| 2000 | 42 | +29.6 | +0.011 |
| | 66 | +19.5, +21.6† | +0.013, +0.0155† |
| | 84 | +8.3**, +10.7 | +0.015**, +0.0155 |
| 2200 | 55 | +13.7** | +0.017** |
| | 63 | +18.9 | +0.0138 |
| | 73 | +11.2** | +0.0156** |

Notes: Fuelling amplitude generally between 20 and 35 mg/shot (pk-pk)

* Fuelling amplitude greater than 50 mg/shot

† Fuelling amplitude less than 10 mg/shot

** Injection timing very retarded (1° CA btdc).

TABLE 5.2 Steady State Gains - Response to Changes in Turbine Inlet Area.

| Nominal Speed (rev/min) | Mean Fuelling (mg/shot) | Steady State Gains (per mm $A_t$) Speed (rev/min) | Boost (bar) |
|---|---|---|---|
| 1000 | 66 | 10.3, 0.8** | .008, .0125** |
| | 104 | 4.5 | .025 |
| 1200 | 68 | -1.0, 1.4** | .025, .02** |
| | 104 | 8.1, 6.4, 6.2** | .044, .041, .045** |
| 1600 | 68 | -2.75**, -4.3 | .036**, .032 |
| | 102 | -4.4, -3.0, -2.5** | .081, .07, .07** |
| | | 0.8 | .055 |
| 2000 | 42 | -16 | .05 |
| | 66 | -17.3, -5.26**, -10. | .067, .048**, .055 |
| | 84 | -6.7, -5.0** | .066, .05** |
| 2200 | 63 | -26 | .07 |

Notes: Turbine inlet area approximately 75% ± 20% in each case.

** indicates injection timing very retarded.

TABLE 5.3 Measurement of diesel torque delay.

| Speed Rev/min | Fuelling % max. fuel | Diesel Torque Delay | | | |
|---|---|---|---|---|---|
| | | Gant Formula | | Present Method | |
| | | msec | °CA | msec | °CA |
| 1530 | 60 ± 38% | 22.8 | 210 | 7.0 | 65° |
| 1050 | 60 ± 41% | 33.3 | 210 | 9.8 | 62° |
| 939 | 60 ± 28% | 37.3 | 210 | 12.8 | 72° |
| 1180 | 60 ± 15% | 29.8 | 210 | 10.0* | 71°* |
| 2000 | 31 ± 4% | 17.5 | 210 | 9.5 † | 113°† |
| 1550 | 78 ± 11% | 22.8 | 210 | 7.6 | 70° |
| 1955 | 69 ± 9% | 17.8 | 210 | 6.0 | 70° |
| 1595 | 79 ± 2.5% | 21.9 | 210 | 21.4† | 205°† |

* Result affected by cylinder-to-cylinder fuelling variations.

† Subject to error due to small amplitude of measured signal.

TABLE 5.4 Comparison of Estimated and Measured Boost Time Constants

| Mean Speed | Mean Turbocharger Speed | Mean Boost Pressure | Rack Voltage | Compressor Efficiency | Break frequency (Hz) | |
|---|---|---|---|---|---|---|
| | | | | | Estimated | Measured |
| 1595 | 71775 | 1.68 | 5.4 | 0.75 | 0.18 | 0.20 |
| 1992 | 80650 | 1.77 | 5.0 | 0.75 | 0.20 | 0.25 |
| 1594 | 58450 | 1.41 | 4.4 | 0.72 | 0.16 | 0.18 |
| 1983* | 85720 | 1.89 | 5.0 | 0.75 | 0.20 | 0.25 |

* timing very retarded

volumetric efficiency assumed: 0.90

TABLE 6.1 Effect of Interaction at Steady State: feedback control of speed and boost pressure.

| Mean Speed rev/min. | Mean Rack Volts | Steady State Gains $g_{11}$ | $g_{12}$ | $g_{21}$ | $g_{22}$ | Typical Interactions Speed | Boost | $\frac{g_{12}\,g_{21}}{g_{11}\,g_{22}}$ |
|---|---|---|---|---|---|---|---|---|
| 1000 | 4.4 | 8.8 | 1 | .0042 | .013 | 0.0021 | 1.8 | 0.05 |
| | 5.4 | 6 | 4.5 | .01 | .025 | 0.0132 | 4.2 | 0.30 |
| 1200 | 4.4 | 10.8<br>14.7 | -1.0<br>1.4 | .006<br>.006 | .025<br>.02 | ±0.0013 | 1.1 | ±0.02 |
| | 5.4 | 5.9 | 6.2 | .01 | .041 | | | |
| | | 8.3 | 8.15 | .013 | .045 | 0.0144 | 2.8 | 0.31 |
| 1600 | 4.4 | 12.5<br>17.7 | -2.7<br>-4.3 | .008<br>.011 | .036<br>.032 | -0.003 | 0.95 | 0.06 |
| | 5.4 | 10.2 | -4.4<br>-2.5 | .013 | .055<br>.081 | -0.025 | 0.9 | -0.04 |
| 2000 | 3.4 | 29.6 | -16 | .011 | .05 | -0.0055 | 0.38 | -0.08 |
| | 4.4 | 19.5 | -17<br>-10 | .013 | .048<br>.067 | -0.0049 | 0.6 | -0.12 |
| | 5.1 | 10.7<br>8.3 | -5<br>-8.1 | .015<br>.0155 | .05<br>.09 | -0.0053 | 0.92 | -0.15 |
| 2200 | 4.4 | 18.9 | -26 | .014 | .07 | -0.01 | 0.47 | -0.27 |

$$k_1 = 0.65 \ \frac{\text{mg/shot}}{\text{rev/min}} \qquad k_2 = 28 \ \frac{\text{mm At}}{\text{bar boost}}$$

Typical changes in reference values assumed to be 500 rev/min and 0.3 bar boost.

TABLE 6.1 Effect of Interaction at Steady State: feedback control of speed and boost pressure.

| Mean Speed rev/min. | Mean Rack Volts | Steady State Gains $g_{11}$ | $g_{12}$ | $g_{21}$ | $g_{22}$ | Typical Interactions Speed | Boost | $\frac{g_{12}\,g_{21}}{g_{11}\,g_{22}}$ |
|---|---|---|---|---|---|---|---|---|
| 1000 | 4.4 | 8.8 | 1 | .0042 | .013 | 0.0021 | 1.8 | 0.05 |
| | 5.4 | 6 | 4.5 | .01 | .025 | 0.0132 | 4.2 | 0.30 |
| 1200 | 4.4 | 10.8 | -1.0 | .006 | .025 | ±0.0013 | 1.1 | ±0.02 |
| | | 14.7 | 1.4 | .006 | .02 | | | |
| | 5.4 | 5.9 | 6.2 | .01 | .041 | 0.0144 | 2.8 | 0.31 |
| | | 8.3 | 8.15 | .013 | .045 | | | |
| 1600 | 4.4 | 12.5 | -2.7 | .008 | .036 | -0.003 | 0.95 | 0.06 |
| | | 17.7 | -4.3 | .011 | .032 | | | |
| | 5.4 | 10.2 | -4.4 | .013 | .055 | -0.025 | 0.9 | -0.04 |
| | | | -2.5 | | .081 | | | |
| 2000 | 3.4 | 29.6 | -16 | .011 | .05 | -0.0055 | 0.38 | -0.08 |
| | 4.4 | 19.5 | -17 | .013 | .048 | -0.0049 | 0.6 | -0.12 |
| | | | -10 | | .067 | | | |
| | 5.1 | 10.7 | -5 | .015 | .05 | -0.0053 | 0.92 | -0.15 |
| | | 8.3 | -8.1 | .0155 | .09 | | | |
| 2200 | 4.4 | 18.9 | -26 | .014 | .07 | -0.01 | 0.47 | -0.27 |

$$k_1 = 0.65 \ \frac{\text{mg/shot}}{\text{rev/min}} \qquad k_2 = 28 \ \frac{\text{mm At}}{\text{bar boost}}$$

Typical changes in reference values assumed to be 500 rev/min and 0.3 bar boost.

TABLE 6.2 Steady State Interaction Effects with Feedback Control of Engine Speed and Air-Fuel Ratio.

| Mean Speed (rev/min) | Mean Rack Volts | Feedback gains ** $K_1$ | $K_2$ | Steady State Gains ** $g_{11}$ | $g_{12}$ | $g_{21}$ | $g_{22}$ | Typical + interactions Speed | AFR | $\frac{g_{12}}{g_{11}}\frac{g_{21}}{g_{22}}$ |
|---|---|---|---|---|---|---|---|---|---|---|
| 1200 | 5.4 | 0.65 | 3 | 6 | 4.5 | -0.11 | 0.7 | .0062 | -1.1 | -0.123 |
| 1600 | 5.4 | 0.65 | 3 | 10.2 | -3.5 | -0.21 | 0.75 | -0.0028 | -1.2 | 0.096 |
| 2200 | 4.4 | 0.65 | 3 | 19 | -26 | -0.27 | 0.9 | -.0082 | -0.58 | 0.416 |
| 1200 | 5.4 | 0.02* | 3 | 6 | 4.5 | -0.11 | 0.7 | -0.21 | o.2 | -0.123 |
| 1600 | 5.4 | 0.02* | 3 | 10.2 | -3.5 | -0.21 | 0.75 | 0.10 | 0.38 | 0.096 |
| 2200 | 4.4 | 0.02* | 3 | 19 | -26 | -0.27 | 0.9 | 0.47 | 0.43 | 0.416 |

** Gains in terms of following units: rev/min, AFR, mg/shot, mm turbine area actuator movement.

+ Typical interactions assuming changes in reference values of 500 rev/min and 3 AFR. Actuator saturation ignored.

* Without speed governing.

Table 7.1 Typical values of terms in Equation 7.1: peak torque condition with 2-speed governor

| Term | Description | Steady State Value |
|---|---|---|
| $f_1$ | Response of F.I.E. speed to engine speed. | 1.0 |
| $k_1$ | Change in fuelling with speed | 0.4% max.fuel/% rated speed (0.0 - 0.6) |
| $g_{11}$ | Engine speed response to fuelling | 0.8% rated speed/% max.fuel (0.6 - 1.0) |
| $f_2$ | Actuator pressure response to boost. | 1.0 |
| $k_2$ | Actuator rod response to boost | 5% turbine area restriction/ % change in boost (absolute) (2.5-10) |
| $g_{22}$ | Boost response to actuator rod | 0.5% change in boost (abs)/ % restriction (0.4-0.6) |
| $g_{12}$ | Speed response to actuator rod | 0.03% rated speed/% restriction (0.02-0.04) |
| $g_{21}$ | Boost response to fuelling | 1.4% boost change (abs)/ % maximum fuel (1.3 - 2.0) |

Table 7.2 Steady state transfer function gains at rated engine speed.

| Term | Steady State Gain | Dimension |
|---|---|---|
| $g_{11}$ | 0.8 (0.6 to 1.0) | % rated speed 1% maximum fuel |
| $g_{12}$ | -0.05 (0.035 to -0.05) | % rated speed/% turbine area |
| $g_{21}$ | 1.0 (0.8 to 1.2) | % boost change (abs)/% maximum fuel |
| $g_{22}$ | 0.35 (0.3 to 0.45) | % abs. boost pressure/% turbine area |

TABLE 8.1 Scaling Applied to Steady State Voltage Gain Matrix.

| Engine Speed | Rack Position (volts) | Steady State Gain Matrix G(O) | Output Scaling $S_o$ | Input Scaling $S_i$ | Diagonalised Gain Matrix G* |
|---|---|---|---|---|---|
| 1200 | 5.4 | $\begin{bmatrix} 1.15 & 0.02 \\ 1.95 & 0.14 \end{bmatrix}$ | $\begin{bmatrix} 0.87 & 0 \\ 0 & 0.26 \end{bmatrix}$ | $\begin{bmatrix} 1 & 0 \\ 0 & 27.5 \end{bmatrix}$ | $\begin{bmatrix} 1 & 0.47 \\ 0.5 & 1 \end{bmatrix}$ |
| 1600 | 5.4 | $\begin{bmatrix} 1.5 & -0.015 \\ 2.0 & 0.33 \end{bmatrix}$ | $\begin{bmatrix} 0.67 & 0 \\ 0 & 0.125 \end{bmatrix}$ | $\begin{bmatrix} 1 & 0 \\ 0 & 24.2 \end{bmatrix}$ | $\begin{bmatrix} 1 & -0.24 \\ 0.25 & 1 \end{bmatrix}$ |
| 2000 | 5.1 | $\begin{bmatrix} 1.15 & -0.045 \\ 2.23 & 0.5 \end{bmatrix}$ | $\begin{bmatrix} 0.87 & 0 \\ 0 & 0.18 \end{bmatrix}$ | $\begin{bmatrix} 1 & 0 \\ 0 & 11 \end{bmatrix}$ | $\begin{bmatrix} 1 & -0.43 \\ 0.4 & 1 \end{bmatrix}$ |
| 1200 | 4.4 | $\begin{bmatrix} 1.57 & -.0025 \\ 1.08 & .067 \end{bmatrix}$ | $\begin{bmatrix} 0.69 & 0 \\ 0 & 0.16 \end{bmatrix}$ | $\begin{bmatrix} 1 & 0 \\ 0 & 93 \end{bmatrix}$ | $\begin{bmatrix} 1 & -0.15 \\ 0.17 & 1 \end{bmatrix}$ |

TABLE 8.2 VALUES OF PRECOMPENSATOR MATRIX WHEN $S_o$ is Fixed.

| Engine Speed | Rack Position (V) | $S_o$ | $G^*S_i$ | $(G^*S_i)^{-1}$ | $S_o^{-1}$ |
|---|---|---|---|---|---|
| 1200 | 5.4 | $\begin{bmatrix} 0.8 & 0 \\ 0 & 0.18 \end{bmatrix}$ | $\begin{bmatrix} 1.15 & 0.55 \\ 1.95 & 3.85 \end{bmatrix}$ | $\begin{bmatrix} 1.15 & -0.16 \\ -0.58 & 0.34 \end{bmatrix}$ | $\begin{bmatrix} 1.15 & 0 \\ 0 & 5.55 \end{bmatrix}$ |
| 1600 | 5.4 | $\begin{bmatrix} 0.8 & 0 \\ 0 & 0.18 \end{bmatrix}$ | $\begin{bmatrix} 1.5 & -0.363 \\ 2.0 & 8.0 \end{bmatrix}$ | $\begin{bmatrix} 0.63 & 0.028 \\ -0.16 & 0.12 \end{bmatrix}$ | $\begin{bmatrix} 1.15 & 0 \\ 0 & 5.55 \end{bmatrix}$ |
| 2000 | 5.1 | $\begin{bmatrix} 0.8 & 0 \\ 0 & 0.18 \end{bmatrix}$ | $\begin{bmatrix} 1.15 & -0.495 \\ 2.23 & 5.5 \end{bmatrix}$ | $\begin{bmatrix} 0.74 & 0.067 \\ -0.30 & 0.155 \end{bmatrix}$ | $\begin{bmatrix} 1.15 & 0 \\ 0 & 5.55 \end{bmatrix}$ |
| 1200 | 4.4 | $\begin{bmatrix} 0.8 & 0 \\ 0 & 0.18 \end{bmatrix}$ | $\begin{bmatrix} 1.56 & -0.25 \\ 1.08 & 6.7 \end{bmatrix}$ | $\begin{bmatrix} 0.62 & 0.023 \\ -0.10 & 0.145 \end{bmatrix}$ | $\begin{bmatrix} 1.15 & 0 \\ 0 & 5.55 \end{bmatrix}$ |

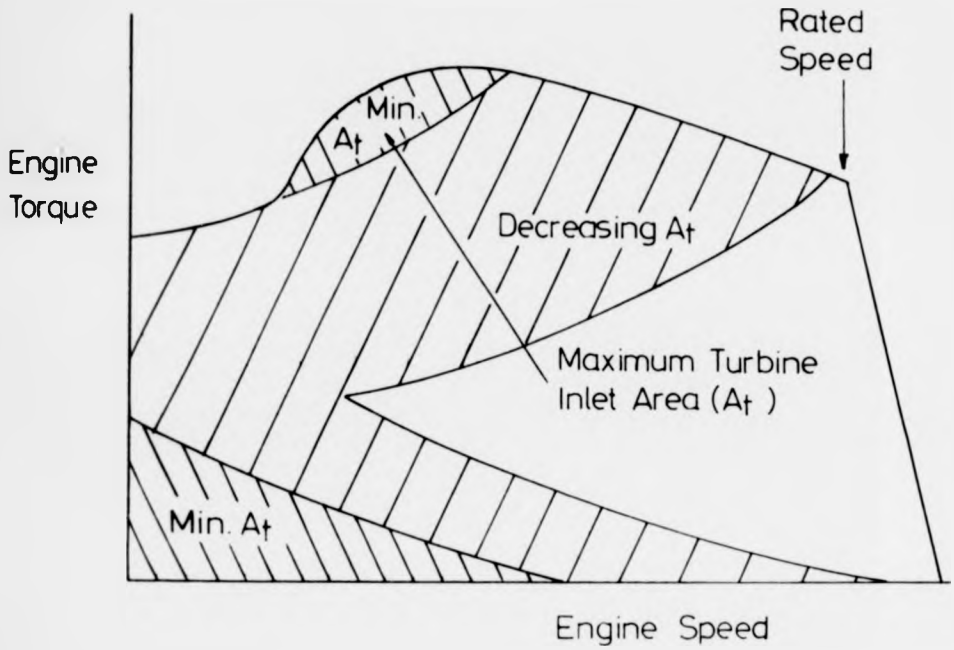


Figure 1.1 Idealised steady state scheduling of turbine inlet area

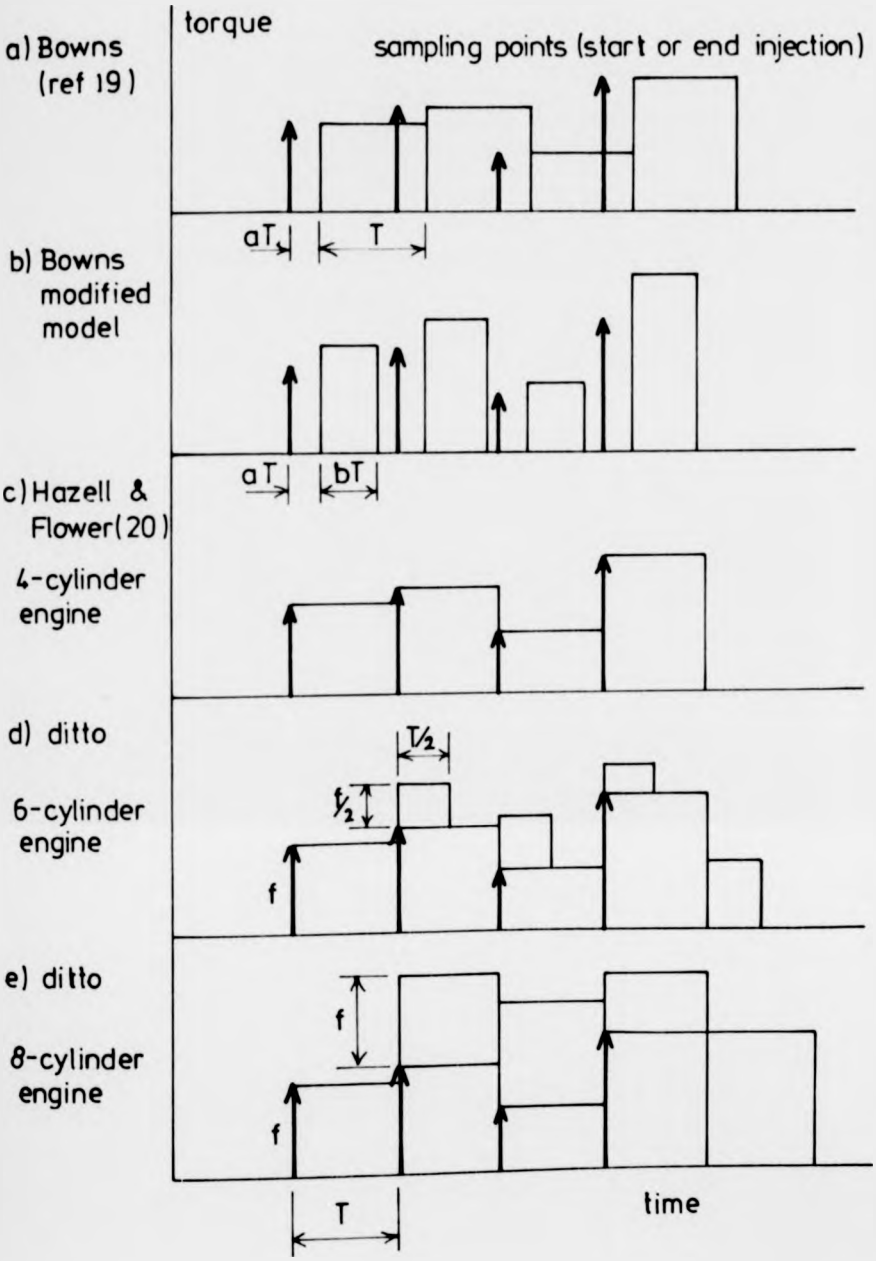


Figure 2.1 Comparison of various diesel engine sampled-data torque models.

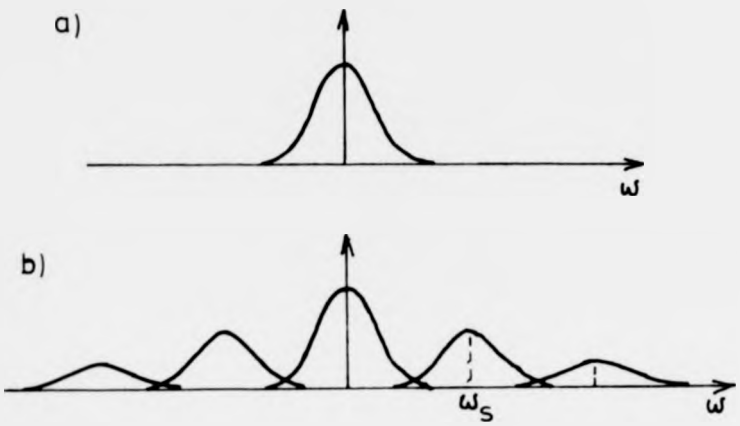


Figure 2.2 Frequency spectra for a) acontinuous system and b) the same system after pulse sampling

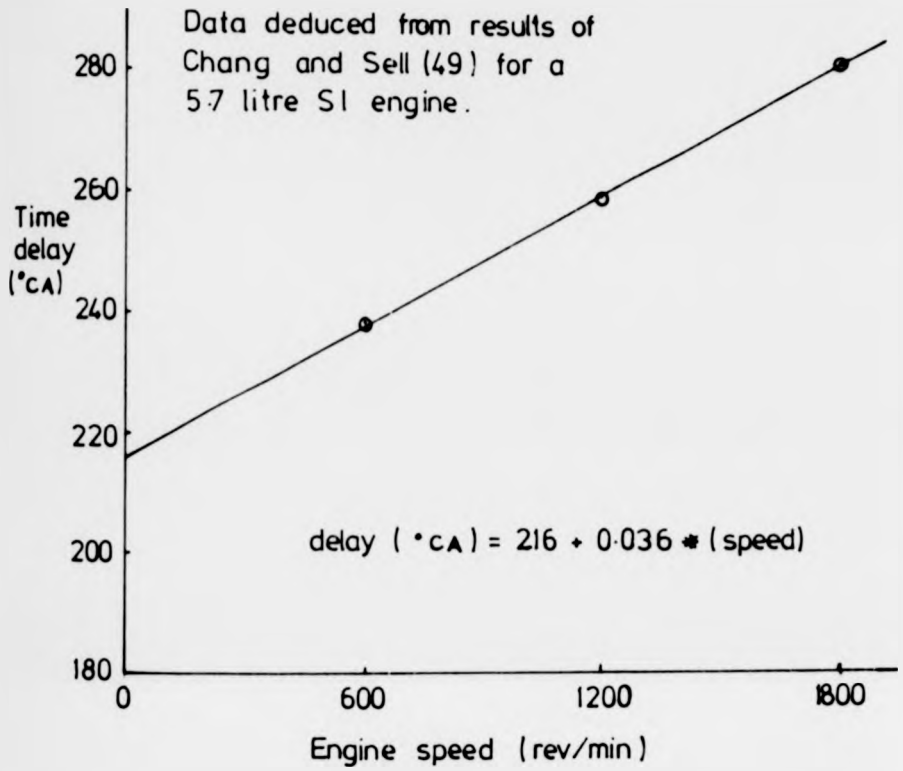


Figure 2.3 Time delay in response of engine speed to throttle movement.

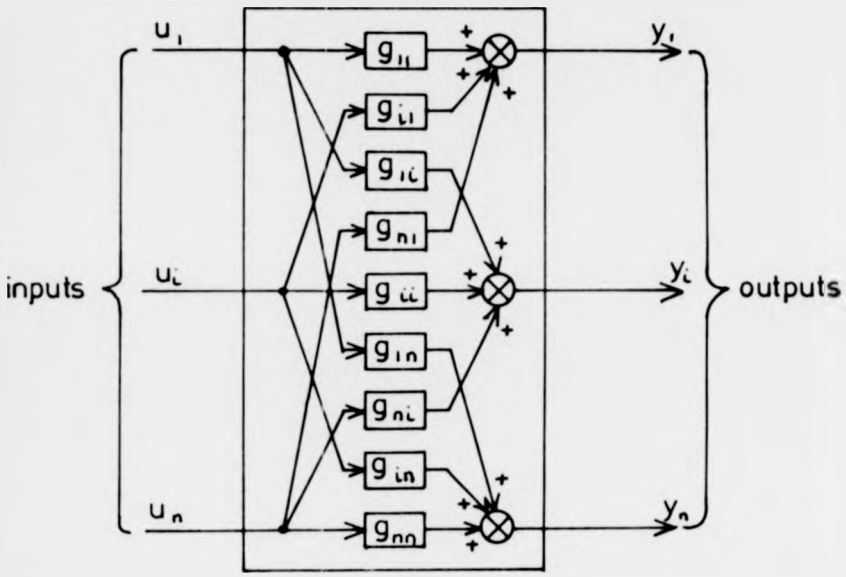


Figure 3.1 Block diagram of example multi-input multi-output system

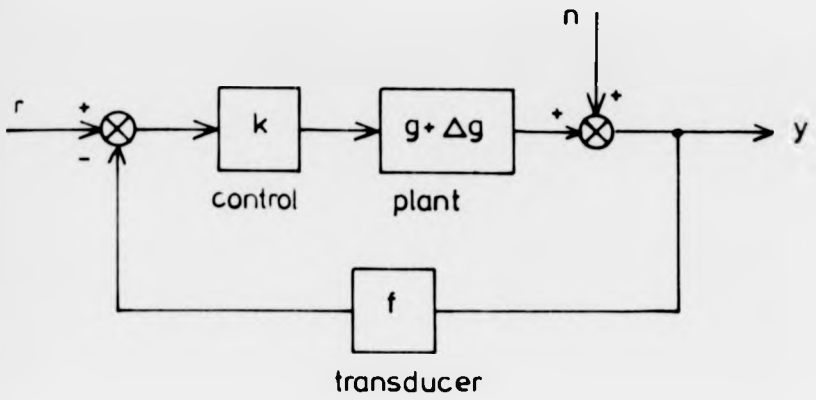


Figure 3.2 SISO system with output noise and variations in plant behaviour.

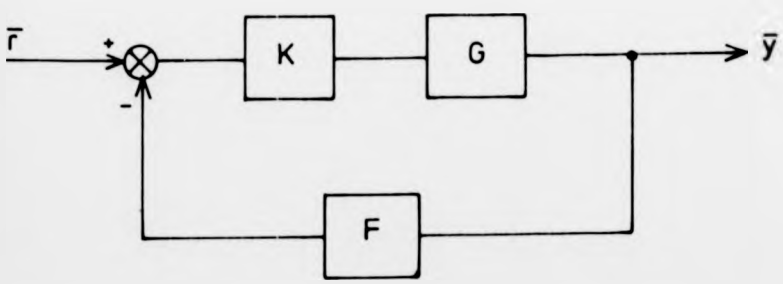


Figure 3.3 Block diagram of MIMO system in matrix form.

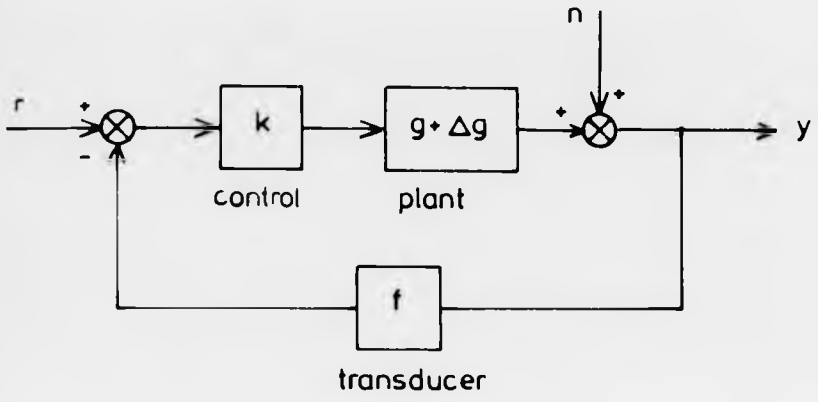


Figure 3.2 SISO system with output noise and variations in plant behaviour.

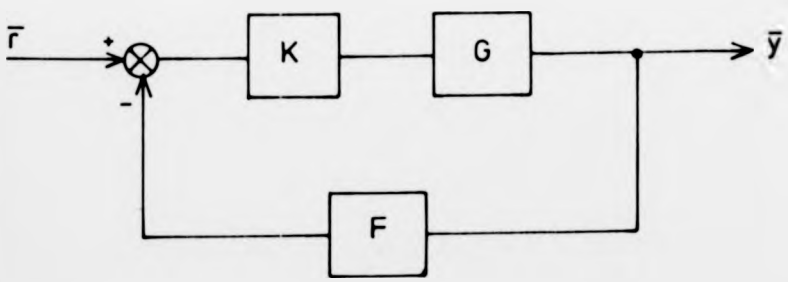


Figure 3.3 Block diagram of MIMO system in matrix form.

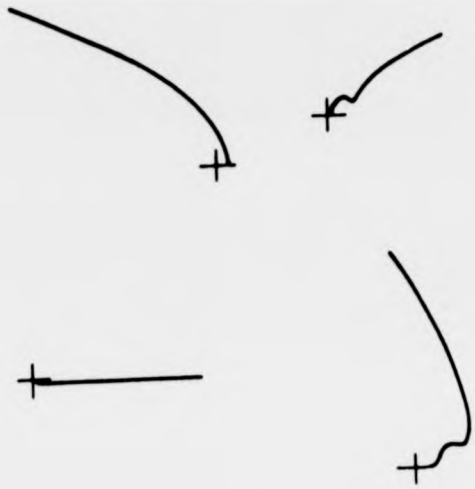

Inverse Nyquist array of two input two output system

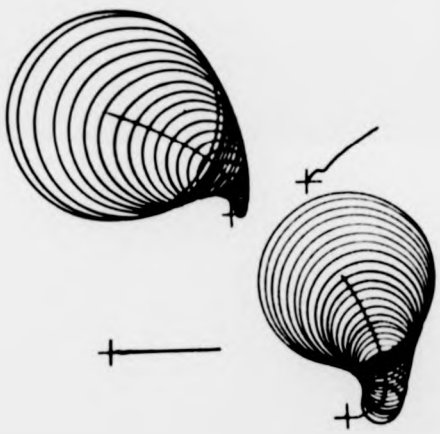

Same array with Gershgorin discs shown

(System is diagonally dominant since discs exclude origins)

Figure 3.4 Example of inverse Nyquist array with Gershgorin discs shown.

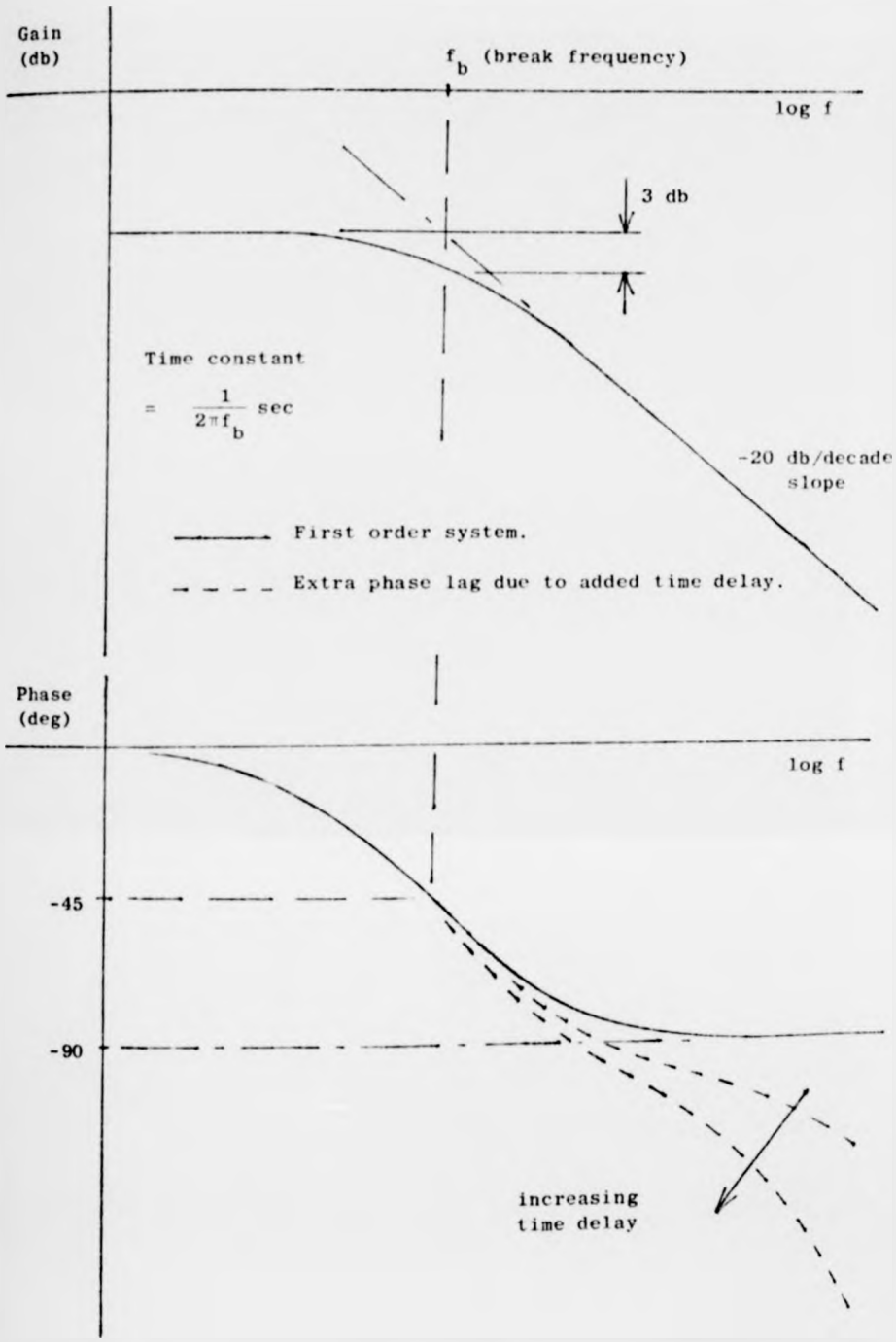


Figure 3.5 Bode diagrams of a first order system with time delay.

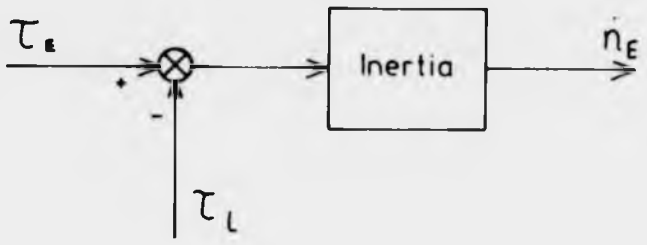


Figure 3.6 Engine-dynamometer system.

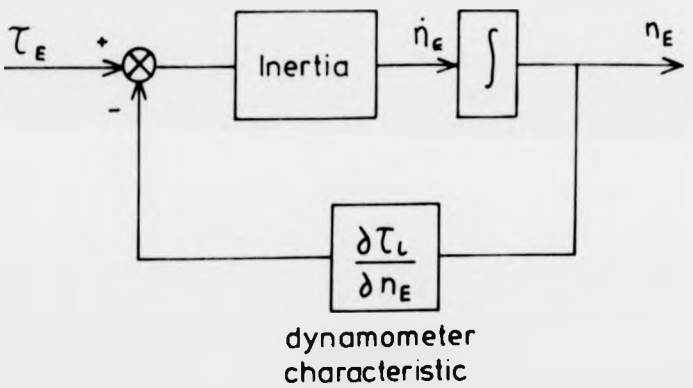


Figure 3.7 Engine-dynameter system with load characteristic.

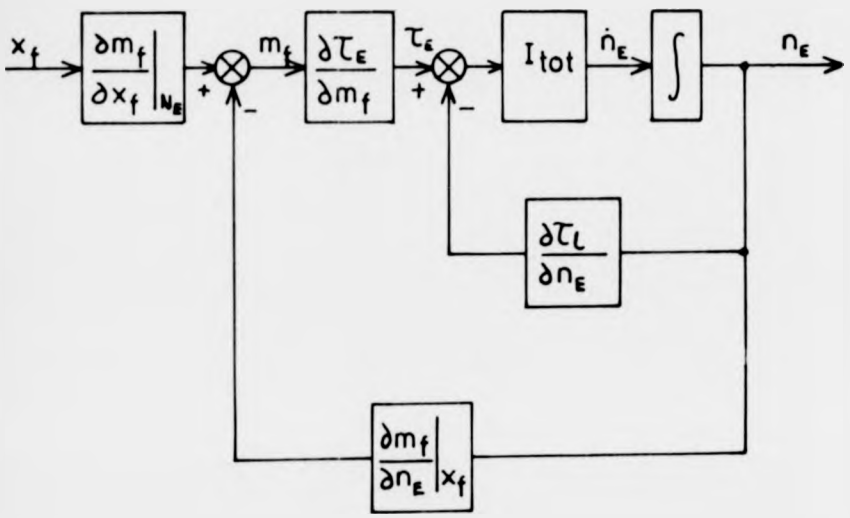


Figure 3.8 Transfer function diagram of system with fuel injection characteristics included.

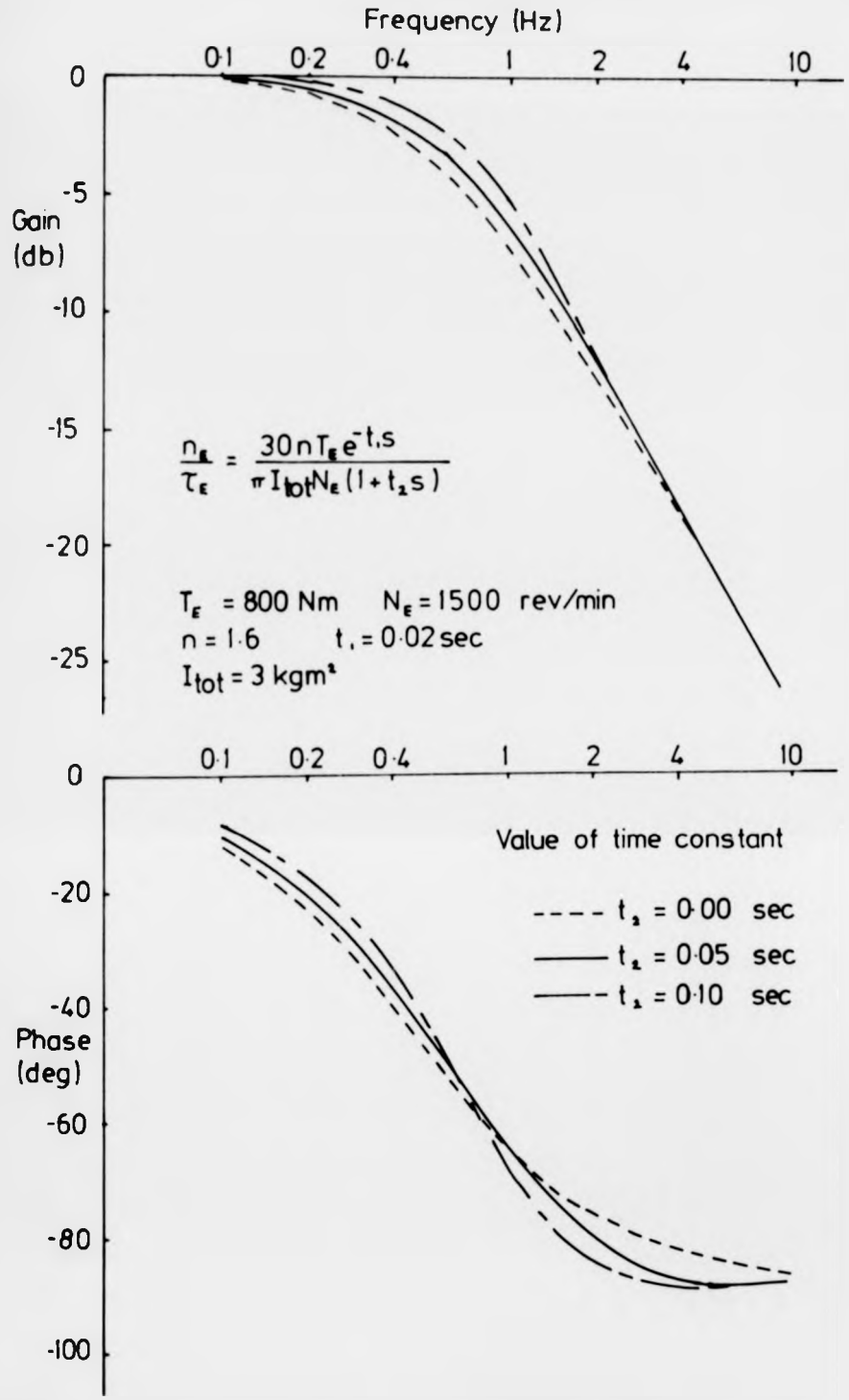


Figure 3.9 Effect of dynamometer time constant on engine speed response (calculated)

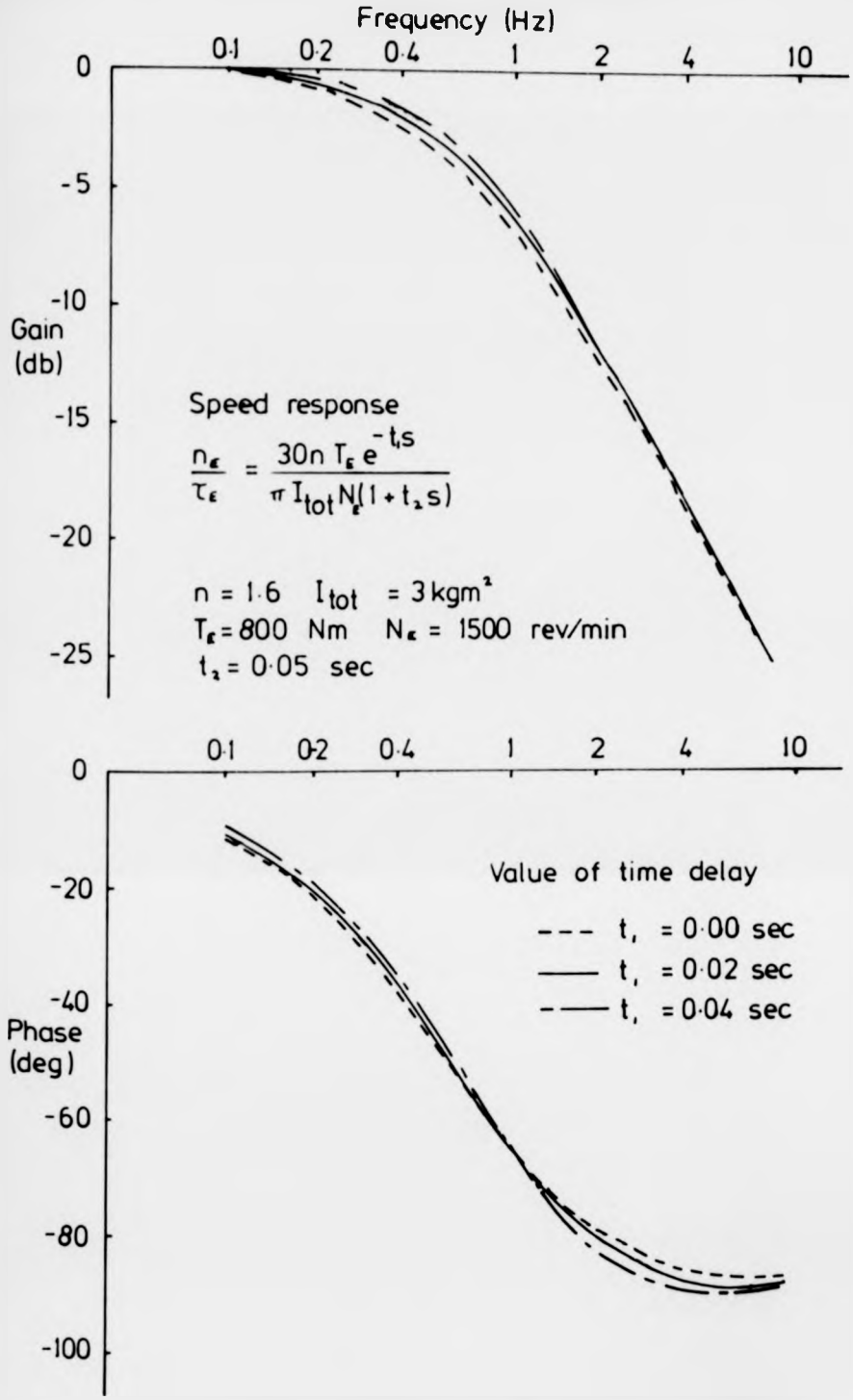


Figure 3.10 Effect of dynamometer time delay on engine speed response (calculated)

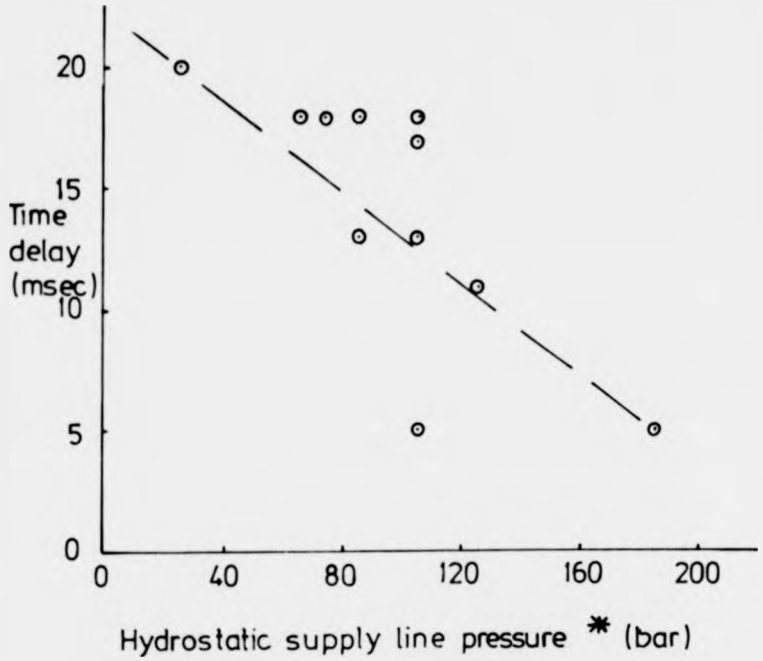


* supply line pressure at start of transient

Figure 3.11 Dynamometer control system time delay against hydrostatic supply line pressure.

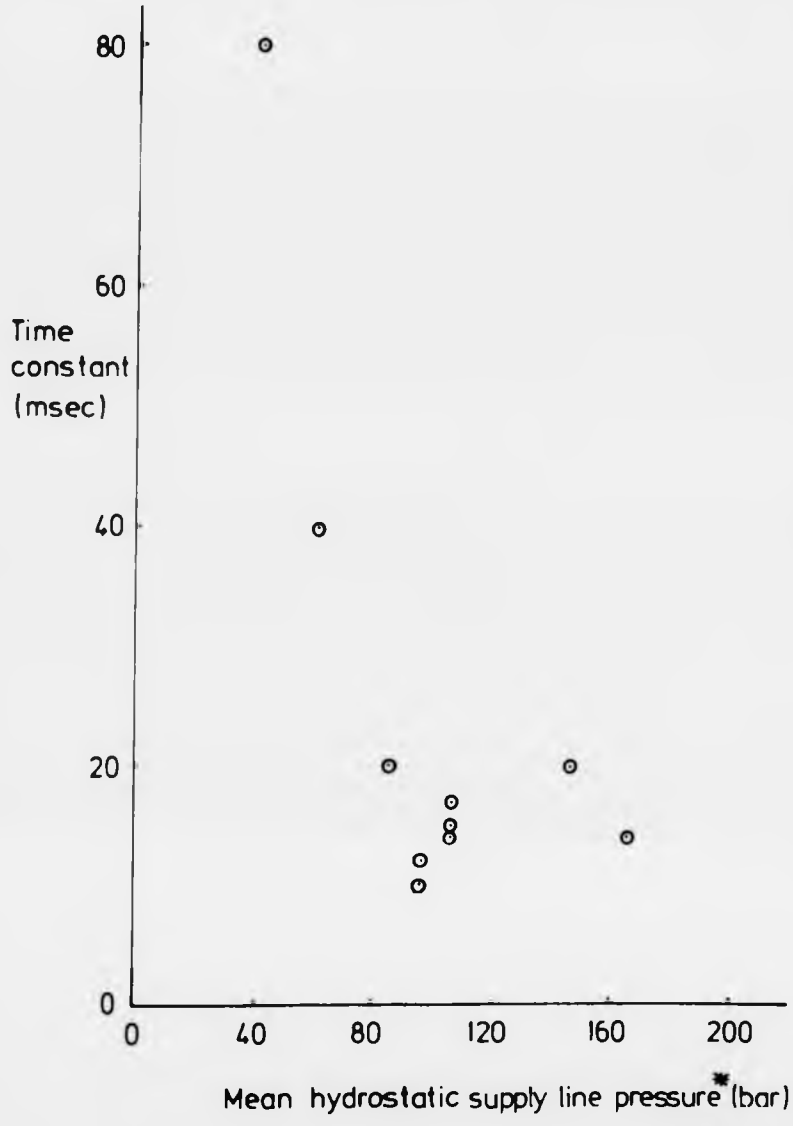


* taken to be the pressure at the start of the transient plus ⅓ the change in pressure.

Figure 3.12 Dynamometer control system time constant against hydrostatic supply line pressure.

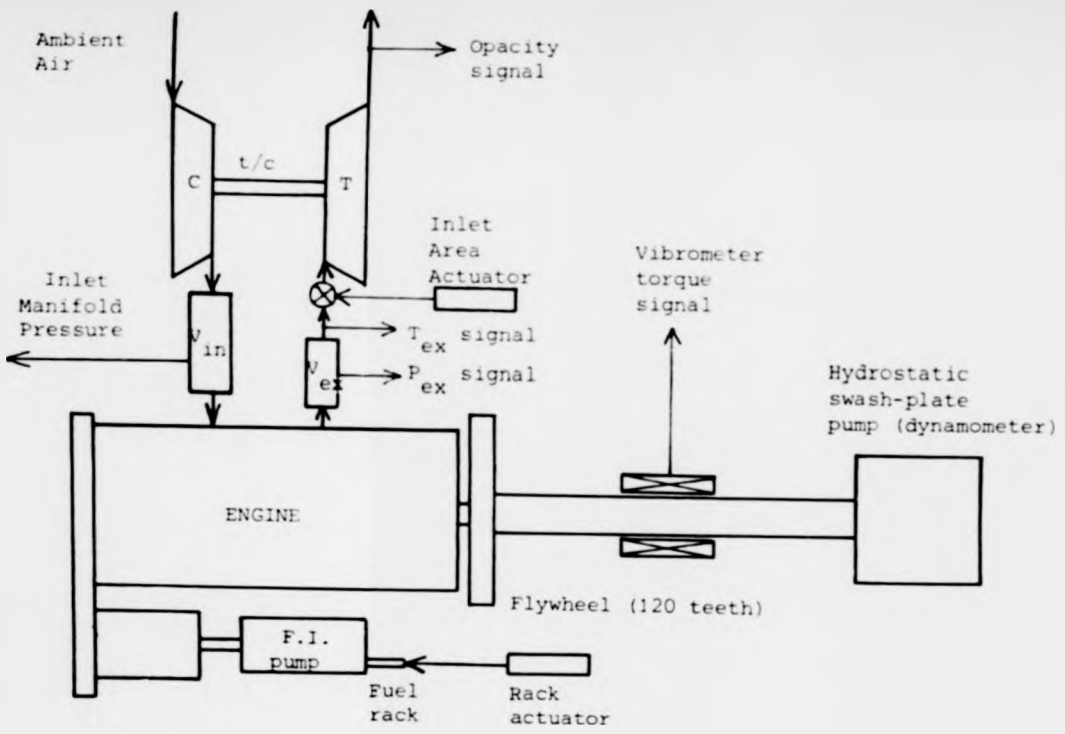


Figure 4.1 Diagram of engine and dynamometer with positions of transducrs and actuators indicated.

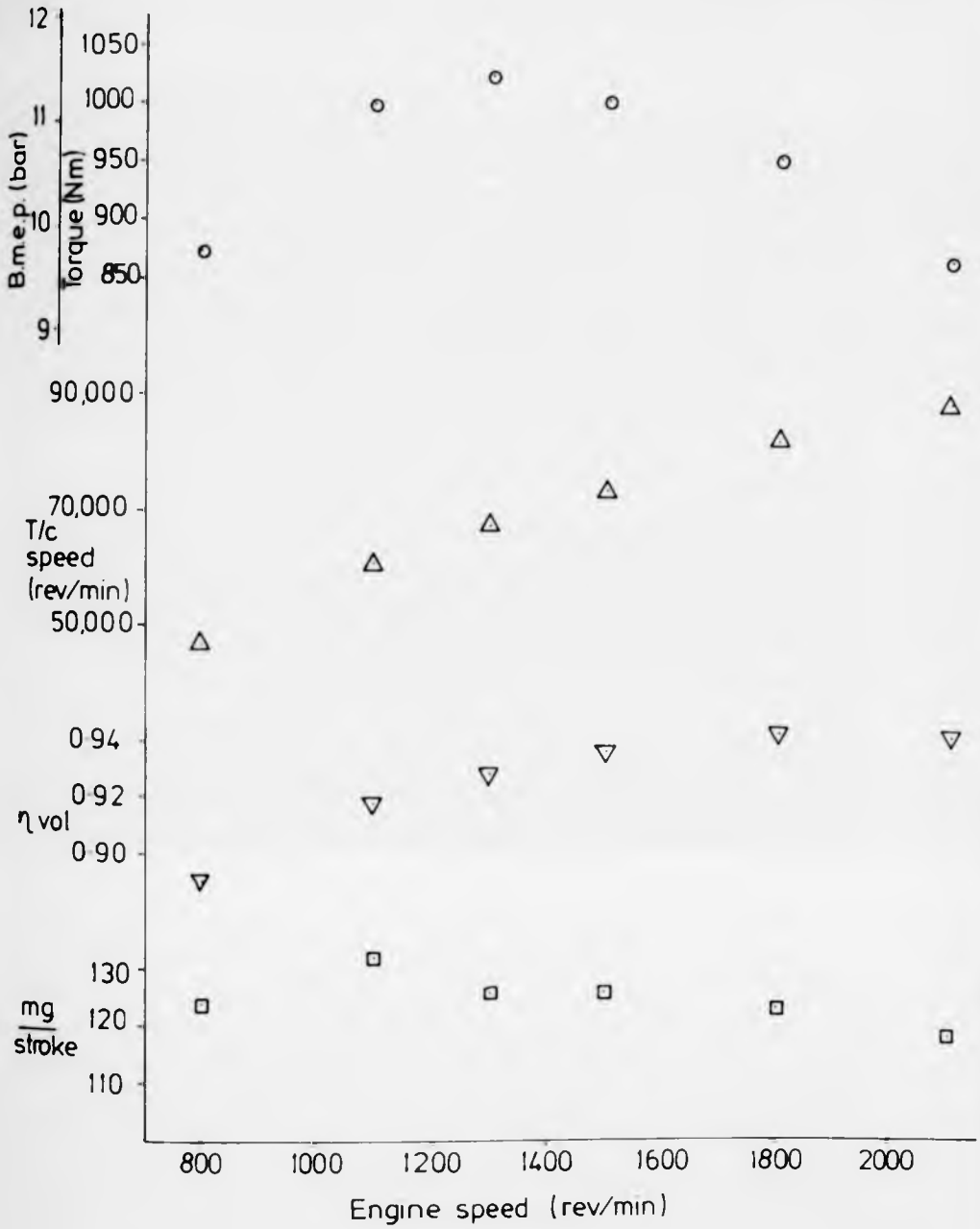


Engine: Leyland TL11
Vsw: 11·1 litre
Turbocharger: Holset H2C
F.I. pump: CAV Majormec

Timing: 22° BTDC (static)
Rating: 190 kW at 2100 rev/min
$P_{amb}$: 23°C
$T_{amb}$: 0·99 bar

Figure 4.2 Full-load performance of TL11 engine.

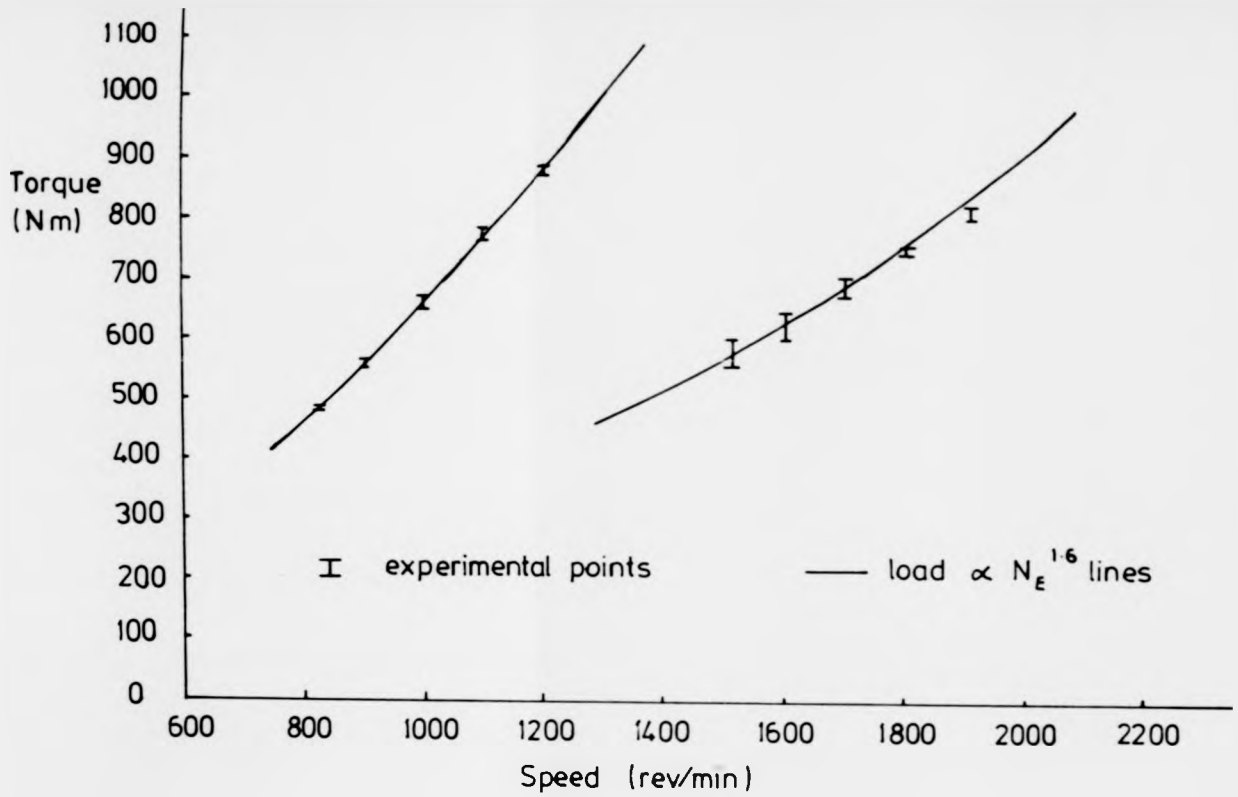


Figure 4.3 Windage characteristics of dynamometer.

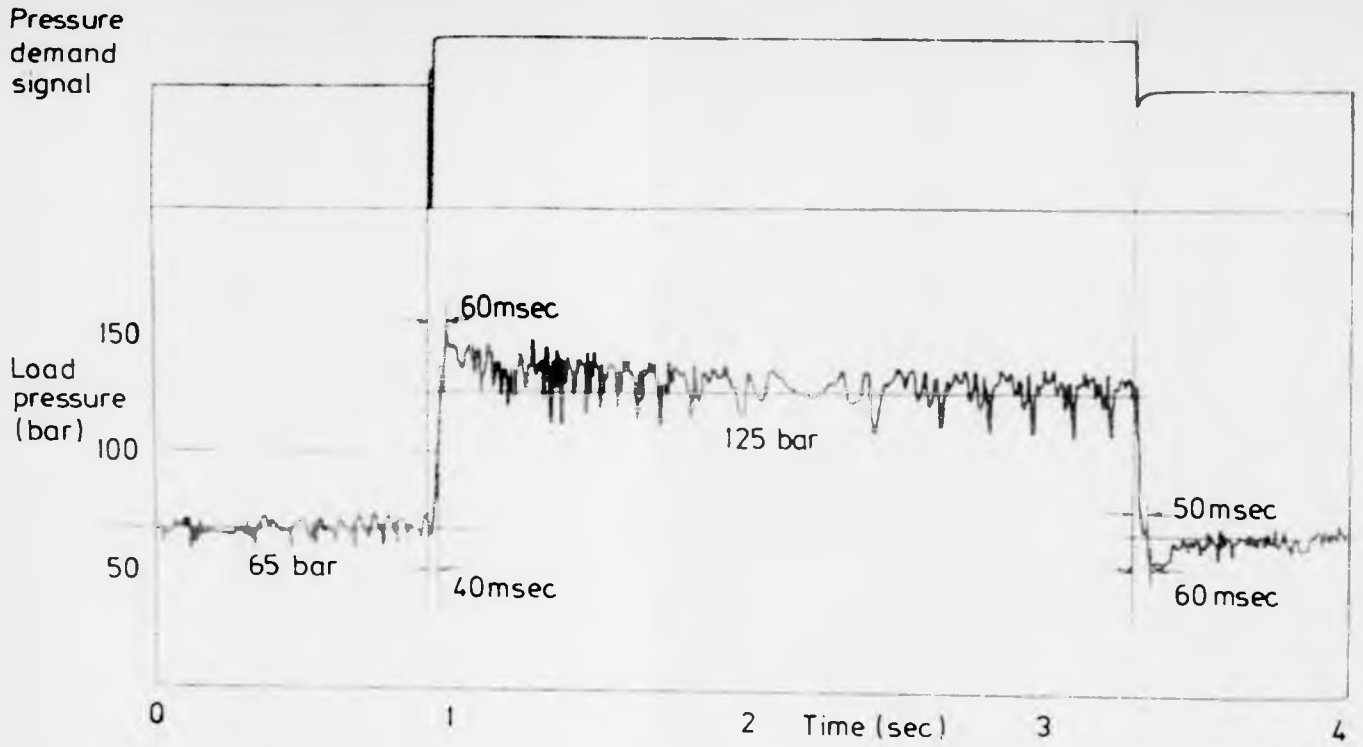


Figure 4.4 Dynamometer load pressure response to step changes in demand voltage, from results of Campbell (74)

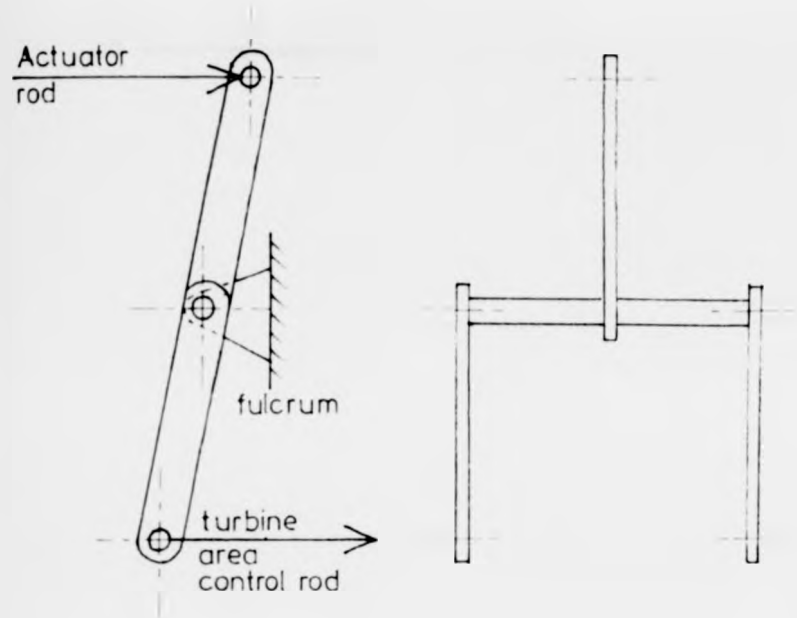


Figure 4 5 Diagram of turbine area control linkage

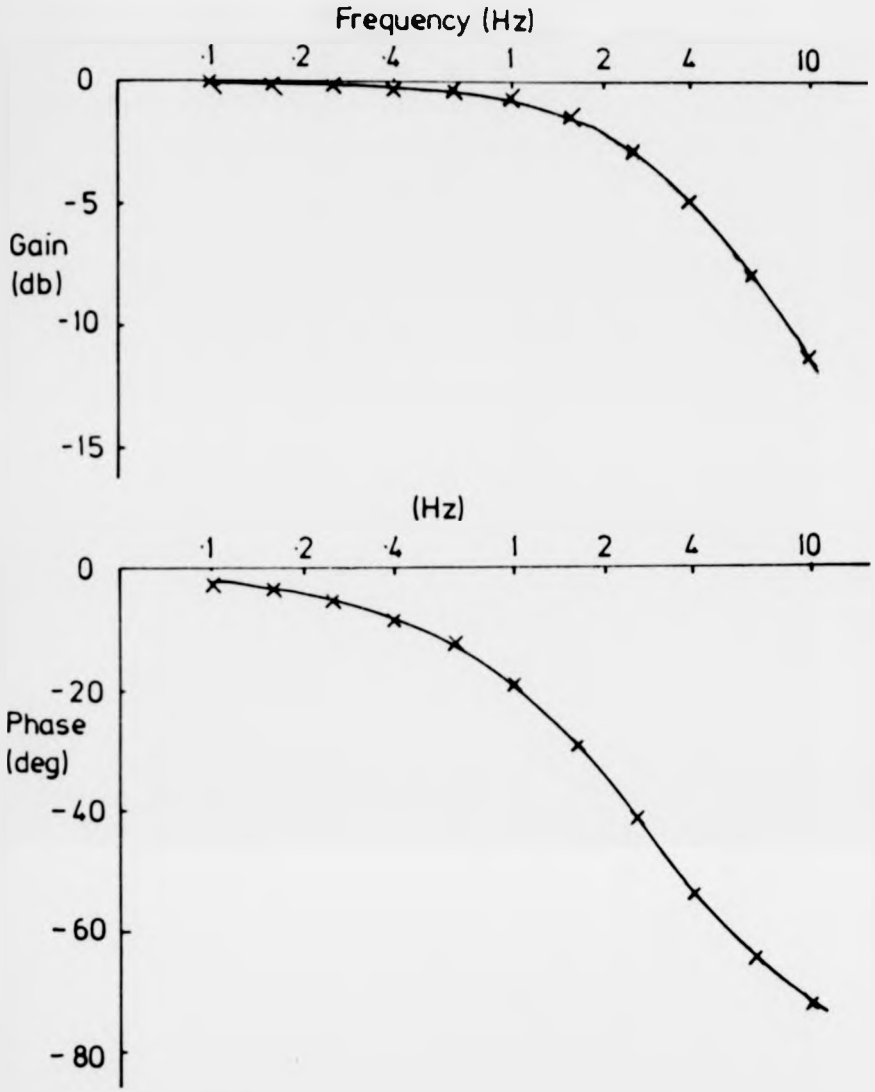


First order system, $f_b \approx 2.83$ Hz

Figure 4.6 Thermocouple signal conditioning response.

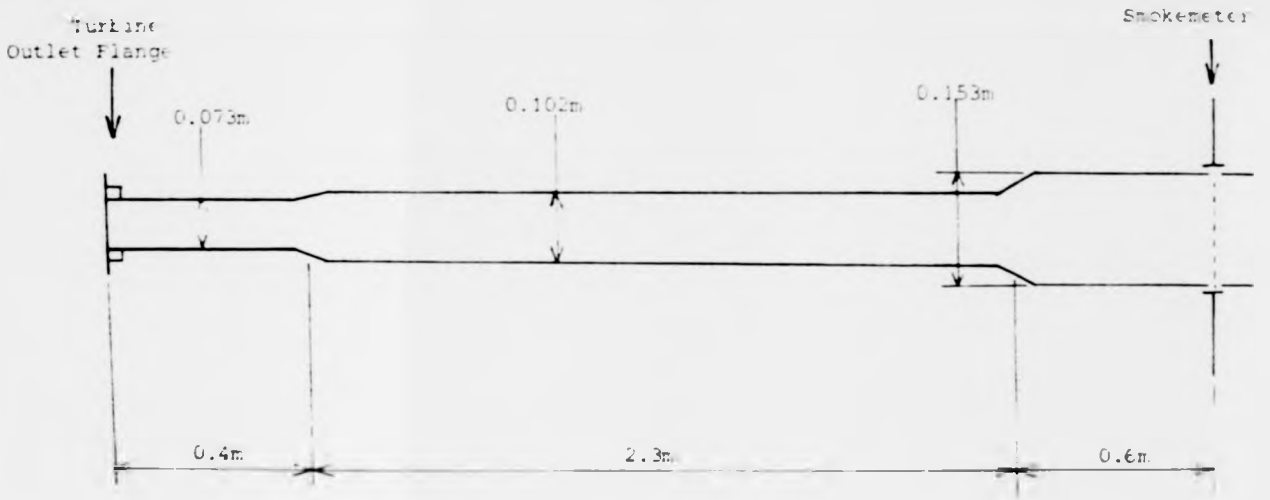


Figure 4.7 Exhaust dimensions showing opacity meter.

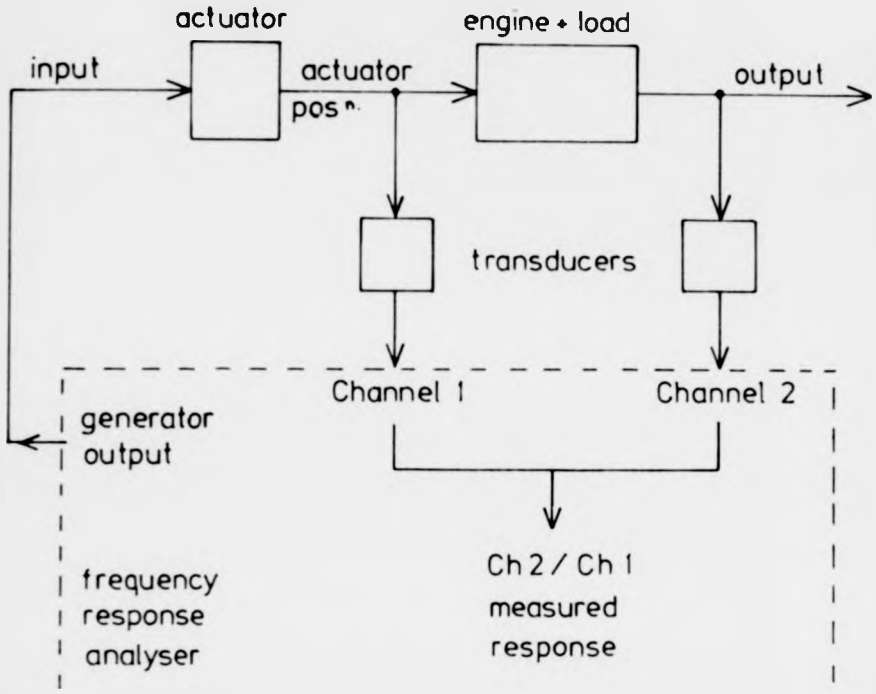


Figure 4.8 Removal of actuator response from frequency response measurements

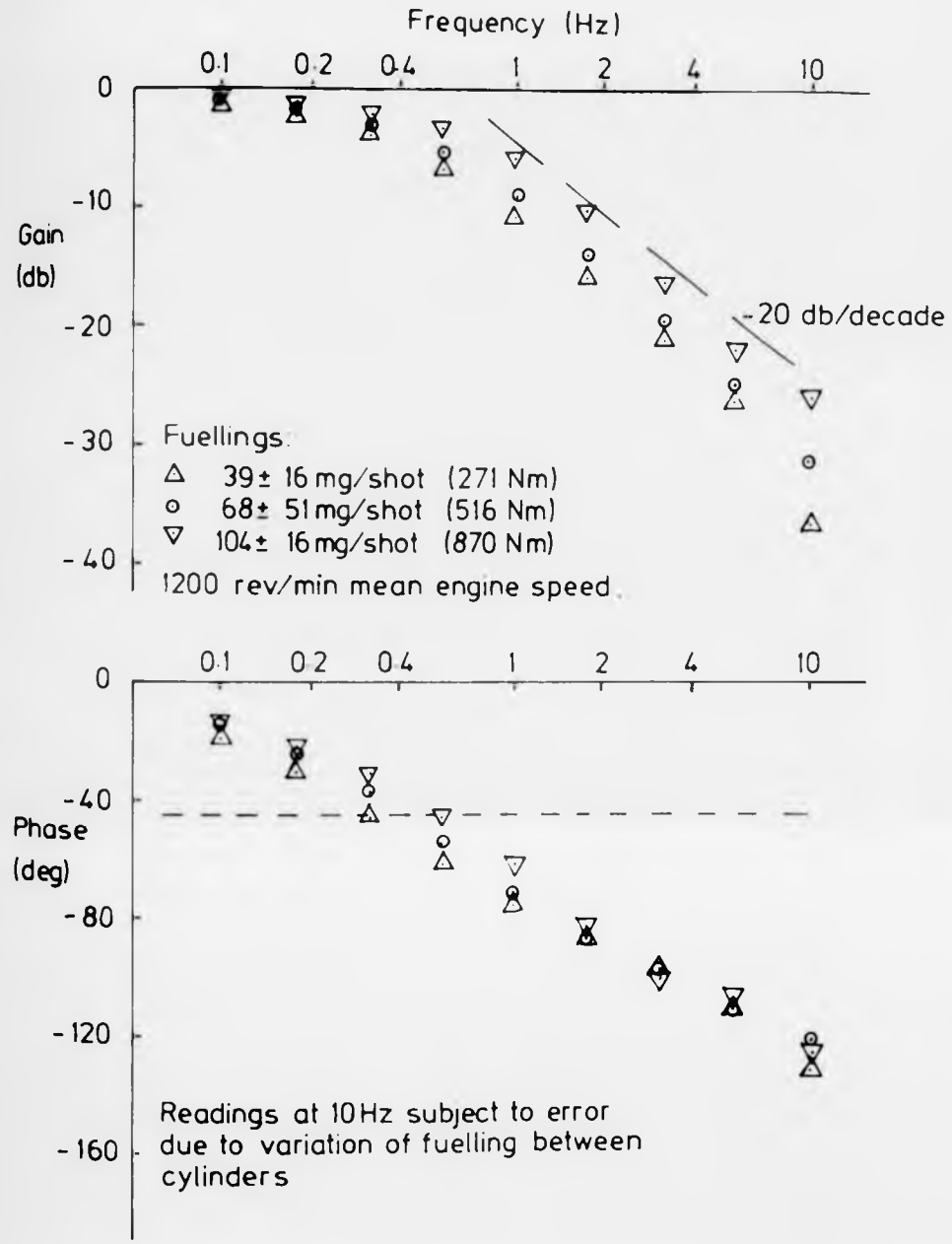


Figure 5.1 Variation of engine speed response with mean fuelling (rack perturbation)

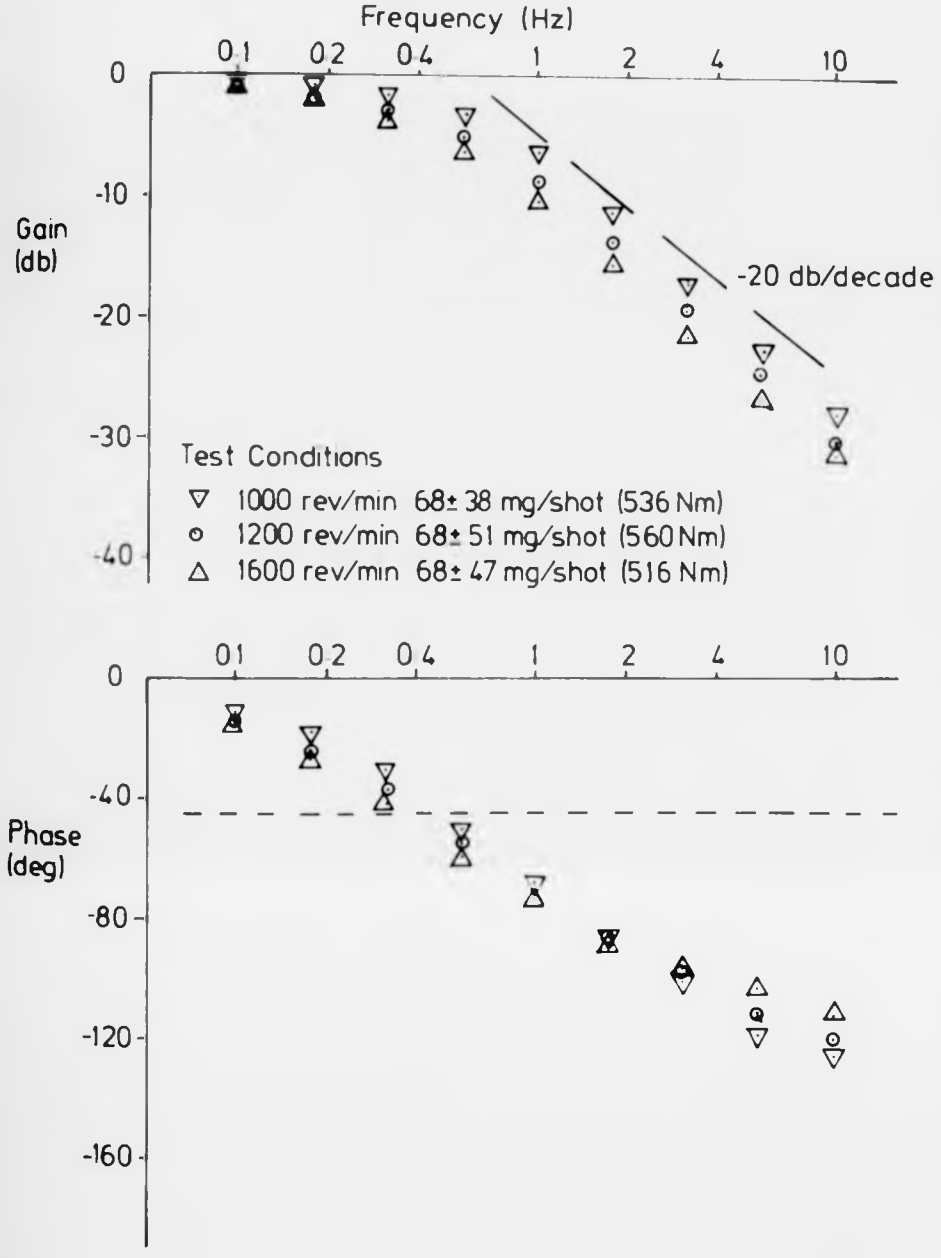


Figure 5.2 Variation of speed response with mean engine speed (rack perturbation)

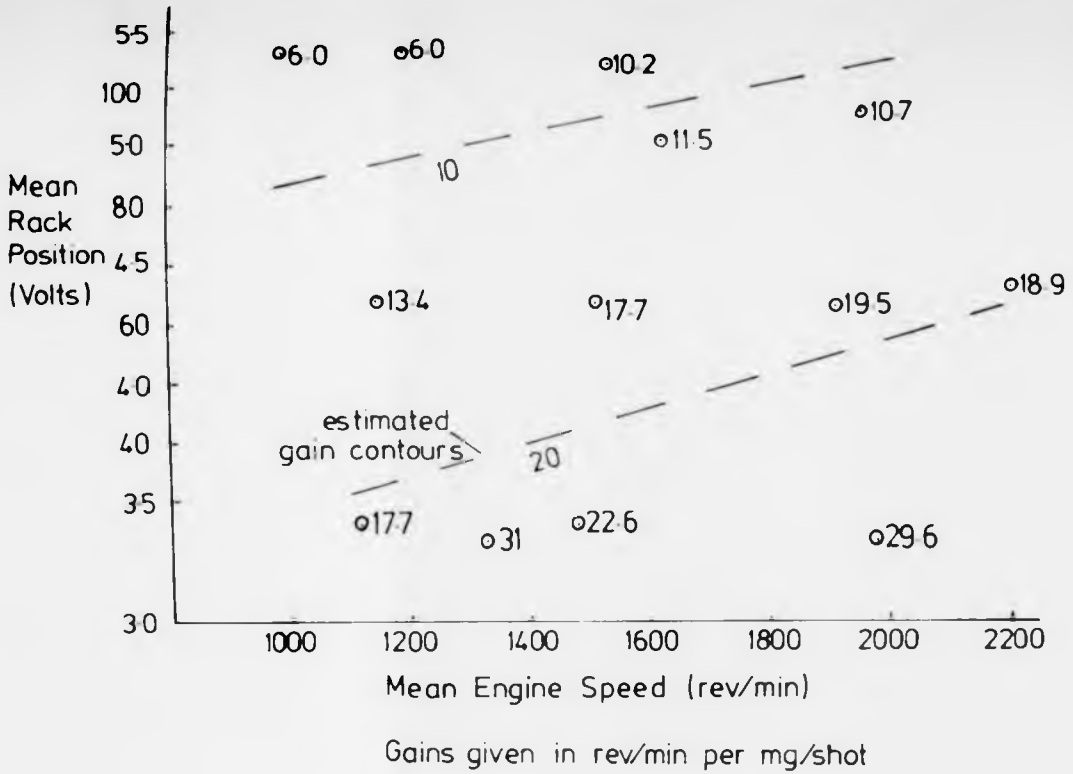


Figure 5.3 Steady state gains: speed response to rack perturbation

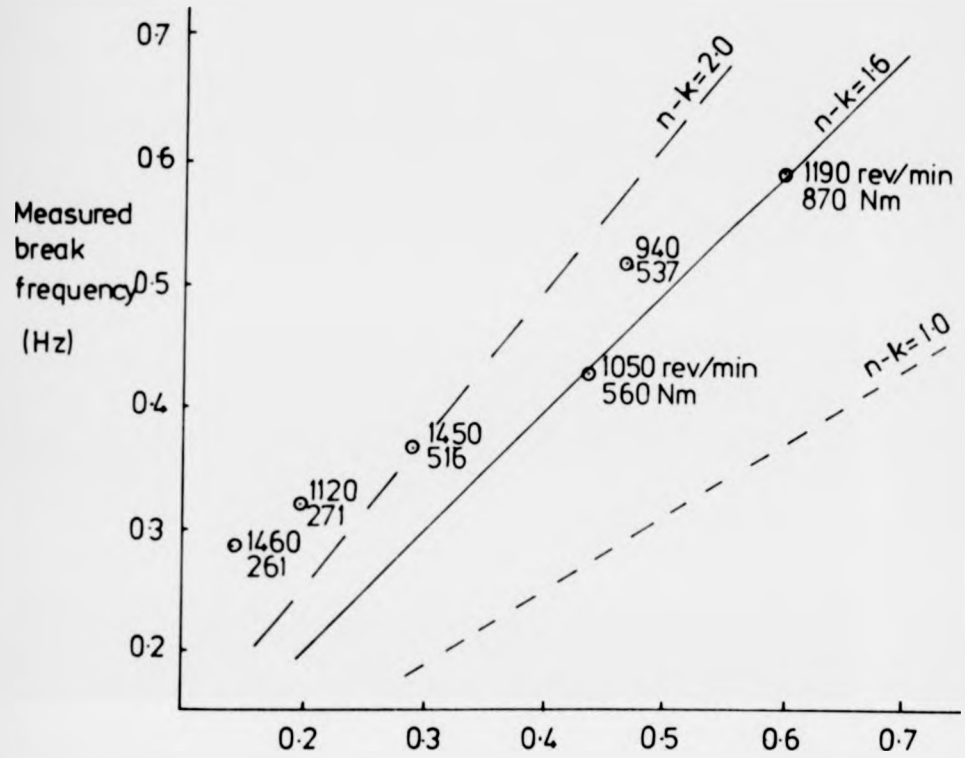


$$fb = \frac{15(n-k)\tau_m}{\pi^2 N_E I_E} \quad \text{[where } (n-k)=1\cdot6\text{]}$$

Figure 5.4 Measured break frequency of speed response against calculated value.

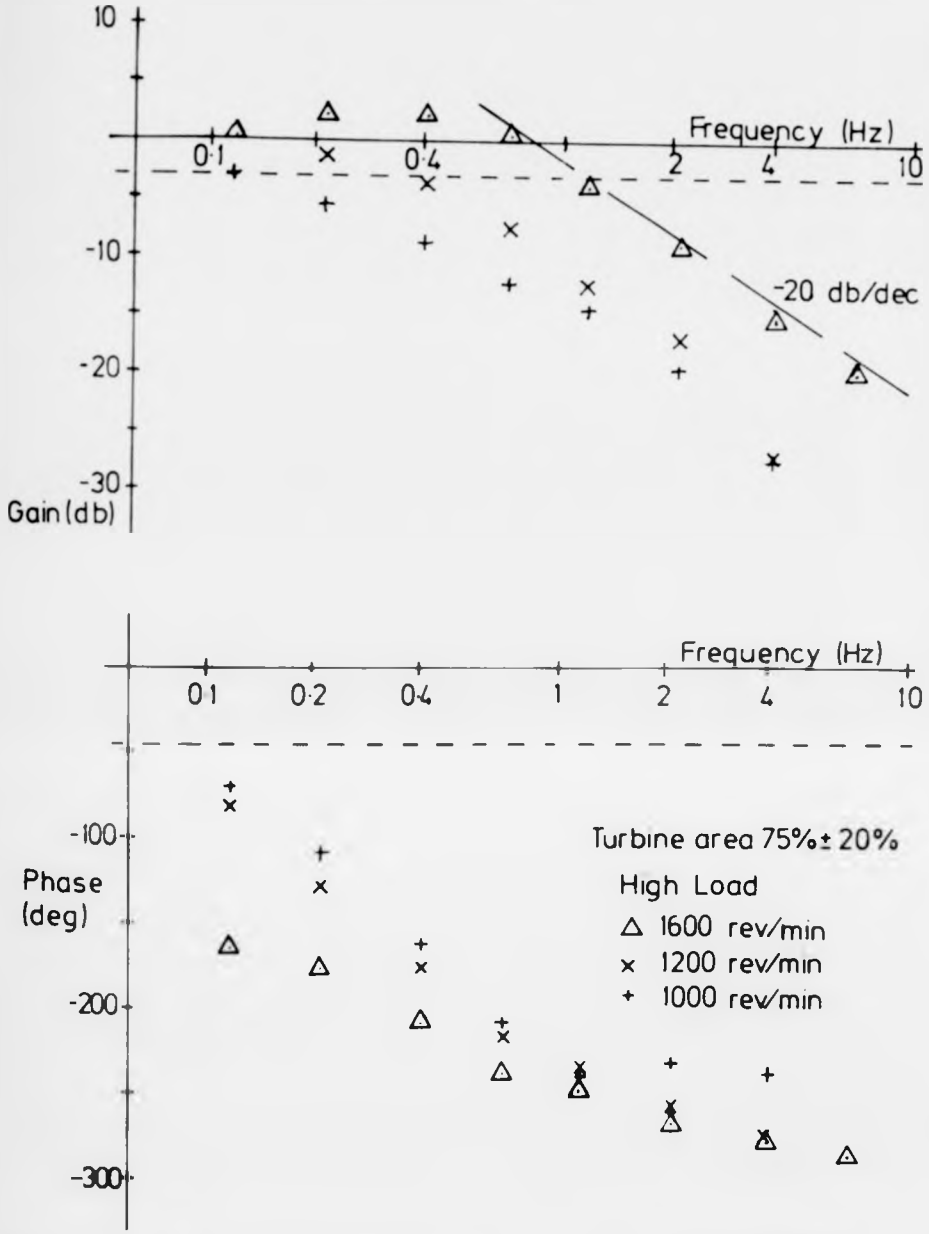


Figure 5.5 Engine speed response to turbine area perturbations

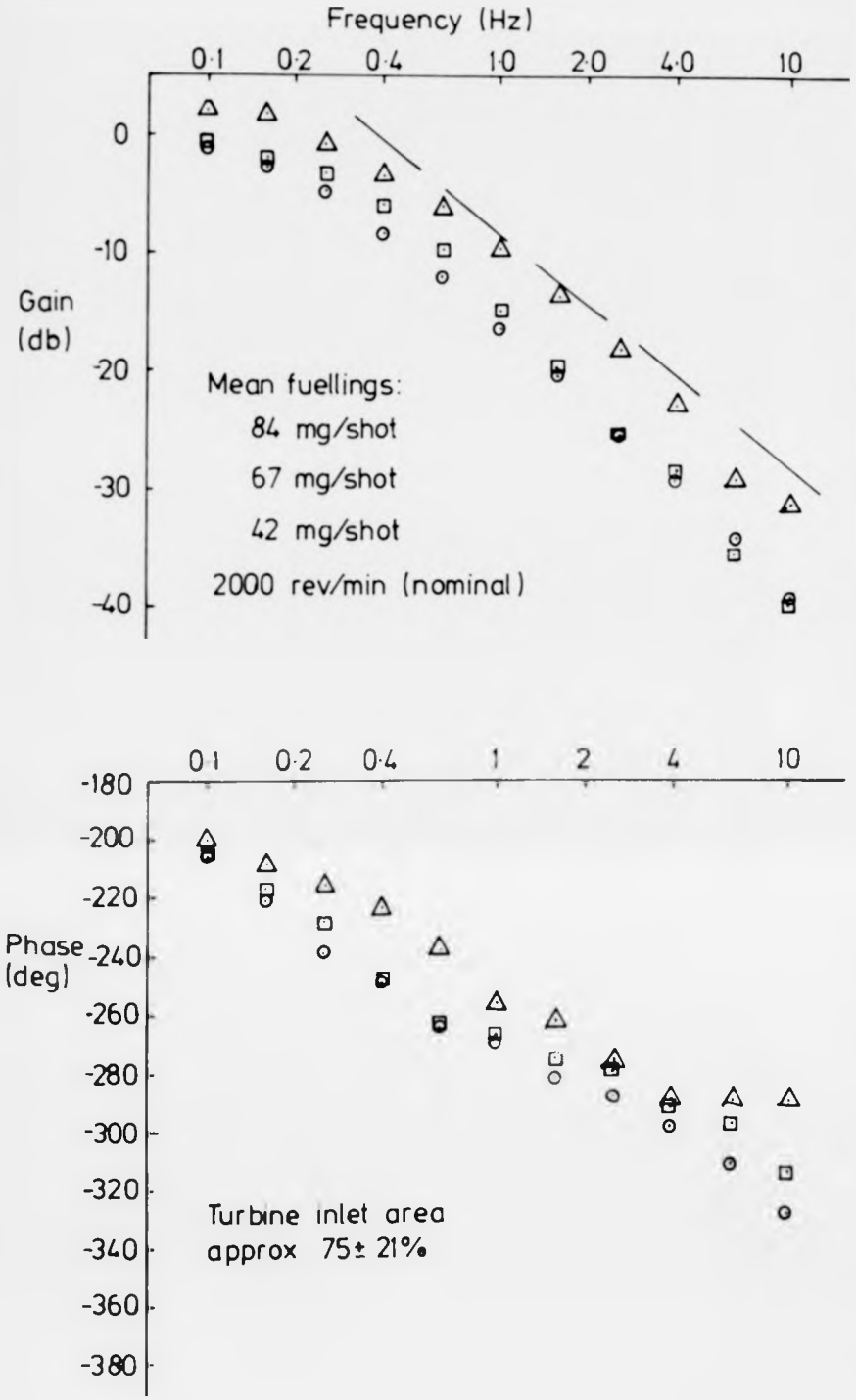


Figure 5.6 Engine speed response to turbine inlet area at different mean fuellings.

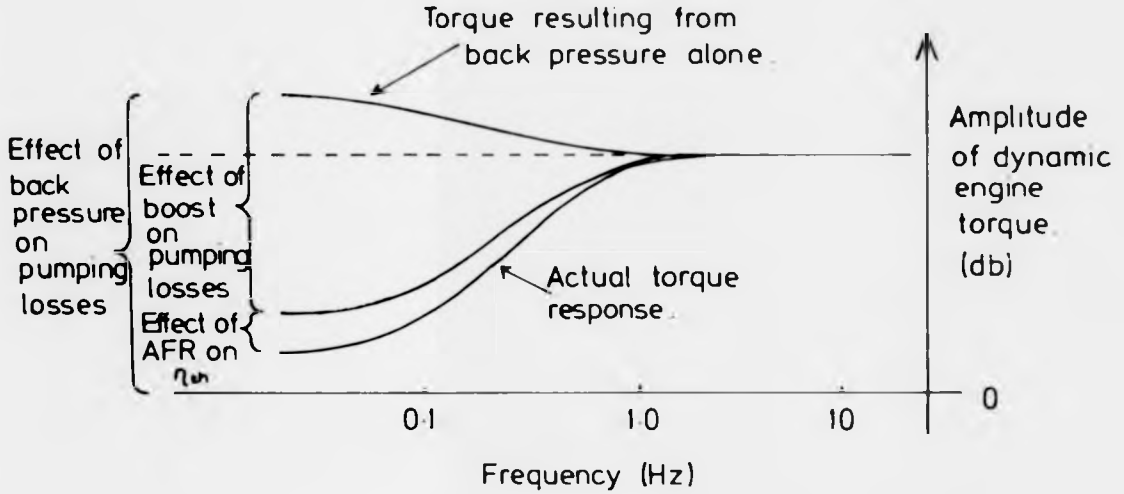


Amplitude of turbine inlet area perturbations assumed constant

Figure 5.7 Diagram illustrating the effect of turbine inlet area perturbation on dynamic engine torque.

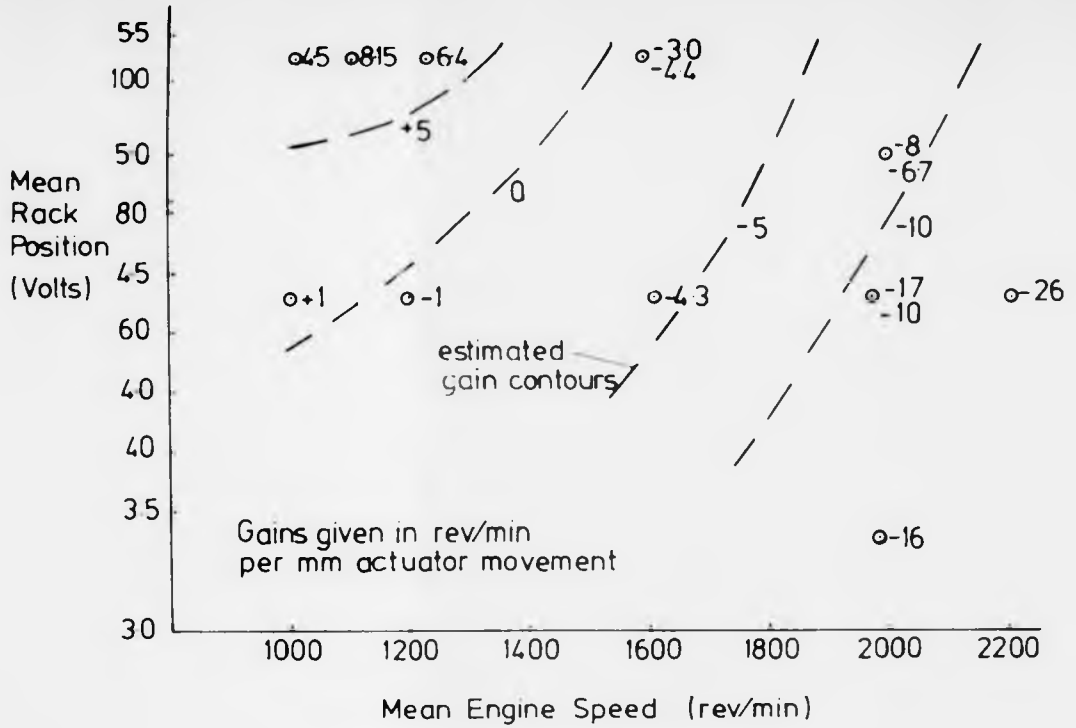


Figure 5.8 Steady state gains: speed response to turbine area

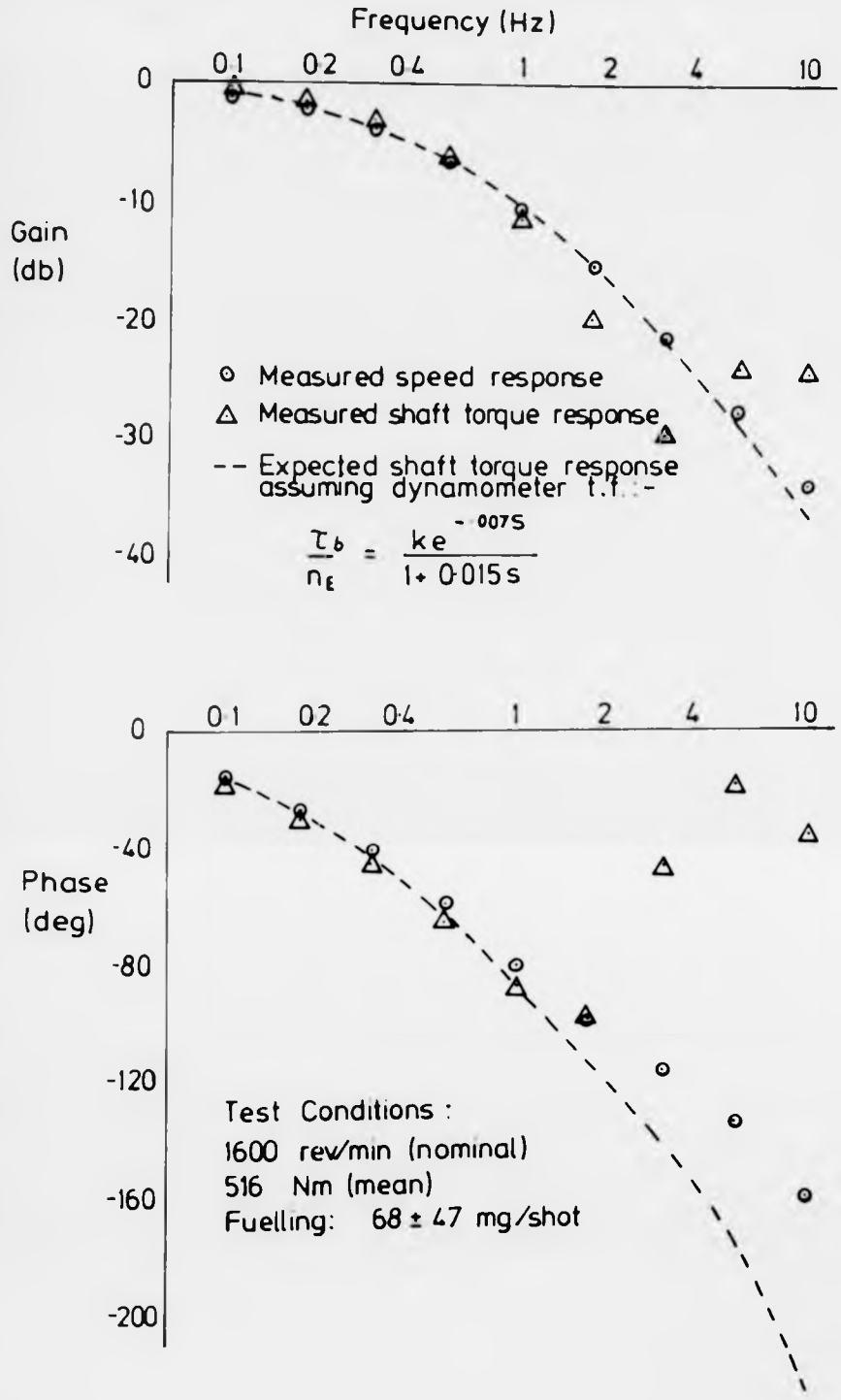


Figure 5.9 Comparison of Measured and Expected Shaft Torque Responses

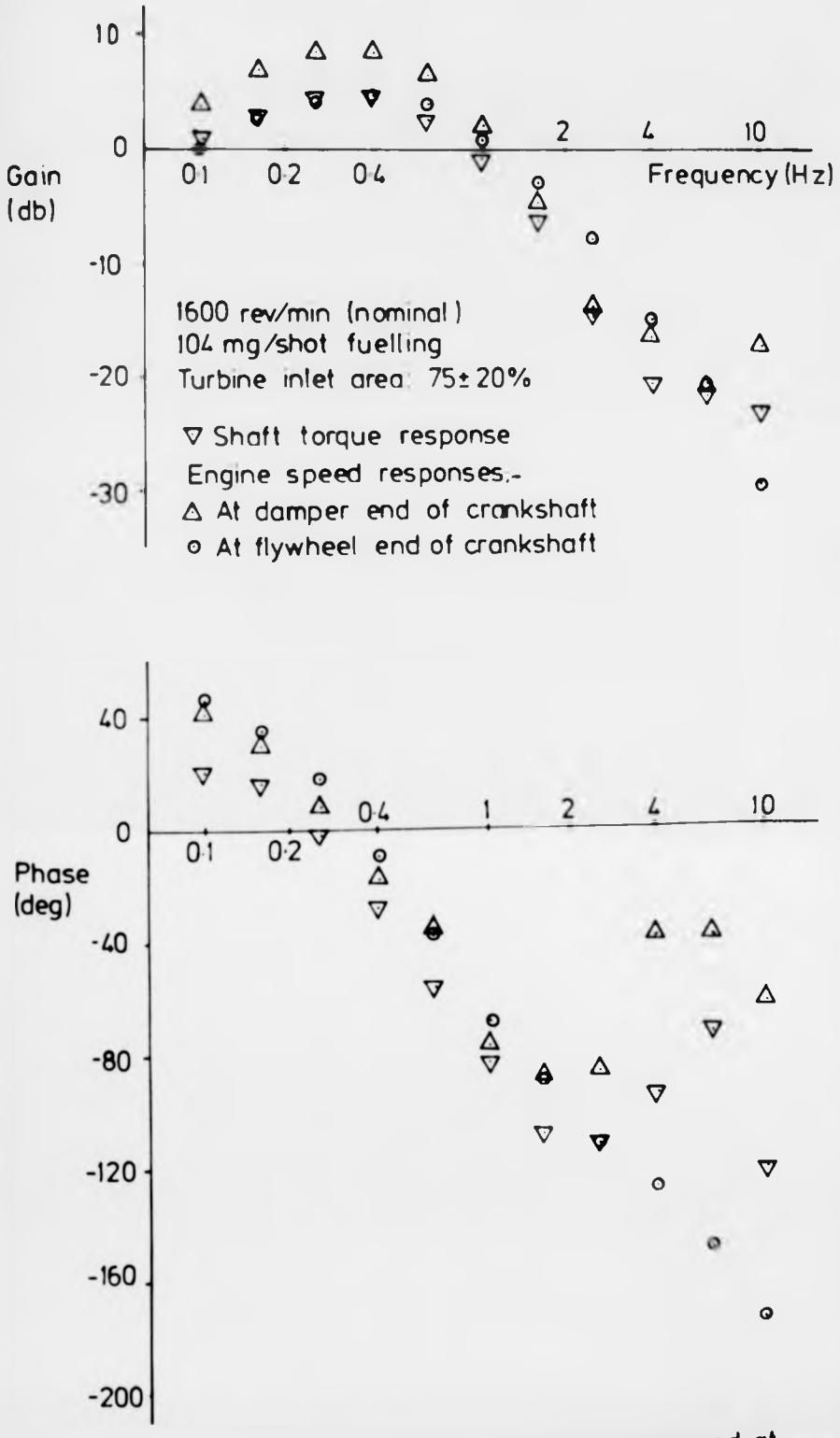


Figure 5.10 Comparison of speed responses measured at flywheel and damper with shaft torque response.

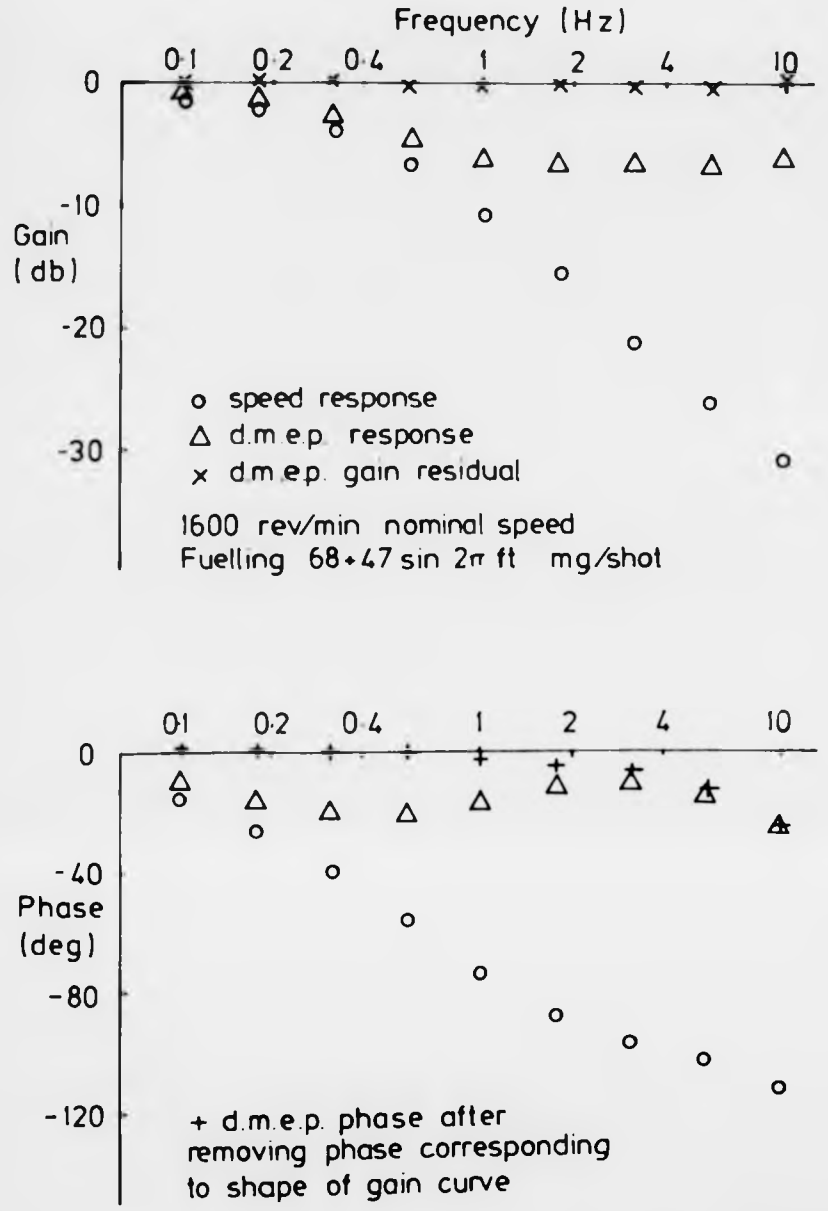


Figure 5.11 D.m.e.p. response : 1600 rev/min, large amplitude fuelling perturbation.

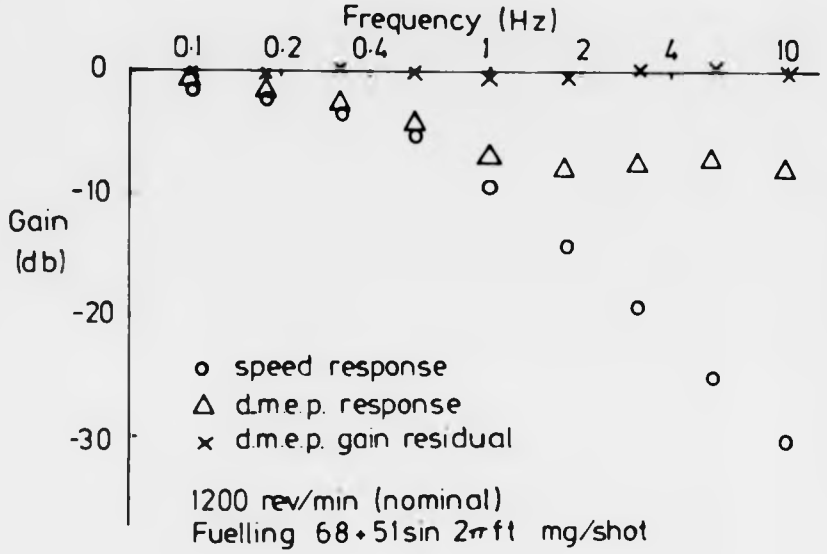


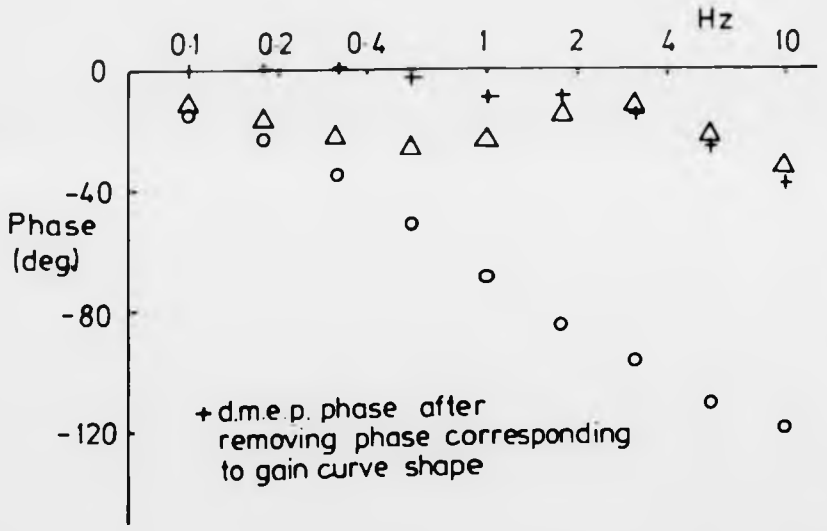


Figure 5.12 D.m.e.p. response: 1200 rev/min, large fuelling amplitude.

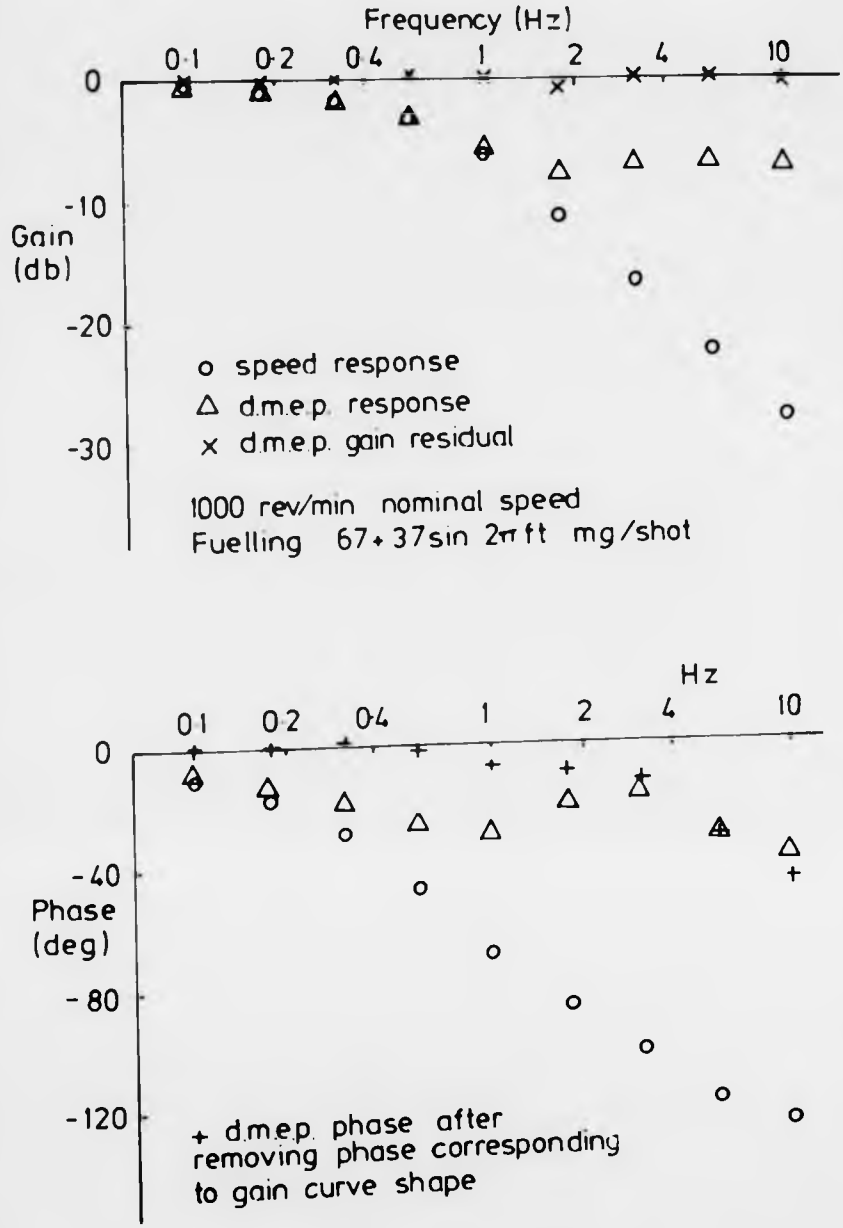


Figure 5.13 D.m.e.p. response: 1000 rev/min with large amplitude of fuelling.

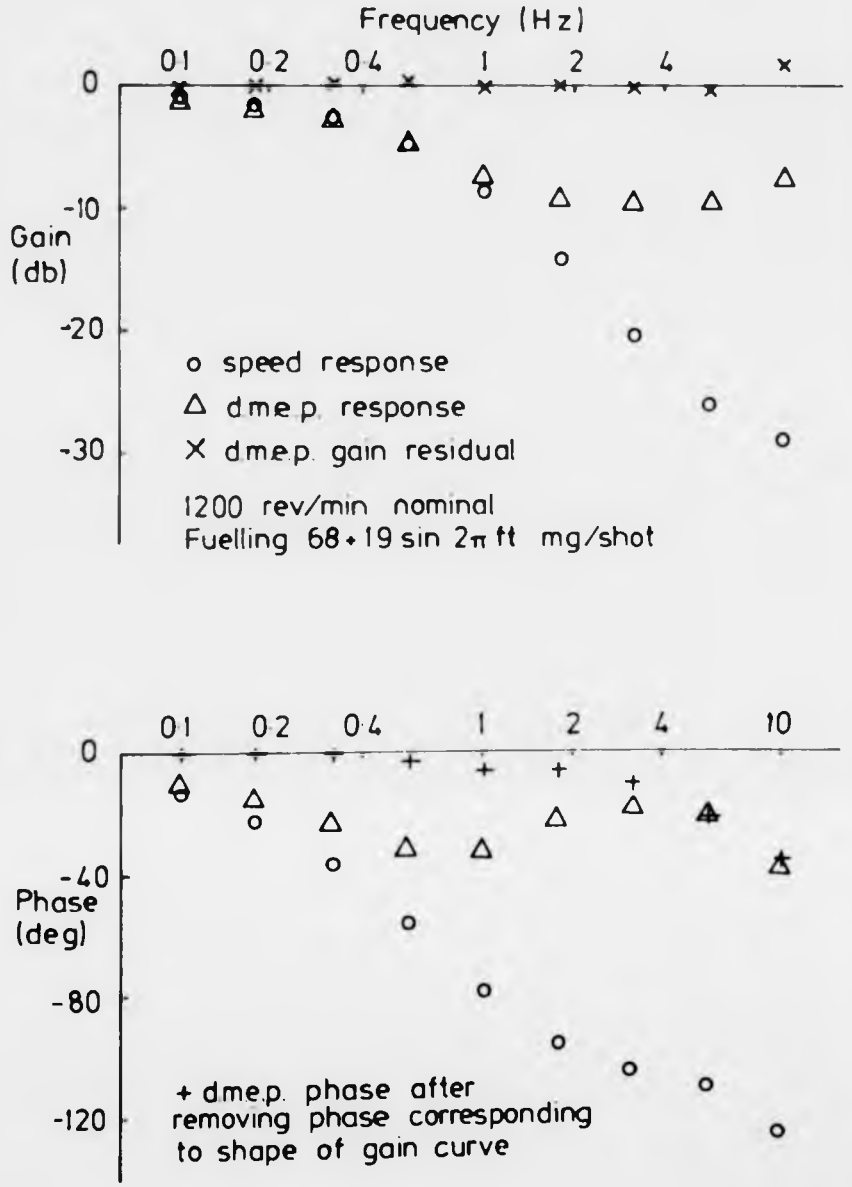


Figure 5.14 D.m.e.p. response: 1200 rev/min with moderate amplitude of fuelling.

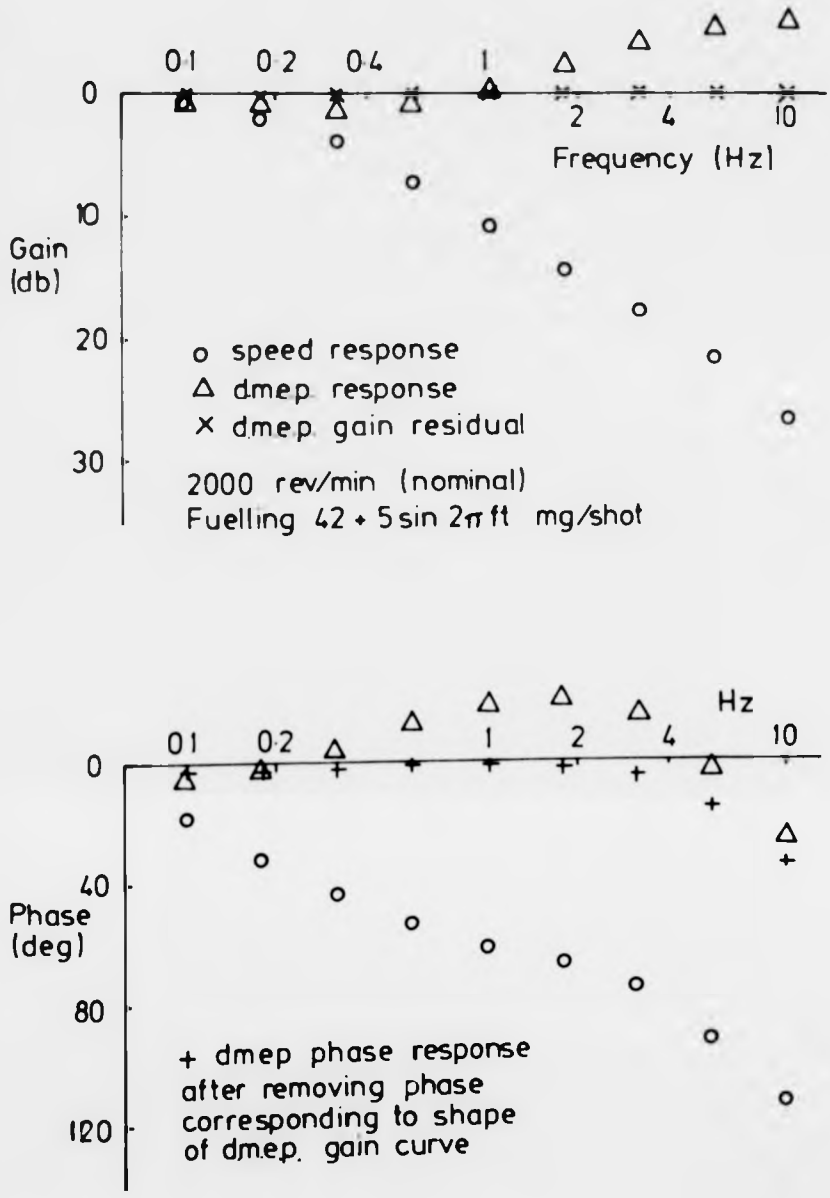


Figure 5.15 Dmep response: 2000 rev/min light load.

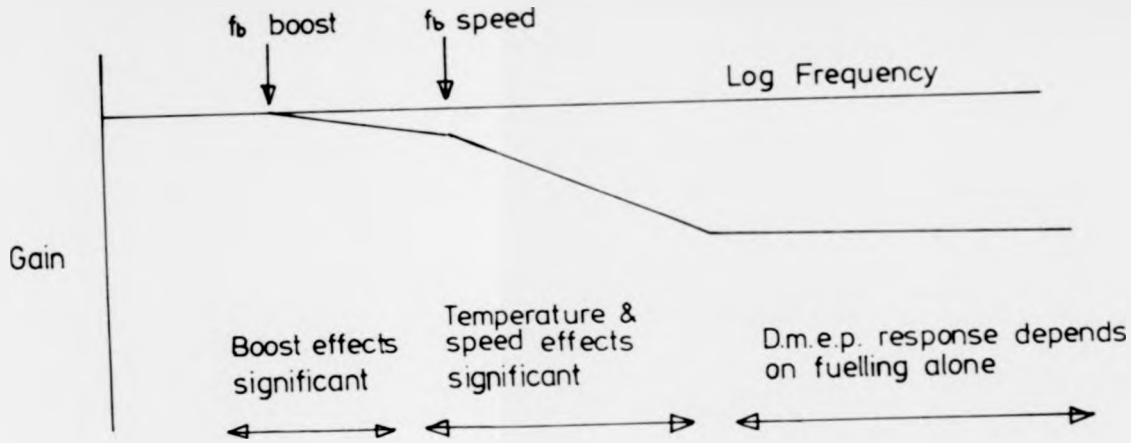


Figure 5.16 Schematic structure of d.m.e.p. response

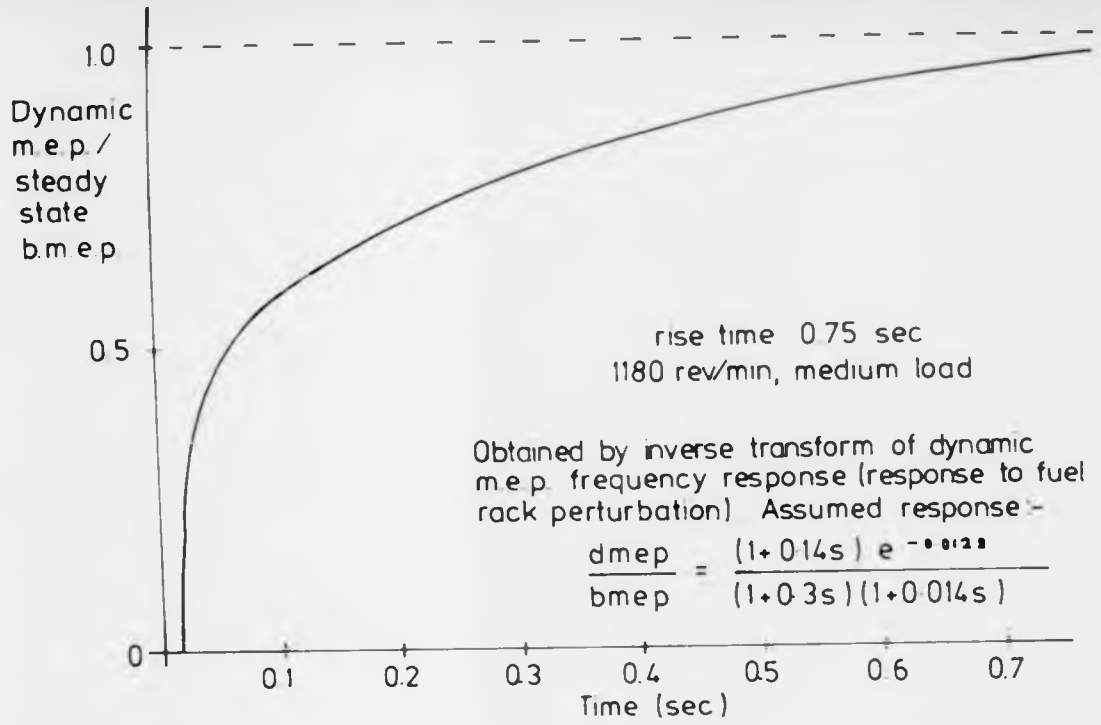


Figure 5.17 Dynamic torque step response

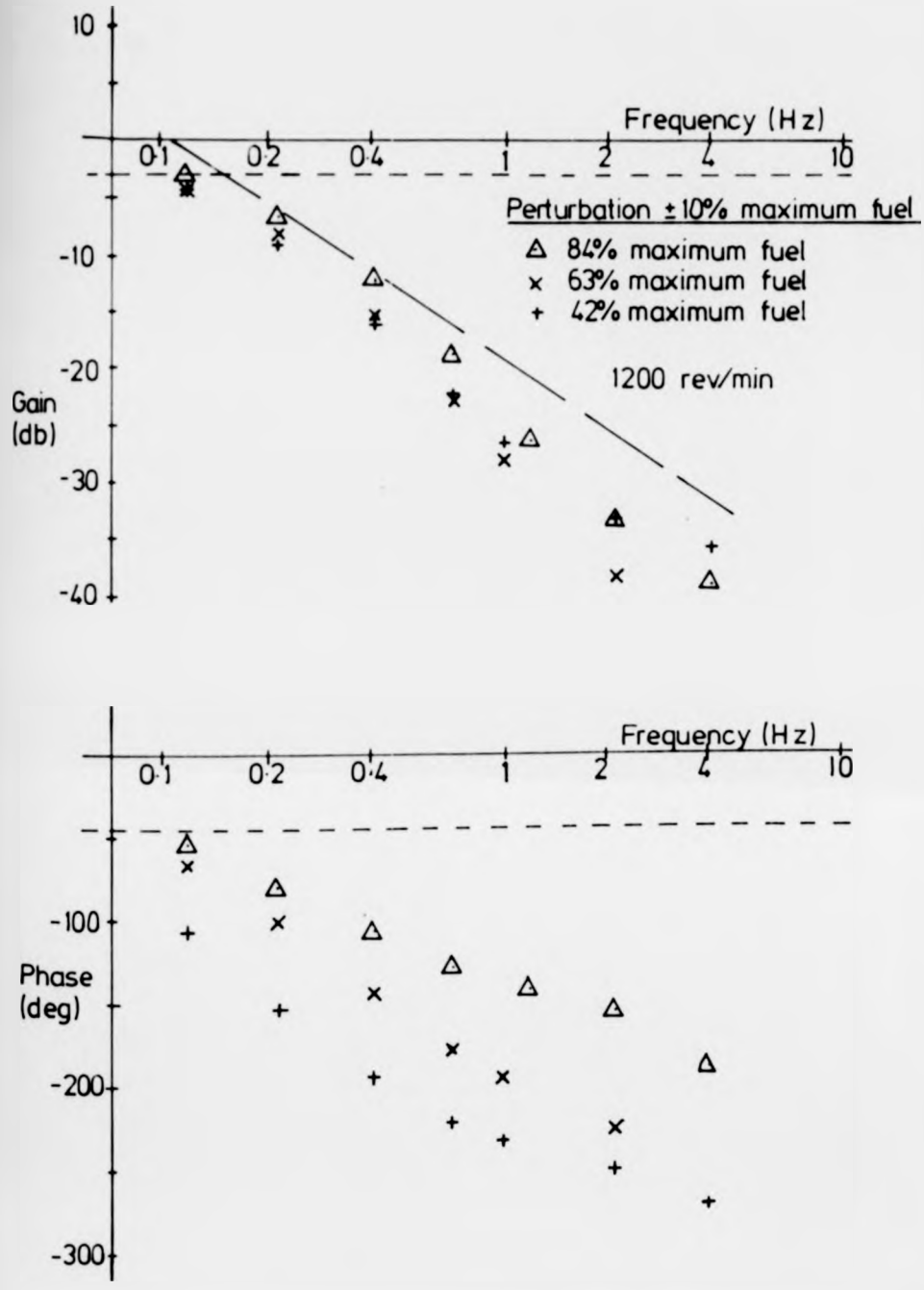


Figure 5.18 Boost pressure response to rack perturbation at different engine loads.

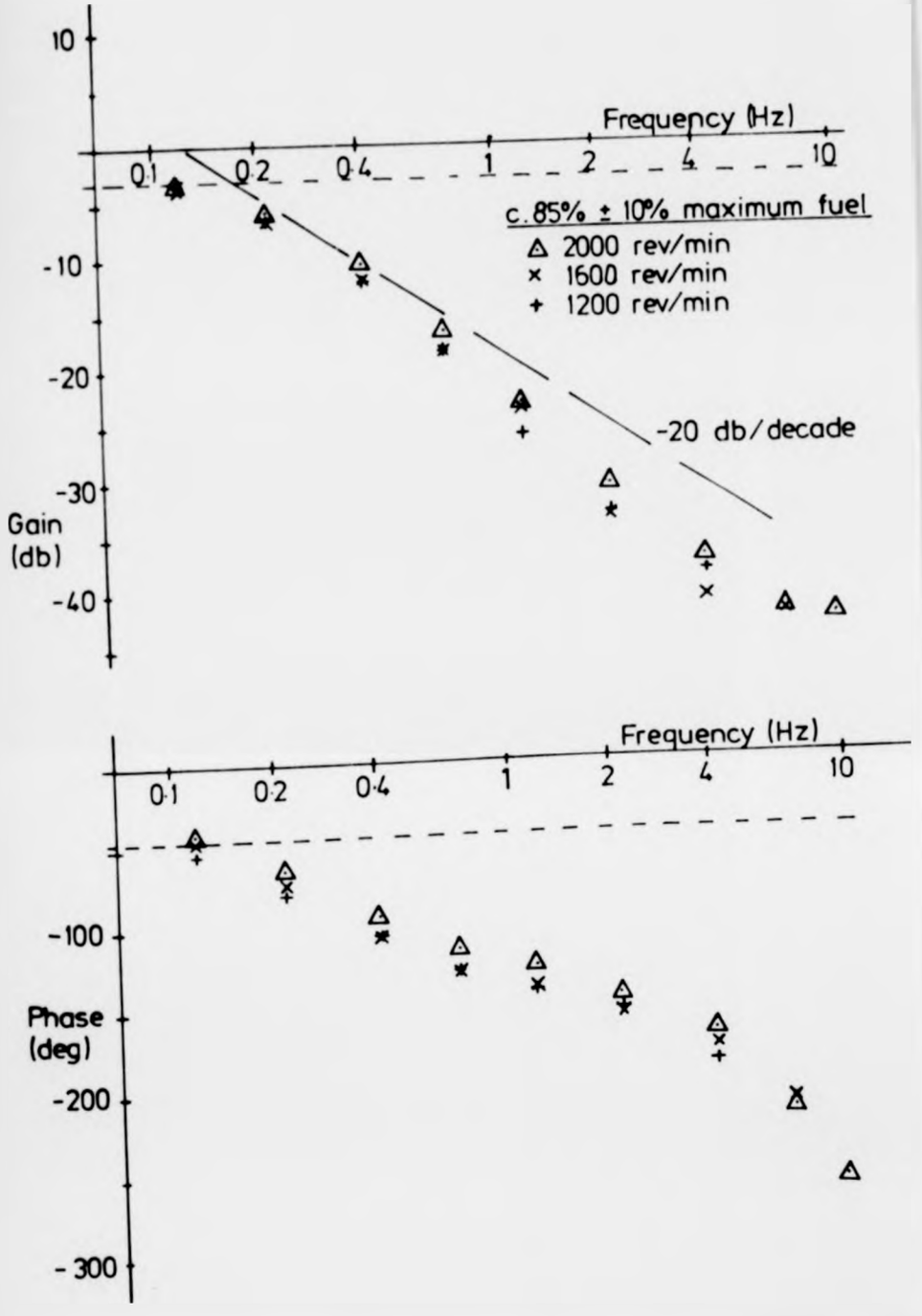


Figure 5.19 Boost pressure response to rack perturbation at different mean speeds.

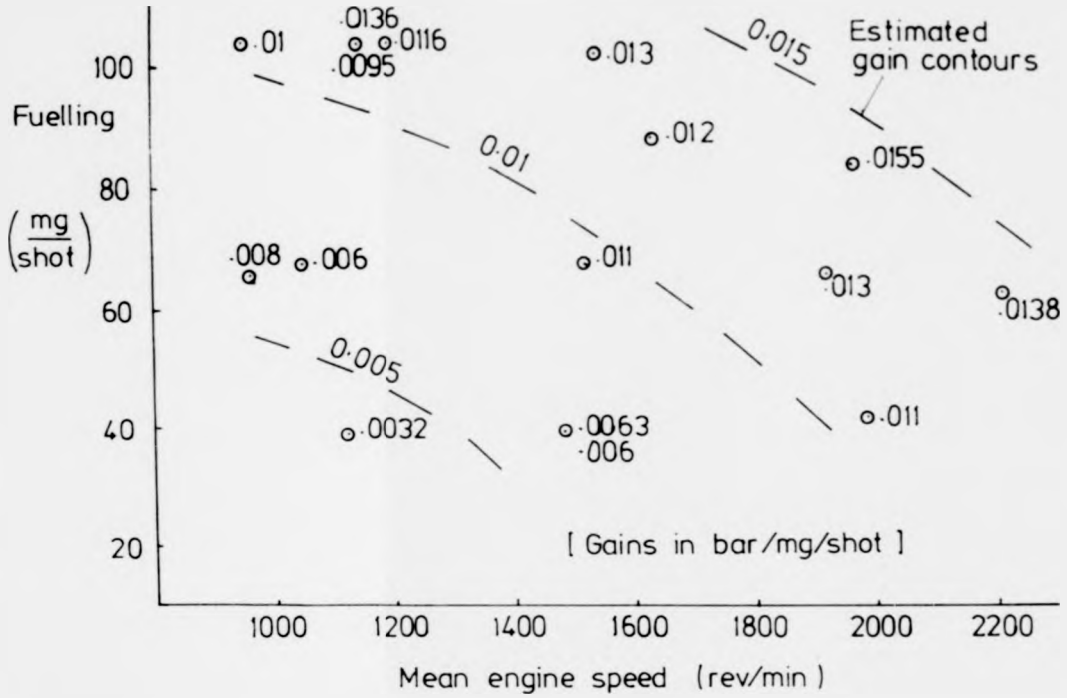


Figure 5.20 Steady state gains: boost response to rack

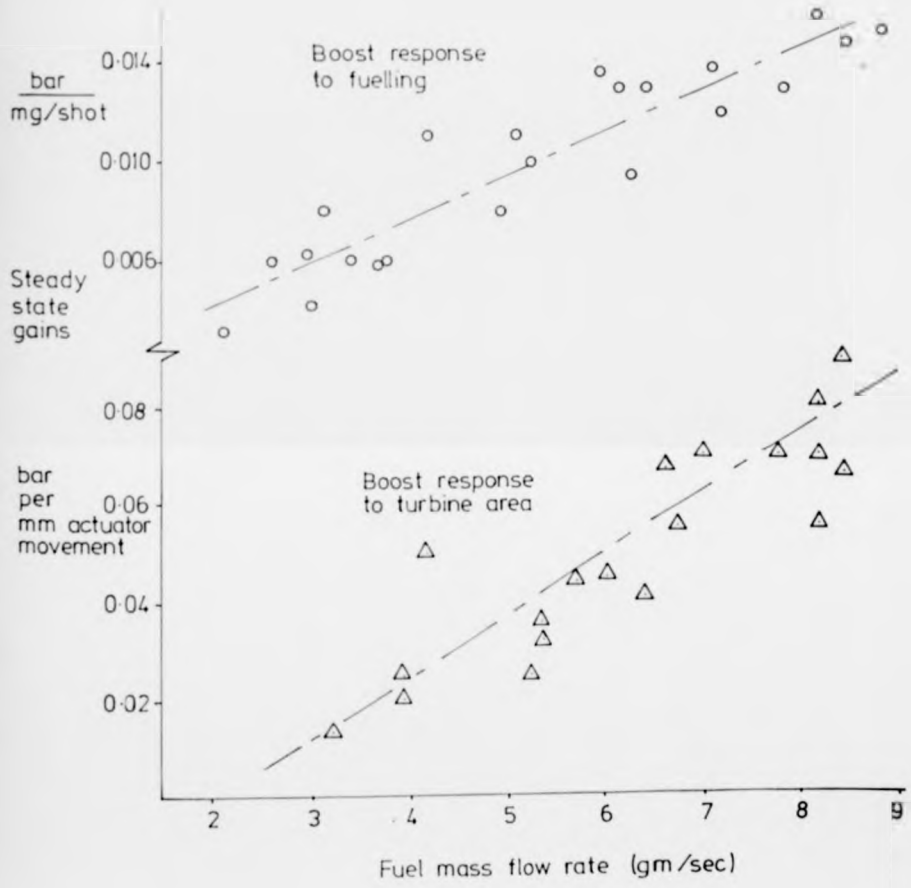


Figure 5.21 Boost steady state gains plotted against fuel mass flow rate.

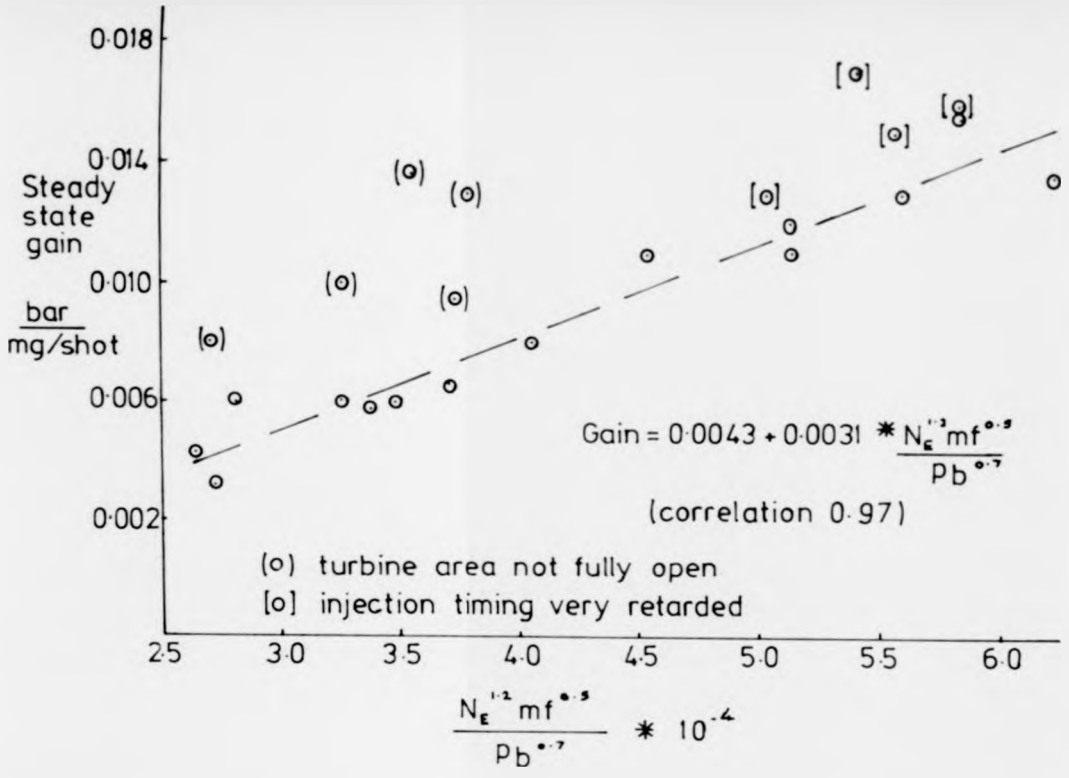


Figure 5.22 Boost steady state gain against dimensionless mass flow (fuel rack perturbation)

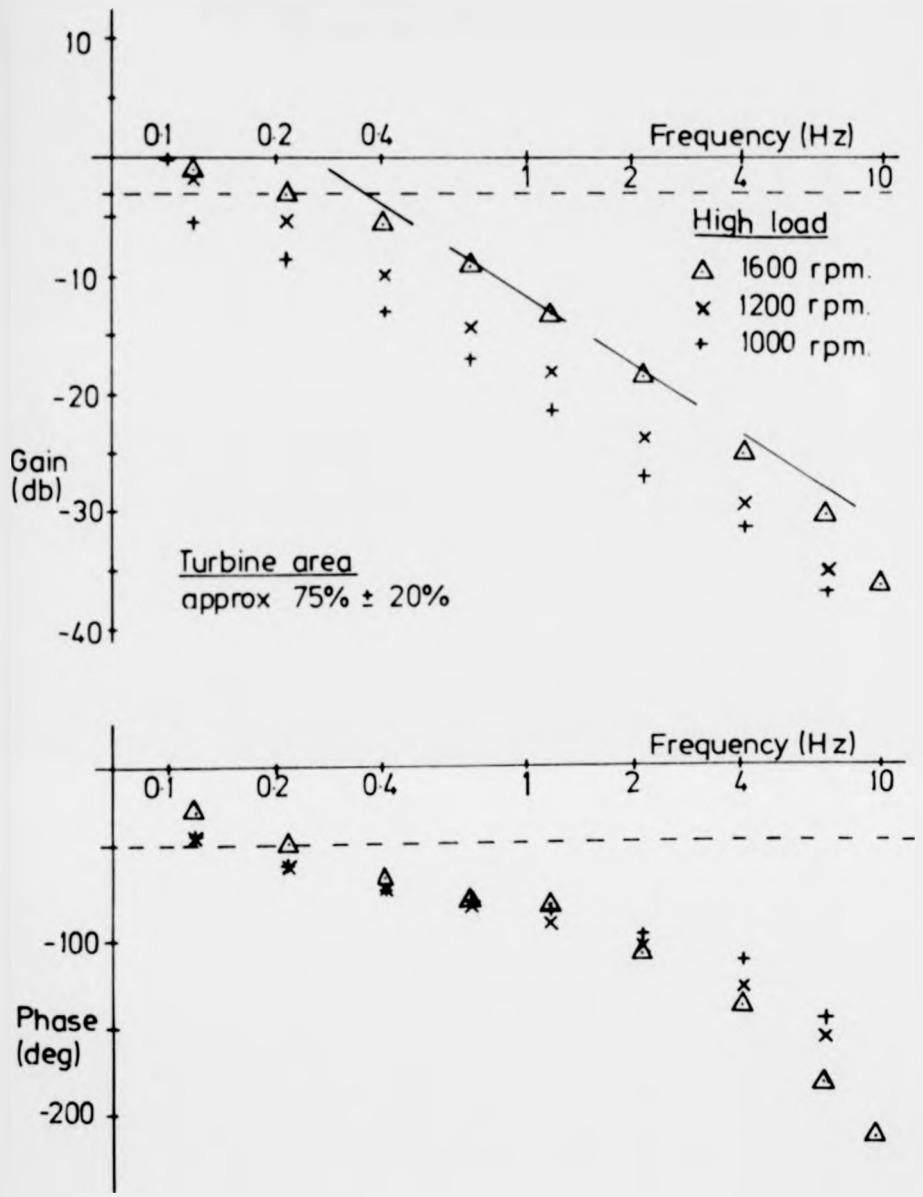


Figure 5.23 Effect of engine speed on boost response to turbine area.

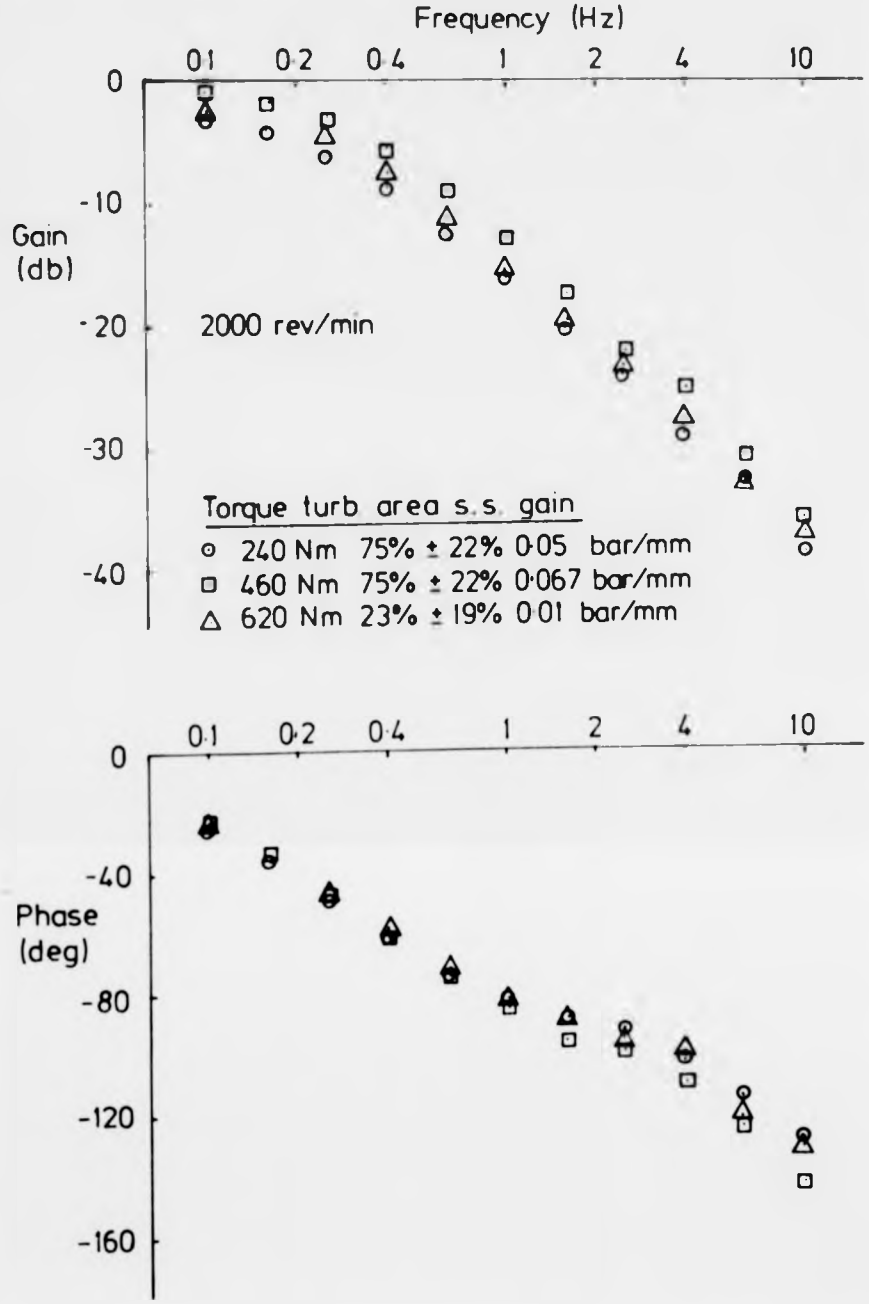


Figure 5.24 Effect of load on boost response to turbine area

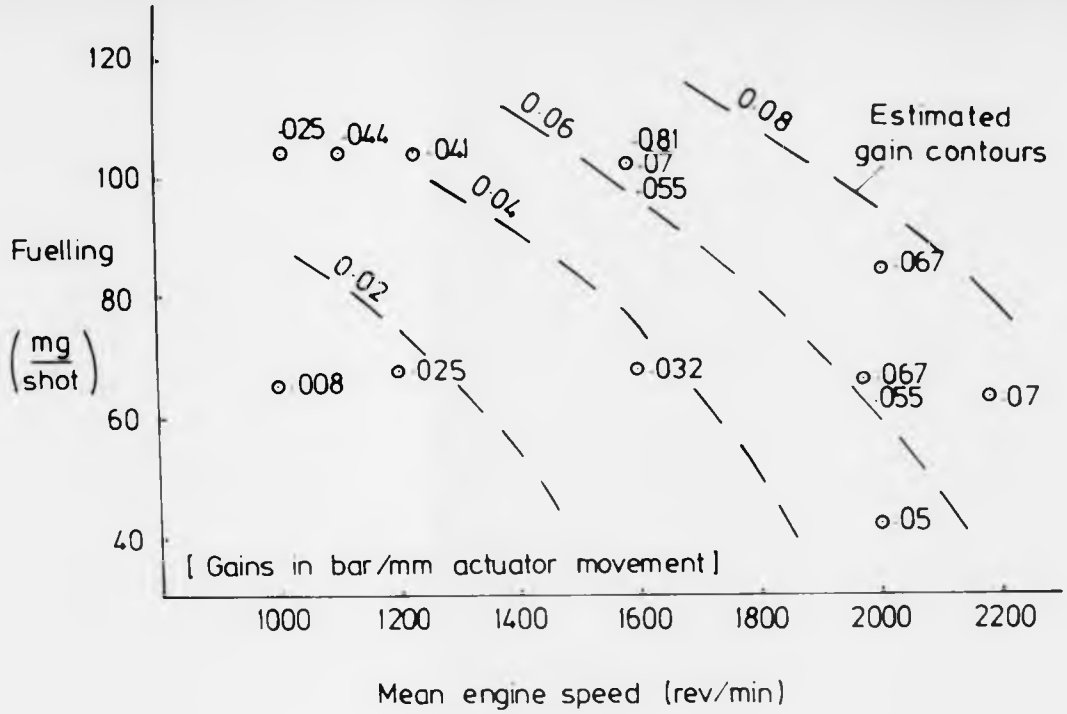


Figure 5.25 Steady state gains: boost response to turbine area

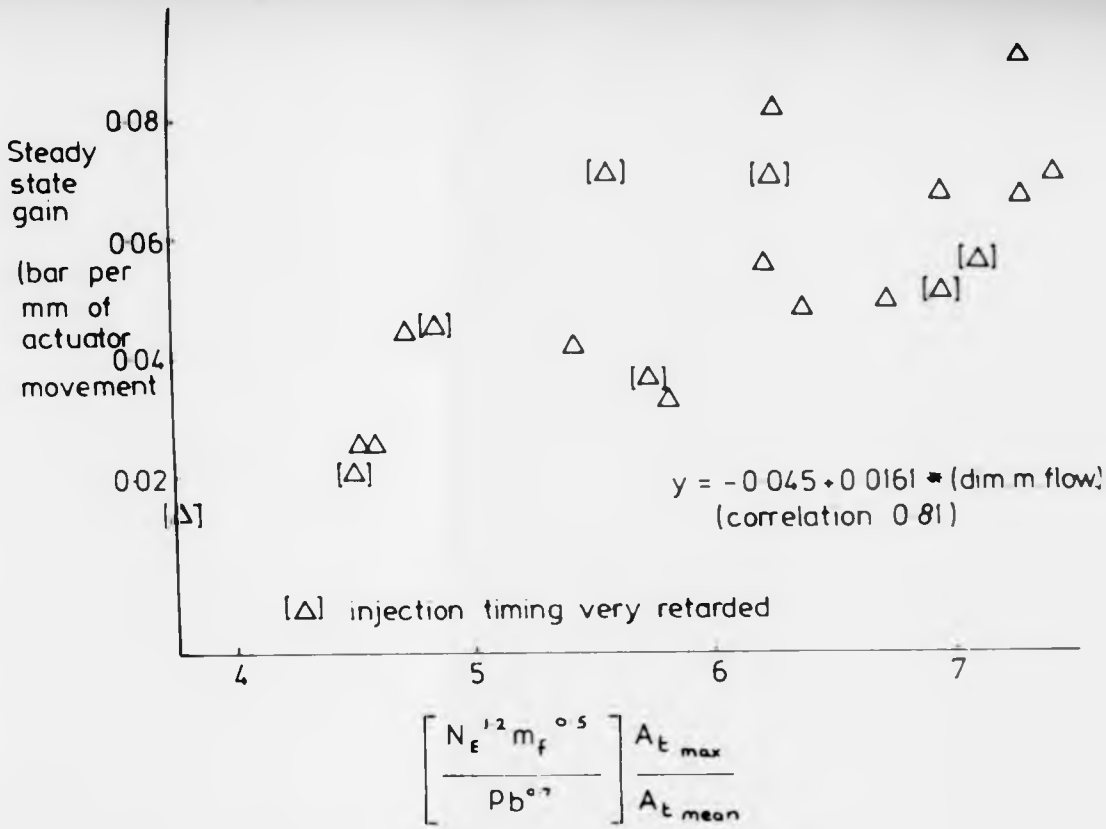


Figure 5.26 Boost steady state gain against dimensionless turbine mass flow (turbine area perturbation)

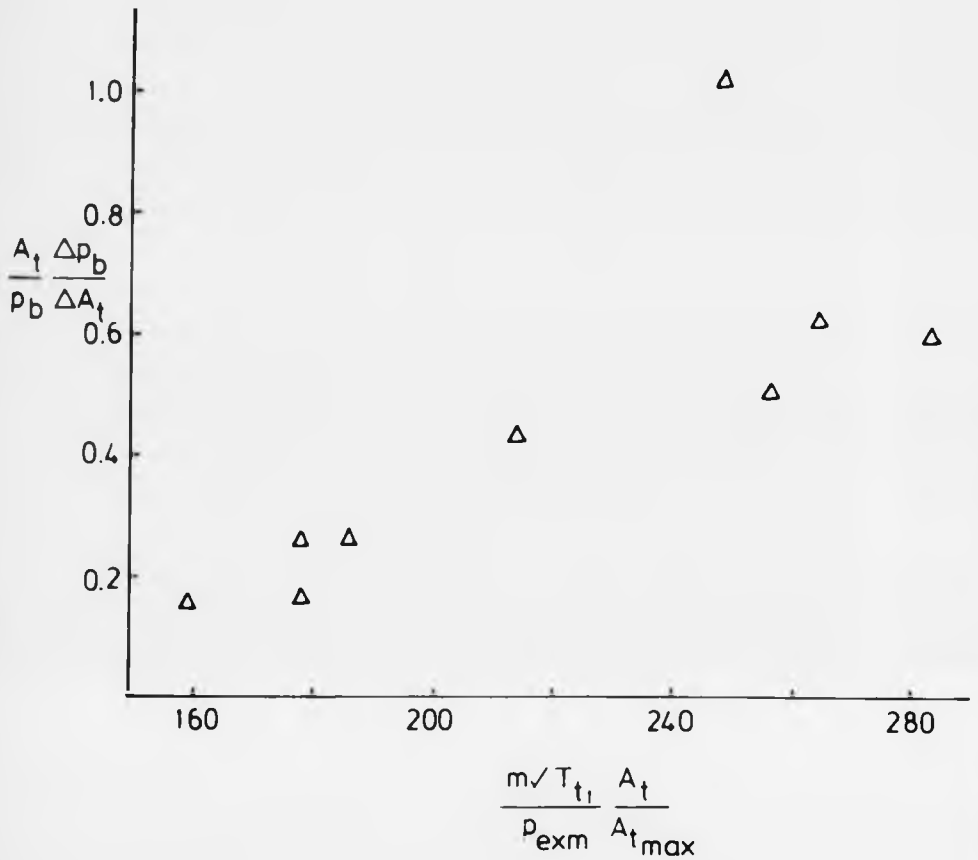


Figure 5.27 Normalised boost gain against dimensionless turbine mass flow

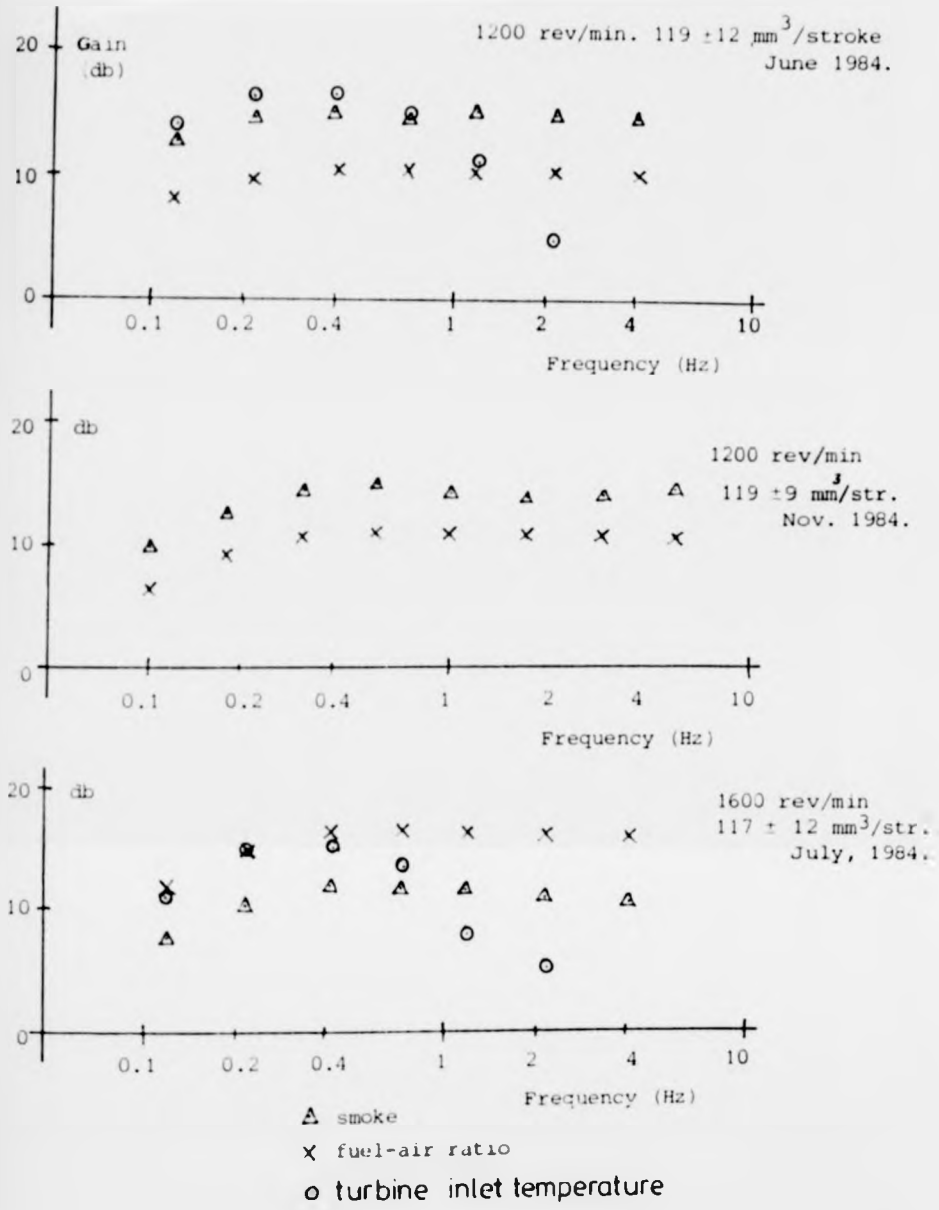


Figure 5 28 Responses of opacity and turbine inlet temperature compared with air-fuel ratio response.

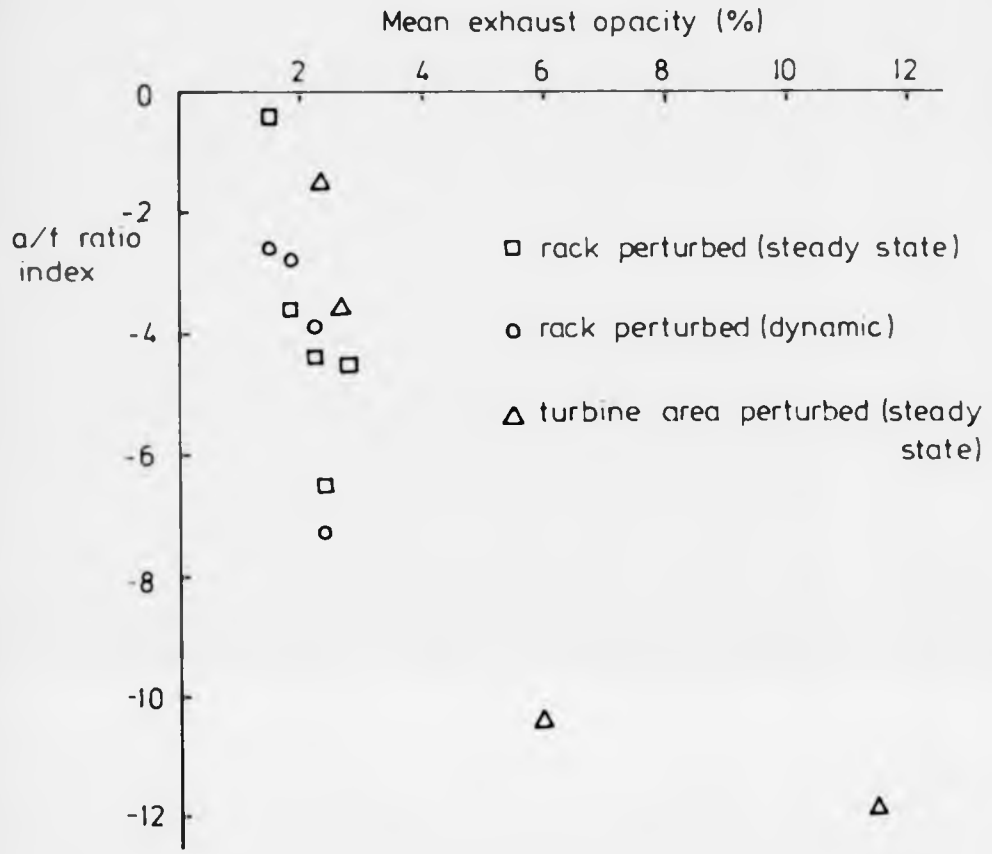


Figure 5.29 Air-fuel ratio index plotted against mean exhaust opacity.

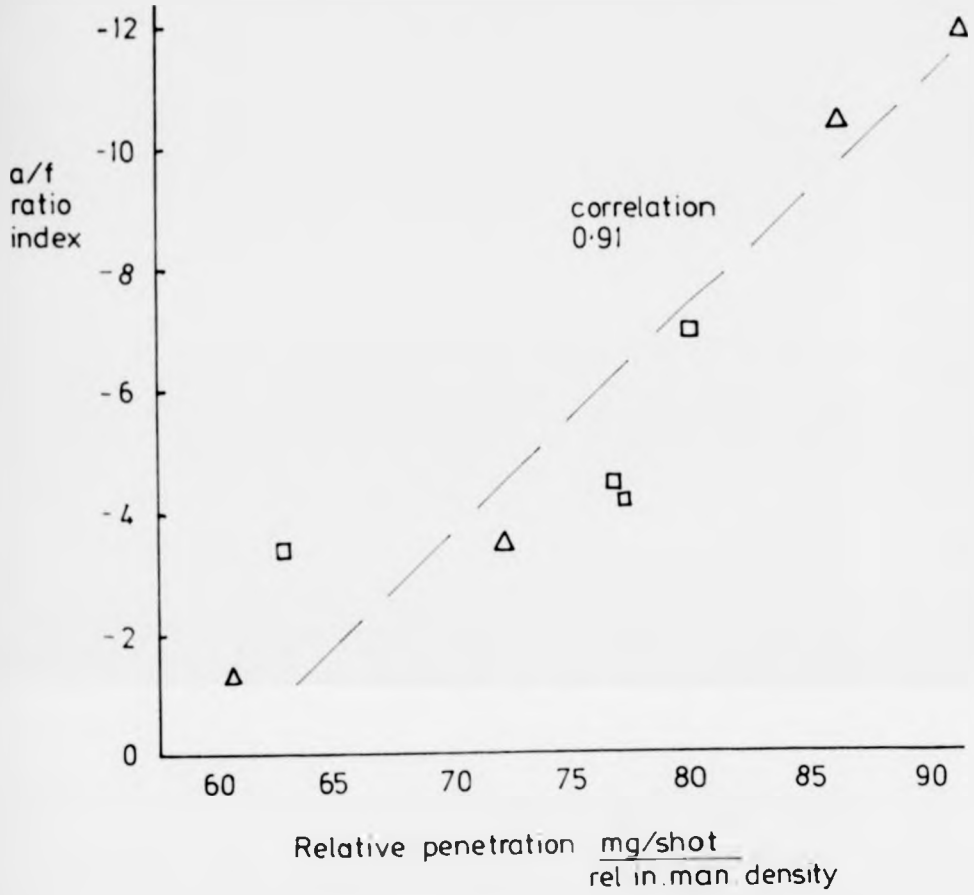


Figure 5.30 Air-fuel ratio index versus relative fuel injection penetration.

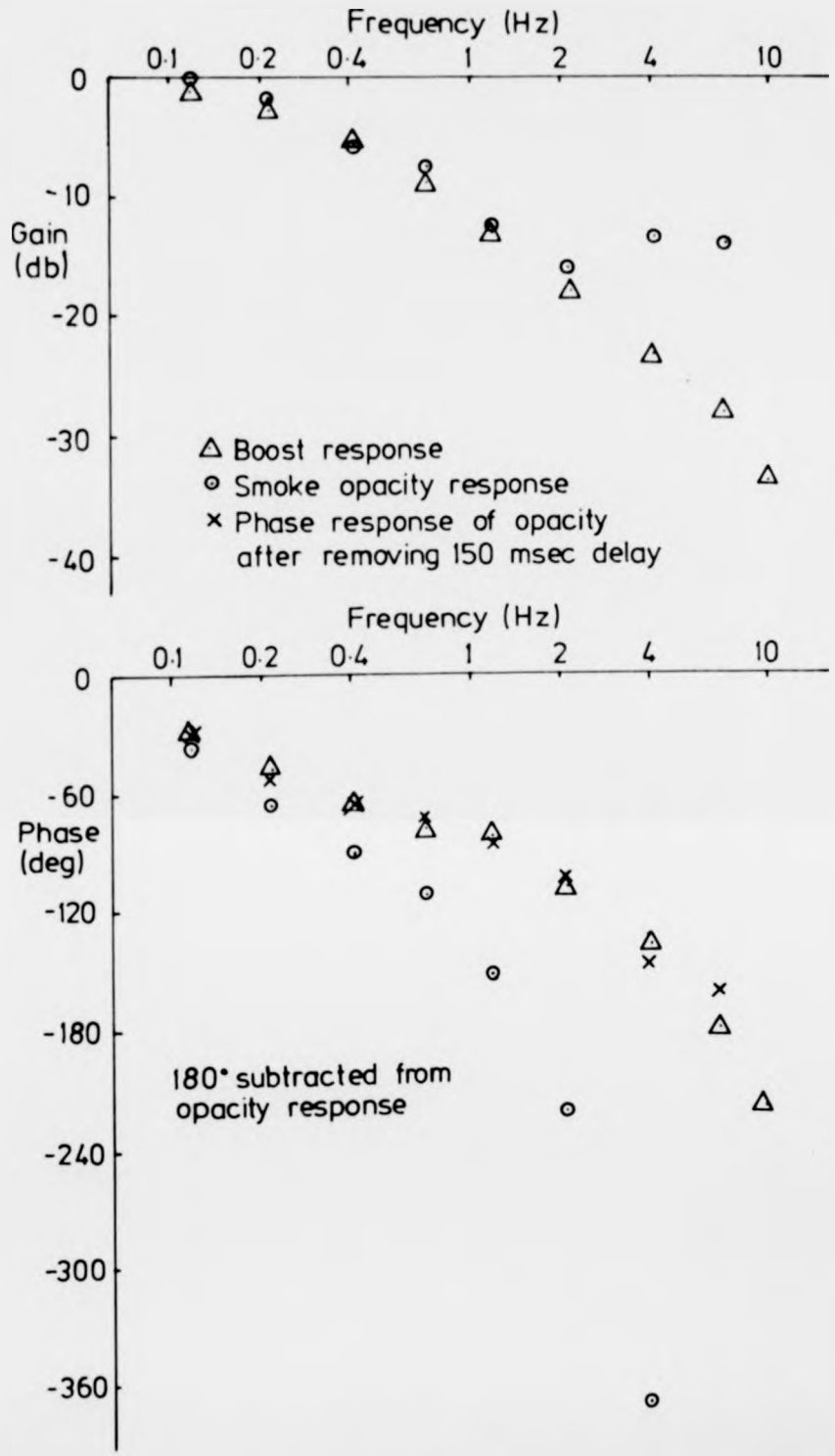


Figure 5.31 Opacity response to turbine area compared with boost response.

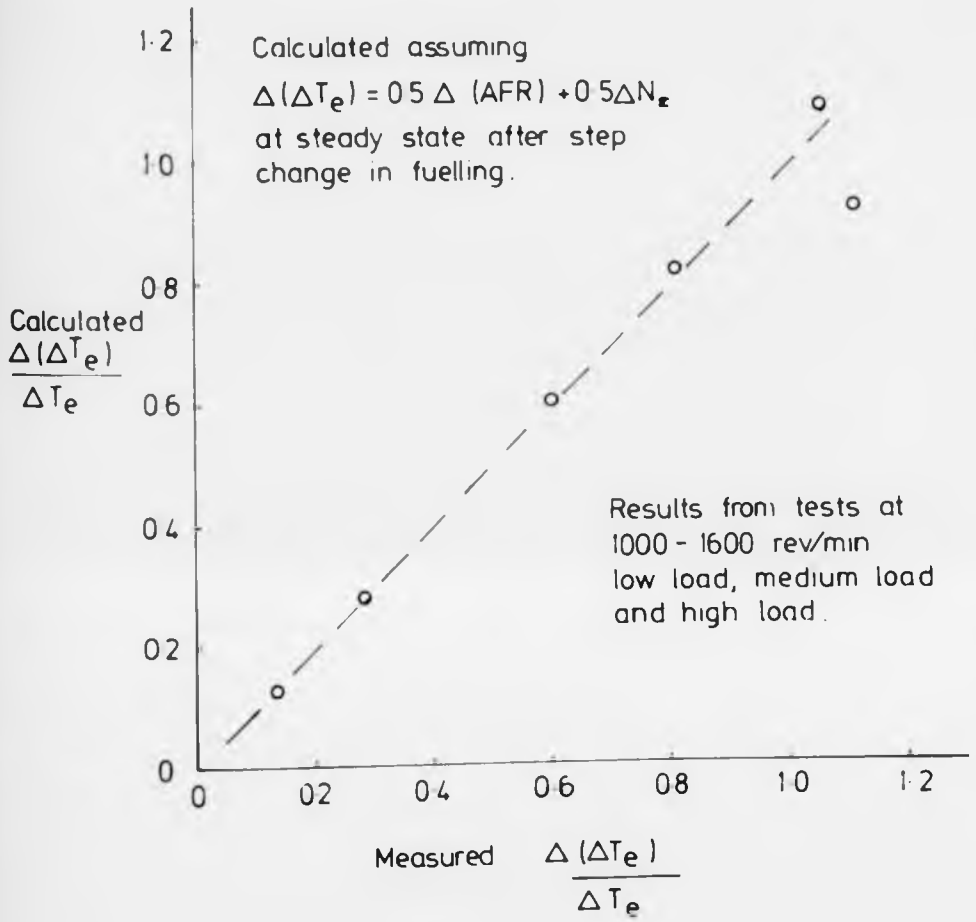


Figure 5.32 Comparison of measured and calculated changes in temperature rise across the engine ($\Delta T_e$)

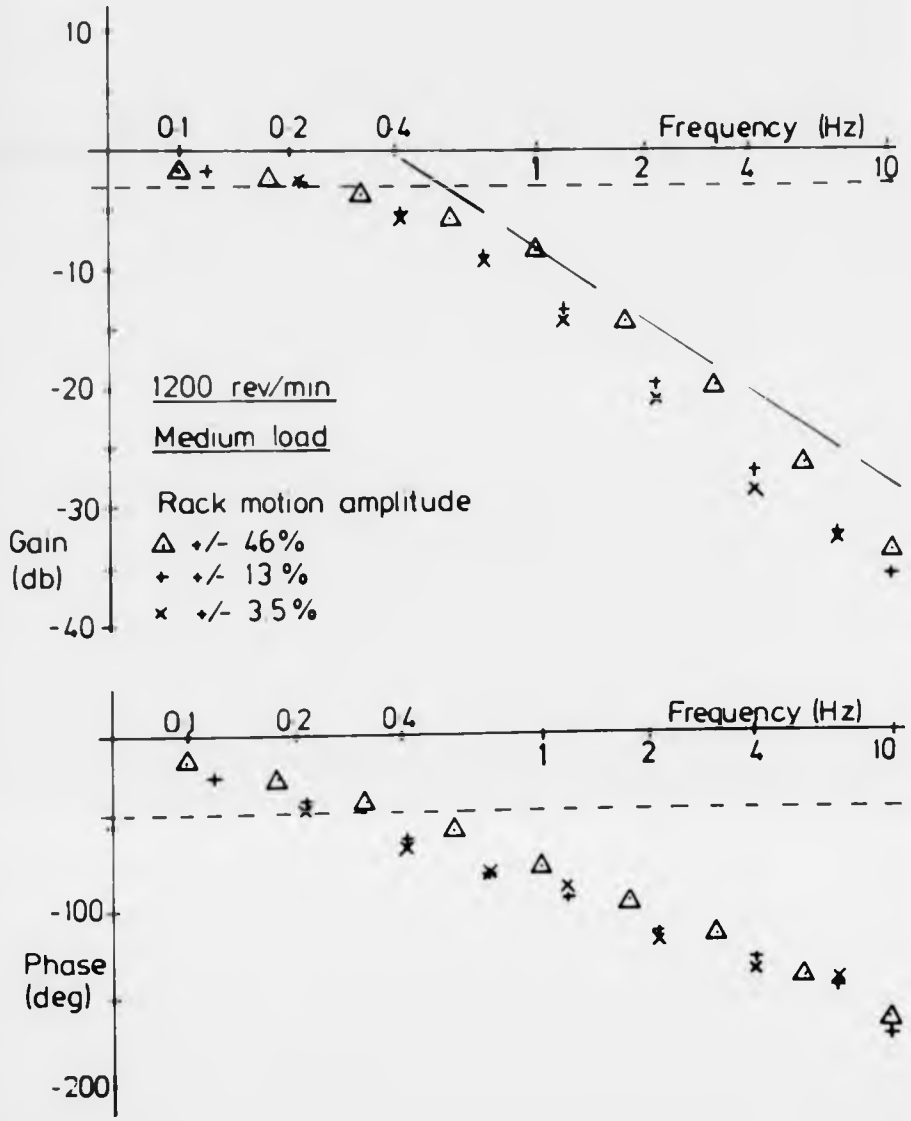


Figure 5.33 Effect of rack motion amplitude on engine speed response.

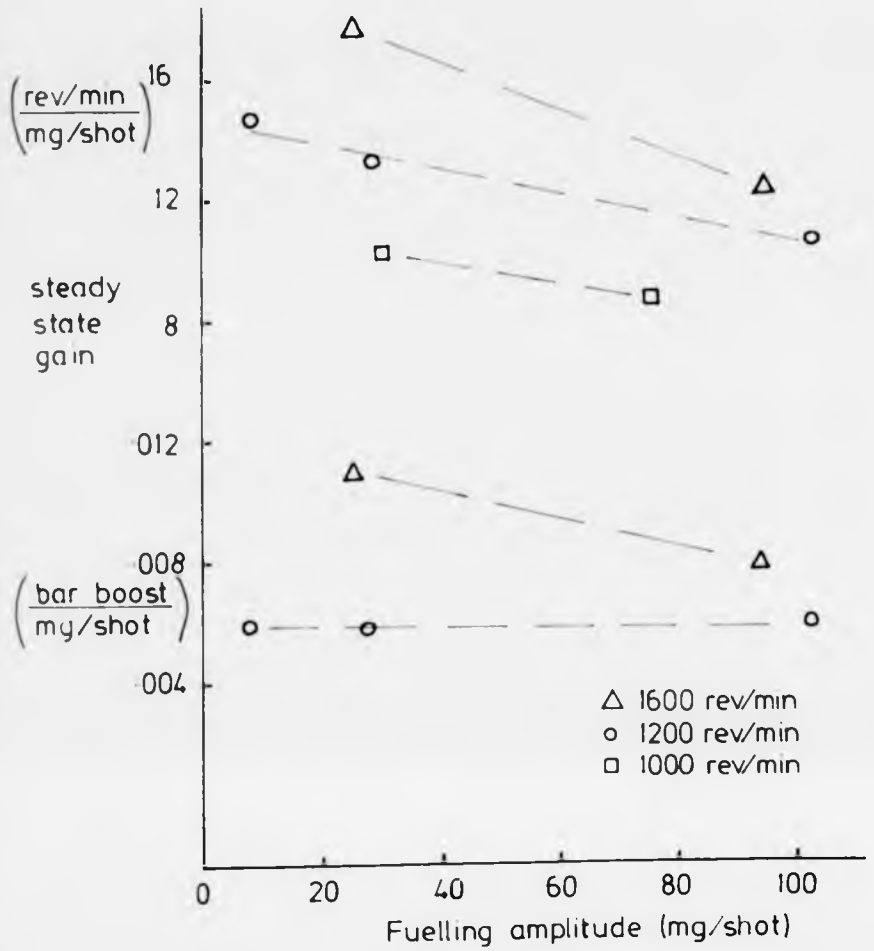


Figure 5.34 Variation of steady state gains with amplitude of perturbation

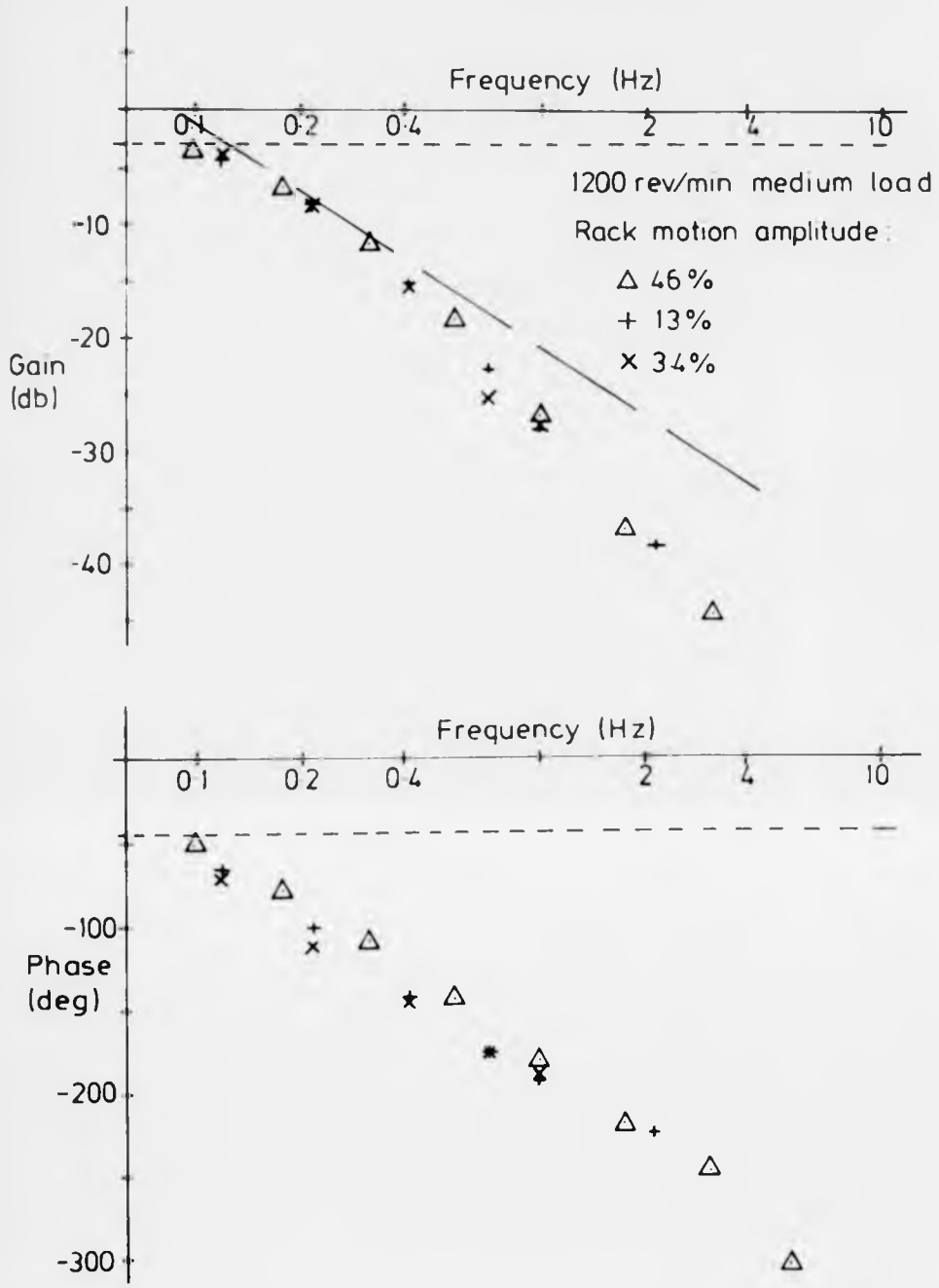


Figure 5.35 Non-linearity: Effect of rack motion amplitude on engine speed response.

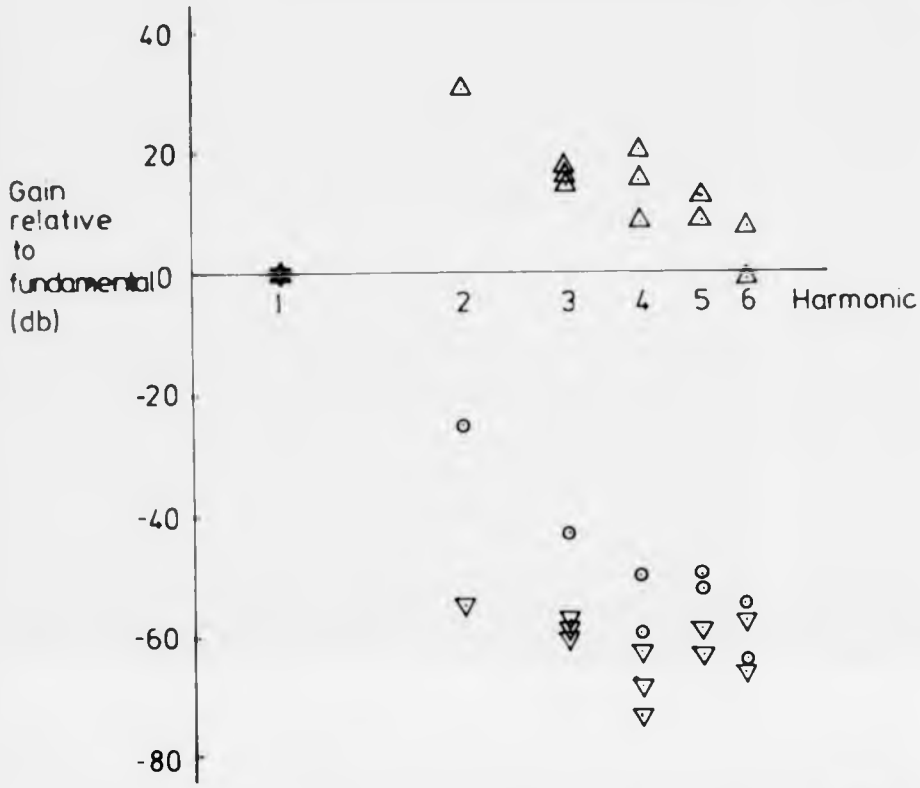


△ speed signal response relative to rack position
o speed signal response relative to tut signal.
▽ rack position signal harmonic content.

1200 rev/min
104 ± 16 mg/shot fuelling
Test frequency 1Hz

Figure 5.36 Amplitude of first six harmonics in engine speed response.

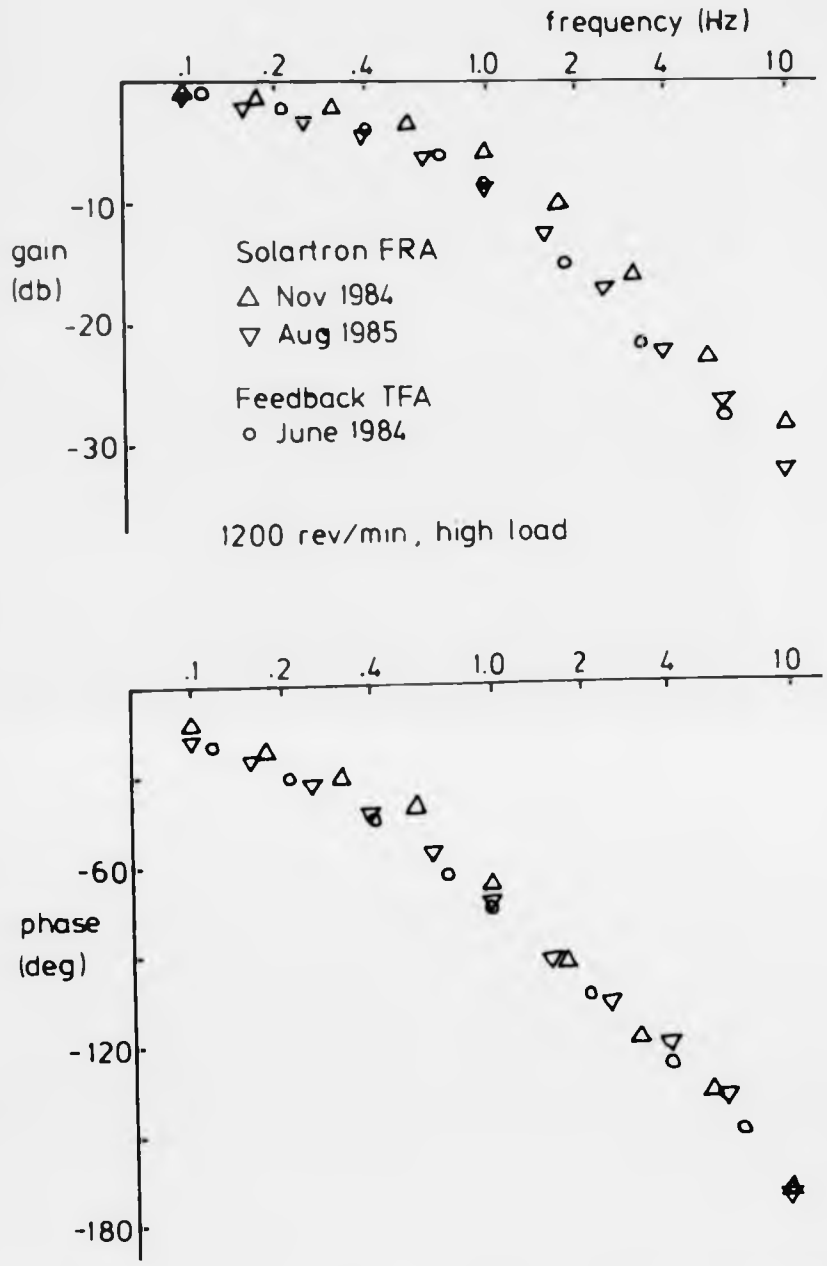


Figure 5.37 Consistency of results: speed response to rack

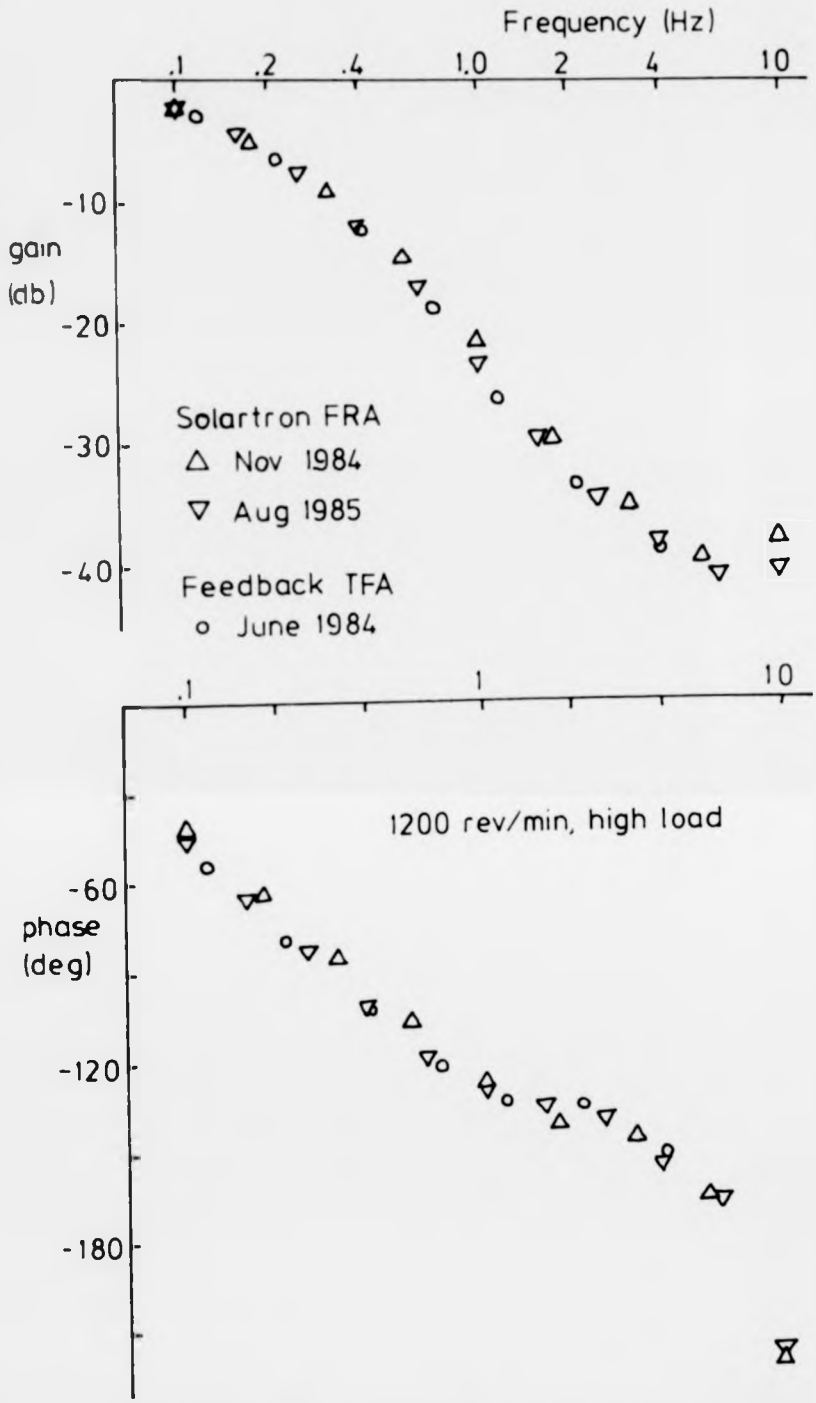


Figure 5.38 Consistency of results: boost response to rack

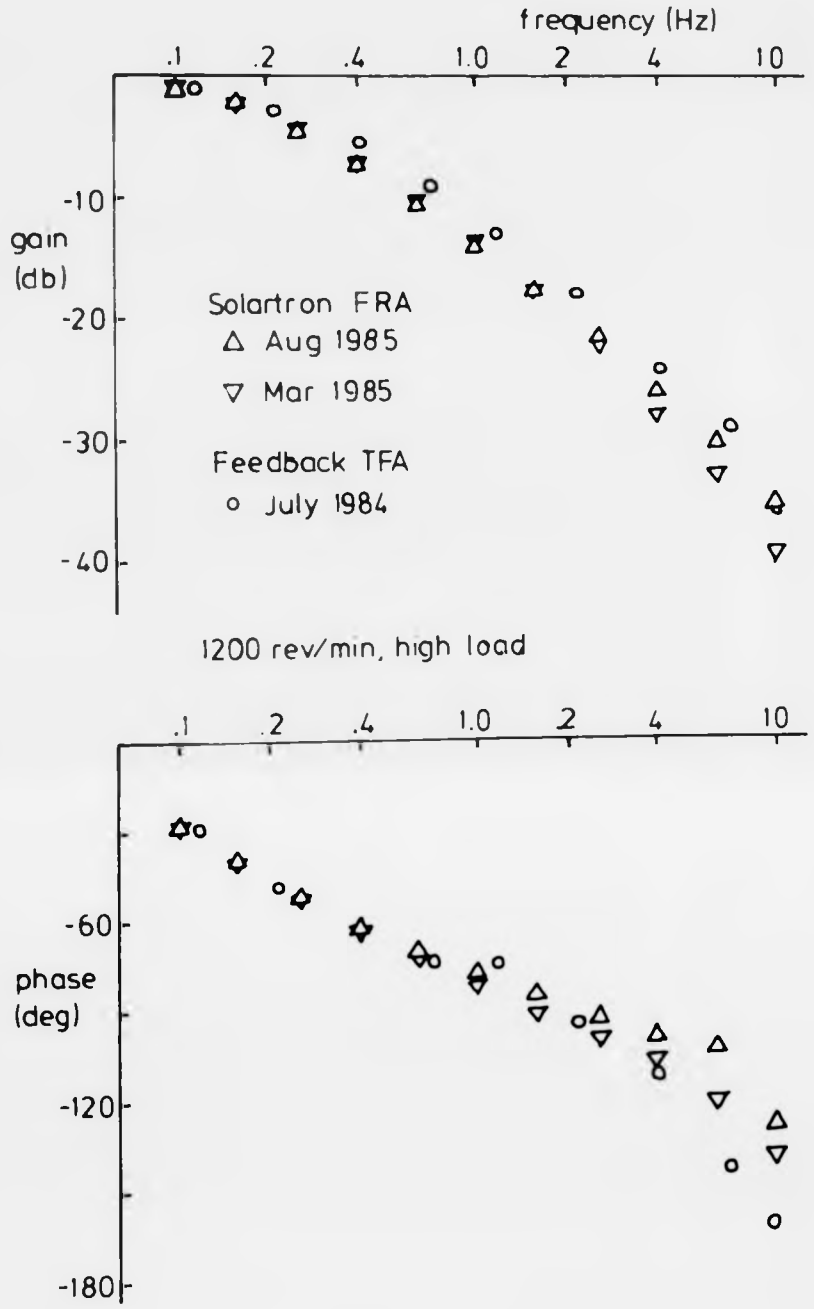


Figure 5.39 Consistency of results: boost response to turbine inlet area

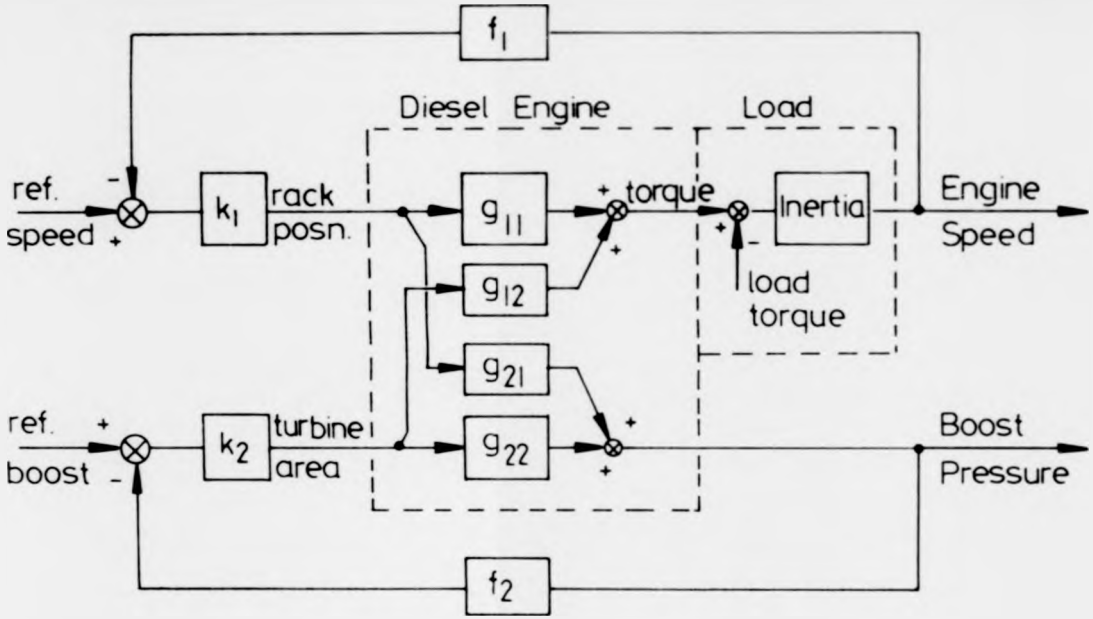


Figure 6.1 Transfer function diagram of a turbocharged diesel engine with VG turbine and seperate feedback control of engine speed and boost pressure

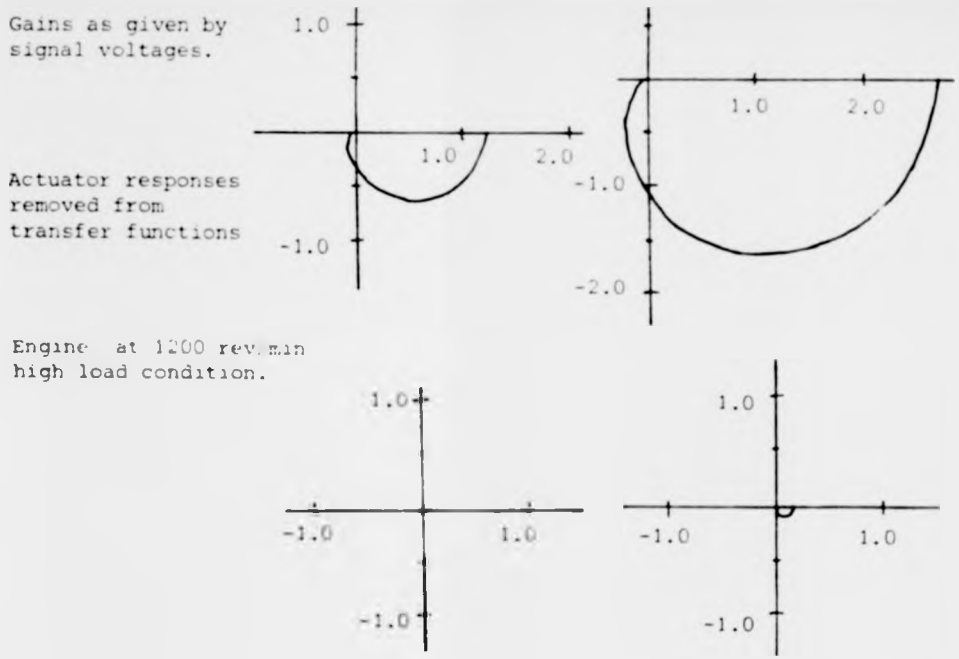


Figure 6.2 Nyquist plots of transfer function matrix.

Engine operating at
1200rev/min, high load.

Inlet and output voltages
scaled to avoid singularity
and achieve near dominance

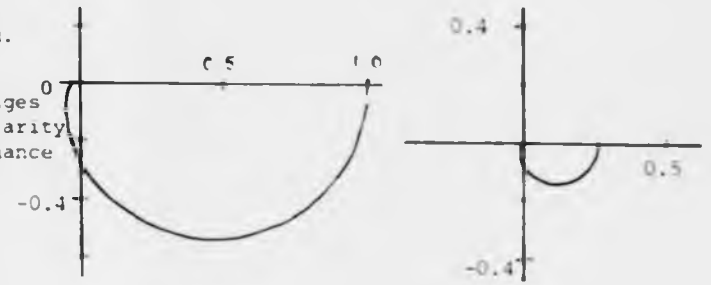


Actuator responses
removed from engine
transfer functions.

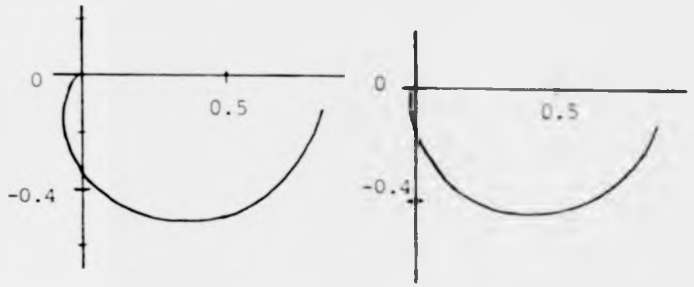


Figure 6.3 Nyquist array after scaling inputs and outputs.

Precompensator matrix designed, using 'align' algorithm, to give best diagonal dominance at 3.3 Hz.

Input and output signals scaled to avoid singularity.

Actuator responses removed.

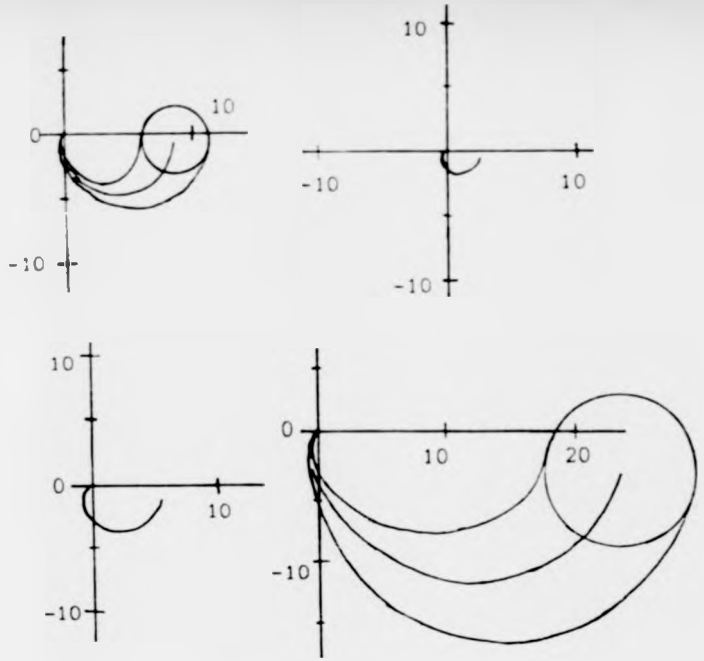


Figure 6.4 Nyquist array with scaling and optimal precompensator.

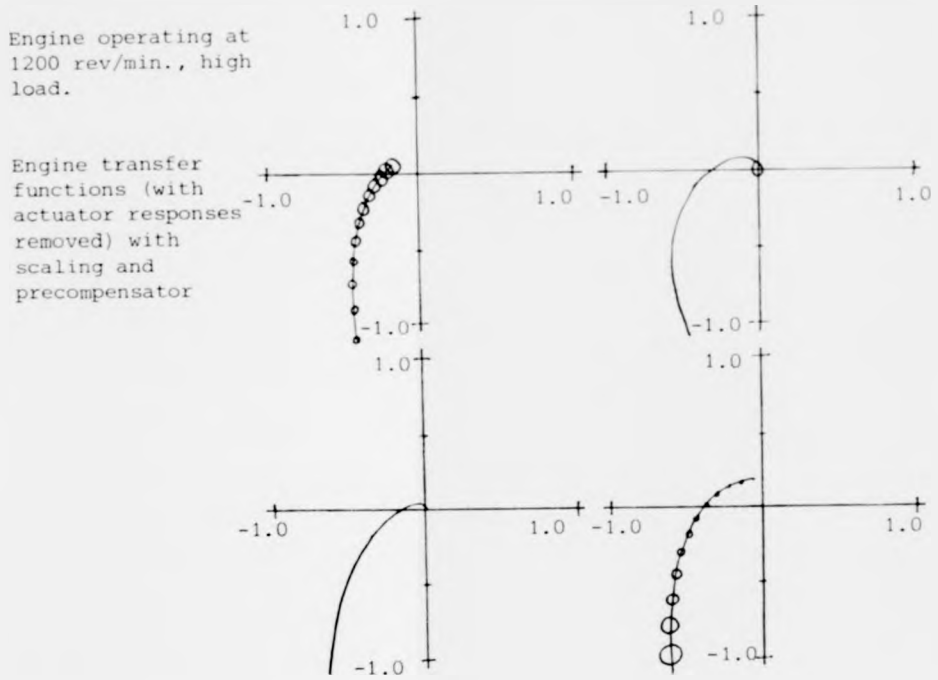


Figure 6.5 Nyquist array expanded near critical point. (Gershgorin discs shown)

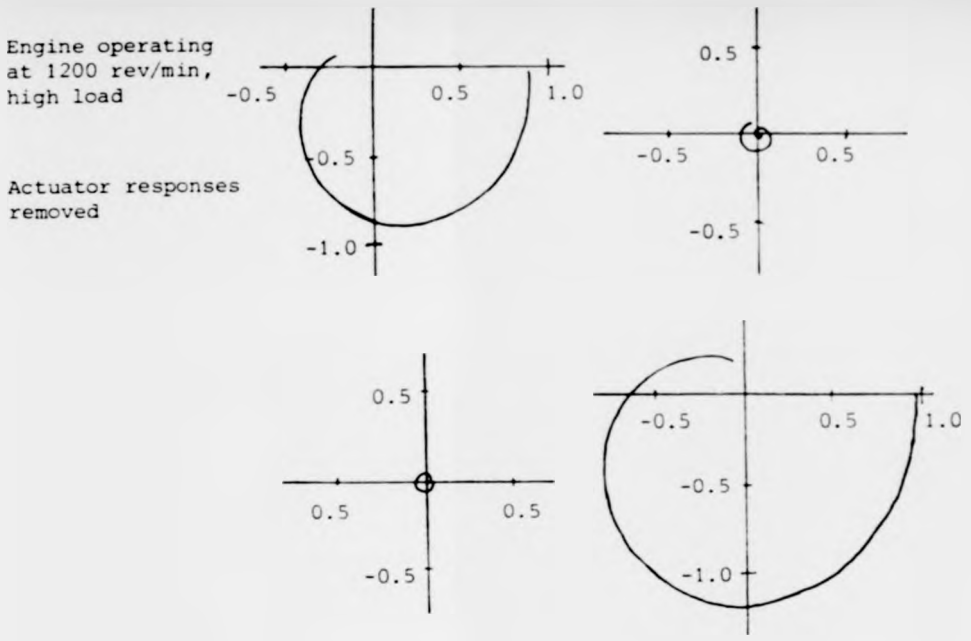


Figure 6.6 Closed loop Nyquist plots of system with scaling and precompensator

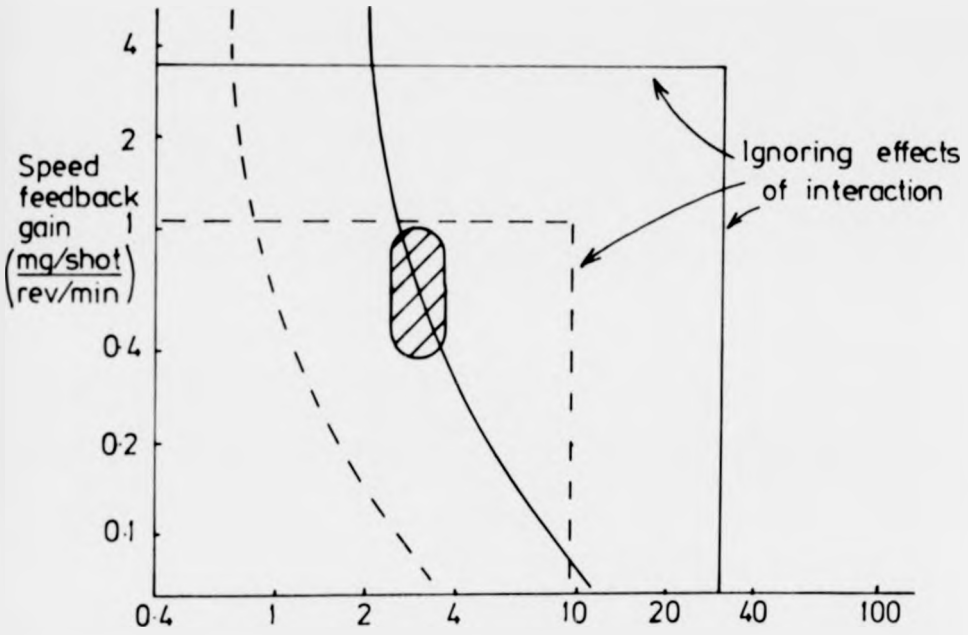


—— lines indicating limits of stability

---- lines indicating safe stability margin

region of desired feedback gains

2200 rev/min medium load ( TL11 engine) load inertia is that of engine, flywheel and dynamometer.

Figure 6.7 Regions of stability in the gain plane with air-fuel ratio as the second variable (max. speed)

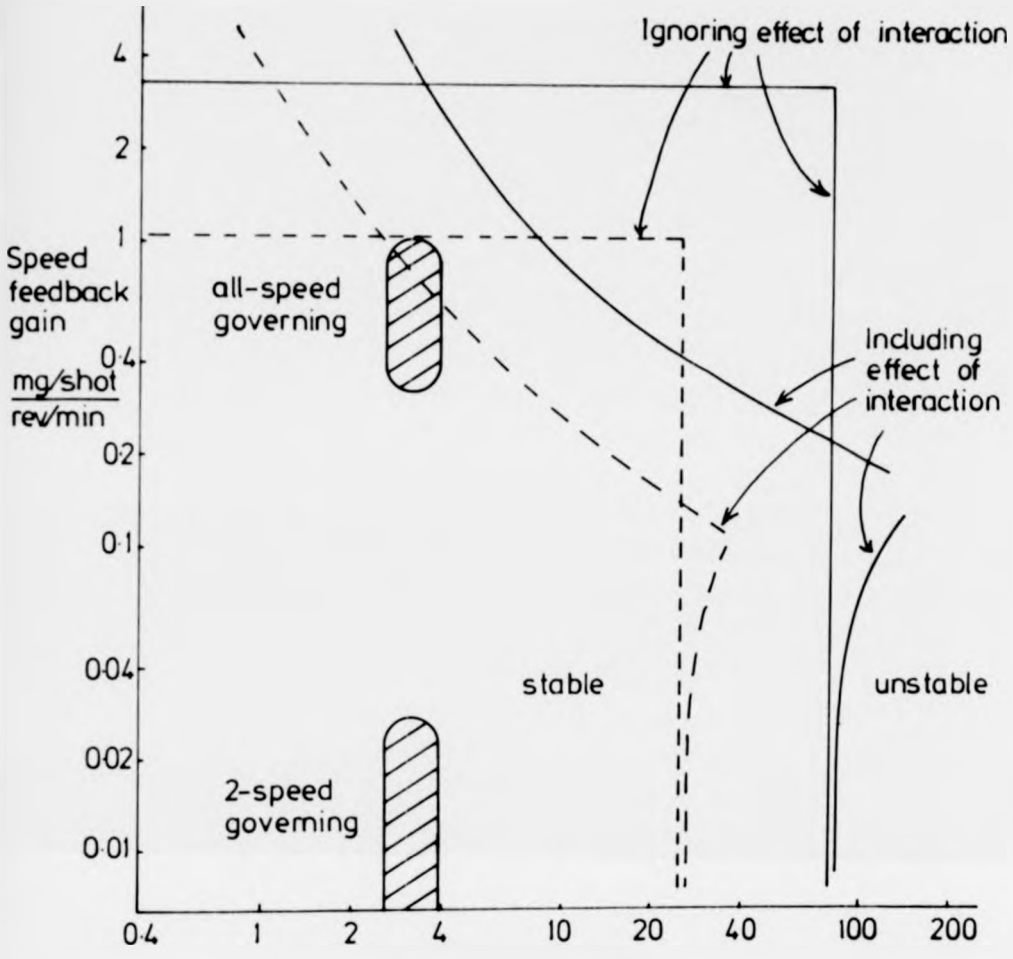


Figure 6.8 Regions of stability in the gain plane with air-fuel ratio as the second variable (peak torque)

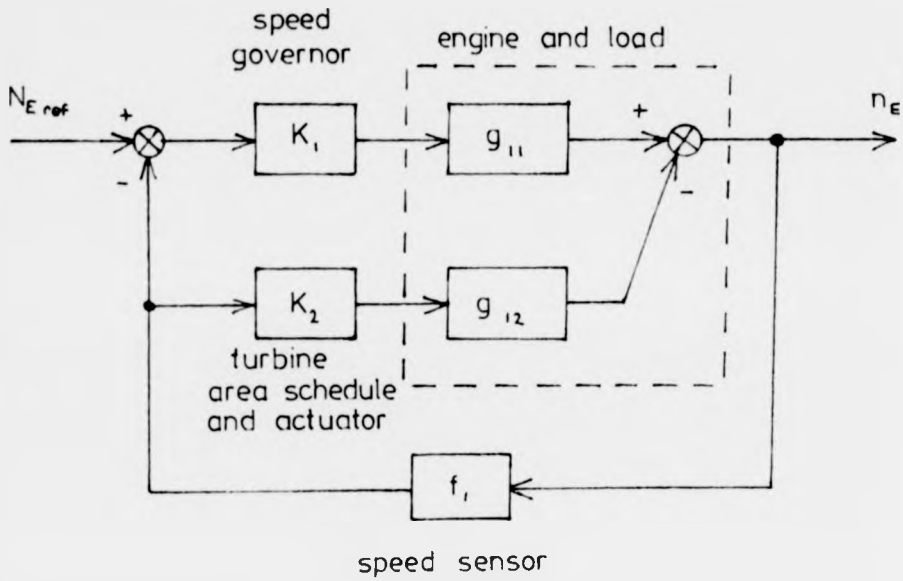


Figure 6.9 Transfer function diagram of engine with scheduling of turbine inlet area according to engine speed.

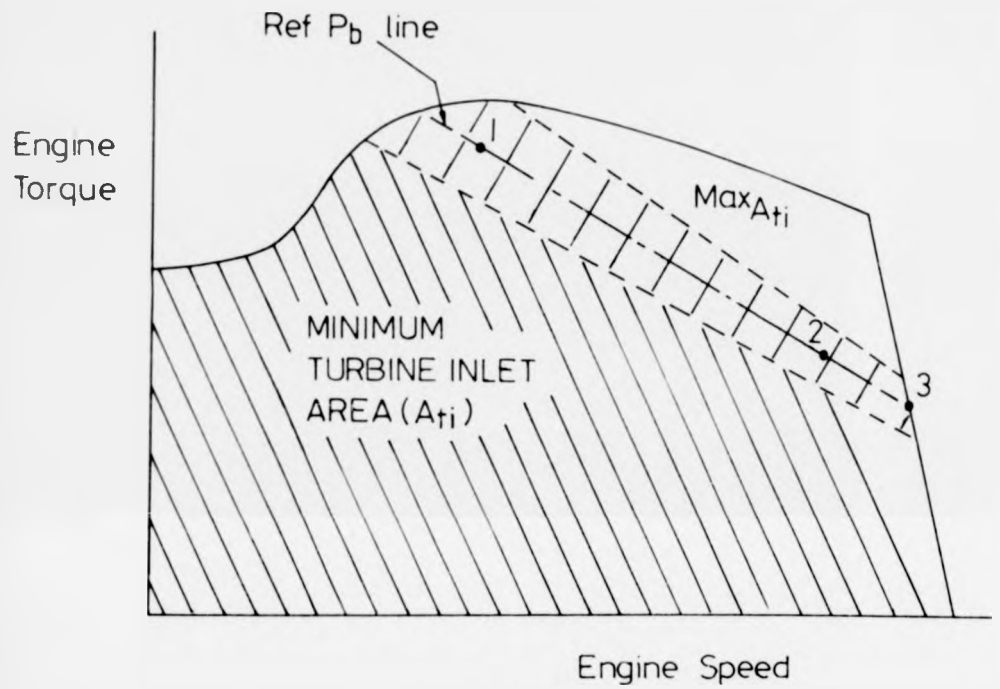


Figure 7.1 Turbine inlet area schedule when actuator is operated by boost pressure.

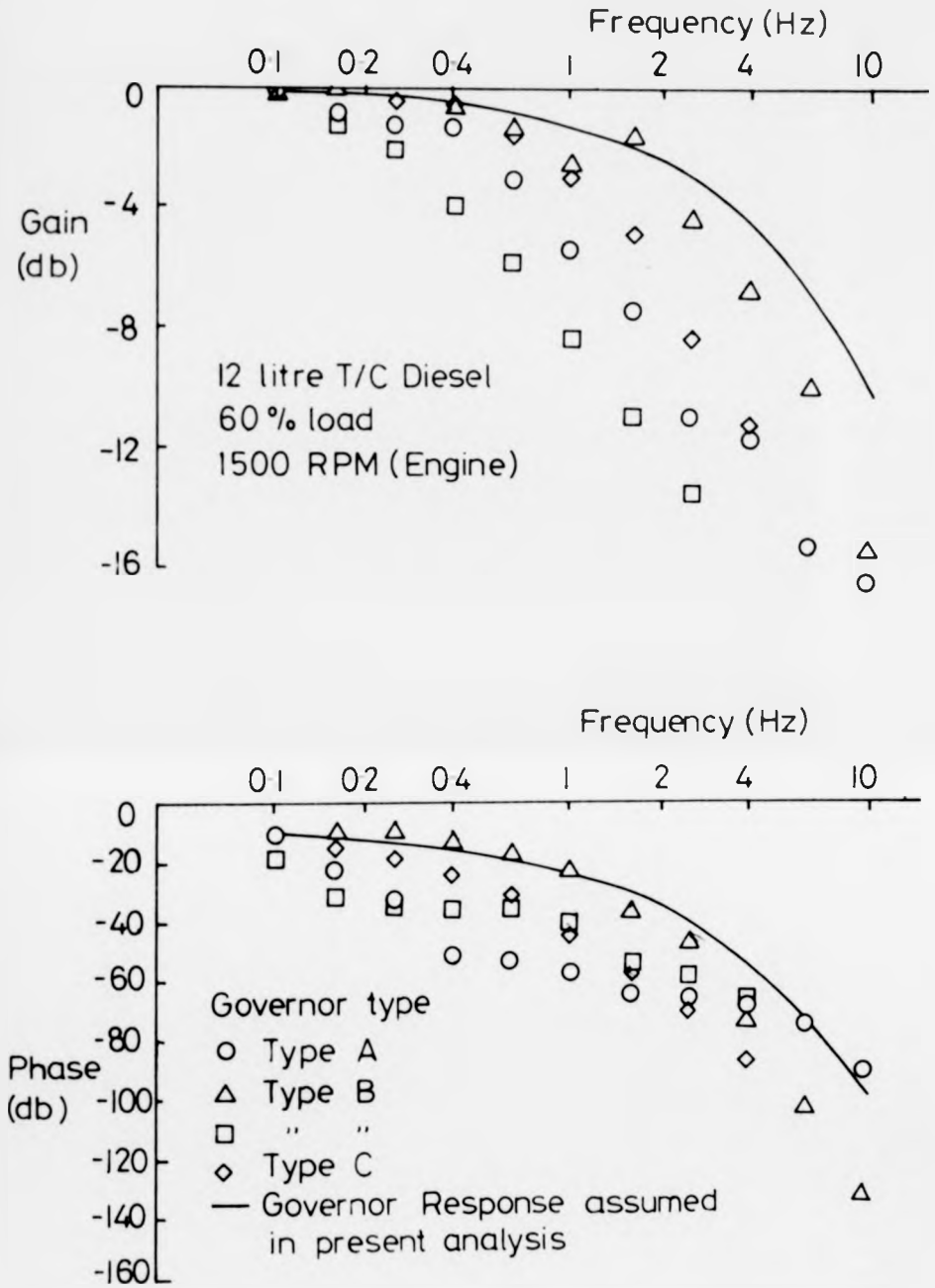


Figure 7.2 Assumed govenor response compared with response measured for similar f.i.e. pumps.

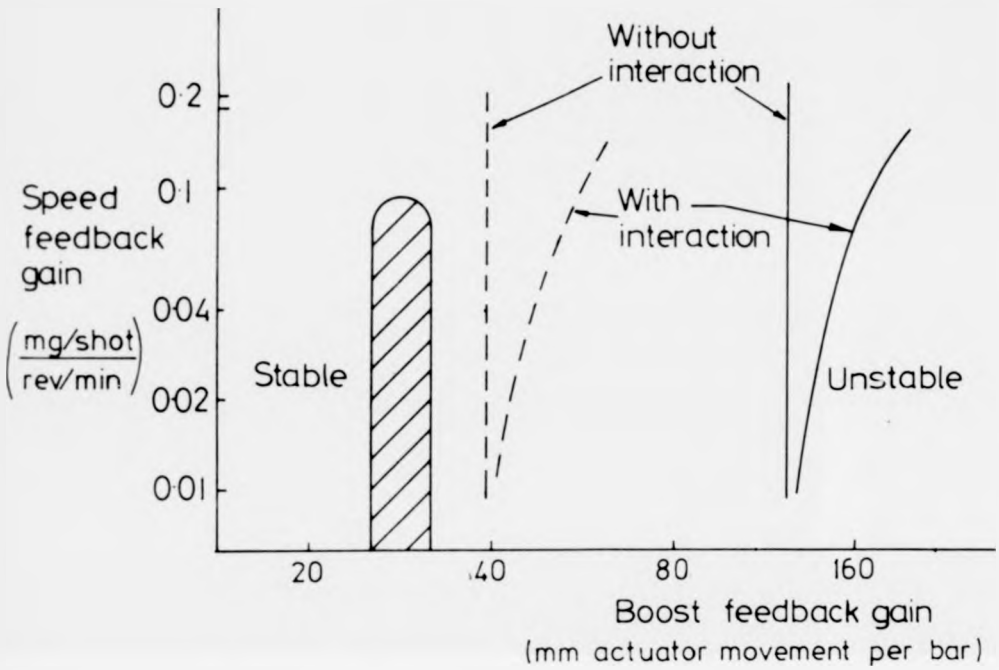


— lines indicating instability

--- lines of safe stability margin

region of desired feedback gains

Actuator responses normal
Turbocharger inertia standard

Figure 7.3 Stability region in the gain plane: peak torque condition without speed governing

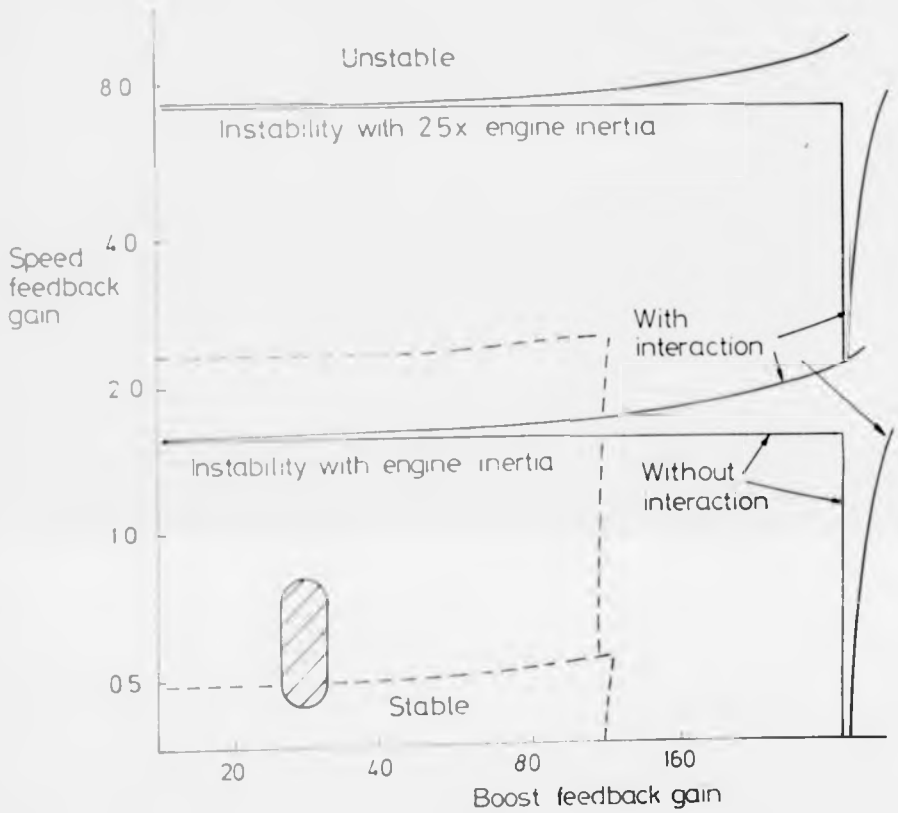


Actuator responses normal
Turbocharger inertia standard

Figure 7 4 Stability region in the gain plane: maximum speed, showing effect of load inertia.

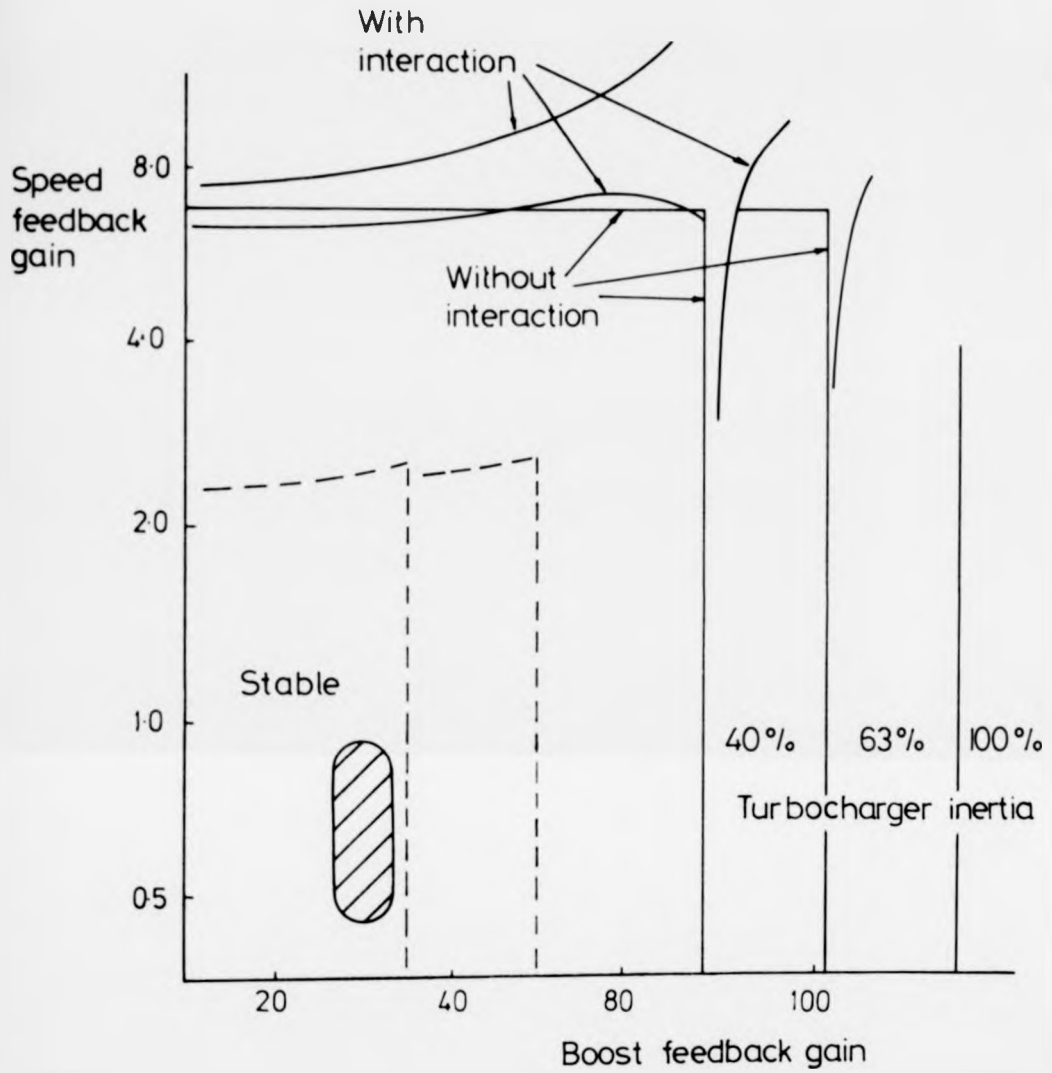


Turbine area actuator response improved
(10 Hz band width with digital control)
Load inertia (total) is 2·5 times engine inertia.

Figure 7.5 Stability in the gain plane: maximum speed governing showing effect of turbocharger inertia.

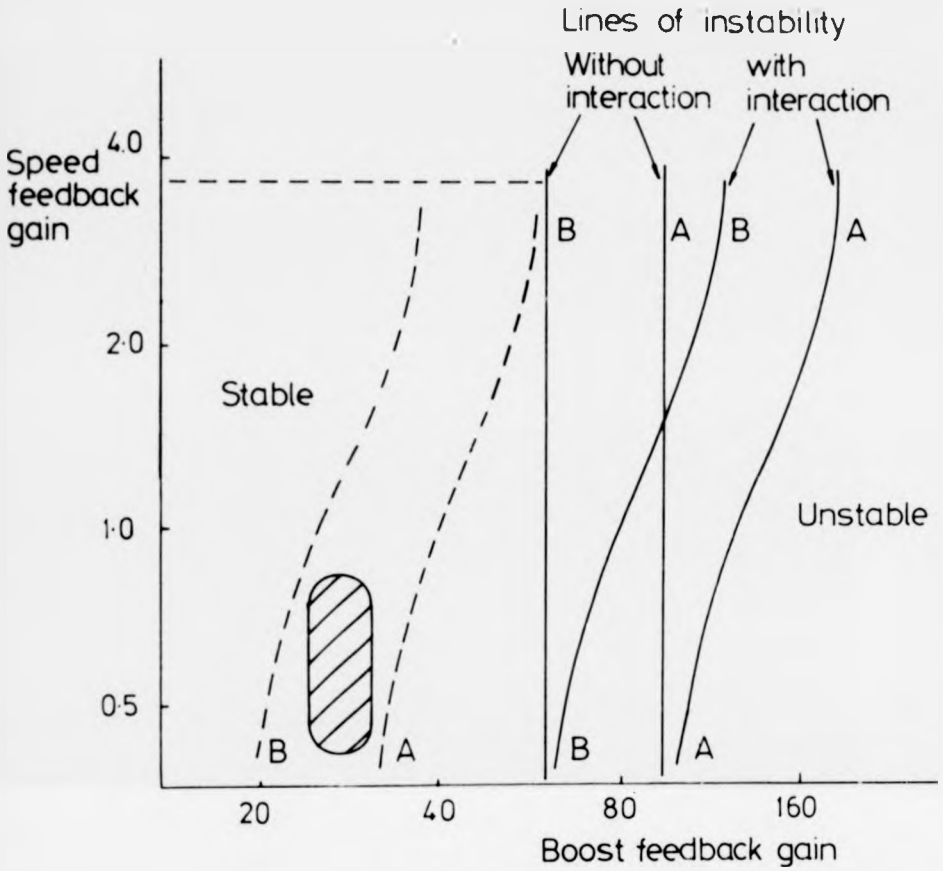


Turbine area actuator response improved
Load inertia (total) is 25 times engine inertia
Lines B-B indicate 40% reduction in t/c inertia

Figure 7.6 Stability region in the gain plane: peak torque condition with speed governing

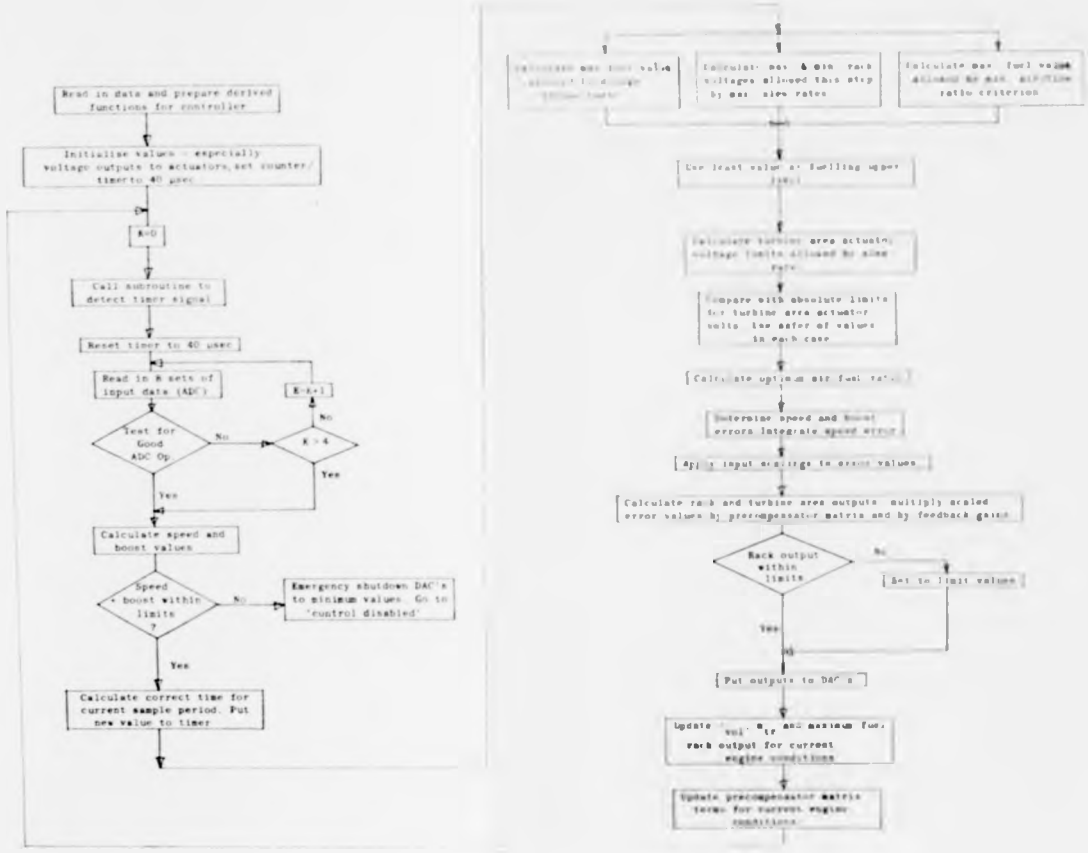


Figure 8.1 Flow diagram showing main features of controller program

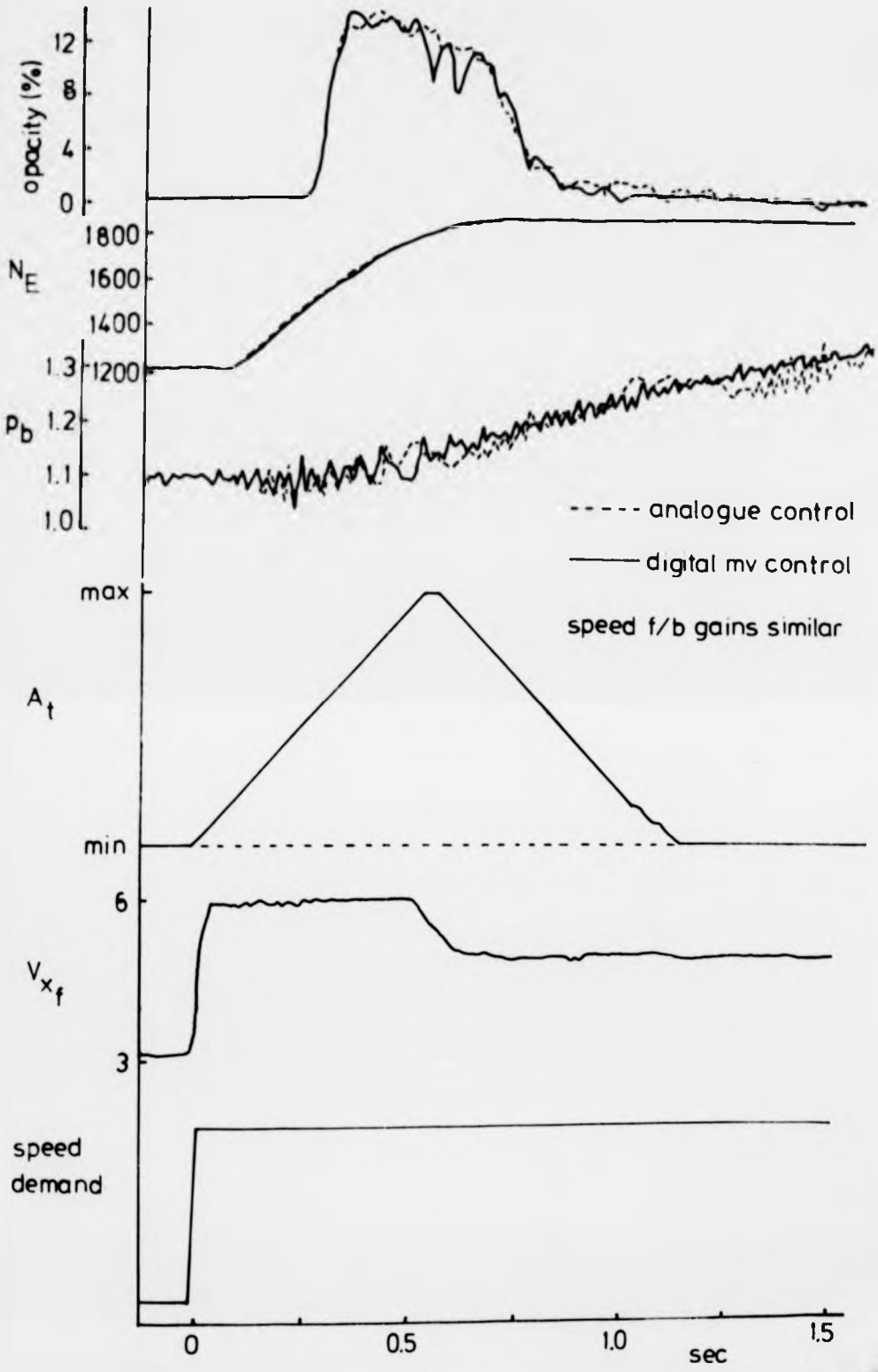


Figure 8.2 Step responses with analogue and digital control

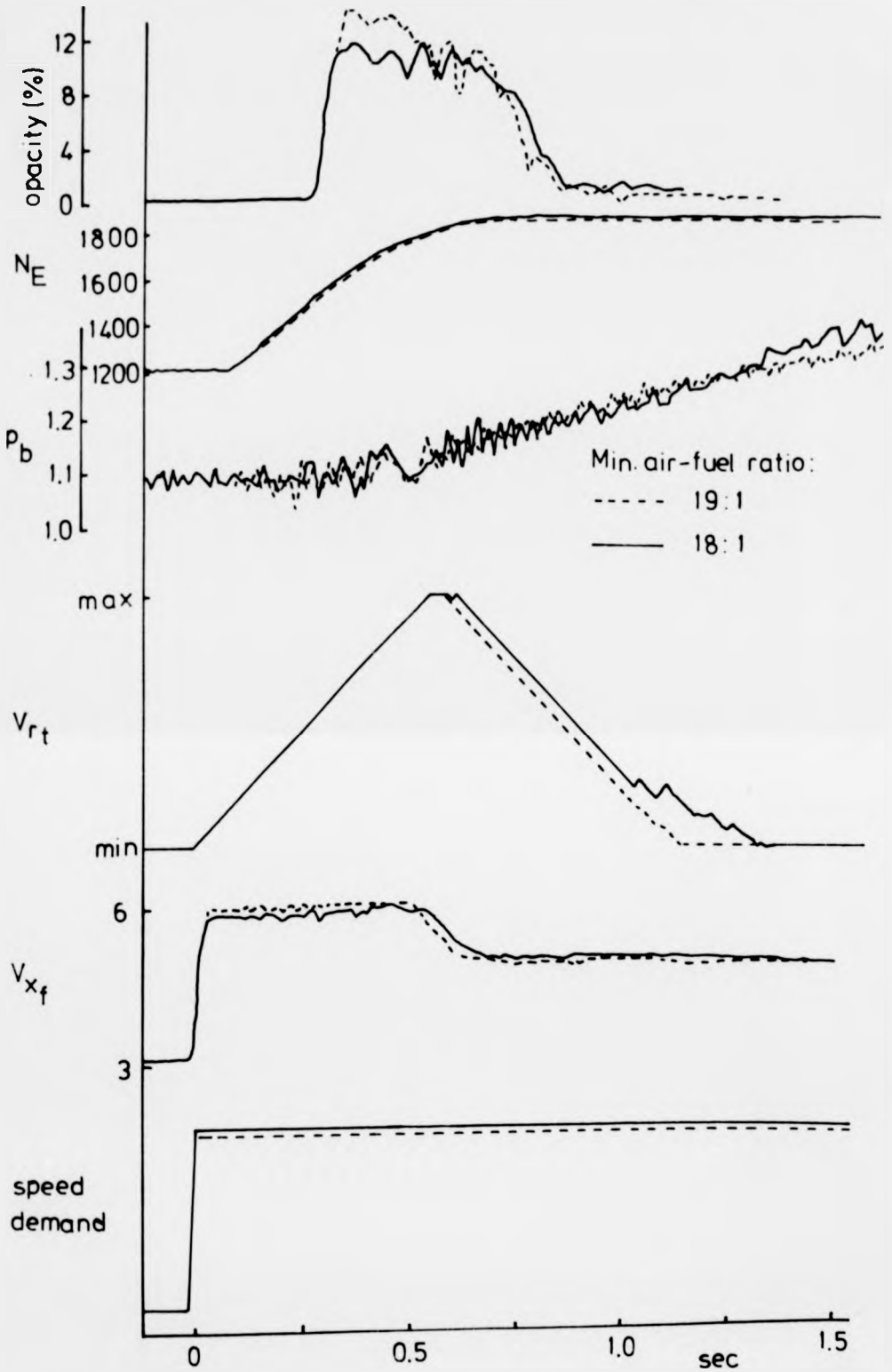


Figure 8.3 Step responses effect of min. air-fuel ratio

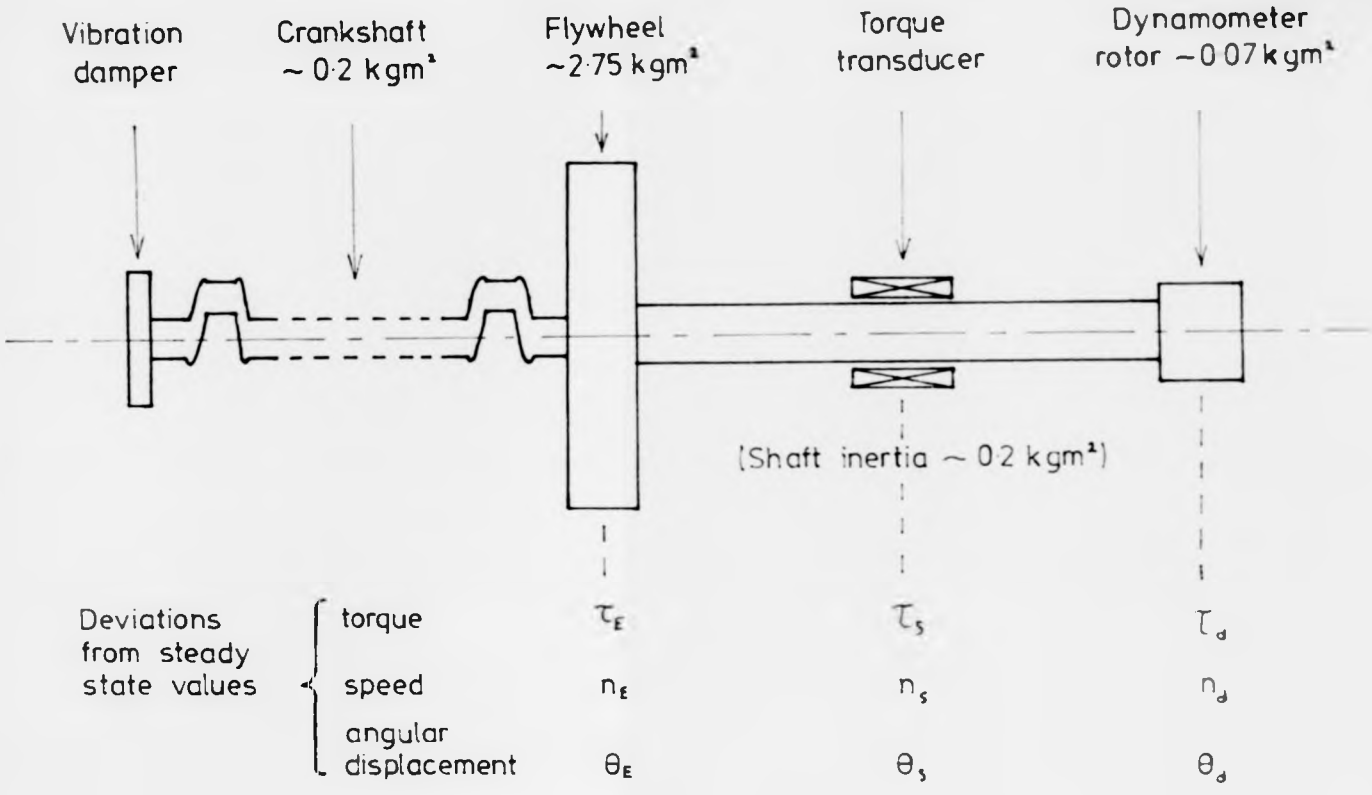


Figure A 3.1 Diagram of engine-dynamometer torsional system

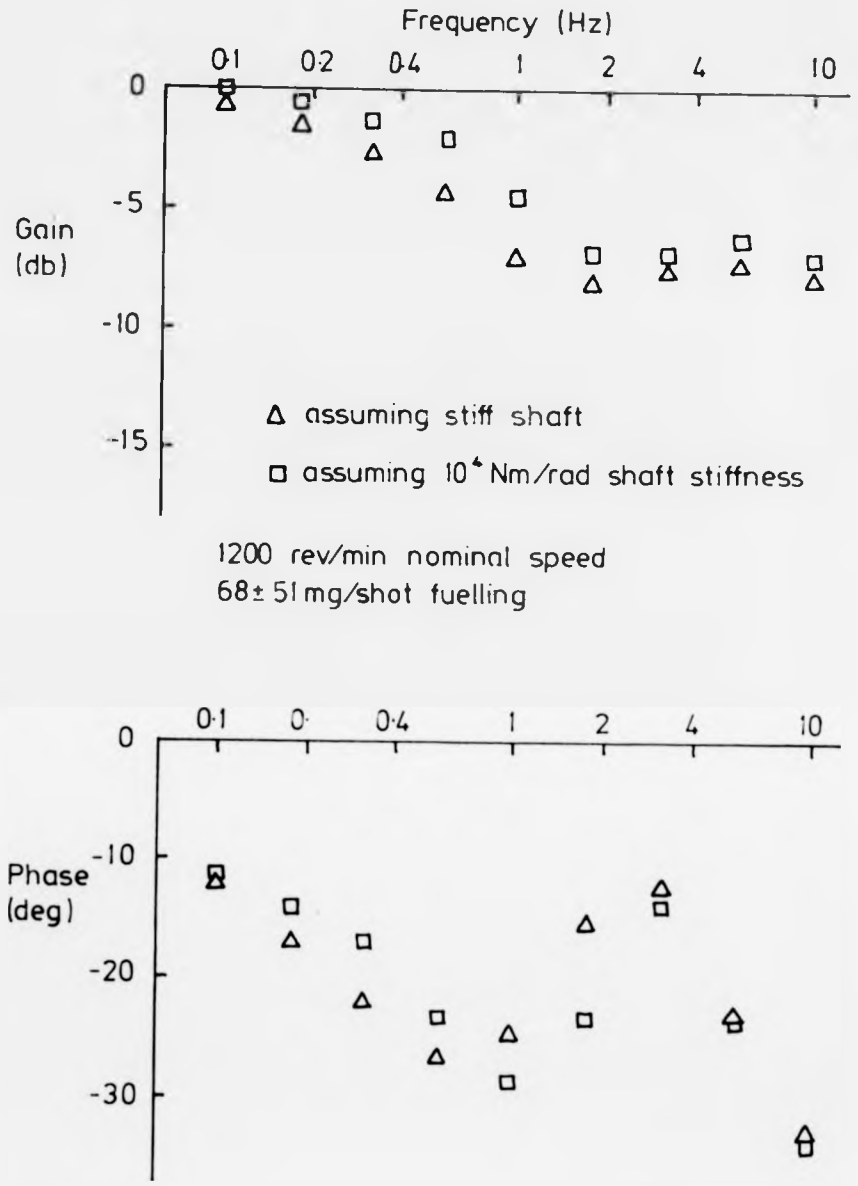


Figure A3.2 Effect of shaft stiffness on calculated d.m.e.p. response at 1200 rev/min.

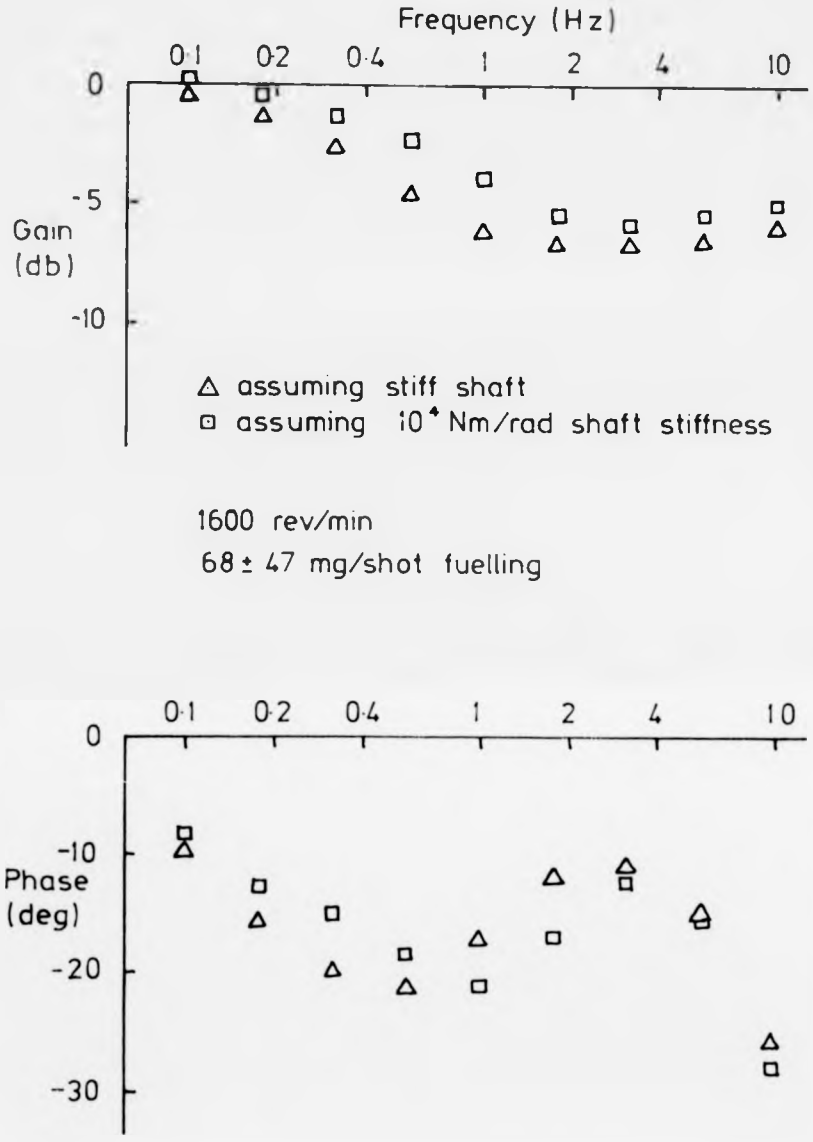


Figure A3.3 Effect of shaft stiffness on calculation of d.m.e.p. response at 1600 rev/min.